

**EXPLORING THE GEOSPATIAL RELATIONSHIPS BETWEEN DEMERSAL FISH
AND SEAFLOOR MORPHOMETRICS ALONG THE SOUTHEAST ATLANTIC
CONTINENTAL SHELF**

A thesis submitted in partial fulfillment of the requirements for the degree

MASTER OF SCIENCE

in

ENVIRONMENTAL STUDIES

by

**FRIEDRICH ALEXANDER KNUTH
NOVEMBER 2014**

at

**THE GRADUATE SCHOOL OF THE UNIVERSITY OF CHARLESTON,
SOUTH CAROLINA AT THE COLLEGE OF CHARLESTON**

Approved by:

Dr. Norman S. Levine

Dr. Laura M. Kracker

Dr. Leslie R. Sautter

Dr. Matthew C. Nowlin

Dr. Amy T. McCandless, Dean of the Graduate School

UMI Number: 1585544

All rights reserved

INFORMATION TO ALL USERS

The quality of this reproduction is dependent upon the quality of the copy submitted.

In the unlikely event that the author did not send a complete manuscript and there are missing pages, these will be noted. Also, if material had to be removed, a note will indicate the deletion.



UMI 1585544

Published by ProQuest LLC (2015). Copyright in the Dissertation held by the Author.

Microform Edition © ProQuest LLC.

All rights reserved. This work is protected against unauthorized copying under Title 17, United States Code



ProQuest LLC.
789 East Eisenhower Parkway
P.O. Box 1346
Ann Arbor, MI 48106 - 1346

ABSTRACT

EXPLORING THE GEOSPATIAL RELATIONSHIPS BETWEEN DEMERSAL FISH AND SEAFLOOR MORPHOMETRICS ALONG THE SOUTHEAST ATLANTIC CONTINENTAL SHELF

A thesis submitted in partial fulfillment of the requirements for the degree

MASTER OF SCIENCE

in

ENVIRONMENTAL STUDIES

by

FRIEDRICH ALEXANDER KNUTH
NOVEMBER 2014

at

THE GRADUATE SCHOOL OF THE UNIVERSITY OF CHARLESTON,
SOUTH CAROLINA AT THE COLLEGE OF CHARLESTON

The 2007 Magnuson-Stevens Fishery Conservation and Management Act mandates understanding geospatial fish-seascape interactions to establish Marine Protected Areas (MPAs). MPAs are successful place-based management tools in protecting Essential Fish Habitat (EFH) and sustaining the resilience of fish populations to commercial and recreational fishing pressures. Accurate MPA delineation remains a difficult task, given the complexity of ocean systems and lack of geospatially precise information. In the southeast Atlantic, the morphometric environment of the seafloor has been found to be a control on EFH. Demersal fish species within the snapper grouper fish complex have shown strong site fidelity and interactions with the seascape (Sedberry and Van Dolah 1984). To this end, morphometric analysis of the seascape is a powerful oceanographic technique for identifying EFH to meet the mandates of the Magnuson-Stevens Act. Modern methods of acoustic data acquisition used to survey seafloor morphometrics and model fish-seascape interactions promise efficiency and minimal environmental impact in the development of better fisheries management information. In July, 2013, the NOAA Ship Pisces collected bathymetric, backscatter and water column data for potential habitat sites along the U.S. Southeast Atlantic continental shelf. A total of 205 km² of seafloor were mapped between Mayport, FL and Wilmington, NC, using the SIMRAD ME70 multibeam echosounder system. In addition, a total of $n = 7410$ fish presences were recorded within the water column, using the SIMRAD EK 60 split-beam echosounder system. These data were processed in CARIS HIPS, QPS Fledermaus, MATLAB and Echoview. This study provides a morphometric characterization and quantitative assessment of fish present within each survey site and identifies features of the bathymetry that help explain the presence of demersal fish. A total of 106 unique maps were created, illustrating seafloor morphometrics and fish distributions across the seascape. In ArcGIS, 14 morphometrics were generated as candidate explanatory variables for fish abundances in small (5-12 cm), medium (12-29 cm) and large (>29 cm) size classes. We explored fish-seascape interactions at two spatial scales in the GIS using a site-wide and 50 x 50 m grid scale. At the site-wide scale, \bar{X} Slope ($R^2 = 0.97$), \bar{X} Slope of Slope ($R^2 = 0.90$) and σ Depth ($R^2 = 0.87$) provided the strongest explanatory power in a bivariate analysis and may be used to help identify EFH at a coarse scale. At a 50 x 50 m grid scale, \bar{X} Slope, \bar{X} Slope of Slope and \bar{X} Backscatter emerged as the strongest contributing variables, when combined in a multivariate analysis. Overall, multivariate model R^2 values were low and not predictive, but allow for the identification of variables contributing to the characterization of fish-seascape interactions at a finer scale.

Copyright © by

Friedrich Alexander Knuth

2014

ii

ACKNOWLEDGEMENTS

This research was funded in part by the College of Charleston Graduate Scholars Award, the Joanna Endowed Scholarship and a continuous Teaching Assistantship awarded through the College of Charleston. I would like to thank Dr. Norman Levine, my advising committee, Dr. Martin Jones and Dr. Daniel McGlenn for their insight, guidance and thoughtful critique throughout the course of this project. In particular, I would like to thank Dr. Laura Kracker for inspiring this project by inviting me out in the summer of 2013 on the NOAA Ship Pisces. Funding for the 2013 stock assessment cruise, led by Stacey Harter and Andrew David from the NOAA Panama City Southeast Fisheries Science Center, was provided by the SAFMC NOAA CRCP grant #NA11NMF4410061. Finally, I would like to thank the MES program, the Department of Geology and Environmental Sciences, the Santee Cooper GIS and Remote Sensing Laboratory, Dr. Leslie Sautter and the entire BEAM team at the College of Charleston for providing the foundations upon which this research stands.

TABLE OF CONTENTS

ABSTRACT	i
LIST OF FIGURES	vi
LIST OF TABLES	xiii
INTRODUCTION	1
FISHERIES MONITORING IN THE SOUTHEAST ATLANTIC	1
BACKGROUND ON MARINE PROTECTED AREAS.....	3
PROJECT OVERVIEW AND STUDY AREA.....	5
Research Objectives	6
METHODS.....	8
DATA ACQUISITION	8
ME70 Multibeam Echo Sounder System (MBES).....	10
EK60 Split-beam Echo Sounder System (SBES).....	12
DATA PROCESSING.....	13
Bathymetry.....	14
Backscatter.....	14
Water Column (Fish) Data.....	15
Morphometric Base Layers.....	16
Explanatory Variables	31
Response Variables	37
MODELING	39
RESULTS	42
50 X 50 M GRID SCALE MULTIVARIATE MODELS	42
SITE-WIDE SCALE BIVARIATE MODELS	44
ERROR ANALYSIS	49
BATHYMETRIC ARTIFACTS	49
BACKSCATTER ARTIFACTS	51
BIAS.....	53
DISCUSSION.....	55
CONCLUSIONS	57
FUTURE WORK.....	59
Analysis at Various Spatial Scales	59
Site-Wide Model Validation	60
Seafloor Classification.....	61
RECOMMENDATIONS.....	61
REFERENCES	63

APPENDIX A, MORPHOMETRICS	I
APPENDIX B, FISH COUNTS.....	LXXXIII
APPENDIX C, MULTIVARIATE OUTPUTS	LXXXVII
APPENDIX D, BIVARIATE OUTPUTS	XC

LIST OF FIGURES

Figure 1. Map of waters governed by the US Regional Fishery Management Councils. (Fishery Councils 2013).....	2
Figure 2. View of acoustically measured fish presences above bathymetry raster surface (VE = 2x). Created in ESRI ArcScene. Knuth 2014.	4
Figure 3. NOAA Ship <i>Pisces</i> (NOAA 2013).	6
Figure 4. SAFMC Deepwater Snapper Grouper MPAs between Florida and North Carolina (SAFMC/SEAMAP/MARMAP 2014).	7
Figure 5. 2013 NOAA Ship <i>Pisces</i> survey sites.	9
Figure 6. ME70 System description. A. Processor Unit. B. Transceiver Unit. C. Power Supply Units. D. Transducer. (Kongsberg Maritime 2014).....	11
Figure 7. Diagram of entire positioning system. (Hashimoto 2013)	11
Figure 8. EK60 System description. A. Color Display. B. Processor Unit. C. Commercial Ethernet switch. D. Transceiver unit. E. Transducers at 38, 120 and 200 kHz. (Kongsberg Maritime 2014).....	12
Figure 9. Conceptual processing workflow of explanatory variable generation. [A] MBES acoustic point data. [B] 2x2 m morphometric base layer raster data. [C] Polygon data containing all 14 explanatory variables. [D] SBES acoustic point data. [E] Subset of data to include demersal fish only [F] Fish count data subset into four response variables. Figure generated in MatchWare MindView 5.....	13
Figure 10. Histogram of 2x2 m raster cells with according depth values in meters (m).	17
Figure 11. Example site Snowy Wreck Two showing distance from sea level to seafloor.	18
Figure 12. Histogram of 2x2 m raster cells with according slope values in degrees (°).	19
Figure 13. Example site Snowy Wreck Two showing maximum rate of change in depth between 2 x 2 m raster cell and eight neighbors.....	20
Figure 14. Histogram of raster cells with according slope of slope.....	21
Figure 15. Example site Snowy Wreck Two showing maximum rate of change in slope between cell and eight neighbors.....	22
Figure 16. Histogram of 2x2 m raster cells with according plan curvature values.	23
Figure 17. Example site Snowy Wreck Two showing rate of change in curvature across the surface.	24
Figure 18. Histogram of 2x2 m raster cells with according rugosity values.	25

Figure 19. Example site Snowy Wreck Two showing ratio of surface area to planar surface area.	26
Figure 20. Histogram of 2x2 m raster cells with according Distance to Shelf Edge values in meters (m) divided by 500.	27
Figure 21. Example site Snowy Wreck Two showing distance of each 2x2 m raster cell to 200 m isobath, known as shelf edge (U.S. Geological Survey 2014, United Nations 1958).	28
Figure 22. Histogram of 2x2 m raster cells with according backscatter values in decibels (dB). ..	29
Figure 23. Example site Snowy Wreck Two showing intensity of the acoustic return.	30
Figure 24. [1] Depth raster at 2x2 m resolution. [2] 50x50 m grid superimposed on depth raster. [3] 2x2 m depth raster cell values averaged within 50x50 m grid cells. [4] Fish occurrences intersected with averaged grid cell values present within 50x50 m grid cells. One cell appears to contain four fish, another one fish and the rest zero.	32
Figure 25. [1] 50x50 m Snowy Wreck Two grid with all response categories and explanatory variables appended ($n = 3643$). [2] Ship track lines intersection with grid cells. [3] Final dataset for Snowy Wreck Two containing only observed fish data ($n=905$).	36
Figure 26. Small, medium and large fish occurrences in survey site Snowy Wreck Two depicted above bathymetric depth map.	38
Figure 27. Conceptual view of ecological predictors related to fish abundance. Actual 14 explanatory surfaces not depicted. Figure generated in ArcScene 10.2.1. Knuth 2014.	39
Figure 28. Example Poisson distribution of All Fish counts recorded within 50 x 50 m cells at survey site Snowy Wreck Two.	40
Figure 29. Relationship between mean site-wide σ of Depth and Fish Count. Small Fish $R^2 = 0.26$, Medium Fish $R^2 = 0.88$ Large Fish $R^2 = 0.87$, All Fish $R^2 = 0.54$	45
Figure 30. Relationship between mean site-wide X Range \times X Variety and Fish Count by size. Small Fish $R^2 = 0.25$, Medium Fish $R^2 = 0.81$ Large Fish $R^2 = 0.87$, All Fish $R^2 = 0.52$	46
Figure 31. Relationship between mean site-wide X Slope and Fish Count. Small Fish $R^2 = 0.36$, Medium Fish $R^2 = 0.81$ Large Fish $R^2 = 0.97$, All Fish $R^2 = 0.70$	47
Figure 32. Relationships between mean site-wide X Slope of Slope and Fish Count. Small Fish $R^2 = 0.27$, Medium Fish $R^2 = 0.82$ Large Fish $R^2 = 0.90$, All Fish $R^2 = 0.61$	48
Figure 33. Error in Bathymetry. The red box highlights refraction error at the outer beams of the ME70. Faint traces of this same type of error for each line can be seen across the map. Fish presences are recorded at nadir in the area between these areas. Thus, bathymetric data associated with fish is unaffected by this error in the outer beams.	50

Figure 34. Error in Backscatter. Here the error at nadir can be clearly seen in a stripe like pattern across the survey site. Fish presences are recorded at nadir and would presumable be heavily impacted by averaging backscatter values within a 50 x 50 m grid at nadir.52

Figure 35. NW (left) and N (right) views of Large Fish sampled along track lines across bathymetric surface at Snowy Wreck Two (VE = 2x). EK 60 sampling bias along track lines depicted in black becomes apparent in N view (right), yet no matter the view Large Fish presences coincide with prominent bottom features. Created in ESRI ArcScene. Knuth 2014. ...54

Figure 36. Survey sites without EK60 water column data. Sites not depicted to scale.60

Figure 37. Location of Bull’s Scarp survey site relative to existing MPAs. I

Figure 38. Depth of sea level to seafloor at Bull’s Scarp. II

Figure 39. Maximum rate of change in depth between 2 x 2 m raster cell and eight neighbors at Bull’s Scarp. III

Figure 40. Maximum rate of change in slope between cell and eight neighbors at Bull’s Scarp. IV

Figure 41. Rate of change in curvature across the surface at Bull’s Scarp. V

Figure 42. Ratio of surface area to planar surface area at Bull’s Scarp. VI

Figure 43. Distance of each 2x2 m raster cell to 200 m isobaths at Bull’s Scarp. VII

Figure 44. Intensity of the acoustic return at Bull’s Scarp. VIII

Figure 45. Location of Cape Lookout One survey site relative to existing MPAs. IX

Figure 46. Depth of sea level to seafloor at Cape Lookout One. X

Figure 47. Maximum rate of change in depth between 2 x 2 m raster cell and eight neighbors at Cape Lookout One. XI

Figure 48. Maximum rate of change in slope between cell and eight neighbors at Cape Lookout One. XII

Figure 49. Rate of change in curvature across the surface at Cape Lookout One. XIII

Figure 50. Ratio of surface area to planar surface area at Cape Lookout One. XIV

Figure 51. Distance of each 2x2 m raster cell to 200 m isobaths at Cape Lookout One. XV

Figure 52. Intensity of the acoustic return at Cape Lookout One. XVI

Figure 53. Location of Cape Lookout Two survey site relative to existing MPAs. XVII

Figure 54. Depth of sea level to seafloor at Cape Lookout Two. XVIII

Figure 55. Maximum rate of change in depth between 2 x 2 m raster cell and eight neighbors at Cape Lookout Two. XIX

Figure 56. Maximum rate of change in slope between cell and eight neighbors at Cape Lookout Two.	XX
Figure 57. Rate of change in curvature across the surface at Cape Lookout Two.	XXI
Figure 58. Ratio of surface area to planar surface area at Cape Lookout Two.	XXII
Figure 59. Distance of each 2x2 m raster cell to 200 m isobaths at Cape Lookout Two.....	XXIII
Figure 60. Intensity of the acoustic return at Cape Lookout Two.	XXIV
Figure 61. Location of Charleston DAR MPA survey site relative to other MPAs.	XXV
Figure 62. Depth of sea level to seafloor at Charleston DAR MPA.	XXVI
Figure 63. Maximum rate of change in depth between 2 x 2 m raster cell and eight neighbors at Charleston DAR MPA.	XXVII
Figure 64. Maximum rate of change in slope between cell and eight neighbors at Charleston DAR MPA.	XXVIII
Figure 65. Rate of change in curvature across the surface at Charleston DAR MPA.	XXIX
Figure 66. Ratio of surface area to planar surface area at Charleston DAR MPA.	XXX
Figure 67. Distance of each 2x2 m raster cell to 200 m isobaths at Charleston DAR MPA.	XXXI
Figure 68. Intensity of the acoustic return at Charleston DAR MPA.	XXXII
Figure 69. Location of N of Edisto MPA survey site relative to existing MPAs.	XXXIII
Figure 70. Depth of sea level to seafloor at N of Edisto MPA.	XXXIV
Figure 71. Maximum rate of change in depth between 2 x 2 m raster cell and eight neighbors at N of Edisto MPA.	XXXV
Figure 72. Maximum rate of change in slope between cell and eight neighbors at N of Edisto MPA.	XXXVI
Figure 73. Rate of change in curvature across the surface at N of Edisto MPA.	XXXVII
Figure 74. Ratio of surface area to planar surface area at N of Edisto MPA.	XXXVIII
Figure 75. Distance of each 2x2 m raster cell to 200 m isobaths at N of Edisto MPA.	XXXIX
Figure 76. Intensity of the acoustic return at N of Edisto MPA.	XL
Figure 77. Location of North Carolina 780 survey site relative to existing MPAs.	XLI
Figure 78. Depth of sea level to seafloor at North Carolina 780.	XLII
Figure 79. Maximum rate of change in depth between 2 x 2 m raster cell and eight neighbors at North Carolina 780.....	XLIII

Figure 80. Maximum rate of change in slope between cell and eight neighbors at North Carolina 780.....	XLIV
Figure 81. Rate of change in curvature across the surface at North Carolina 780.	XLV
Figure 82. Ratio of surface area to planar surface area at North Carolina 780.	XLVI
Figure 83. Distance of each 2x2 m raster cell to 200 m isobaths at North Carolina 780.....	XLVII
Figure 84. Intensity of the acoustic return at North Carolina 780.	XLVIII
Figure 85. Location of North Carolina 780 survey site relative to existing MPAs.	XLIX
Figure 86. Depth of sea level to seafloor at North Carolina 780.	L
Figure 87. Maximum rate of change in depth between 2 x 2 m raster cell and eight neighbors at North Carolina 780.....	LI
Figure 88. Maximum rate of change in slope between cell and eight neighbors at North Carolina 780.....	LII
Figure 89. Rate of change in curvature across the surface at North Carolina 780.	LIII
Figure 90. Ratio of surface area to planar surface area at North Carolina 780.	LIV
Figure 91. Distance of each 2x2 m raster cell to 200 m isobaths at North Carolina 780.....	LV
Figure 92. Intensity of the acoustic return at North Carolina 780.	LVI
Figure 93. Location of Snowy Wreck One survey site relative to existing MPAs.	LVII
Figure 94. Depth of sea level to seafloor at Snowy Wreck One.....	LVIII
Figure 95. Maximum rate of change in depth between 2 x 2 m raster cell and eight neighbors at Snowy Wreck One.	LIX
Figure 96. Maximum rate of change in slope between cell and eight neighbors at Snowy Wreck One.	LX
Figure 97. Rate of change in curvature across the surface at Snowy Wreck One.	LXI
Figure 98. Ratio of surface area to planar surface area at Snowy Wreck One.	LXII
Figure 99. Distance of each 2x2 m raster cell to 200 m isobaths at Snowy Wreck One.	LXIII
Figure 100. Intensity of the acoustic return at Snowy Wreck One.	LXIV
Figure 101. Location of Snowy Wreck Two survey site relative to existing MPAs.	LXV
Figure 102. Depth of sea level to seafloor at Snowy Wreck Two.	LXVI
Figure 103. Maximum rate of change in depth between 2 x 2 m raster cell and eight neighbors at Snowy Wreck Two.....	LXVII

Figure 104. Maximum rate of change in slope between cell and eight neighbors at Snowy Wreck Two.	LXXVIII
Figure 105. Rate of change in curvature across the surface at Snowy Wreck Two.	LXIX
Figure 106. Ratio of surface area to planar surface area at Snowy Wreck Two.	LXX
Figure 107. Distance of each 2x2 m raster cell to 200 m isobaths at Snowy Wreck Two.....	LXXI
Figure 108. Intensity of the acoustic return at Snowy Wreck Two.	LXXII
Figure 109. Location of South of North Florida MPA survey site relative to existing MPAs.	LXXIII
Figure 110. Depth of sea level to seafloor at South of North Florida MPA.....	LXXIV
Figure 111. Maximum rate of change in depth between 2 x 2 m raster cell and eight neighbors at South of North Florida MPA.	LXXV
Figure 112. Maximum rate of change in slope between cell and eight neighbors at South of North Florida MPA.	LXXVI
Figure 113. Rate of change in curvature across the surface at South of North Florida MPA.	LXXVII
Figure 114. Ratio of surface area to planar surface area at South of North Florida MPA.	LXXVIII
Figure 115. Distance of each 2x2 m raster cell to 200 m isobaths at South of North Florida MPA.	LXXIX
Figure 116. Intensity of the acoustic return at South of North Florida MPA.	LXXX
Figure 117. Cape Lookout One fish distributions.	LXXX
Figure 118. Cape Lookout Two fish distributions.	LXXXII
Figure 119. North of Edisto MPA fish distributions.	LXXXIII
Figure 120. North Carolina 780 fish distributions.	LXXXIV
Figure 121. Snowy Wreck One fish distributions.	LXXXV
Figure 122. Snowy Wreck Two fish distributions.	LXXXVI
Figure 123. Relationship between X Depth and Fish Count by site. Highest $R^2 = 28\%$	XC
Figure 124. Relationships between X Distance to Shelf Edge and Fish Count by site. Highest $R^2 = 69\%$	XCI
Figure 125. Relationships between X Plan Curvature and Fish Count by site. Highest $R^2 = 69\%$	XCII

Figure 126. Relationships between X Rugosity and Fish Count by site. Highest $R^2 = 26\%$... XCIII

Figure 127. Relationships between X High Rugosity and Fish Count by site. Highest $R^2 = 8\%$
..... XCIV

Figure 128. Relationships between X Max Rugosity and Fish Count by site. Highest $R^2 = 42\%$
..... XCV

Figure 129. Relationships between σ Rugosity and Fish Count by site. Highest $R^2 = 17\%$... XCVI

Figure 130. Relationships between X Backscatter and Fish Count by site. Highest $R^2 = 43\%$
..... XCVII

Figure 131. Relationships between Backscatter Kurtosis and Fish Count by site. Highest $R^2 = 57\%$ XCVIII

Figure 132. Relationships between σ Backscatter and Fish Count by site. Highest $R^2 = 61\%$
..... XCIX

LIST OF TABLES

Table 1. Summary of 2013 survey sites.	8
Table 2. Description of Base Layer Morphometrics.	16
Table 3. Description of 14 Explanatory Variables.	31
Table 4. Pearson’s Variable Correlation Matrix. Correlations greater than an absolute value of 0.5 are shown in bold font. Significant correlations greater than an absolute value of 0.9 are shown in bold font and parenthesis.	34
Table 5. Summary of fish counts normalized by area for sites with fish data.	37
Table 6. Poisson Regression for All Fish $n = 7410$	42
Table 7. Poisson Regression for Large Fish $n = 680$	42
Table 8. Poisson Regression for Medium Fish $n = 2858$	43
Table 9. Poisson Regression for Small Fish $n = 3955$	43
Table 10. Average variable contribution to overall model R^2	44

INTRODUCTION

FISHERIES MONITORING IN THE SOUTHEAST ATLANTIC

In 1996, the Magnuson-Stevens Fishery Conservation and Management Act, as amended through 2007, established eight regional fisheries management councils to manage U.S. fisheries (Figure 1) (Magnuson-Stevens 2007). Their mission is to develop fisheries management plans based on sound scientific advice and in a fully transparent and public process (Fishery Councils 2013). Some of the fish species subject to overfishing within South Atlantic Fisheries Management Council's (SAFMC) waters include Red Grouper, Red Snapper, Snowy Grouper, Speckled Hind, Vermillion Snapper and Warsaw Grouper (SAMFC, Snapper Grouper Page 2013). For these and other fish species, the Magnuson-Stevens act defines Essential Fish Habitat (EFH) as "...those waters and substrate necessary to fish for spawning, breeding, feeding or growth to maturity." It further mandates the management councils to identify, describe, map and protect EFH as follows (Magnuson-Stevens 2007; SAFMC, MPA Information Page 2013):

- "The general distribution and geographic limits of EFH for each life history stage should be presented in the form of maps."
- "Ultimately, these data should be incorporated into a GIS to facilitate analysis and presentation."

Snapper grouper populations are seafloor dwelling demersal fish that express strong site fidelity. Studies on coral reef habitats in the US Virgin Islands and patchy reef systems along the southeast Atlantic continental shelf have found the morphometric environment of the seafloor to

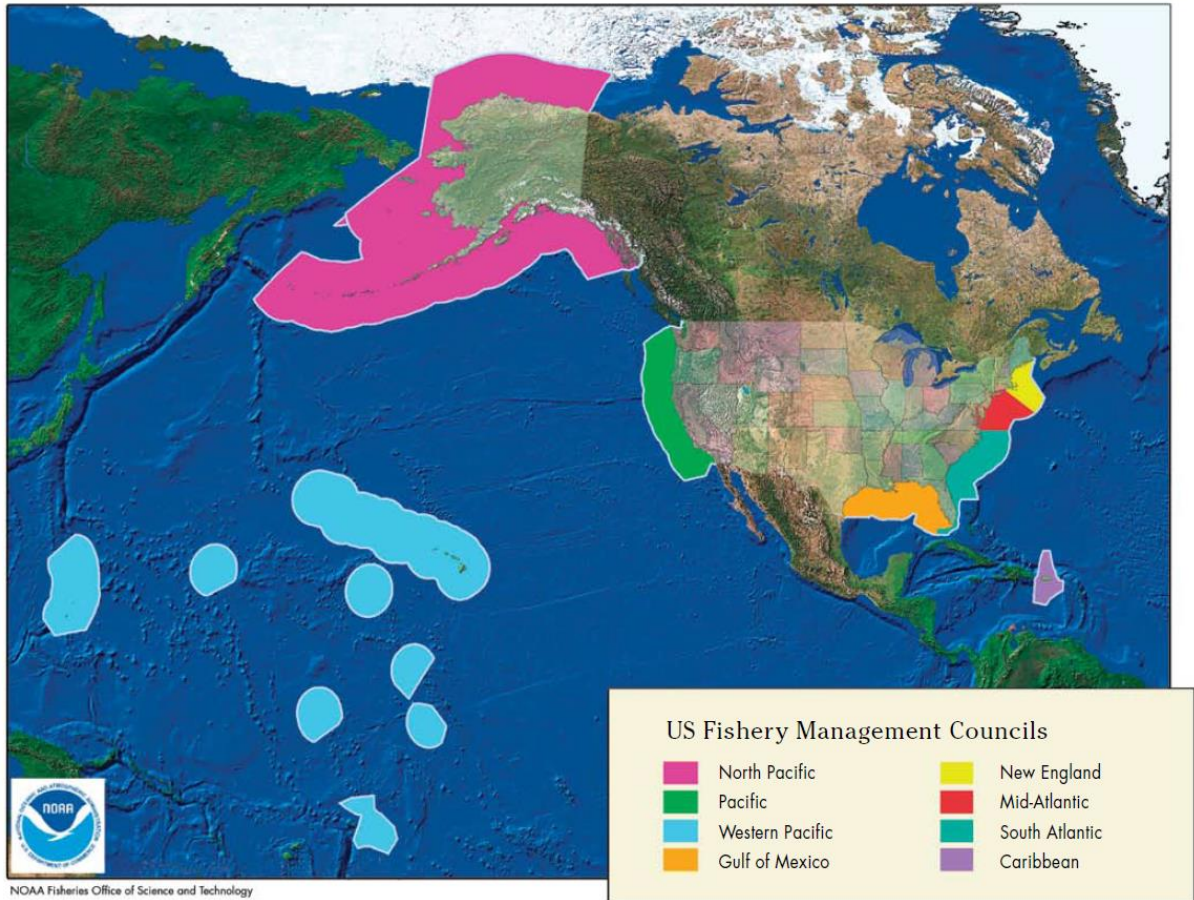


Figure 1. Map of waters governed by the US Regional Fishery Management Councils. (Fishery Councils 2013)

function as a control on snapper grouper species richness, abundance and total biomass (Costa, et al. 2014; Pittman, Costa and Battista 2009; Sedberry and Van Dolah 1984). The SAFMC protects EFH for these species through place-based management systems, known as Marine Protected Areas (MPAs) (Harter, *et al.* 2009). It defines MPAs as: “A network of specific areas of marine environments reserved and managed for the primary purpose of aiding in the recovery of overfished stocks and to ensure the persistence of healthy fish stocks, fisheries, and associated habitats. Such areas may include naturally occurring or artificial bottom and water column habitats, and may include prohibition of harvest on seasonal or permanent time periods to achieve desired fishery conservation and management goals.” (SAFMC, MPA Info Page, 2013).

Traditionally, data collection on fish in and outside of MPAs has been achieved via trawl, SCUBA and Remotely Operated Vehicle (ROV) surveys (Kendall, Bauer and Jeffrey 2007; Harter, *et al.* 2009; Sedberry and Van Dolah 1984). While all three methods have the advantage of visually identifying fish species, these methods are time and labor intensive, and lack the ability to measure the exact location and distribution of fish size classes present across the seascape (Figure 2). This deficit has, until recently, made precise fish-seascape interaction analysis in a GIS nearly impossible or imprecise at best (Kracker, Kendall and McFall 2008). To meet the mandates set forth by the Magnuson-Stevens act, modern methods of acoustic bathymetric and water column data acquisition allow for unprecedented measurement and understanding of spatially intricate fish-seascape relationships. This information can aid in the rapid visualization, assessment and ultimately protection of EFH (Costa, *et al.* 2014; Pittman, Costa and Battista 2009; Kracker, Kendall and McFall 2008; Kracker, *et al.* 2010). These methods are not intended to replace the visual identification of species specific abundances in the ocean. In fact, these techniques cannot identify fish to species. Rather, they have the potential to augment, expedite and ultimately improve visual surveys and stock assessment strategies by characterizing the spatial distribution and dimension of multiple trophic levels (size classes) throughout the water column and across the seascape.

BACKGROUND ON MARINE PROTECTED AREAS

In 1957, R.J.H. Beverton and S.J. Holt conceptualized the first formal description of a Marine Protected Area as a policy measure to conserve marine species and increase fishery yields (Beverton and Holt 1957). The idea came in response to observations of increased fish stock in the North Sea after World War II. Previously popular fishing grounds had been riddled with mines, which created a *de facto* moratorium on all fishing activity within those desirable

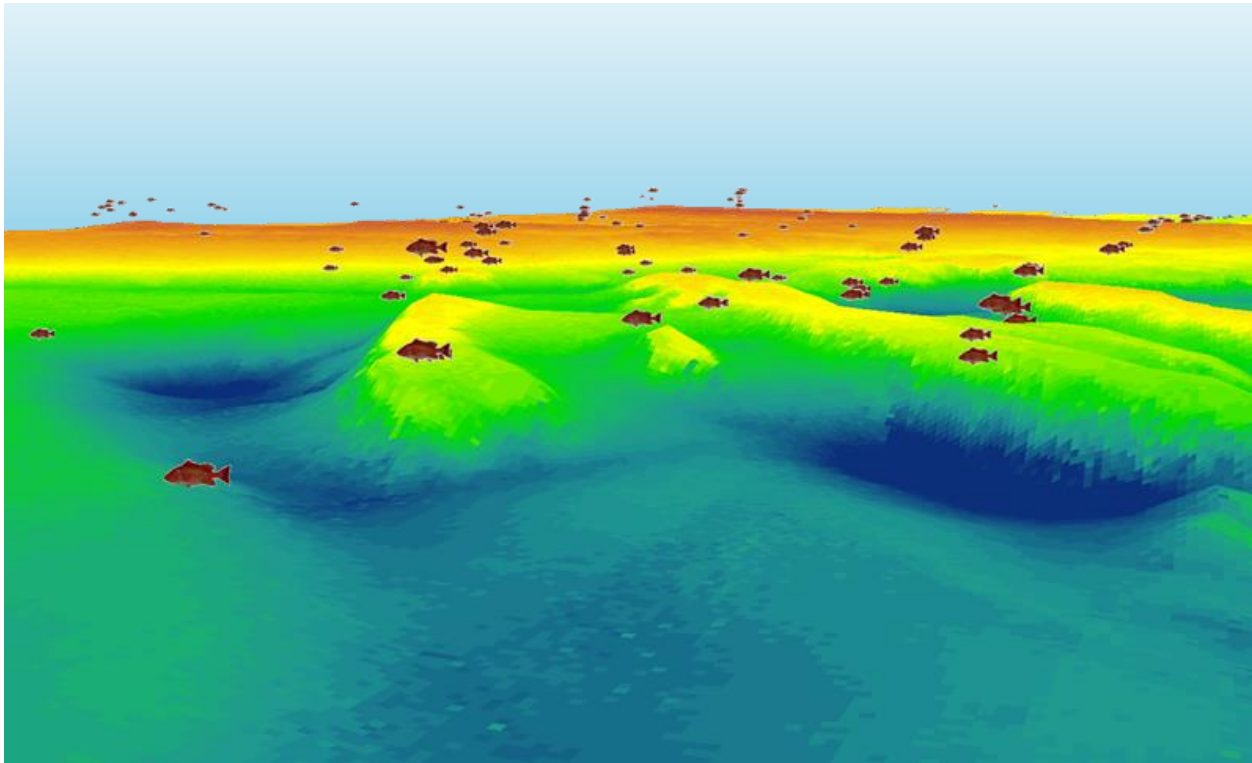


Figure 2. View of acoustically measured fish presences above bathymetry raster surface (VE = 2x). Created in ESRI ArcScene. Knuth 2014.

waters (Beverton and Holt 1957). As was expected, populations flourished within the previously popular fishing grounds. With time, increasing stock levels were also being observed outside the inaccessible fishing grounds, which lead to the idea of deliberately creating MPAs (Beverton and Holt 1957). In retrospect, the concept seems rather intuitive. We designate the boundaries of critical fish habitat as off limits to fishing activity, populations rebound within, and fisheries outside the MPAs receive a steady influx of fish stock. Once an area, designated as an MPA, has reached its carrying capacity in terms of fish density, fish begin to seek lesser competition for food and shelter outside the MPA boundaries (Abesamis and Russ 2005). This is known as density-dependent spillover (Grüss, et al. 2011). Spillover maintains a sustainable yield to the fishing industry, while larval dispersal from within MPA boundaries ensures a steady proliferation of the species to new and unprotected habitats (White, et al. 2011).

The bottom line in any MPA design must be that fish stock replenishment through spillover from an MPA is significant enough to offset the loss of fishing grounds to fisherman. The ideal scenario is that once an MPA is established, species, both target and non-target, are attracted to areas of high biological productivity. We can conceptualize this as density-dependent spill-in (Christie, *et al.* 2010; Eggleston and Parsons 2008; Gerber, *et al.* 2005). Once an MPA has reached capacity, in terms of biomass, density-dependent spillover of low to moderate movement species occurs, which finally leads to an increased fishery yield (Abesamis and Russ 2005; Russ, *et al.* 2004; Williams, *et al.* 2009; Harter, *et al.* 2009).

PROJECT OVERVIEW AND STUDY AREA

This study was conducted as part of a scientific research cruise aboard the NOAA Ship *Pisces* during the period of July 1st through the 14th, 2013 (Figure 3). The cruise was funded by the SAFMC with the primary mission to visually assess the snapper grouper fishery and coral habitat outside existing MPA boundaries along the Southeast Atlantic coast (Figure 4). Stacey Harter and Andrew David, of the NOAA Panama City Southeast Fisheries Science Center, were the principal investigators, along with John Reed from Florida Atlantic University. Fish stock and coral habitat were assessed using *in situ* observations via video transmitted from the ROV Phantom S2, operated by Lance Horn and Glenn Taylor from the Undersea Vehicles Program of University of North Carolina Wilmington. ROV dives were conducted based on bathymetric maps either previously created or generated on board.

RESEARCH OBJECTIVES

1. Collect and process water column and bathymetric data for potential habitat sites along the U.S. South Atlantic continental shelf.
2. Provide a morphometric characterization and quantitative assessment of fish populations present within each survey site.
3. Identify morphometric features of the bathymetry that may explain the presence of demersal fish.

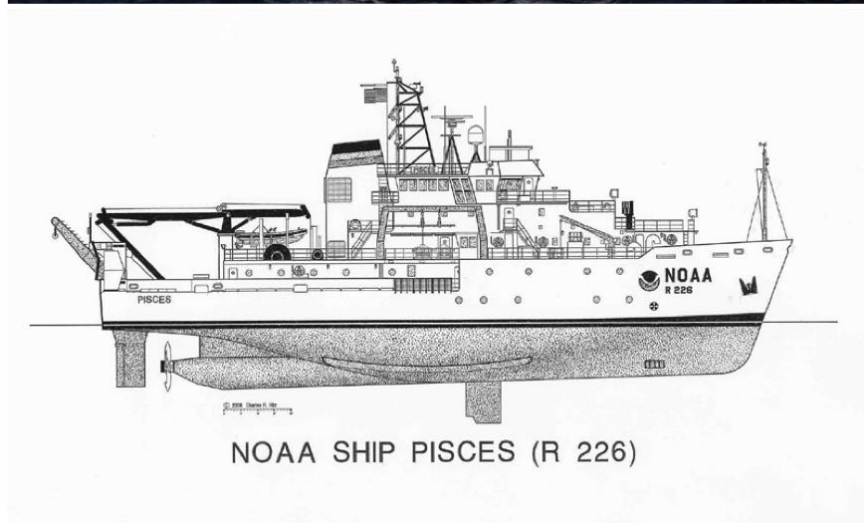
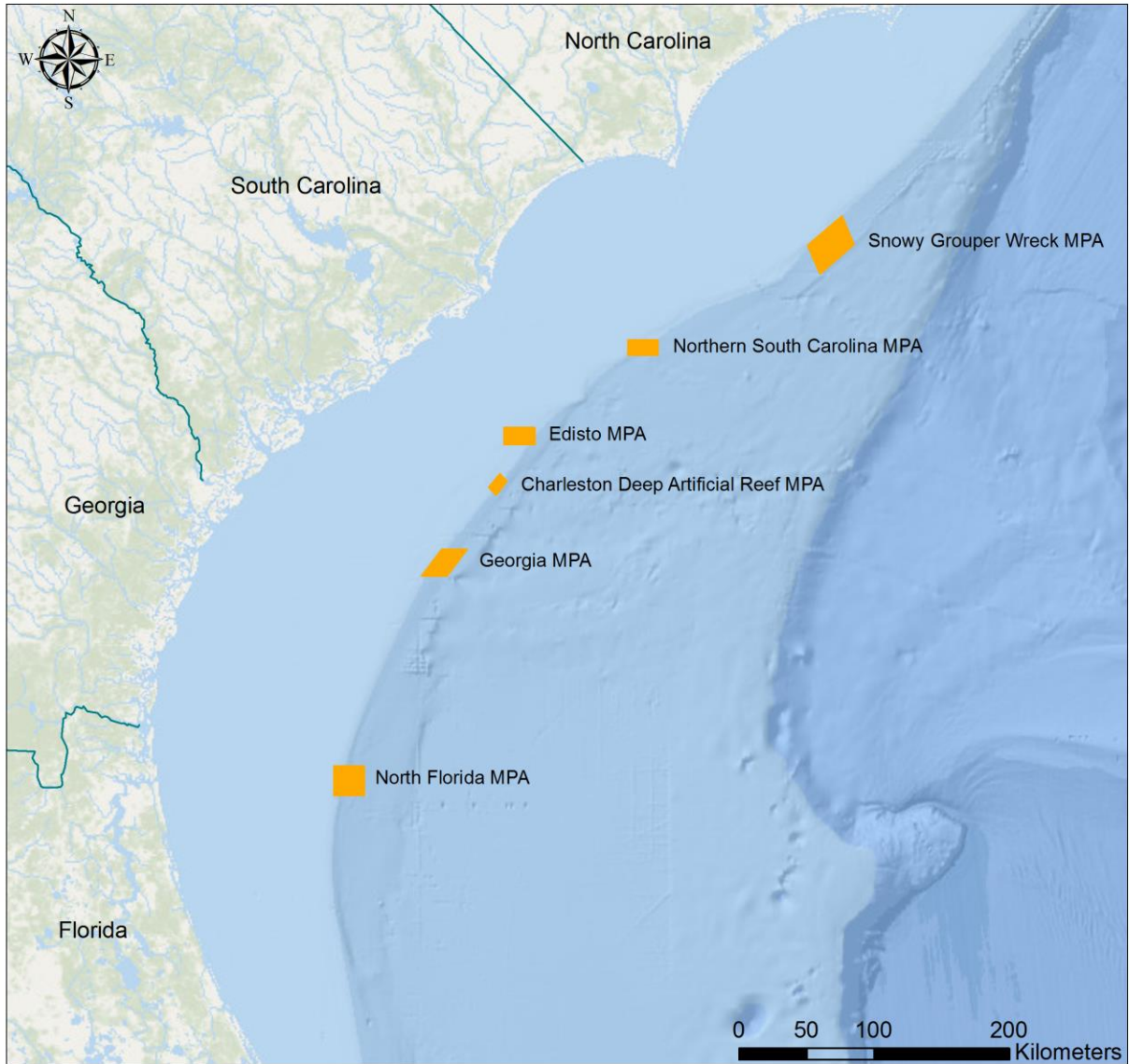


Figure 3. NOAA Ship *Pisces* (NOAA 2013).



Legend

- State Boundaries
- Marine Protected Areas (MPAs)

Friedrich Knuth (c)
College of Charleston
2014

Source: SAFMC online GIS database, NOAA, SEAMAP, MARMAP, ESRI (base layer)

Coordinate System: WGS 1984 Web Mercator

Figure 4. SAFMC Deepwater Snapper Grouper MPAs between Florida and North Carolina (SAFMC/SEAMAP/MARMAP 2014).

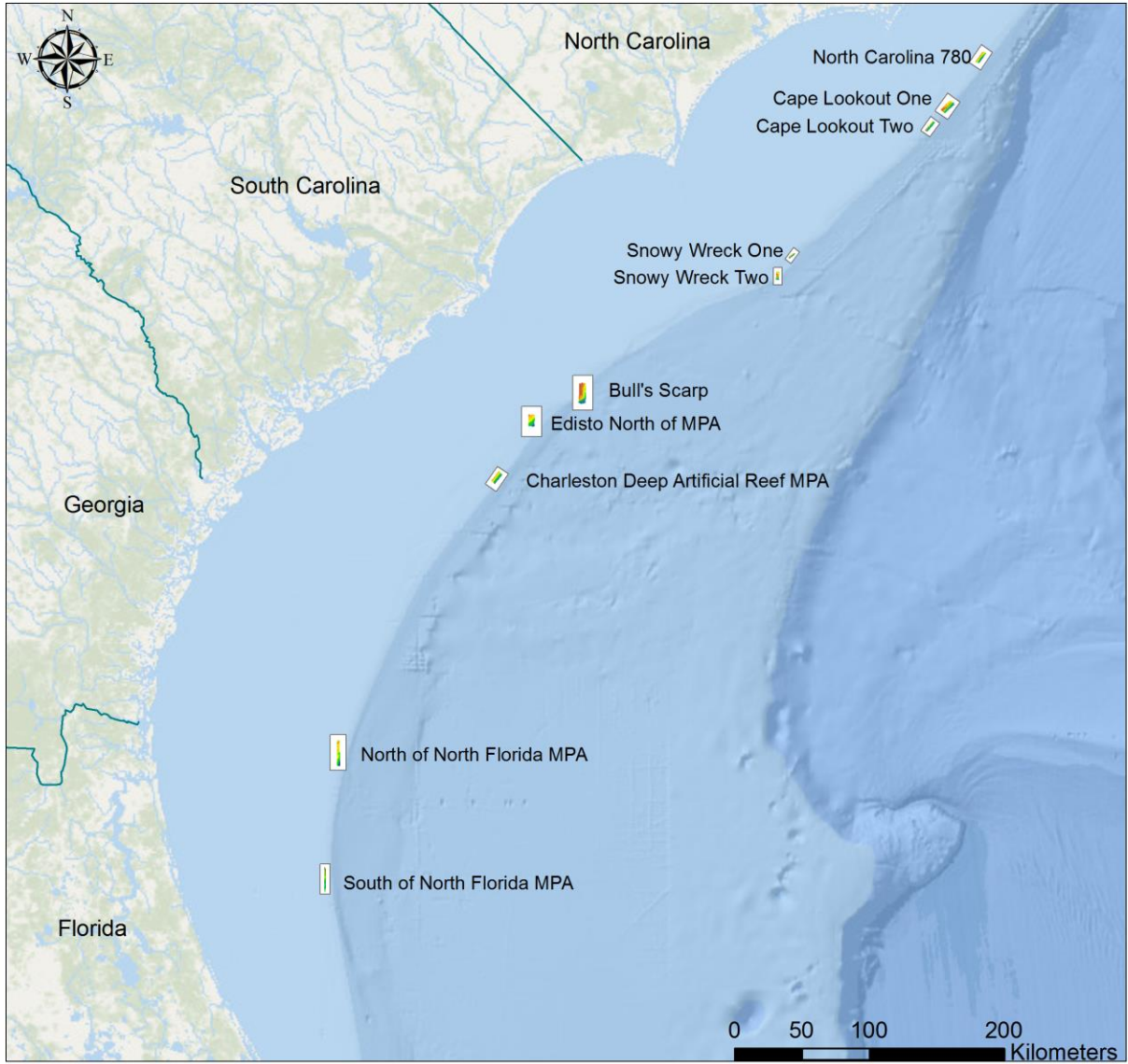
METHODS

DATA ACQUISITION




Ten potential habitat sites were acoustically mapped between Mayport, FL and Wilmington, NC, for a total of 205 km² and $n = 7410$ fish counts at six out of ten sites (Figure 5 and Table 1). Mapping operations were conducted from 07/01/2013 to 07/14/2013 between 8:00PM and 8:00AM. Bathymetry, backscatter and water column data were acquired using the SIMRAD ME70 (bathymetry / backscatter) and EK60 (water column) echo sounder systems. Water column data was collected for six out of the ten sites, leaving four sites for potential future predictive habitat model validation.

Table 1. Summary of 2013 survey sites.

Survey Site	Fish Count (<i>n</i>)	Area (km ²)	Min Depth (m)	Max Depth (m)
Cape Lookout One	2285	26	53	147
Snowy Wreck Two	2052	9	62	121
North of Edisto MPA	1181	25	50	142
Cape Lookout Two	1160	10	72	120
North Carolina 780	658	14	66	96
Snowy Wreck One	74	4	71	100
Bull's Scarp	No Data	52	45	250
Charleston DAR MPA	No Data	21	100	120
North of North Florida MPA	No Data	30	43	74
South of North Florida MPA	No Data	15	52	72



Legend

-  State Boundaries
-  Survey Sites
-  Shallow
Deep

Friedrich Knuth (c)
College of Charleston
2014

Source: SAFMC online GIS database, NOAA,
SEAMAP, MARMAP, ESRI (base layer)

Coordinate System: WGS 1984 Web Mercator

Figure 5. 2013 NOAA Ship Pisces survey sites.

ME70 MULTIBEAM ECHO SOUNDER SYSTEM (MBES)

The ME70 is a scientific multibeam echo sounder system (Figure 6), that operates in the 70 to 120 kHz range, emitting 45 beams within the swath fan (Figure 7) (Cutter, Berger and Demer 2010). It sends between 64 and 5120 pulses per μ s resulting in individual pings, each tagged with an individual time stamp, representing the two-way travel time. Each ping is converted to a point fixed in three-dimensional space by a defined x, y and z value. The z value represents depth and is determined from the two-way travel time of the acoustic signal, while the x and y values are provided by the Global Positioning System (GPS) on board the ship and respective corrections. Various factors, such as the pitch, roll, heave, tide and relative positioning of the echo sounder system to the GPS must be accounted for in determining the exact location of each point on the seafloor (Figure 7). Some automated and manual removal of false values occurs during primary data acquisition, in an effort to reduce the dataset to detections within the expected range of the seafloor and remove obviously false values. Further, errant returns outside the expected depth range were removed during the conversion process from .raw files to .gsf files using a MATLAB script provided by Tom Weber from the University of New Hampshire (UNH). Because the *Pisces* did not have the ME70 bathymetry package, it was necessary to use this script for bottom detection and to prepare the data for import and further processing in CARIS HIPS and Fledermaus FMGT.

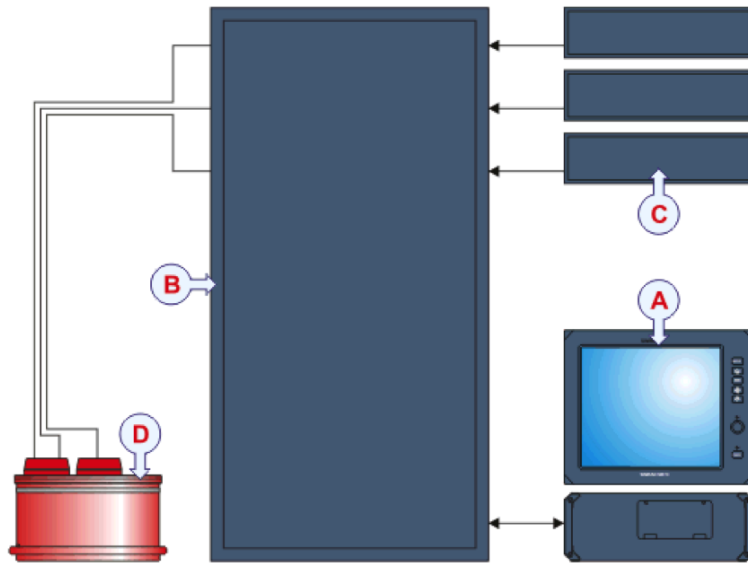


Figure 6. ME70 System description. A. Processor Unit. B. Transceiver Unit. C. Power Supply Units. D. Transducer. (Kongsberg Maritime 2014)

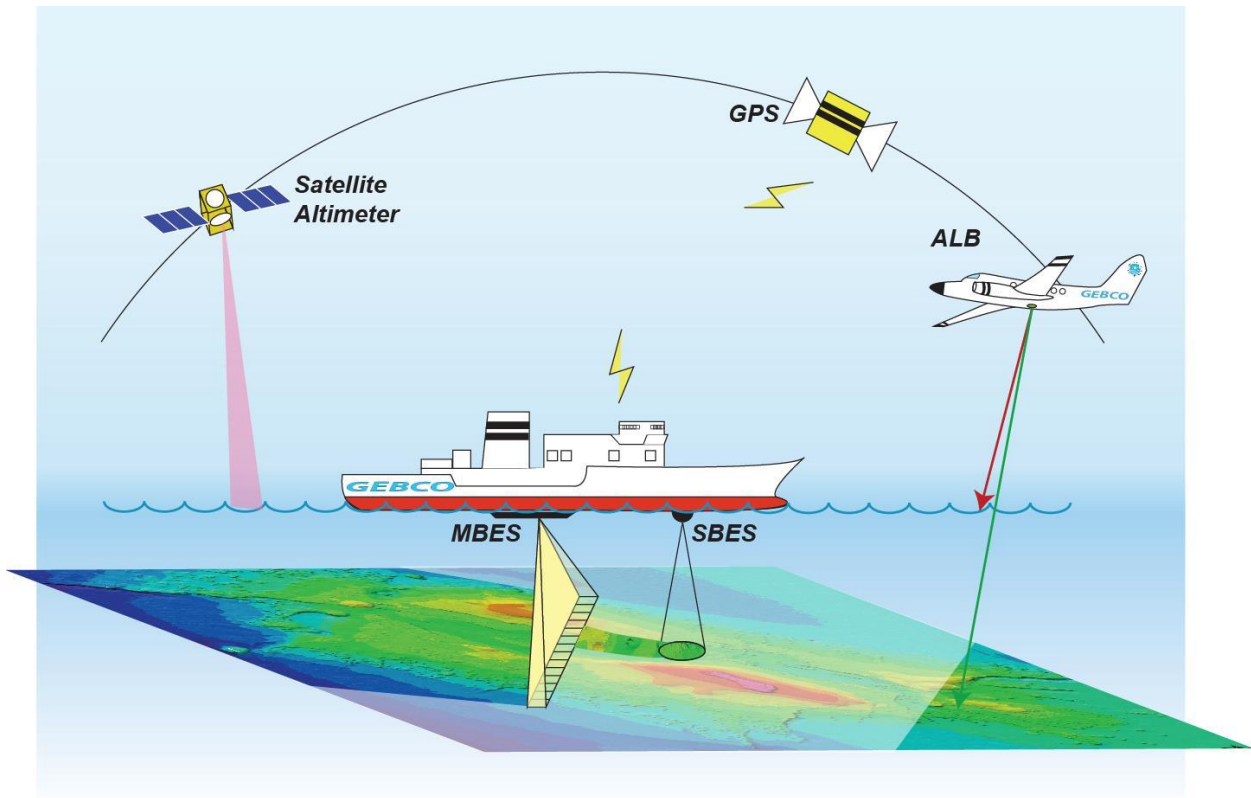


Figure 7. Diagram of entire positioning system. (Hashimoto 2013)

EK60 SPLIT-BEAM ECHO SOUNDER SYSTEM (SBES)

The EK60 is a scientific split-beam echo sounder system (Figure 8). The system on the Pisces operates at 38, 120 and 200 kHz. The data from the 120 transducer was processed to detect seafloor dwelling and pelagic fish present within the water column. Much like with the ME70, a ping return is recorded and assigned the according x, y and z value based on GPS location and the two-way acoustic travel time. Once the data is acquired it is exported to the Echoview software for further processing.

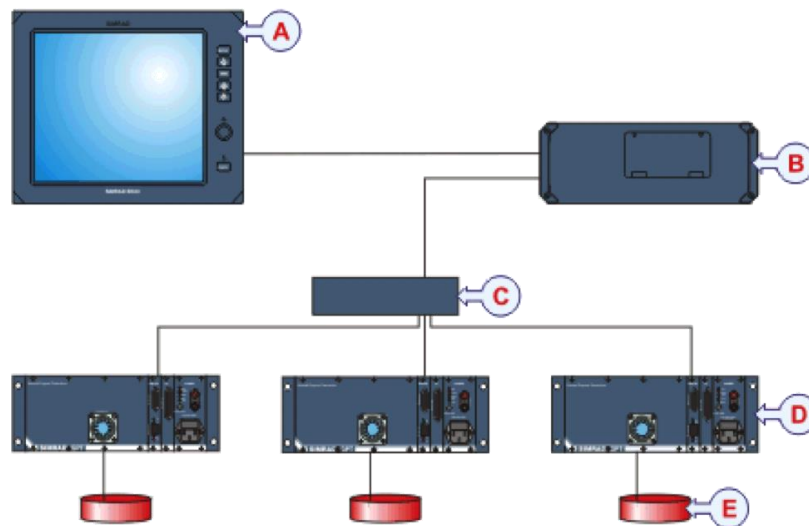


Figure 8. EK60 System description. A. Color Display. B. Processor Unit. C. Commercial Ethernet switch. D. Transceiver unit. E. Transducers at 38, 120 and 200 kHz. (Kongsberg Maritime 2014)

DATA PROCESSING

A diagram showing the conceptual overview of explanatory variable and response generation can be seen below in Figure 9.

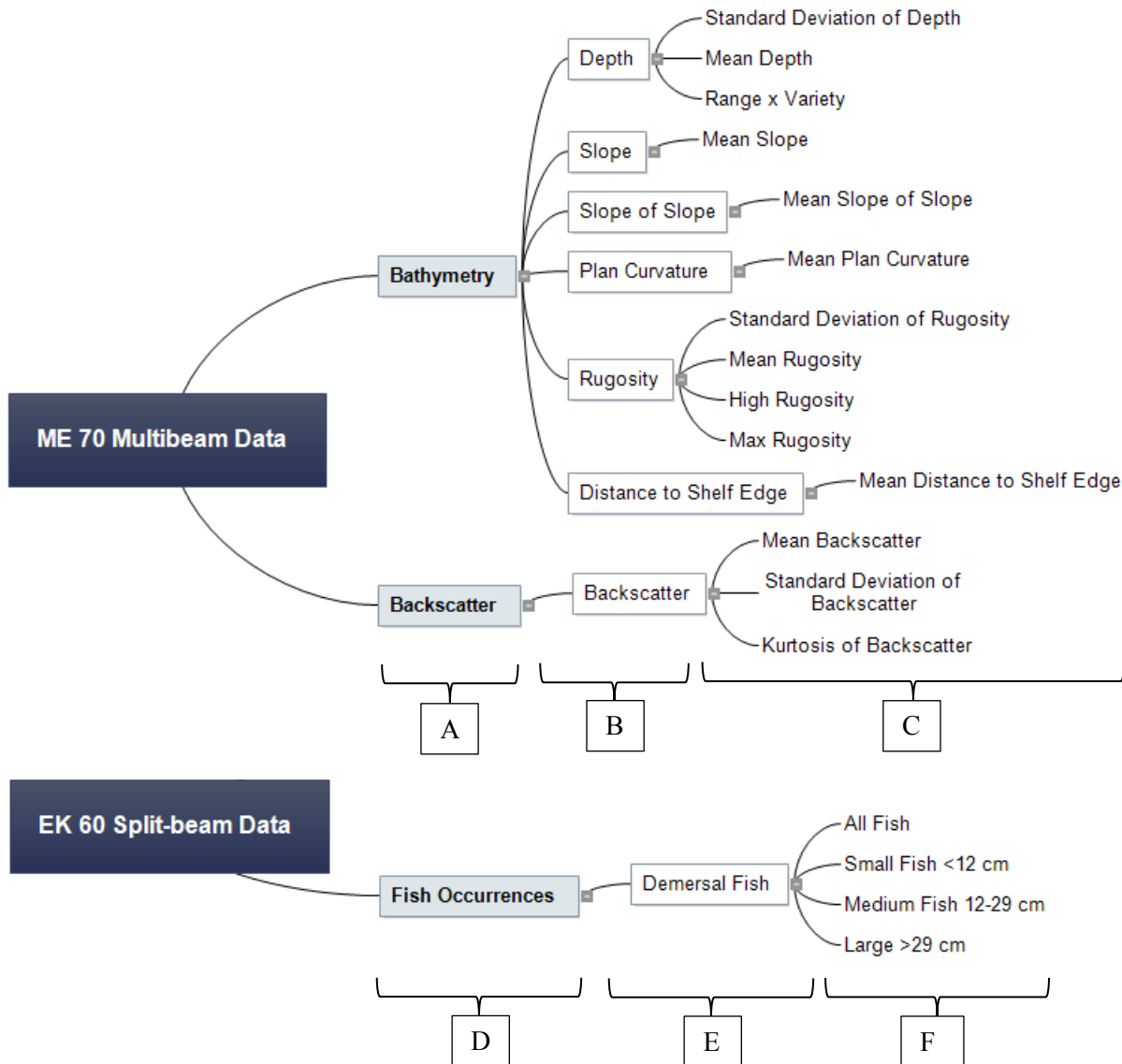


Figure 9. Conceptual processing workflow of explanatory variable generation. [A] MBES acoustic point data. [B] 2x2 m morphometric base layer raster data. [C] Polygon data containing all 14 explanatory variables. [D] SBES acoustic point data. [E] Subset of data to include demersal fish only [F] Fish count data subset into four response variables. Figure generated in MatchWare MindView 5.

BATHYMETRY

Bathymetry is derived via the time it takes for an acoustic ping to travel from the ME70's transducer, to the seafloor and back to its transceiver. Acoustic data collected by the MBES was processed in CARIS HIPS 7.1. Corrections were applied in the respective HIPS editors to account for, pitch, roll, heave, sound velocity, tidal influences and the timing of GPS signals. Once all plausible points were given an x, y and z value, any remaining artifacts (false values) were removed via manual and automated cleaning techniques. In order to derive a continuous raster surface from the point cloud we applied the CUBE (Combined Uncertainty and Bathymetric Estimator) algorithm to arrive at the most likely hypothesis for a raster surface representing the true bathymetry of the seafloor. CUBE was developed by Brian Calder at the Center for Coastal and Ocean Mapping (CCOM), a Joint Hydrographic Center (JHC) between NOAA and UNH. Bathymetry rasters for each of the ten survey sites were processed at a 2 x 2 meter resolution. Any minor gaps in the data were interpolated using the Interpolate function in HIPS. Each raster was then exported as an ESRI ASCII Grid and subsequently imported into an ESRI file geodatabase ready for analysis in ArcMap. Finally, track lines were exported as .dxf files and imported into the file geodatabase as line feature vector files.

BACKSCATTER

Backscatter represents the intensity of the acoustic return signal and is measured in decibels (dB). The more negative the return value, the less energy is contained in the signal and vice versa. In a relative sense, lower values correspond to a softer seabed and higher values correspond to a harder seabed. Just like bathymetry, backscatter data was obtained from the ME70 MBES, but processed in QPS Fledermaus FMGT 7.3. All necessary information about the backscatter return is embedded in the .all and subsequent .gsf files. Once the .all files had been

converted into the .gsf files they were imported into Fledermaus FMGT. FMGT uses the GeoCoder engine, which is a collection of algorithms developed by Luciano Fonseca at CCOM JHC, designed to reduce noise in the data and provide the cleanest mosaicked raster representation of the backscatter image reflecting off the seafloor. After this raster image was created at a 2 x 2 m resolution, it was exported as an ArcView Grid and imported into an ESRI file geodatabase, ready for further analysis in ArcMap.

WATER COLUMN (FISH) DATA

EK60 water column data is acquired via three distinct frequencies travelling through the water column and reflecting off targets. Data from the 120 kHz transducer was used for processing in Myriax Echoview 5.3 in order to target snapper and grouper fish species, ensure that the signal reaches the seafloor, and allow for discrimination between fish and the seafloor. The sound pressure wave reflects off of the fish swim bladder and returns an acoustic signal that contains information about time and decibel strength from which depth and size of the fish are derived (Foote 1983). Once data were imported from the SIMRAD acquisition software into Echoview, only pings representing fish larger than 5 cm and within 20 m of the seafloor were retained for this analysis. Echoview outputs a data table with the size class, coordinates and distance above the seafloor for each fish measured. This data table was then imported into ArcGIS using the Make XY Even Layer tool and converted to a point file containing all the necessary information for further analysis.

MORPHOMETRIC BASE LAYERS

Morphometric base layers were created in ESRI ArcGIS 10.2 for all ten survey sites and are described in (Table 2). For illustration purposes, the following maps depicting each base layer are all showing survey site Snowy Wreck Two. A complete collection of all 70 (seven per site) base layers can be found in Appendix A.

Table 2. Description of Base Layer Morphometrics.

Base Layer Morphometrics	Unit	Description	Analytical Tool in ArcGIS
1. Depth	Meters	Distance from sea level to seafloor	-
2. Slope	Degrees	Slope of maximum change in depth between cell and eight neighbors	Slope function in Spatial Analyst
3. Slope of Slope	Degrees of Degrees	Slope of maximum change in slope between cell and eight neighbors	Slope function in Spatial Analyst
4. Plan Curvature	(+) convex (-) concave	Maximum curvature of surface perpendicular to slope direction within 3 x 3 cell neighborhood	Curvature function in Spatial Analyst
5. Rugosity	Ratio Value	Ratio of surface area to planar area within 3 x 3 cell neighborhood	Surface Area and Ratio function in DEM Surface Toolbox
6. Distance to Shelf	Meters	Distance of the centroid of each pixel to the 200 m isobath	Euclidean distance function in Spatial Analyst
7. Backscatter	Decibels	Intensity of acoustic return	-

DEPTH

The depth layer represents the distance from the surface of the ocean to the seafloor. The histogram, seen in Figure 10, shows depth values ranging from -65 to -121. The majority of values, seen as spikes in the histogram, are around -75 and -85 m depth. Figure 11 represents the 2 x 2 m Depth raster derived from the acoustic bathymetry data processed in HIPS. Lower values correspond to deeper depths and high values to shallower depths. The two peaks in the histogram around -75 and -85 m depth can be seen as orange and green values in the raster image.

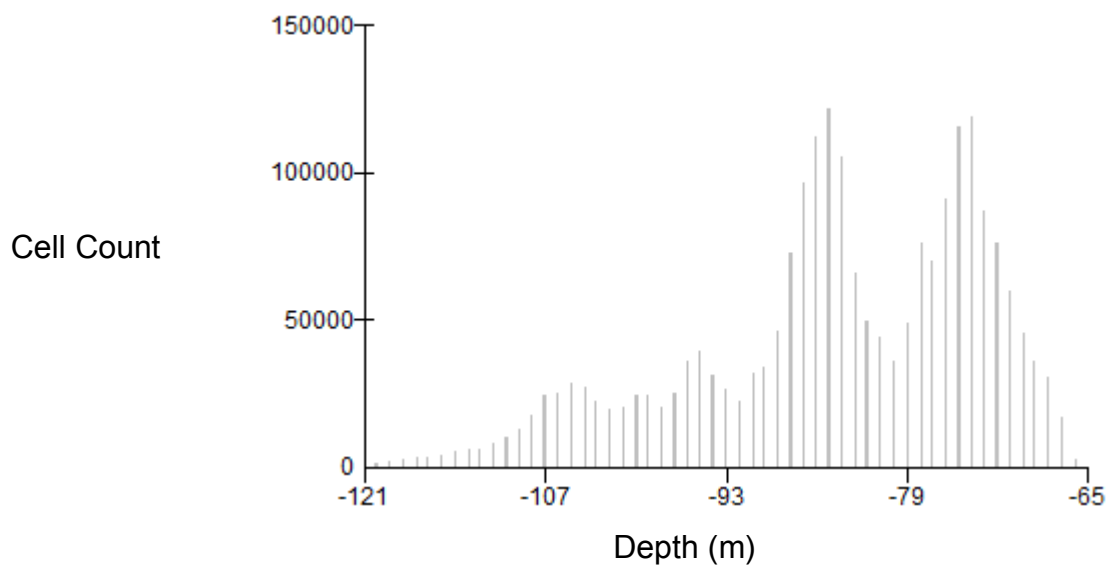


Figure 10. Histogram of 2x2 m raster cells with according depth values in meters (m).

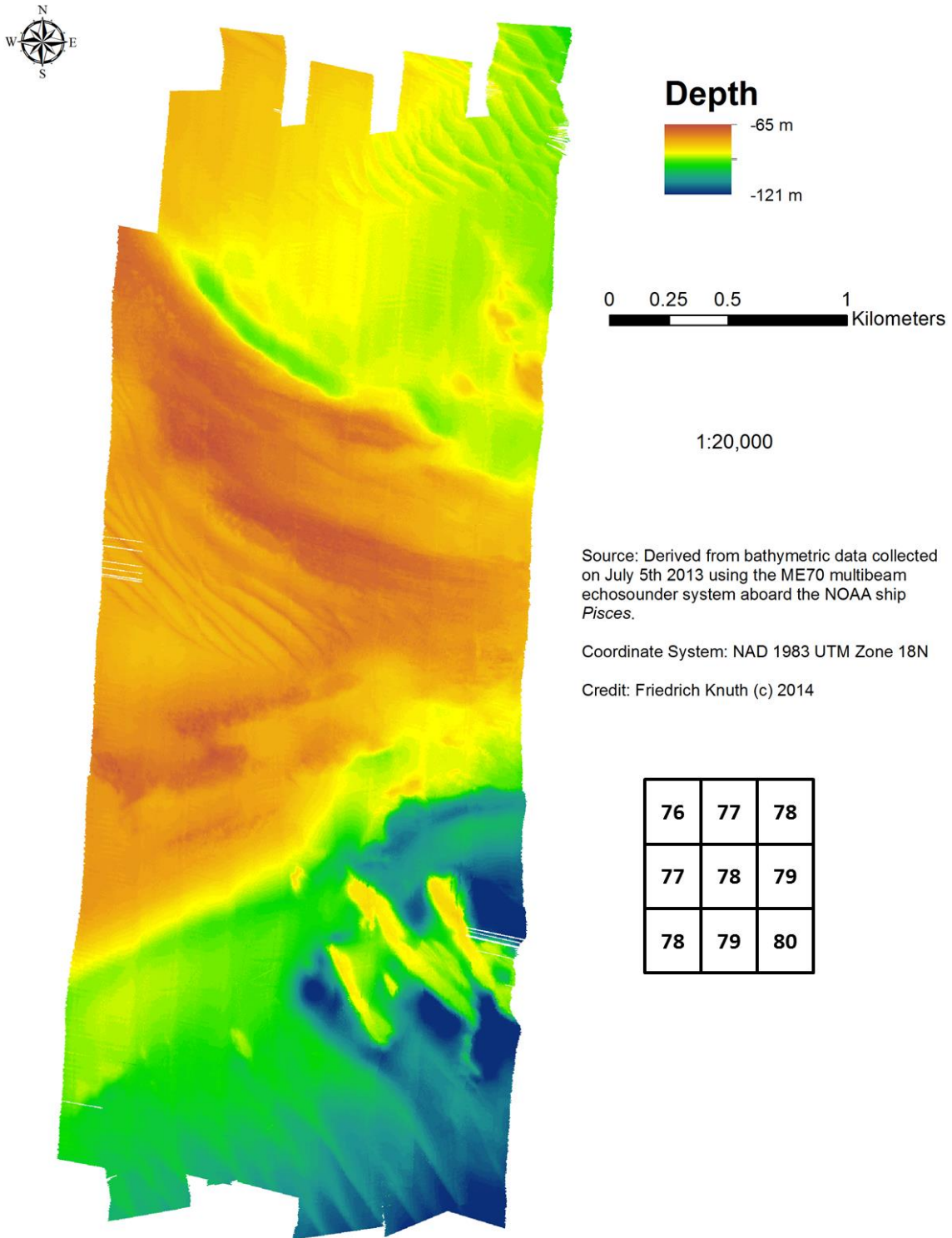


Figure 11. Example site Snowy Wreck Two showing distance from sea level to seafloor.

SLOPE

Slope represents the change in elevation over distance, derived from the bathymetry raster. Slope values range from 0° (flat) to 76° (steep) at a 2 x 2 m grid scale, as can be seen in the histogram in Figure 12. The majority of values have a 0° slope, indicating that this area is predominantly flat. The raster image, seen in Figure 13, was created using the Slope tool in the Spatial Analyst toolbox in ArcGIS at a 2 x 2 m resolution. Some steep areas can be seen in red in the SE corner of the map, surrounding what seem to be three SE-NW striking plateaus.

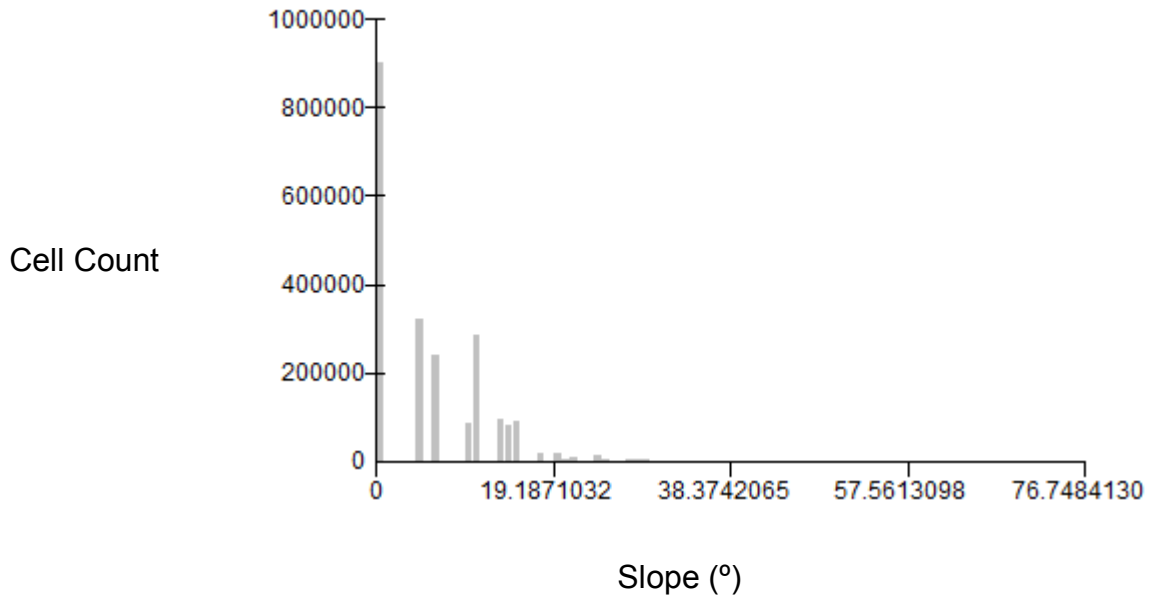


Figure 12. Histogram of 2x2 m raster cells with according slope values in degrees (°).

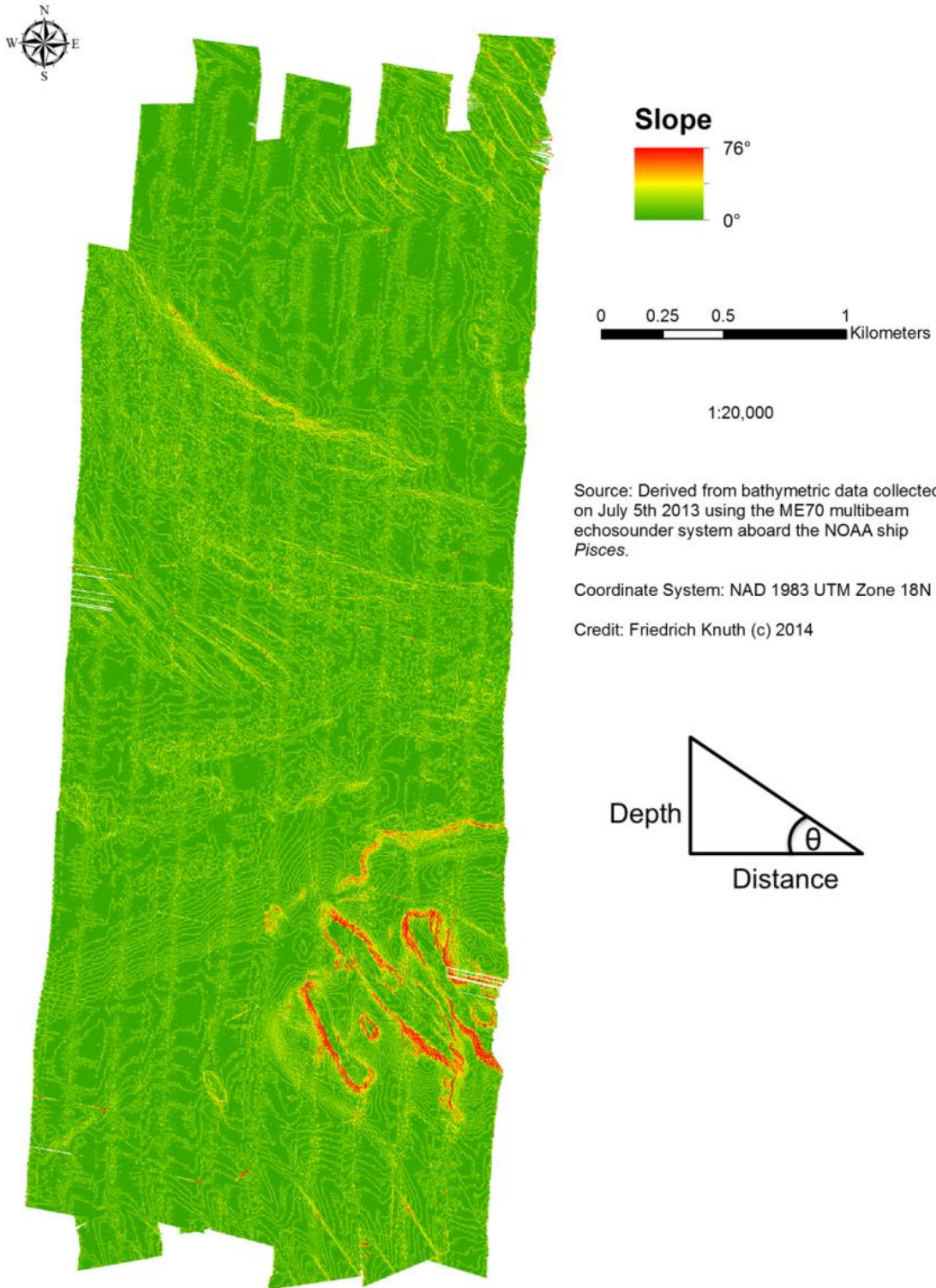


Figure 13. Example site Snowy Wreck Two showing maximum rate of change in depth between 2 x 2 m raster cell and eight neighbors.

SLOPE OF SLOPE

Slope of slope represents the change in slope over a given distance, also known as general curvature (Jeness 2013). The histogram, seen in Figure 14, shows the majority of the survey area to be flat, with little to no change in slope. The 2 x 2 m raster image, seen in Figure 15, was created using the Slope tool in the Spatial Analyst toolbox in ArcGIS, by taking the slope of the previously created slope raster. The more the slope is changing the higher the degree of convexity or concavity, which is why slope of slope is often conceived of a general measure of curvature in a given area. Again, the highest degree of curvature can be seen surrounding the plateaus in the SE corner of the study area.

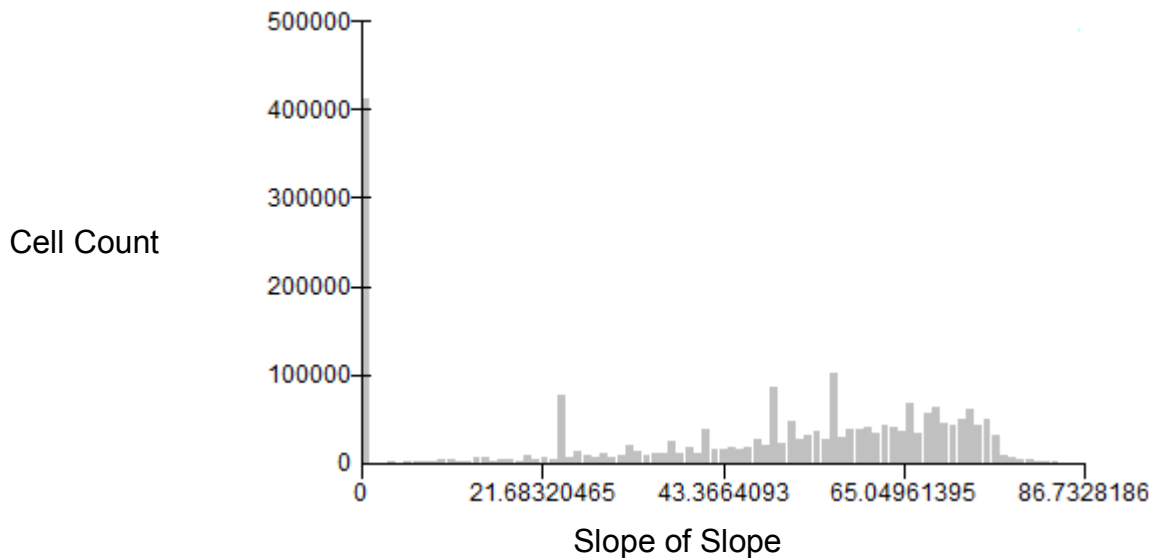


Figure 14. Histogram of raster cells with according slope of slope.

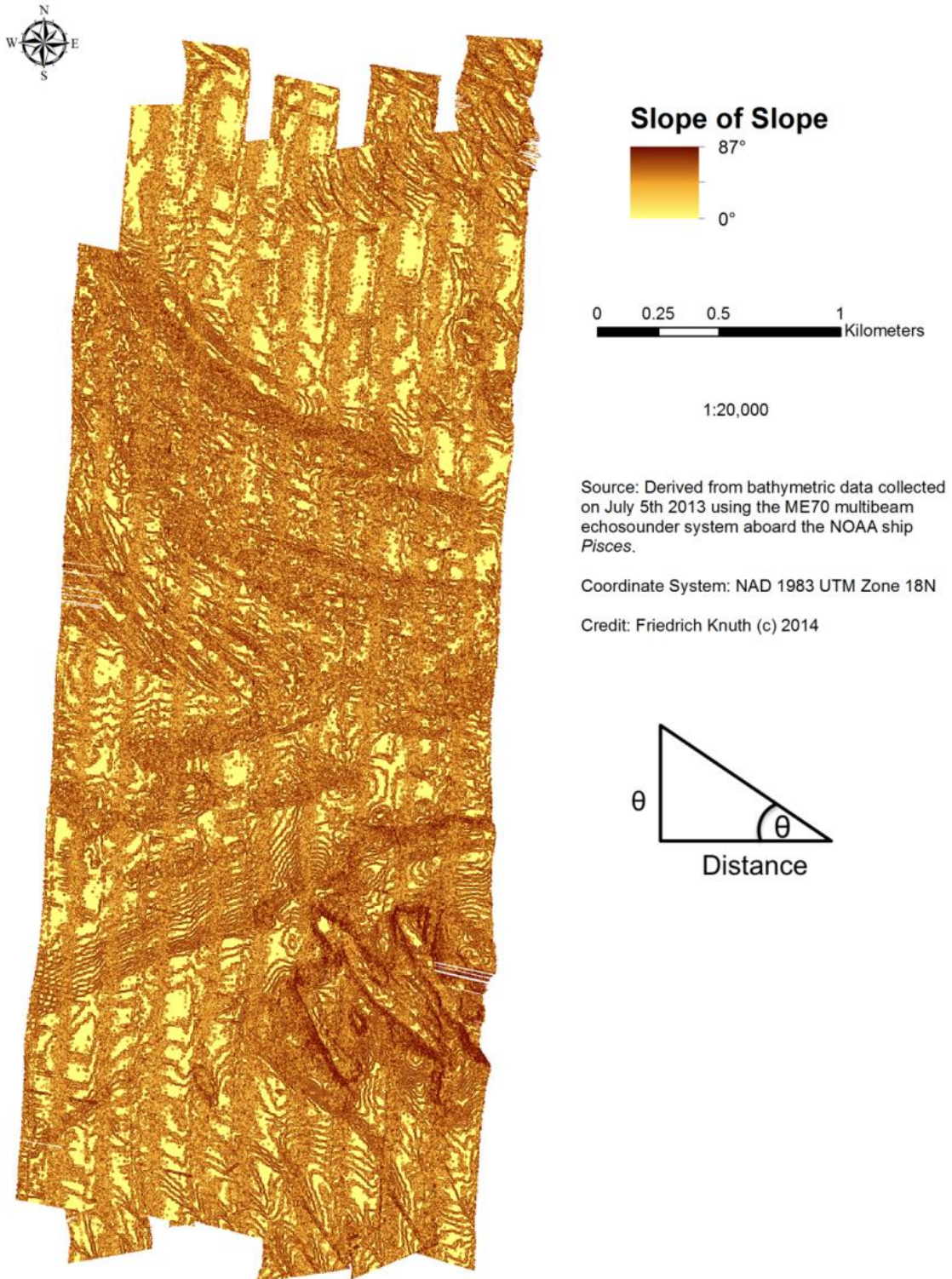


Figure 15. Example site Snowy Wreck Two showing maximum rate of change in slope between cell and eight neighbors.

PLAN CURVATURE

Plan Curvature, also known as planform curvature, is derived from the bathymetry raster and represents the curvature of the surface perpendicular to the slope direction. This is different than the Plan Curvature listed in the DEM Surface Toolbox, provided by Jeff Jeness from Jeness Enterprises. Here Plan Curvature is referred to as Cross-Sectional Curvature (Jeness 2013). It is represented by the vector measuring the maximum rate of change in concavity (-) or convexity (+) and thereby expresses crests and valleys. The dataset can conceptually be split between negative values, representing areas of concavity and positive values, representing areas of convexity (Figure 16). As can be seen in the histogram, the majority of the values are around 0. The plan curvature raster was calculated using the Curvature tool in the ArcGIS Spatial Analyst from the bathymetry raster at a 2 x 2 m resolution (Figure 17). Again, we see that the majority of the values are around 0, which is reflected in the tan color on the map.

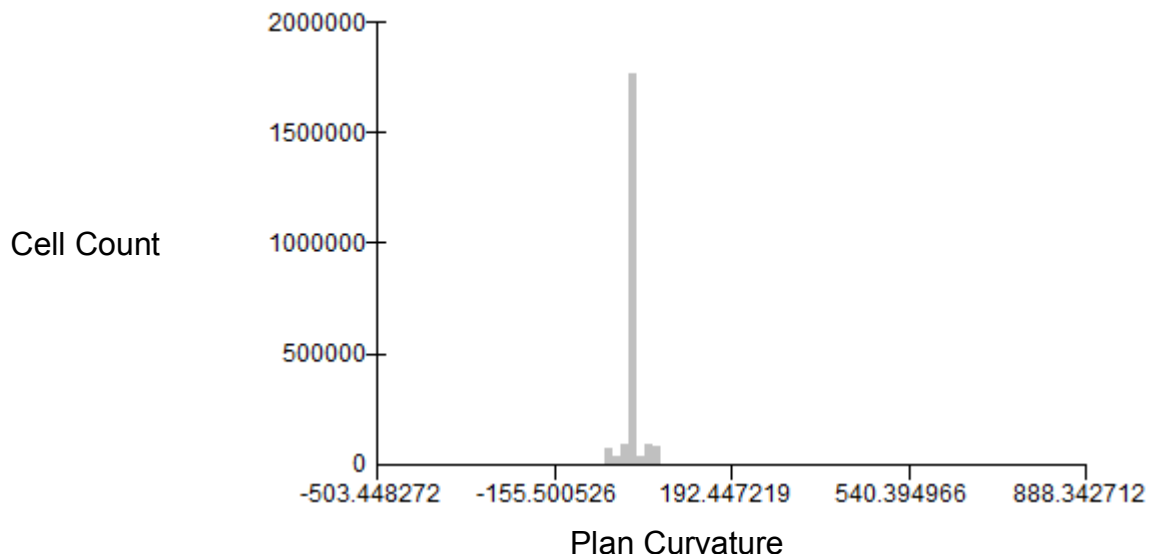


Figure 16. Histogram of 2x2 m raster cells with according plan curvature values.

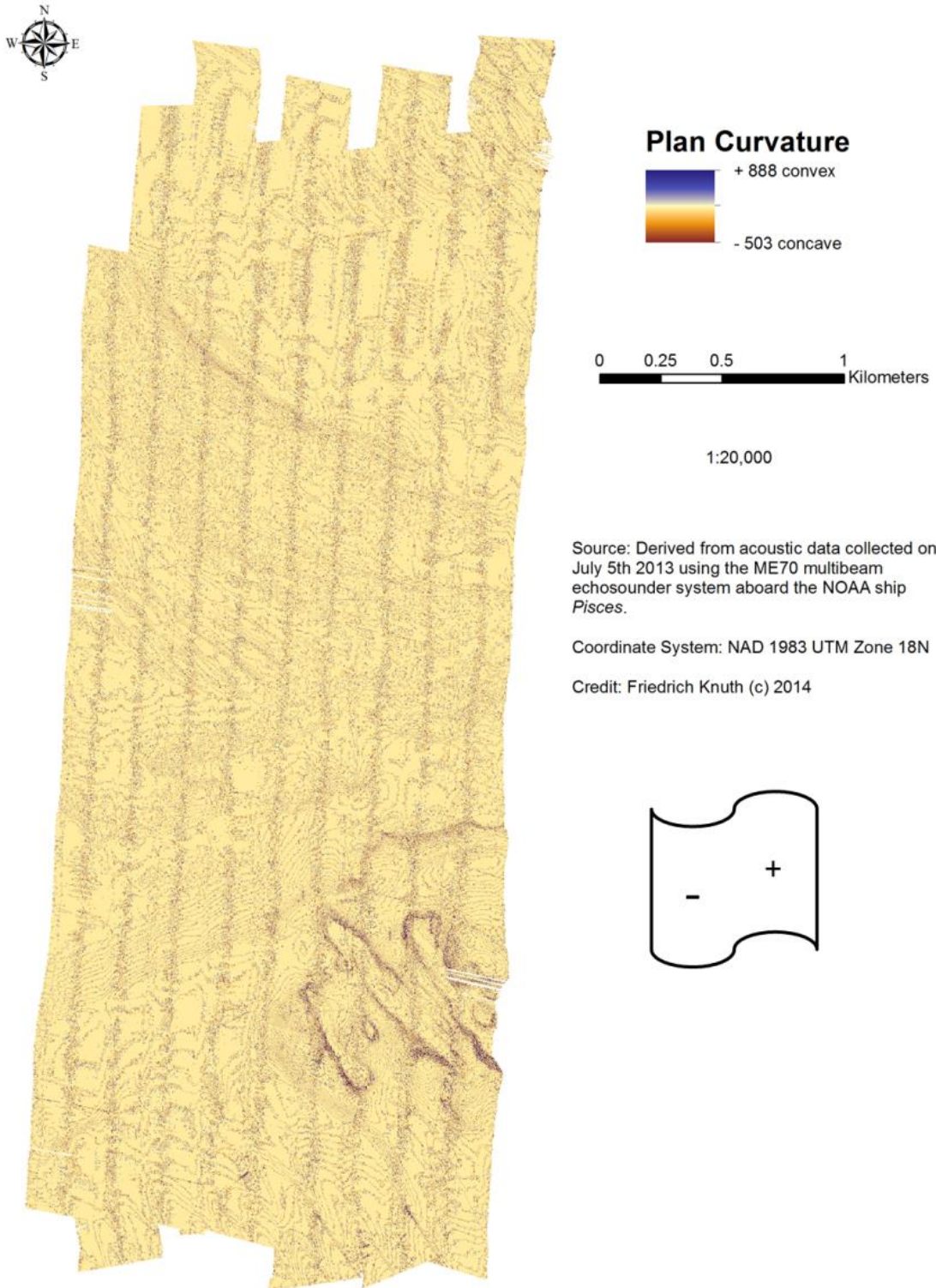


Figure 17. Example site Snowy Wreck Two showing rate of change in curvature across the surface.

RUGOSITY

Rugosity is a measure of topographic complexity and represents the total surface area divided by the planar surface area. Using the DEM Surface Toolbox created by Jeff Jenness we were able to calculate the rugosity raster. The tool divides the surface area by the planar surface area using a 3 by 3 cell grid system. The central pixel within the 3 by 3 grid receives a values representative of the surrounding bathymetry. If there is a lot of variability surrounding the pixel, the value will be high, usually up to around 4. If there is no variability at all the value will be 1 (Figure 18 and Figure 19). Most values seen in the histogram and on the map are around 1, with little to no rugosity.

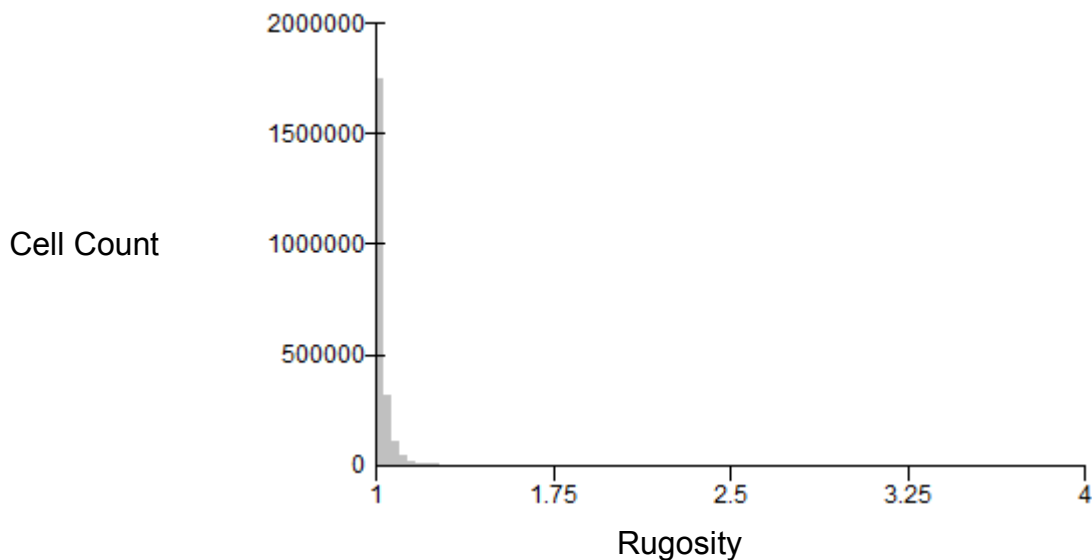


Figure 18. Histogram of 2x2 m raster cells with according rugosity values.

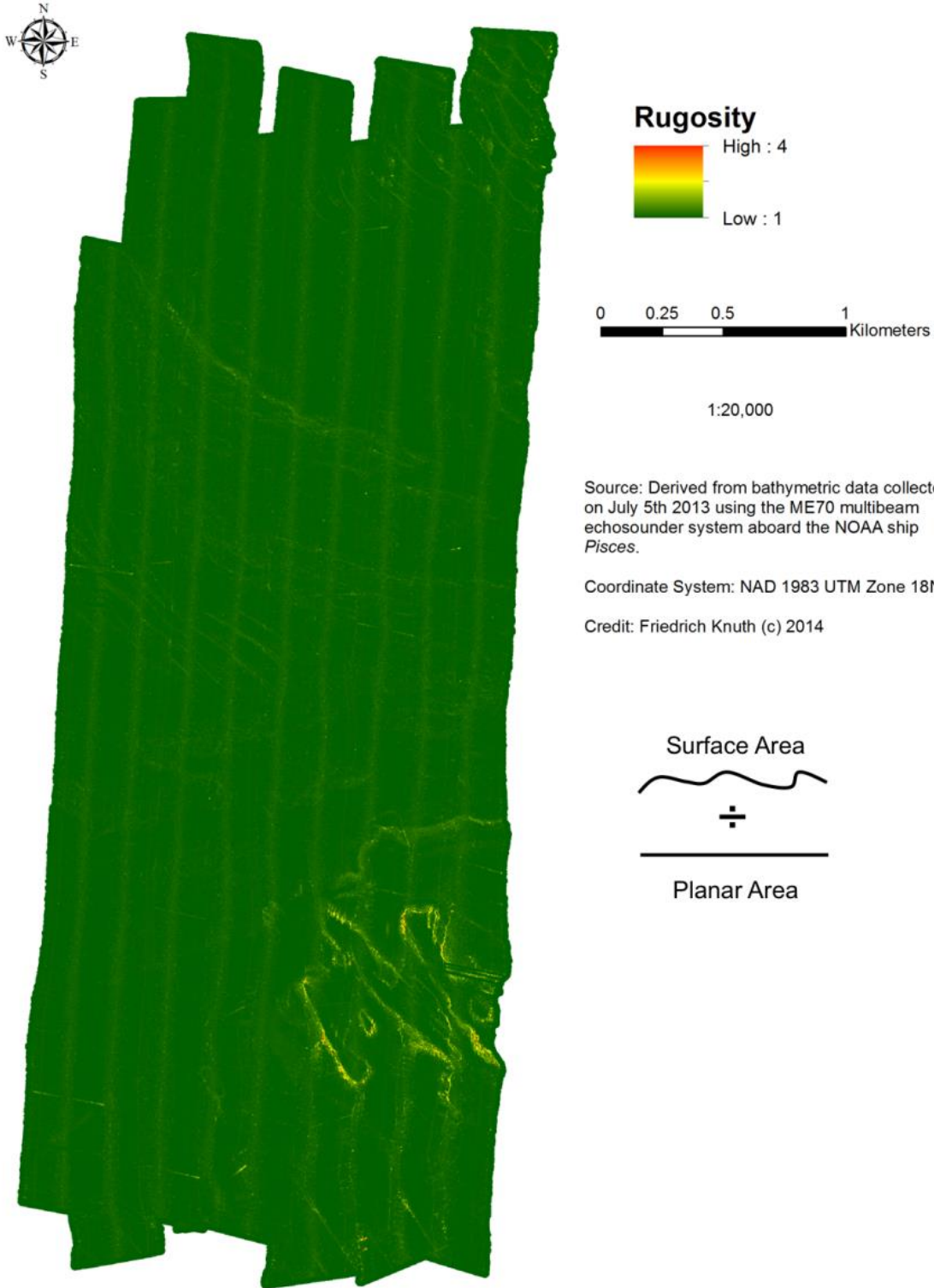


Figure 19. Example site Snowy Wreck Two showing ratio of surface area to planar surface area.

DISTANCE TO SHELF

The Distance to Shelf variable is calculated using the Near tool in the ArcGIS Analysis toolbox. First a point is created for each 2 x 2 m pixel within the bathymetry raster grid. Then the linear shortest distance of each point to the 200 m isobath, known as the shelf edge, is calculated using the Near function (U.S. Geological Survey 2014; United Nations 1958). These values are appended to the attribute tables of the points. Each point is then converted back into a pixel or cell to form a continuous raster representing the distance to the shelf edge in the form of a gradient. We then transformed the data to a half kilometer scale by dividing the meter distance values by 500, which amplifies the relative variance between values (Figure 20 and Figure 21).

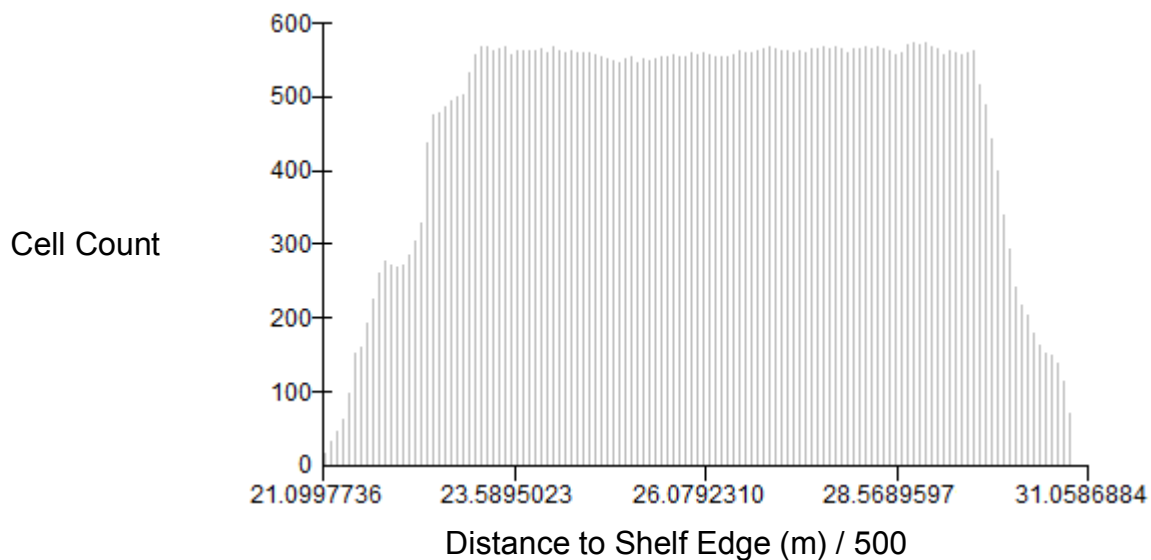


Figure 20. Histogram of 2x2 m raster cells with according Distance to Shelf Edge values in meters (m) divided by 500.

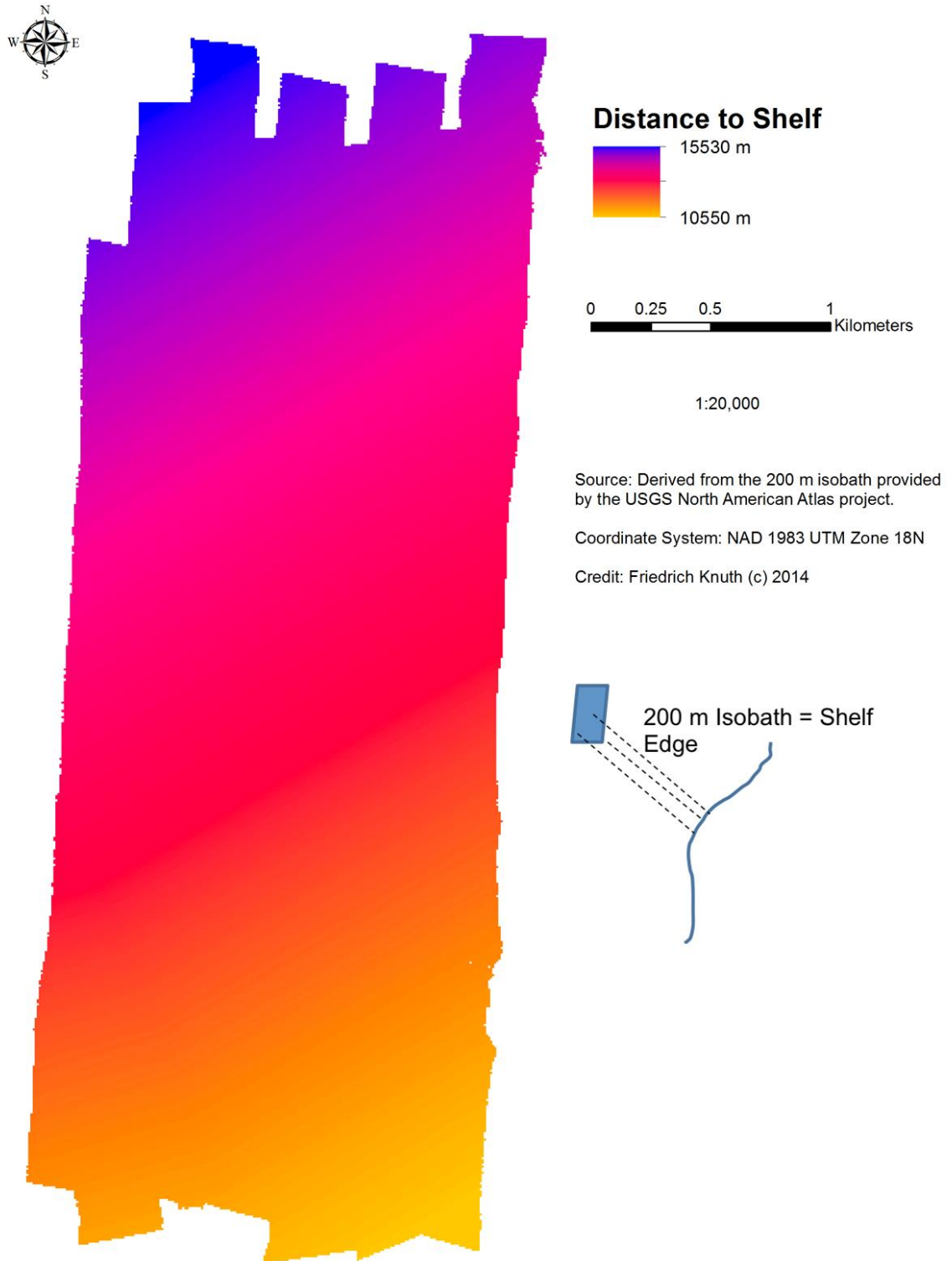


Figure 21. Example site Snowy Wreck Two showing distance of each 2x2 m raster cell to 200 m isobath, known as shelf edge (U.S. Geological Survey 2014, United Nations 1958).

BACKSCATTER

Backscatter represents the intensity of the acoustic return bouncing off the seafloor and is measured in decibels. Lower, more negative (-), values correspond to softer bottom types, while higher values reflect harder bottom types (Figure 22). As can be seen in the histogram, the mean and median values seem to be around -22 and follows a normal distribution. The final raster, representing the backscatter surface, was created at a 2 x 2 m resolution from acoustic data processed in FMGT (Figure 23) Lighter colors represent harder seabed, while darker hues represent softer seabed.

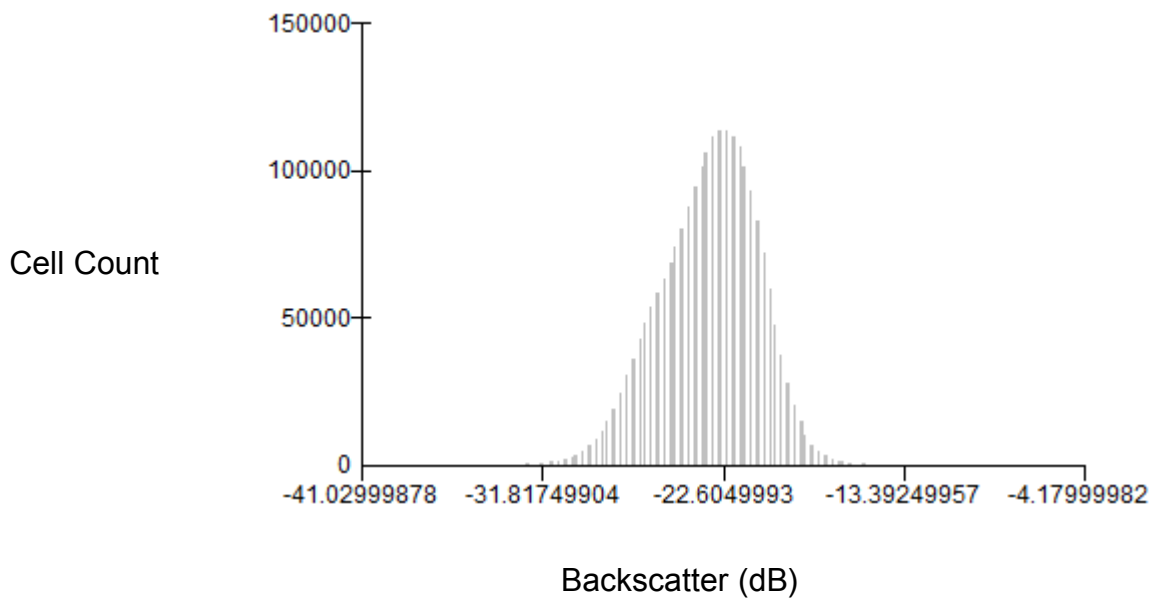


Figure 22. Histogram of 2x2 m raster cells with according backscatter values in decibels (dB).

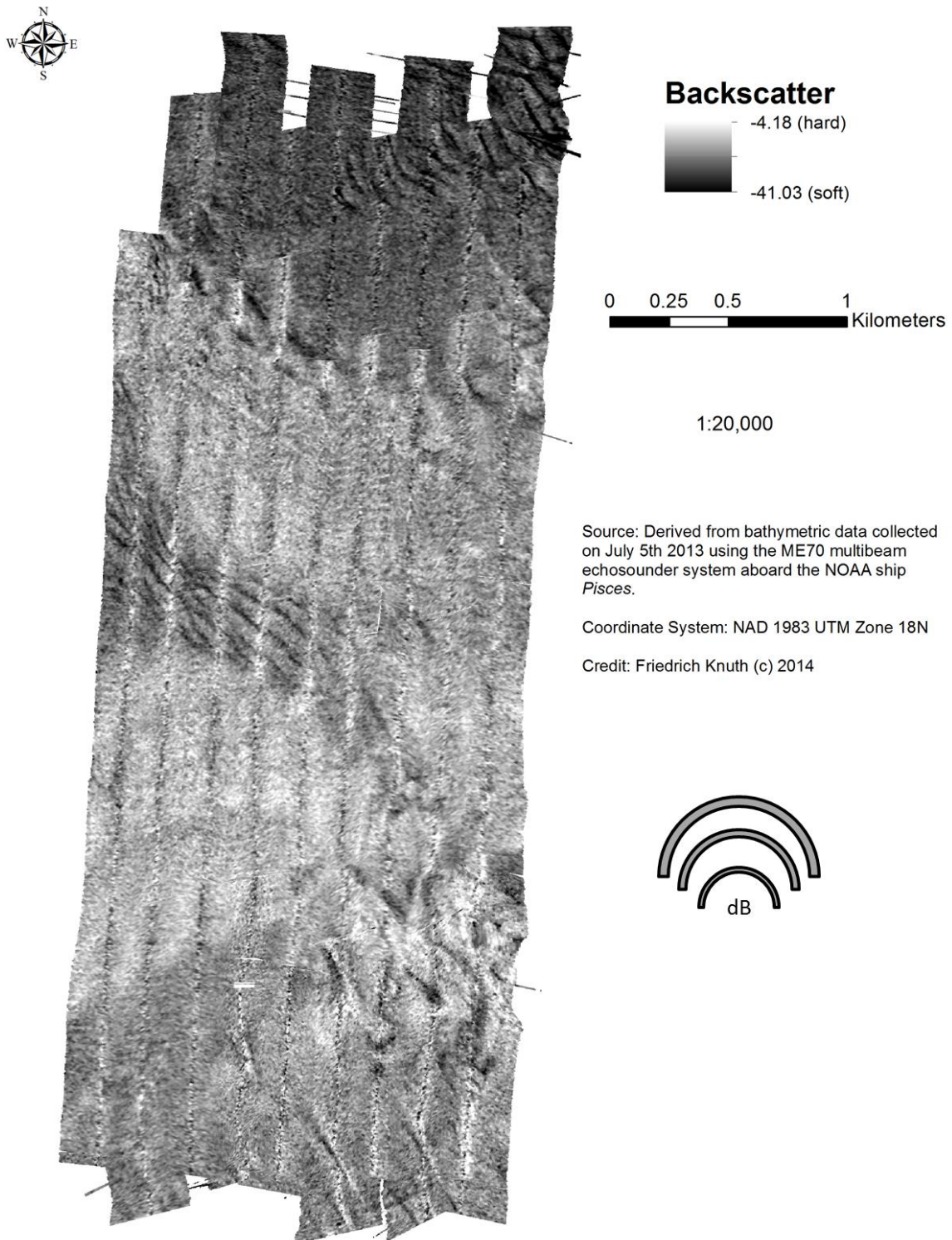


Figure 23. Example site Snowy Wreck Two showing intensity of the acoustic return.

EXPLANATORY VARIABLES

In ArcGIS 10.2, 14 explanatory variables were derived from the seven morphometric base layers (Table 3).

Table 3. Description of 14 Explanatory Variables

50 x 50 m grid and Site-Wide Explanatory Variables		Unit	Description	Analytical Tool in ArcGIS
1.	\bar{X} Depth	Meters	Mean distance from sea level to seafloor	Zonal Statistics in Spatial Analyst
2.	σ Depth	Meters	Variance of depth values about the mean	Zonal Statistics in Spatial Analyst
3.	\bar{X} Range x \bar{X} Variety	-	Range of depth values multiplied by Variety of depth values	Zonal Statistics in Spatial Analyst
4.	\bar{X} Slope	Degrees	Mean slope of maximum change in depth between cell and eight neighbors.	Zonal Statistics in Spatial Analyst
5.	\bar{X} Slope of Slope	Degrees	Mean slope of maximum change in slope between cell and eight neighbors.	Zonal Statistics in Spatial Analyst
6.	\bar{X} Plan Curvature	(+) convex (-) concave	Mean curvature of surface perpendicular to slope direction.	Zonal Statistics in Spatial Analyst
7.	\bar{X} Rugosity	-	Mean ratio of surface area to planar area in a 3 x 3 cell neighborhood.	Zonal Statistics in Spatial Analyst
8.	Max Rugosity	-	Maximum rugosity	Zonal Statistics in Spatial Analyst
9.	σ Rugosity	-	Variance of rugosity values about the mean	Zonal Statistics in Spatial Analyst
10.	High Rugosity	-	If (\bar{X} Rugosity + σ Rugosity) < Max Rugosity, (\bar{X} Rugosity + σ Rugosity) else Max Rugosity.	Con () statement in Field Calculator
11.	\bar{X} Distance to Shelf	Meters	Mean distance of the centroid of each pixel to the 200 m isobath	Zonal Statistics in Spatial Analyst
12.	\bar{X} Backscatter	Decibels	Mean value of intensity of acoustic return	Zonal Statistics in Spatial Analyst
13.	σ Backscatter	Decibels	Variance of backscatter values about the mean	Zonal Statistics in Spatial Analyst
14.	Backscatter Kurtosis	-	$\frac{\sigma^4}{\sigma^2}$	Field Calculator

Zonal statistics for each explanatory variable were calculated by overlaying the relevant morphometric base layer with a 50 x 50 meter grid. The 50 m grid size was chosen because it represents the approximate size of patchy reef structures along the Southeast Atlantic continental shelf (Kendall, Bauer and Jeffrey 2007, Kendall, et al. 2003, Kracker, Kendall and McFall 2008). Each 50 x 50 m grid cell was intersected with small, medium, large and all fish, giving us respective count (abundance) data for each grid cell (Figure 24).

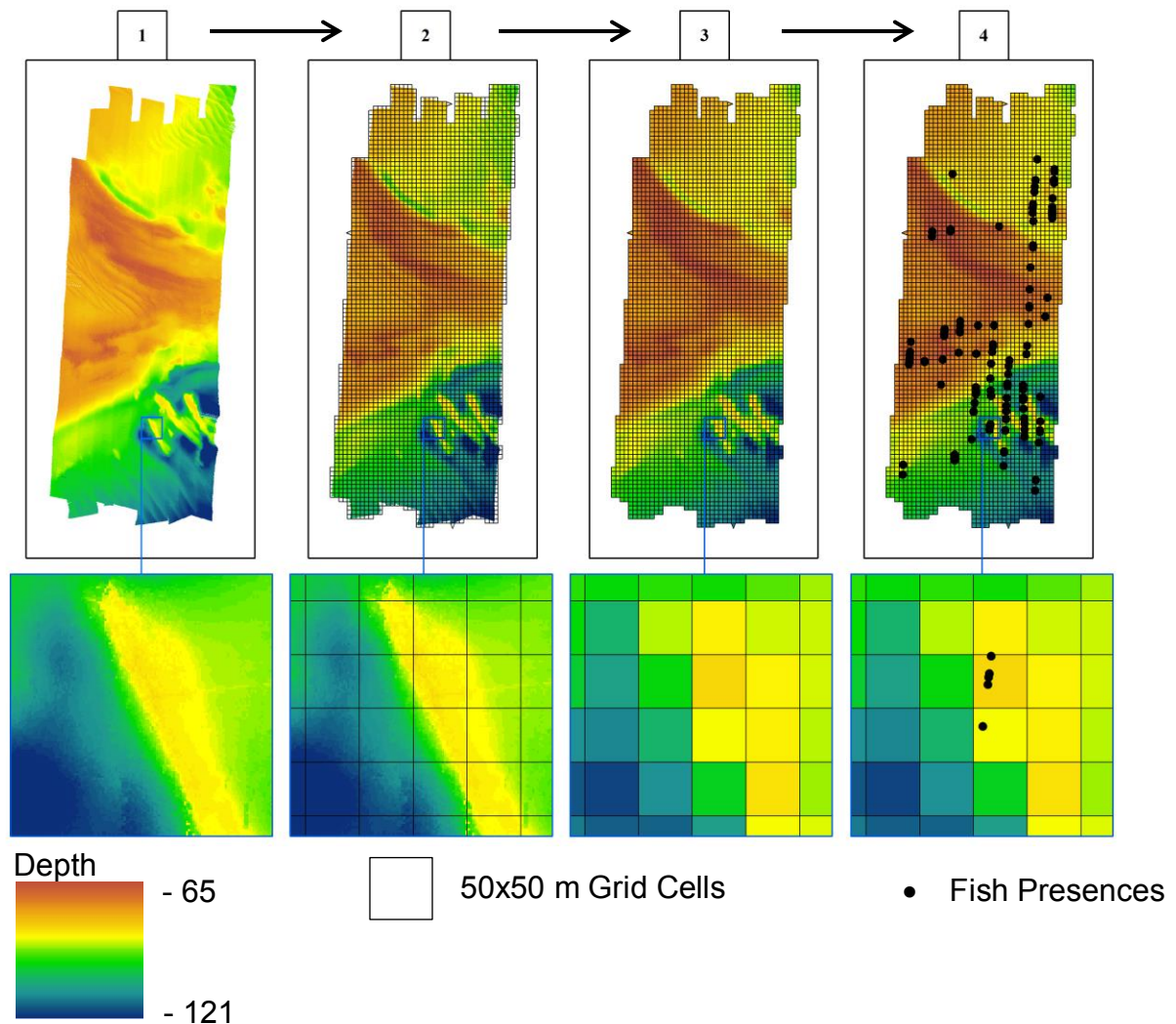


Figure 24. [1] Depth raster at 2x2 m resolution. [2] 50x50 m grid superimposed on depth raster. [3] 2x2 m depth raster cell values averaged within 50x50 m grid cells. [4] Fish occurrences intersected with averaged grid cell values present within 50x50 m grid cells. One cell appears to contain four fish, another one fish and the rest zero.

Range x Variety, High Rugosity and Kurtosis of Backscatter have previously never been included as candidates in similar studies exploring spatial ecological relationships between the seafloor and fish. (Brown, et al. 2011, Costa, et al. 2014, Pittman, Costa and Battista 2009). The Range x Variety variable represents the range of depth values within a 50x50 m grid multiplied by the variety (unique values) of depth values within the same grid. If a grid has a high range and high variety of values, we can consider it to be a topographically complex area. Subsequently a high range, but low variety could represent a steep ridge, while a low range and low variety represents a flat area. High Rugosity is derived from a conditional statement that calculates the values for a 50 x 50 m cell to be the mean plus one standard deviation of all 2 x 2 m values within a given 50 x 50 m grid cell, unless that value exceeds the maximum rugosity value within the grid cell, in which case that is assigned as the value for the 50 x 50 meter cell. Kurtosis of Backscatter is a measure that describes the shape of the histogram peak and its tail weights. This measure better describes the overall distribution by capturing the height and breadth of the histogram and was applied to the 2 x 2 m backscatter raster values present within each 50x50 m grid. This metric has the potential to capture variation in range that is lost by a simple standard deviation metric. A complete variable correlation matrix is compiled in Table 4. The Pearson's correlation represents the strength of the association between variables. Significant correlations between variables are highlighted in bold and set in parenthesis.

Table 4. Pearson’s Variable Correlation Matrix. Correlations greater than an absolute value of 0.5 are shown in bold font. Significant correlations greater than an absolute value of 0.9 are shown in bold font and parenthesis. (Table continued on next page)

	\bar{X} Depth	σ Depth	\bar{X} Range x \bar{X} Variety	\bar{X} Distance to Shelf	\bar{X} Plan Curvature	\bar{X} Slope
σ Depth	-0.306					
\bar{X} Range x \bar{X} Variety	-0.241	(0.907)				
\bar{X} Distance to Shelf	0.605	-0.348	-0.218			
\bar{X} Plan Curvature	0.028	0.015	0.009	0.010		
\bar{X} Slope	-0.374	0.849	0.727	-0.432	0.068	
\bar{X} Slope of Slope	-0.348	0.537	0.337	-0.501	0.063	0.813
\bar{X} Rugosity	-0.166	0.419	0.422	-0.137	0.042	0.481
High Rugosity	-0.088	0.268	0.290	-0.039	0.022	0.274
Max Rugosity	-0.208	0.360	0.373	-0.136	0.054	0.372
σ Rugosity	-0.043	0.175	0.207	0.015	0.010	0.152
\bar{X} Backscatter	-0.287	0.320	0.200	-0.615	-0.017	0.289
Backscatter Kurtosis	-0.015	0.009	0.005	-0.017	0.015	0.015
σ Backscatter	-0.358	0.207	0.145	-0.206	0.032	0.376

	\bar{X} Slope of Slope	\bar{X} Rugosity	High Rugosity	Max Rugosity	σ Rugosity	\bar{X} Backscatter	Backscatter Kurtosis
\bar{X} Rugosity	0.336						
High Rugosity	0.161	(0.948)					
Max Rugosity	0.218	0.757	0.832				
σ Rugosity	0.059	0.880	0.985	0.837			
\bar{X} Backscatter	0.315	0.109	0.062	0.129	0.035		
Backscatter Kurtosis	0.018	0.008	0.005	0.008	0.003	0.012	
σ Backscatter	0.364	0.197	0.115	0.188	0.065	0.143	0.052

Fish are only detected within the 7 degree beam of the EK60 echo sounder system, resulting in a circular footprint with a diameter of approximately $0.12 \times \text{depth}$. This is a small portion of the swath covered by the MBES. Therefore, survey track lines, which represent nadir, were intersected with the composite 50 x 50 m multibeam grid. Values within each grid cell for all 14 explanatory variables and fish counts within each cell were extracted, to select only grid cells that were actually surveyed by the EK 60 (Figure 25). The 50 x 50 meter grid both approximates the swath covered by the EK 60 and reef features in this area.

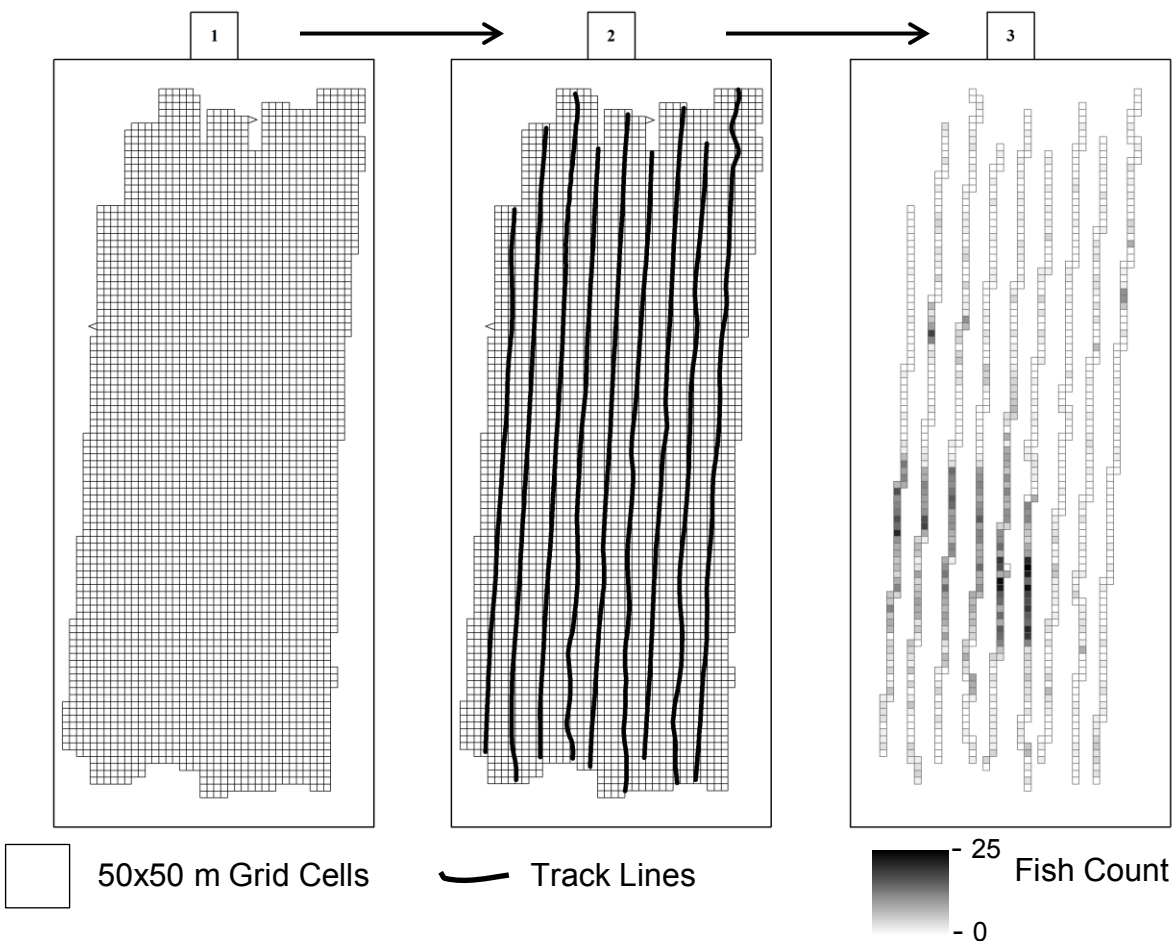


Figure 25. [1] 50x50 m Snowy Wreck Two grid with all response categories and explanatory variables appended ($n = 3643$). [2] Ship track lines intersection with grid cells. [3] Final dataset for Snowy Wreck Two containing only observed fish data ($n=905$).

In order to analyze the data at the site wide scale, all 50 x 50 m grid cell explanatory variables were averaged by site. The sum of the fish counts by site was then normalized by dividing the total site-wide fish count by the total area of surveyed 50 x 50 m grid cells (Table 5). Both the 50 x 50 m and site-wide attribute tables were then exported as a comma separated values (.csv) files, ready for statistical analysis in Minitab 17.

Table 5. Summary of fish counts normalized by area for sites with fish data.

Survey Site	50 x 50 m grid area surveyed by EK60 (km ²)	<i>n</i> All Fish / km ²	<i>n</i> Large Fish / km ²	<i>n</i> Medium Fish / km ²	<i>n</i> Small Fish / km ²
Snowy Wreck Two Cape	2.33	881	69	329	483
Lookout One Cape	8.70	263	39	124	100
Lookout Two North Carolina 780 N of Edisto MPA	3.76	309	24	150	135
	5.18	127	9	44	73
	5.52	214	7	26	181
Snowy Wreck One	1.56	47	4	47	49

RESPONSE VARIABLES

Any fish smaller than 5 cm and higher than 20 m in the water column above the seafloor were excluded from the analysis, in an effort to focus our analysis on seafloor dwelling demersal fish only. Fish data points were grouped into small (5-12 cm), medium (12-29 cm) and large (>29 cm) size classes (Figure 26) (Kracker, et al. 2010, Costa, et al. 2014). Four final response variables were thereby generated: Small Fish, Medium Fish, Large Fish and All Fish. The final dataset only included fish data for six out of ten survey sites: Cape Lookout One, Cape Lookout Two, Snowy Wreck One, Snowy Wreck Two, North of Edisto MPA and North Carolina 780. As we can see in the example Figure 26, large fish seem to be converging around the

topographically complex plateaus in the SE section of this survey area, while all fish size classes seem to be avoiding, what appear to be mega ripples in the mid-western and north-eastern sections of the survey area. This preliminary heuristic evaluation supports the idea that there may be a relationship between seafloor morphology and the presence of fish at this and other sites. A complete catalogue of fish distributions across all six surveyed sites can be seen in Appendix B.

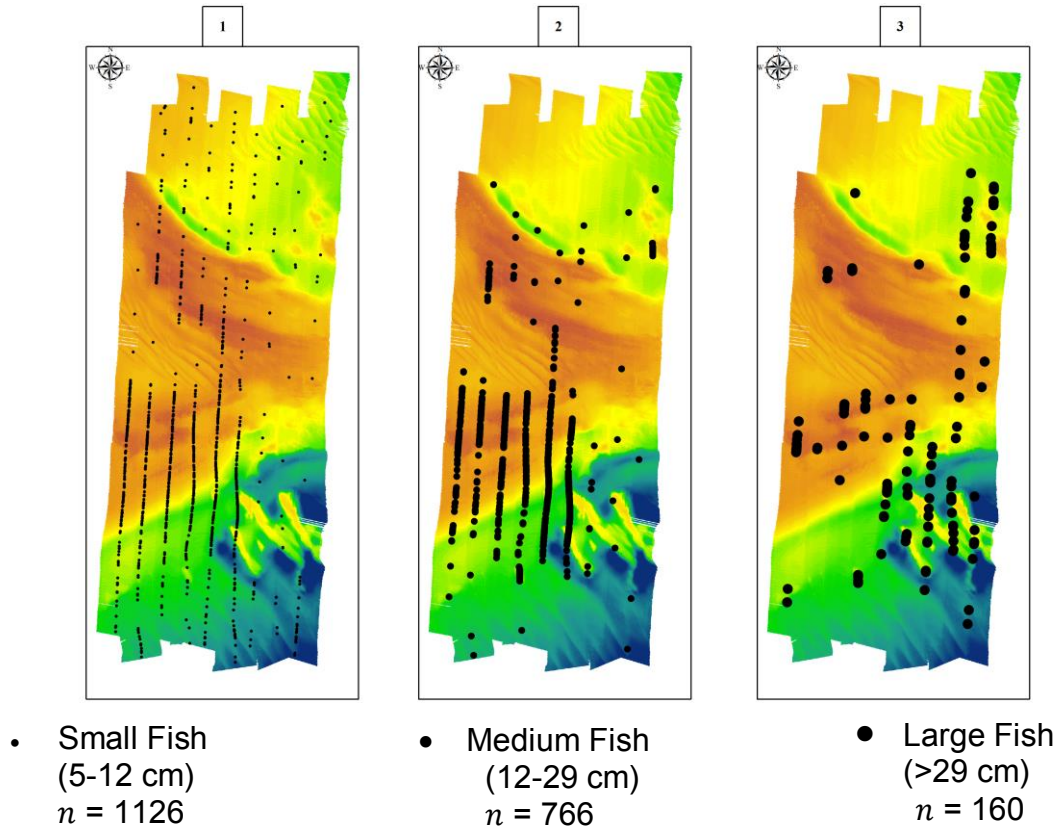


Figure 26. Small, medium and large fish occurrences in survey site Snowy Wreck Two depicted above bathymetric depth map.

MODELING

A conceptual view of ecological seafloor predictors being related to fish can be seen in **Figure 27**.

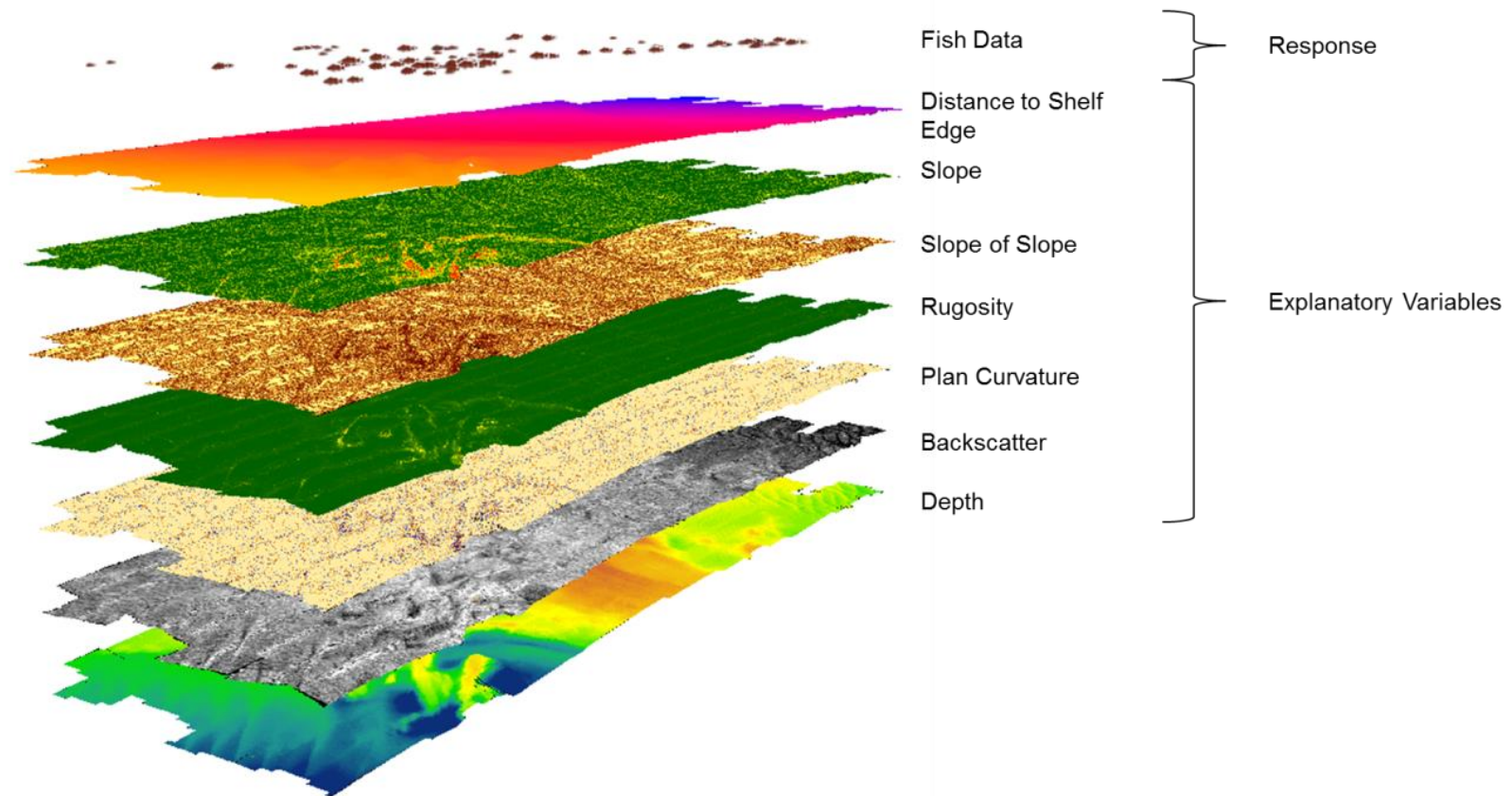


Figure 27. Conceptual view of ecological predictors related to fish abundance. Actual 14 explanatory surfaces not depicted. Figure generated in ArcScene 10.2.1. Knuth 2014.

50 X 50 M GRID SCALE USING MULTIVARIATE ANALYSIS

Fish occurrences within a 50 x 50 m grid are recorded as rare positive whole integers following a Poisson distribution (Figure 28). For this reason, a Poisson regression Generalized Linear Model (GLM) was used to explore the relationship between fish count and explanatory variables derived from the base layers (University of Massachusetts 2007). In Minitab 17, any variables with a P-value > 0.05 and an insignificant Chi Square value were removed using a stepwise regression ($\alpha = 0.05$). A Chi Square value was deemed insignificant if its removal resulted in a minimal (< 1%) reduction in overall R^2 performance for the model and did not drastically increase the overall model AIC value. Finally, if any two variables expressed Variable Inflation Factor (VIF) > 7.5 these were excluded from the final model in an effort to avoid collinearity between explanatory variables. A VIF cut-off between 5 and 10 is commonly used as a good general indicator of collinearity (ESRI 2013; Flom 1999). A sample regression output from Minitab 17 displaying the successive model selection process can be seen in Appendix C.

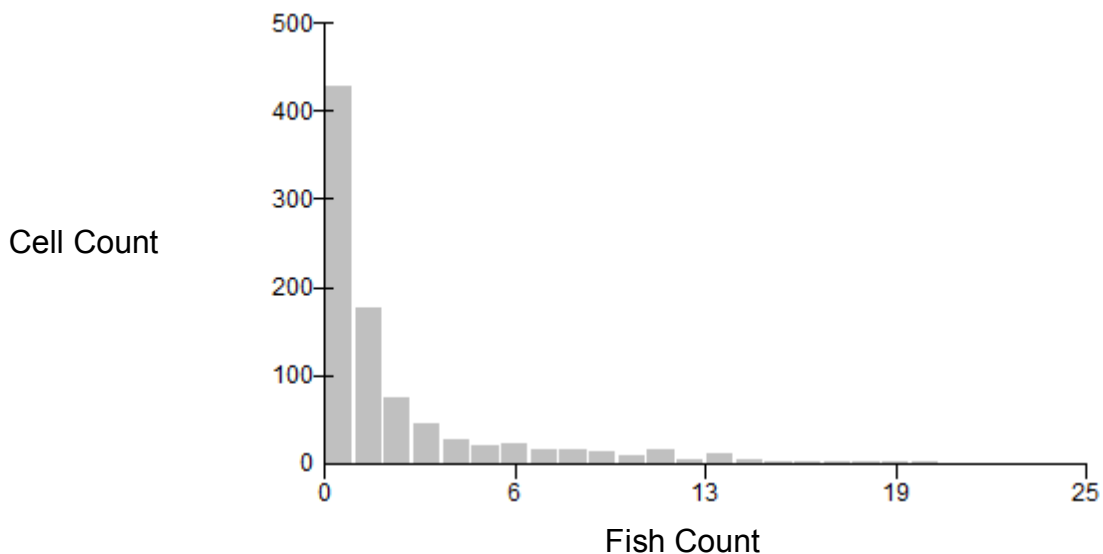


Figure 28. Example Poisson distribution of All Fish counts recorded within 50 x 50 m cells at survey site Snowy Wreck Two.

SITE-WIDE SCALE USING BIVARIATE ANALYSIS

At the site-wide scale, the dataset consists of six data points, one per site (Table 5). In Microsoft Excel a bivariate regression analysis was applied by plotting an exponential regression line to explain the variance in fish counts by site. Because of the small site-wide dataset of six data points, a conservative R^2 of 0.80 was chosen to be the criterion for stating that there may be a significant relationship between fish abundance and a given variable.

RESULTS

50 X 50 M GRID SCALE MULTIVARIATE MODELS

The following are results from the Poisson regression at a 50 x 50 m scale. All Fish together were modeled with an R^2 of 0.10 (Table 6). The highest model R^2 was observed for Medium Fish at 0.15, followed by Large Fish at 0.13 and Small Fish at 0.03, as can be seen in Table 6 through Table 9.

Table 6. Poisson Regression for All Fish $n = 7410$

Contributing Variables (X_n)	P-Value	Chi-Square	VIF	Variable R^2	Model Contribution	Coefficient (β_n)
Slope \bar{X}	0.000	896	2.49	4%	36%	0.18773
Backscatter \bar{X}	0.000	818	1.09	3%	33%	0.11574
Range $\bar{X} \times$ Variety \bar{X}	0.000	385	2.22	2%	16%	-0.004517
Rugosity σ	0.000	187	3.94	1%	8%	2.815
Rugosity \bar{X}	0.000	174	5.15	1%	7%	-6.335

$$\begin{aligned} \text{Model } R^2 &= 0.10 \\ \text{Constant } (\beta_0) &= 7.798 \\ \text{All Fish} &= e^{\beta_0 + \beta_n X_n} \end{aligned}$$

Table 7. Poisson Regression for Large Fish $n = 680$

Contributing Variables (X_n)	P-Value	Chi-Square	VIF	Variable R^2	Model Contribution	Coefficient (β_n)
Slope of Slope \bar{X}	0.000	228	1.17	8%	64%	0.07697
Backscatter \bar{X}	0.000	127	1.17	5%	36%	0.1753

$$\begin{aligned} \text{Model } R^2 &= 0.13 \\ \text{Constant } (\beta_0) &= -2.355 \\ \text{Large Fish} &= e^{\beta_0 + \beta_n X_n} \end{aligned}$$

Table 8. Poisson Regression for Medium Fish $n = 2858$

Contributing Variables (X_n)	P-Value	Chi-Square	VIF	Variable R^2	Model Contribution	Coefficient (β_n)
Backscatter \bar{X}	0.000	759	1.16	9%	63%	0.04894
Slope of Slope \bar{X}	0.000	445	1.16	6%	37%	0.20610

Model $R^2 = 0.15$
 Constant (β_0) = 1.132
 Medium Fish = $e^{\beta_0 + \beta_n X_n}$

Table 9. Poisson Regression for Small Fish $n = 3955$

Contributing Variables (X_n)	P-Value	Chi-Square	VIF	Variable R^2	Model Contribution	Coefficient (β_n)
Slope \bar{X}	0.000	205	2.54	0.97%	32%	0.12377
Rugosity σ	0.000	152	3.63	0.72%	24%	3.372
Rugosity \bar{X}	0.000	145	4.41	0.69%	23%	-7.999
Range $\bar{X} \times$ Variety \bar{X}	0.000	77	1.79	0.36%	12%	-0.003173
Backscatter \bar{X}	0.000	55	1.39	0.26%	9%	0.3006

Model $R^2 = 0.03$
 Constant (β_0) = 6.106
 Medium Fish = $e^{\beta_0 + \beta_n X_n}$

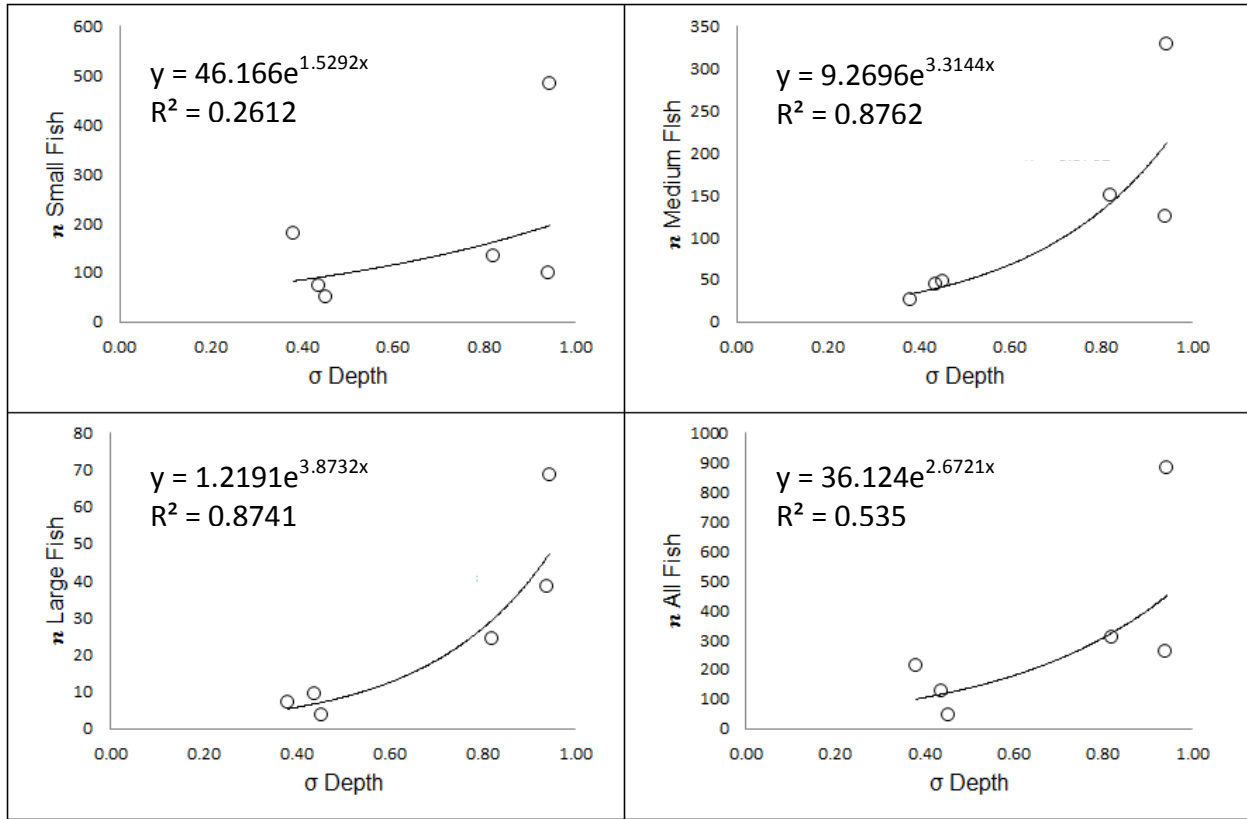
Overall, \bar{X} Slope, \bar{X} Slope of Slope, \bar{X} Backscatter, Range $\bar{X} \times$ Variety \bar{X} , Rugosity σ and Rugosity \bar{X} emerged as the strongest variables contributing to the overall combined explanatory power of a given model. Table 10 highlights the average model contribution, whenever a variable ended up in the final model for all, small, medium and large fish. The maximum variance in fish abundance explained by these multivariate models was 15%. Since the predictive power of these models is weak, ecological inferences should be made cautiously. The results point towards an ecological relationship between the combination of \bar{X} Slope, \bar{X} Slope of Slope, \bar{X} Backscatter and Range $\bar{X} \times$ Variety \bar{X} and the presence of fish at the 50 x 50 m scale.

Table 10. Average variable contribution to overall model R^2

Explanatory Variable	Average Model Contribution
Slope of Slope \bar{X}	51%
Backscatter \bar{X}	44%
Slope \bar{X}	34%
Rugosity σ	16%
Rugosity \bar{X}	15%
Range $\bar{X} \times$ Variety \bar{X}	14%

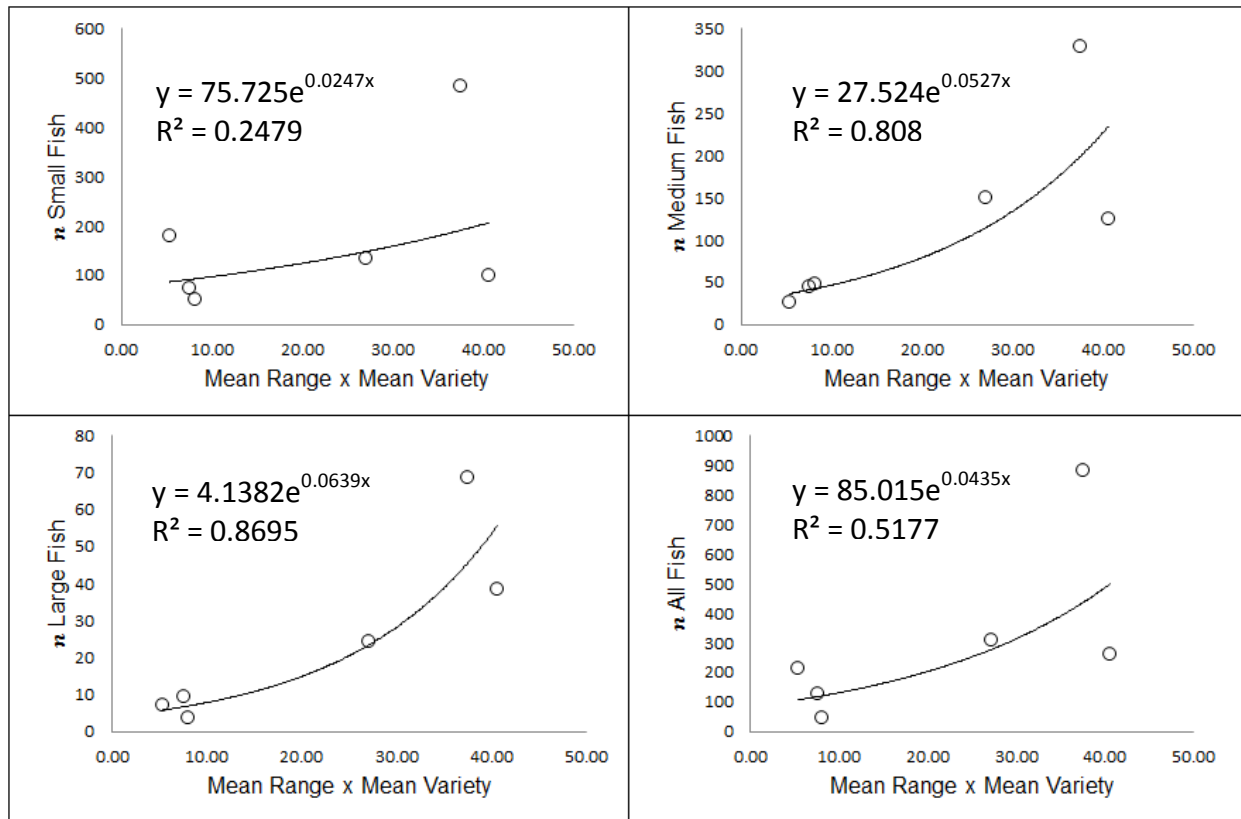
SITE-WIDE SCALE BIVARIATE MODELS

Figure 29 through Figure 32 indicate significant ($R^2 > 0.80$) bivariate relationships between site-wide variables σ Depth, \bar{X} Range \times \bar{X} Variety, \bar{X} Slope, \bar{X} Slope of Slope and the abundance of large and medium fish. Due to only six data points being modeled, ecological inferences should be made with caution. Still, the high R^2 values and predictive potential of the site-wide models is very promising. Modeling expected vs actual fish counts at the site-wide scale can supply very valuable information on assessing the performance of MPAs and impact of anthropogenic fishing pressures outside MPA boundaries. No other explanatory variables expressed an $R^2 > 0.80$ (Appendix D).



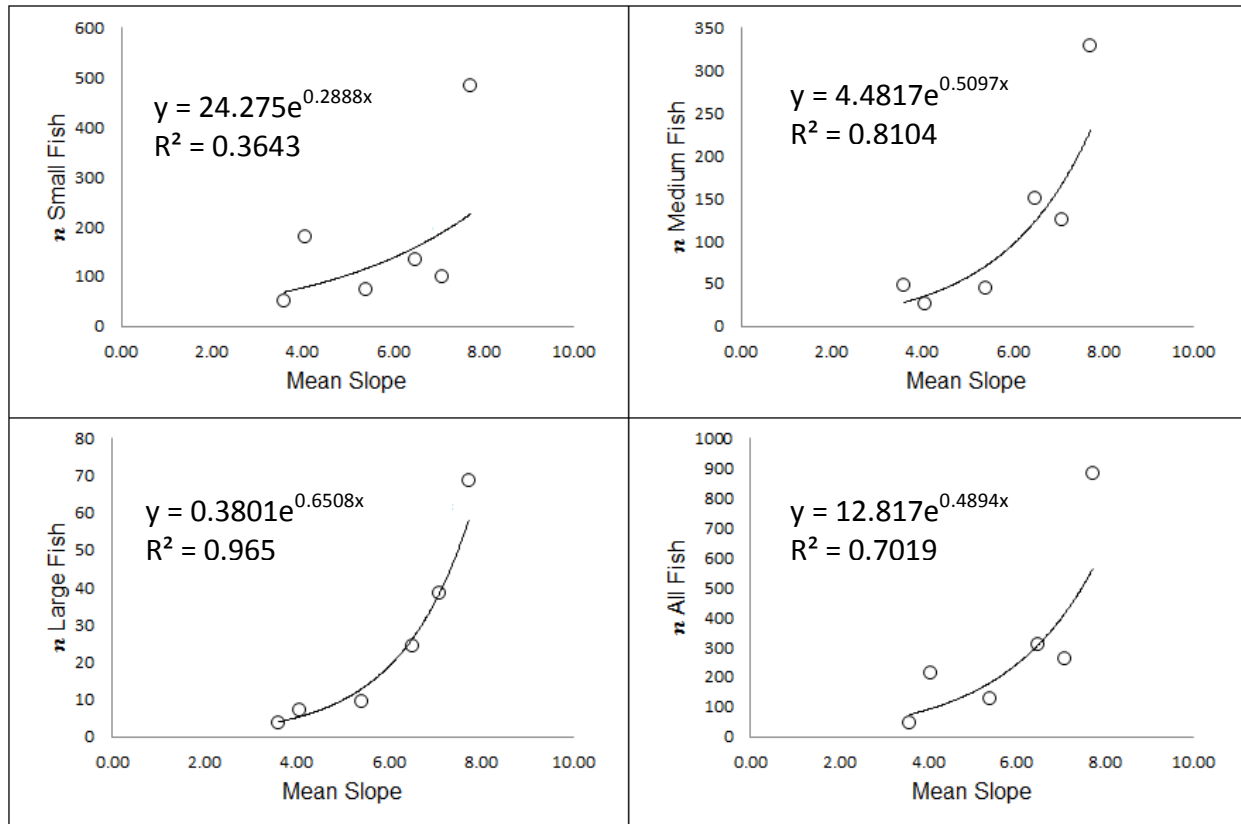
Site	σ of Depth	All Fish	Large Fish	Medium Fish	Small Fish
Snowy Wreck Two	0.94	881	69	329	483
Cape Lookout Two	0.82	309	24	150	135
Cape Lookout One	0.94	263	39	124	100
N of Edisto MPA	0.38	214	7	26	181
North Carolina 780	0.44	127	9	44	73
Snowy Wreck One	0.45	47	4	47	49

Figure 29. Relationship between mean site-wide σ of Depth and Fish Count. Small Fish $R^2 = 0.26$, Medium Fish $R^2 = 0.88$ Large Fish $R^2 = 0.87$, All Fish $R^2 = 0.54$.



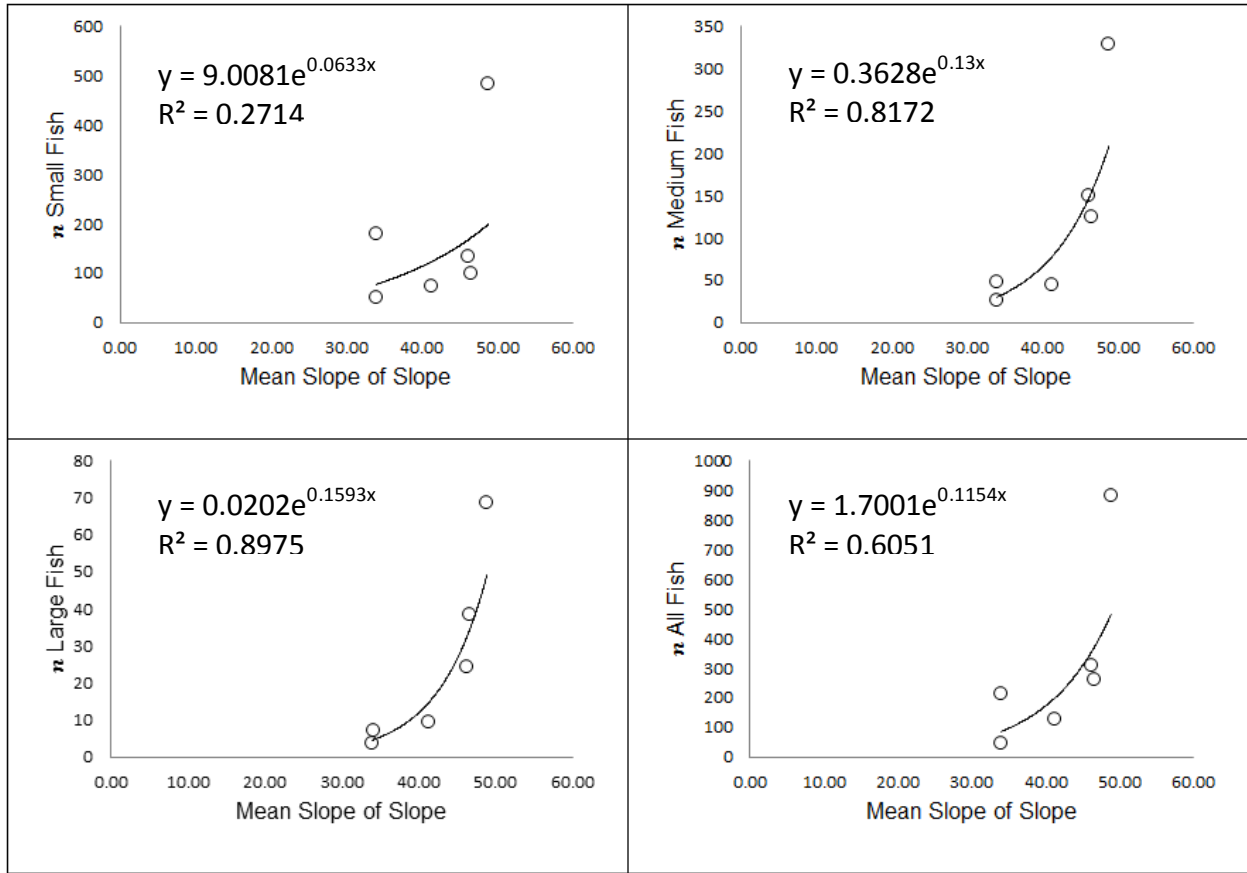
Site	\bar{X} Range \times \bar{X} Variety	All Fish	Large Fish	Medium Fish	Small Fish
Snowy Wreck Two	37.58	881	69	329	483
Cape Lookout Two	27.16	309	24	150	135
Cape Lookout One	40.64	263	39	124	100
N of Edisto MPA	5.32	214	7	26	181
North Carolina 780	7.55	127	9	44	73
Snowy Wreck One	8.12	47	4	47	49

Figure 30. Relationship between mean site-wide \bar{X} Range \times \bar{X} Variety and Fish Count by size. Small Fish $R^2 = 0.25$, Medium Fish $R^2 = 0.81$ Large Fish $R^2 = 0.87$, All Fish $R^2 = 0.52$.



Site	\bar{X} Slope	All Fish	Large Fish	Medium Fish	Small Fish
Snowy Wreck Two	7.73	881	69	329	483
Cape Lookout Two	6.51	309	24	150	135
Cape Lookout One	7.10	263	39	124	100
N of Edisto MPA	4.08	214	7	26	181
North Carolina 780	5.41	127	9	44	73
Snowy Wreck One	3.60	47	4	47	49

Figure 31. Relationship between mean site-wide \bar{X} Slope and Fish Count. Small Fish $R^2 = 0.36$, Medium Fish $R^2 = 0.81$ Large Fish $R^2 = 0.97$, All Fish $R^2 = 0.70$.



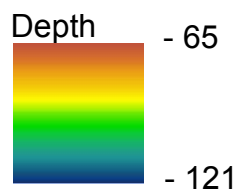
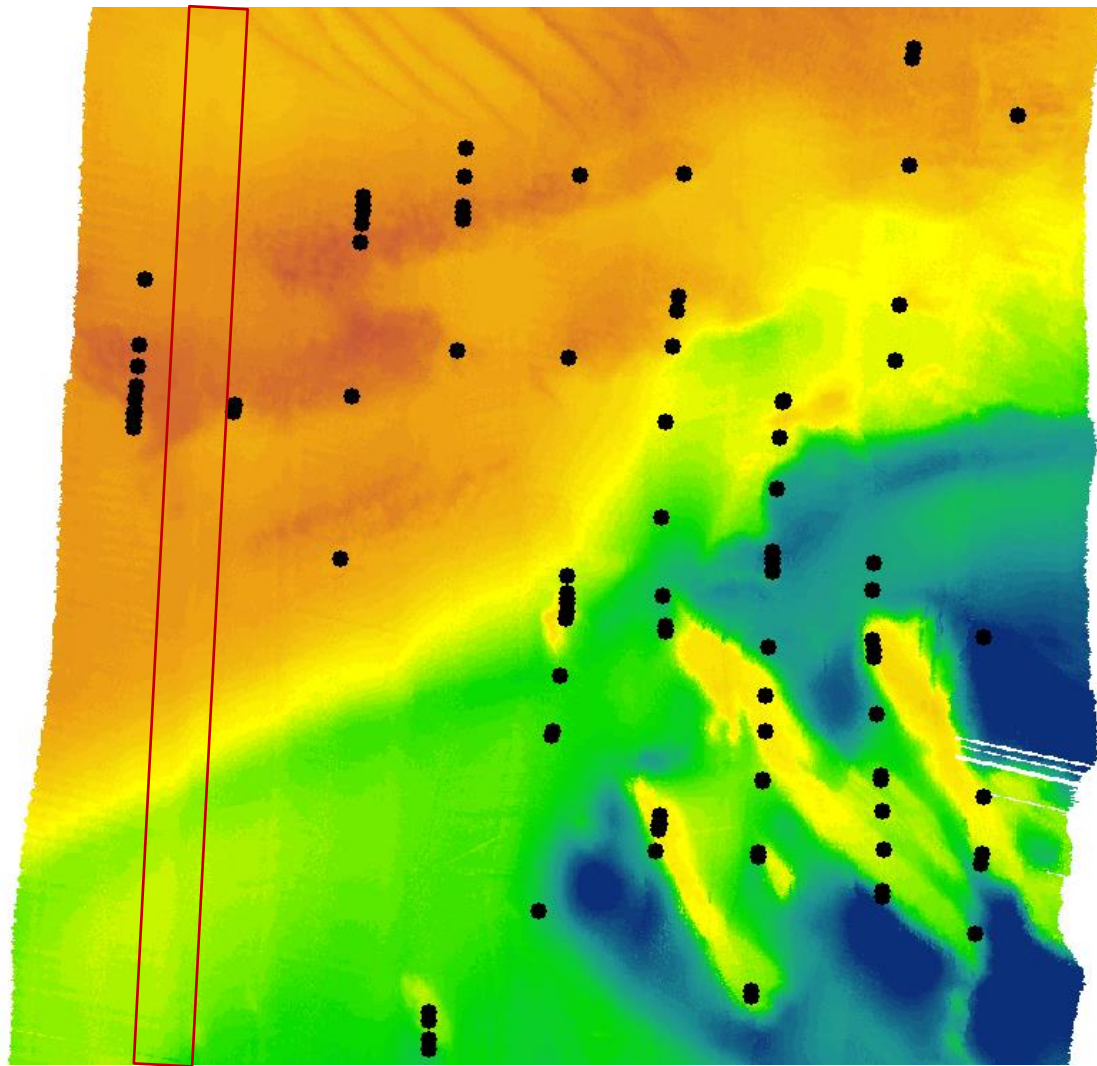
Site	\bar{X} Slope of Slope	All Fish	Large Fish	Medium Fish	Small Fish
Snowy Wreck Two	48.91	881	69	329	483
Cape Lookout Two	46.21	309	24	150	135
Cape Lookout One	46.61	263	39	124	100
N of Edisto MPA	34.09	214	7	26	181
North Carolina 780	41.34	127	9	44	73
Snowy Wreck One	33.94	47	4	47	49

Figure 32. Relationships between mean site-wide \bar{X} Slope of Slope and Fish Count. Small Fish $R^2 = 0.27$, Medium Fish $R^2 = 0.82$ Large Fish $R^2 = 0.90$, All Fish $R^2 = 0.61$.

ERROR ANALYSIS

BATHYMETRIC ARTIFACTS

Artifacts (false representations of the seafloor) along outer beams, due to refraction errors and a lack of accurate tide corrections, are visible in bathymetric raster data for each survey site. This is due to outer beams within the ME70 swath fan not receiving sufficient corrections applied in CARIS HIPS editors. Generally, data at nadir tends to be most accurate, while data in the outer beams must travel the furthest through the water column and is therefore most affected by variations in the sound velocity profile of the water column and temporal variation of mean sea-level height. Because these artifacts manifest themselves as actual differences in the depth map, false values for all derivative morphometric base layers are calculated and could factor in as cascading effects on explanatory variable performance in the final analysis. However, since we extracted 50 x 50 m grids that intersect with the track line at nadir, our final analysis only includes data +/- 50 m around nadir and remains unaffected by these artifacts appearing in the outer beams (Figure 33).



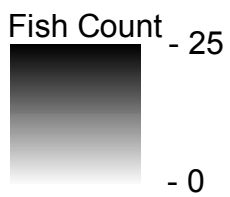
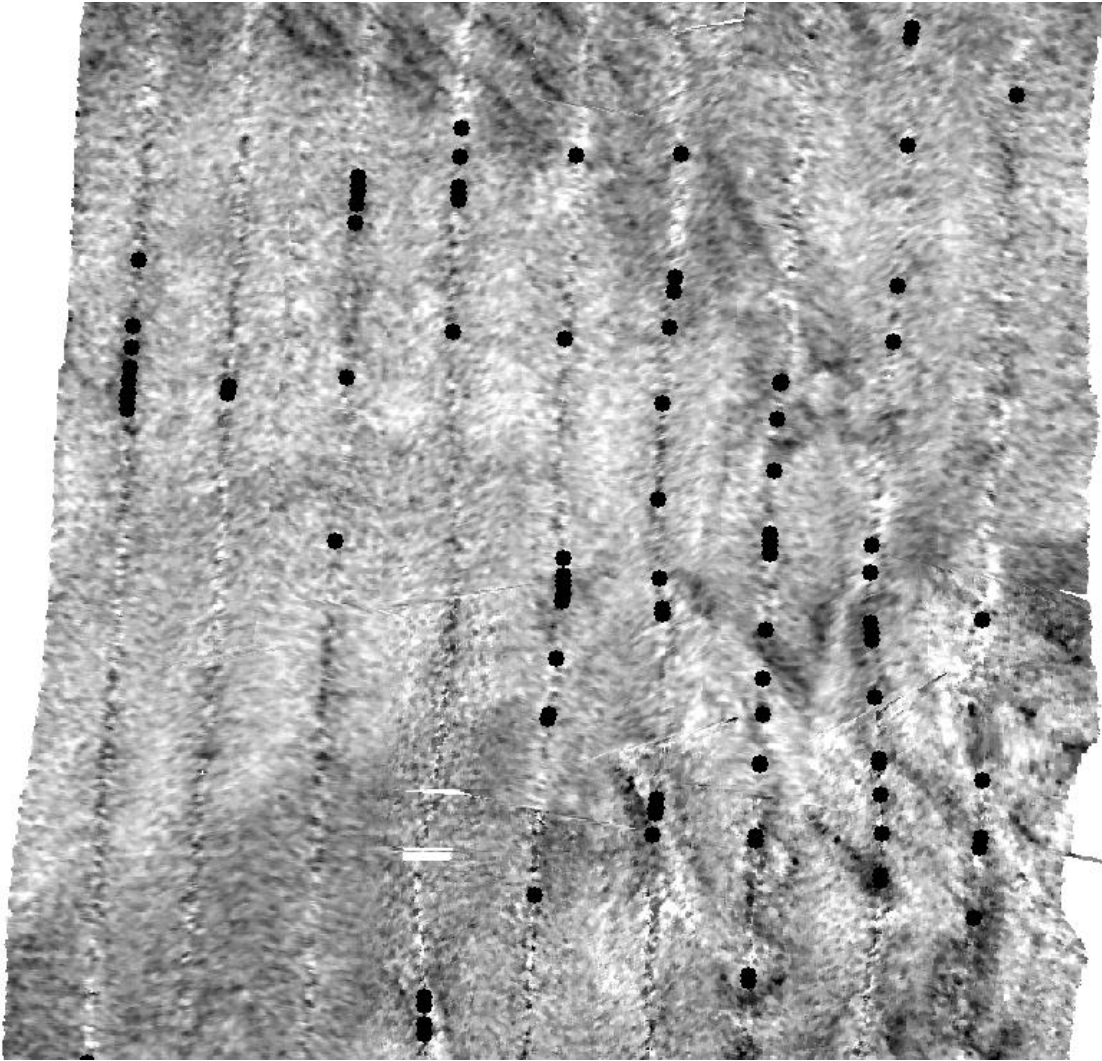
 Box Highlighting Error

 Fish Presences

Figure 33. Error in Bathymetry. The red box highlights refraction error at the outer beams of the ME70. Faint traces of this same type of error for each line can be seen in parallel across the map. Fish presences are recorded at nadir and thus remain unaffected by the error in the outer beams.

BACKSCATTER ARTIFACTS

Unlike bathymetry, backscatter data tends to suffer from the most noise occurring along the center of track lines at nadir (Figure 34). Since fish occurrences are recorded very close to nadir, the backscatter data directly beneath the fish is most often not representative of the true seabed surrounding the fish. Thus, the extracted 50 x 50 m grids are potentially strongly affected by this false data. To combat this potential affect on Mean Backscatter the Standard Deviation of Backscatter and Kurtosis was included. A 50 x 50 m grid area that only barely covers the center line of the ship track may have low Standard Deviation of Backscatter values. Conversely, an area that predominantly covers the area at nadir showed a high random variability in Backscatter values. Since either Standard Deviation or Kurtosis are not correlated with Mean Backscatter values and account for this variability, they may add explanatory power for the abundance of fish. Ultimately, the Standard Deviation of Backscatter and Kurtosis did not contribute to the overall model performance and Mean Backscatter alone emerged with a signal strong enough to contribute to the overall model performance as was seen in the Poisson regression outputs in Table 6.



• Fish Presences

Figure 34. Error in Backscatter. Here the error at nadir can be clearly seen in a stripe like pattern across the survey site. Fish presences are recorded at nadir and would presumably be heavily impacted by averaging backscatter values within a 50 x 50 m grid at nadir.

BIAS

There are three prominent biases in the sampling method used for this data. First, the discrepancy between area surveyed by the ME70 multibeam system and area surveyed by the EK60 split beam system is the greatest cause for bias in the data (Figure 35). Even though the dataset was subset into 50 x 50 meter grids to both approximate the swath covered by the EK60 and reef features in this area, some portions of the 50 x 50 m grid area likely to have remained un-surveyed by the EK60. This may have resulted in an underestimate of fish presences within each 50 x 50 meter grid and subsequent site-wide grid. Second, clustering, as observed by examining the presence of large fish in the SE section of Snowy Wreck Two seen in Figure 26 is unaccounted for by the Poisson regression at the 50 x 50 m scale and likely contributed to the overall lack-of-fit and low explanatory power of each model (Steele 2014). Finally, third, surveys were only conducted at night. Thus any inferences made about the fish-seascape relationship can only be made on nocturnal movement patterns, while diurnal movement patterns remain unexplored.

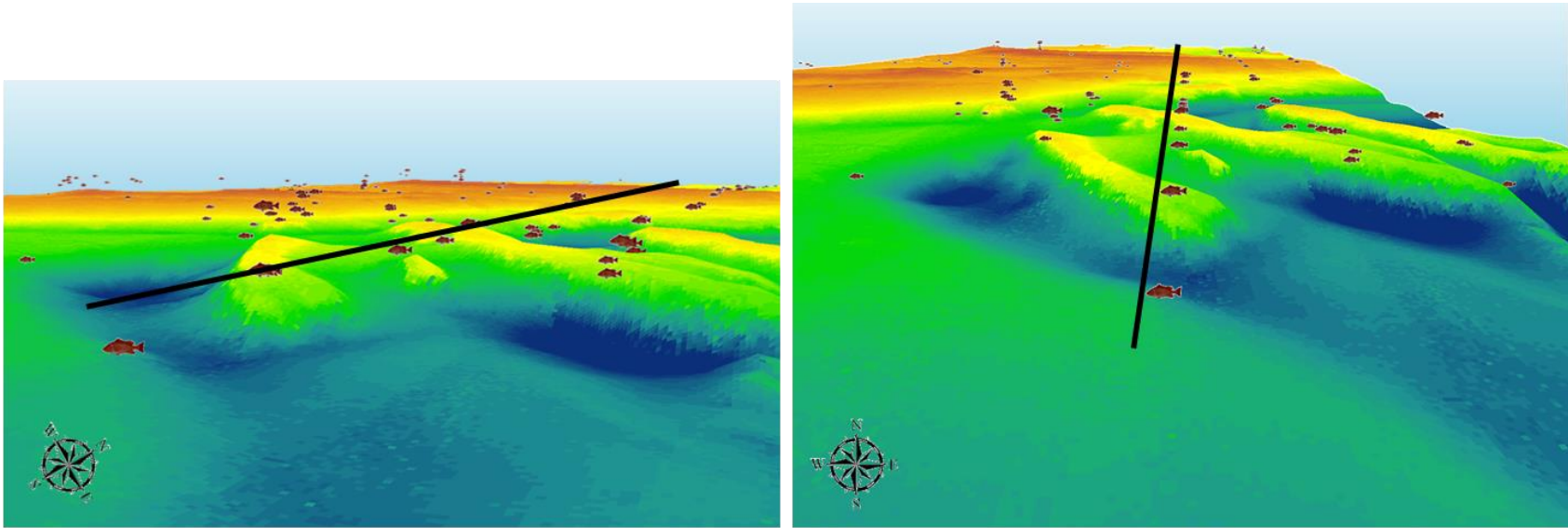


Figure 35. NW (left) and N (right) views of Large Fish sampled along track lines (black) across bathymetric surface at Snowy Wreck Two (VE = 2x). EK 60 sampling bias along track lines depicted in black becomes apparent in N view (right), yet no matter the view Large Fish presences coincide with prominent bottom features. Created in ESRI ArcScene. Knuth 2014.

DISCUSSION

At a high level, this study shows us two very important things. First, at different scales, different statistical methods (bivariate vs multivariate) are required based on the nature of the response. At a site-wide scale we had only six responses with respective fish counts being explained by the average value for a given explanatory value across the entire survey site. Using a multivariate regression approach here would have resulted in only \bar{X} Slope remaining as the final significant predictor variable. All other variables would have been dropped, due to insignificant P-values, as their contribution to the overall explanatory of the multivariate model performance was insignificant and overshadowed by \bar{X} Slope. Thus, even though these other variables showed a strong predictive relationship with the abundance of fish when plotted in a bivariate model, this information would have been lost in a multivariate model. At a 50 x 50 m grid scale, the nature of the response is few whole integers following a Poisson distribution and presented as counts. Plotting a simple bivariate exponential regression line here would attempt to plot thousands of continuous data points along the X axis for a given explanatory variable to only few (<30) fish counts within each 50 x 50 m grid along the Y axis. This results in an insignificant R^2 value and no correlation between explanatory variables and fish abundance would become apparent. For this reason a multivariate Poisson model was used to properly fit the response distribution and combine the explanatory power of candidate morphometric variables.

Second, \bar{X} Slope, \bar{X} Slope of Slope, and \bar{X} Backscatter emerged as the most significant variables contributing to overall multivariate model performance at the 50 x 50 m grid scale (Table 6). At the site-wide scale, \bar{X} Slope, \bar{X} Slope of Slope, σ Depth and \bar{X} Range \times \bar{X} Variety, emerged as the strongest bivariate contributors in explaining the variance in fish abundance (Figure 29 through Figure 32). \bar{X} Slope and \bar{X} Slope of Slope seem to be important variables, regardless the scale of analysis. σ Depth and \bar{X} Range \times \bar{X} Variety, appear to be significant contributors at a coarse site-wide scale, while at a fine 50 x 50 m scale \bar{X} Backscatter emerges as a more important variable than σ Depth or \bar{X} Range \times \bar{X} Variety. Given the understanding that different statistical methods were used, depending on the response, it is valid to make this comparison and attribute the relative importance to explanatory variables.

Finally, when comparing Figure 29 and Figure 30, it is interesting to note the similarity in σ Depth and \bar{X} Range \times \bar{X} Variety scatter plots at a site-wide scale. At the site-wide scale σ Depth (R^2 Medium Fish = 0.88) outperformed \bar{X} Range \times \bar{X} Variety (R^2 Medium Fish = 0.81), while at a 50 x 50 m scale, \bar{X} Range \times \bar{X} Variety emerged as the stronger contributing variable. σ Depth and \bar{X} Range \times \bar{X} Variety shared a VIF $>$ 7.5 during model selection. σ Depth was subsequently eliminated, because it had a lower Chi Square value, thus contributing less to the overall model performance. Both metrics describe the diversity in depth values across the seascape, which can be conceived of as a measure of topographic complexity. Because σ Depth outperformed \bar{X} Range \times \bar{X} Variety at the site-wide scale, while \bar{X} Range \times \bar{X} Variety outperformed σ Depth at the 50 x 50 m scale, both variables should be included in future modeling attempts, as one may hold greater explanatory power than the other, given the scale.

CONCLUSIONS

This work aligns with mandates set forth by the Magnuson-Stevens act to present data on the South Atlantic fishery in the form of maps and for these to be analyzed in a GIS. 106 unique maps were created, describing the morphometric nature of the seafloor and distribution of fish in various size classes across the seascape. A complete catalogue of these maps can be seen in Appendix A and Appendix B. This qualitative data will hopefully provide managers with new fisheries information and aid in future management decisions. Quantitative relationships were explored in the GIS and presented in the form of statistical outputs. These results were presented in the Results section of this work. Research objectives for this study were met as follows:

1. Collect and process water column, bathymetric and backscatter data for potential habitat sites along the U.S. South Atlantic continental shelf.
 - 10 Sites surveyed during 2014 cruise aboard the NOAA Ship *Pisces*
 - 205 km² of Bathymetry and Backscatter acquired and processed.
 - 7401 Fish Counts acquired and processed.
 - Backscatter and bathymetry images of the seafloor provide direct information about relative hard and soft bottom as well as the topographic nature of the seascape and can be used in preliminary qualitative visual habitat assessments.

2. Provide a morphometric characterization and quantitative assessment of fish populations present within each survey site.

- Seven Base Layers created for 10 sites (70 total) that describe the morphometric nature of the seafloor in the form of maps (Appendix A).
- Small, medium and large fish distributions mapped across bathymetry at six survey sites, for a total of 36 maps (Appendix B).
- Visual correlations and clustering allow for qualitative assessment of fish populations by size class across each survey site.

3. Identify morphometric features of the bathymetry that may explain the presence of demersal fish.

- 14 explanatory morphometric variables created at the site-wide and 50 x 50 m grid scale
- Fish responses generated for all, small, medium and large fish counts
- Statistically analyzed the fish-seascape relationship at the site-wide and 50 x 50 m scale
 - Slope \bar{X} , Slope of Slope \bar{X} and Depth σ are important explanatory variables at the site-wide scale
 - Slope \bar{X} , Slope of Slope \bar{X} and Backscatter \bar{X} are important explanatory variables at the 50 x 50 m scale
- Site-wide models are most useful here in understanding the direct relationships between morphometric variables and fish counts. The high bivariate model R^2 values suggest that this form of analysis may be used to evaluate MPA performance, better understand fishing pressures outside MPA boundaries and aid in identifying future Essential Fish Habitat for demersal fish species.

- The 50 x 50 m scale captures the patchy nature of reefs along the southeast Atlantic continental shelf and allows for ecological inferences to be made, revealing Backscatter \bar{X} as an important explanatory variable. The transitional scale at which Backscatter \bar{X} becomes more important than the overall Depth σ remains to be determined in future analyses at various spatial scales.

FUTURE WORK

ANALYSIS AT VARIOUS SPATIAL SCALES

Different scales require different statistical approaches. At a site-wide scale we used a bivariate exponential regression line to model the relationship between fish and morphometrics, while at the 50 x 50 m scale we used a multivariate generalized linear Poisson regression to model fish-seascape relationships. These statistical tools are chosen based on the nature of the response, as illustrated in the Methods section and discussed in the Discussion section. Depth σ emerged as the more significant bivariate predictor at the site-wide scale, while at the 50 x 50 m grid scale, Backscatter \bar{X} was the more important contributor to multivariate model performance. This indicates that further analysis is required at various spatial scales to better understand the transitional scale range at which Backscatter \bar{X} becomes more important than Depth σ . Analysis at the 20 m, 50 m, 100 m, 250 m, 500 m, 1 km and site-wide scale are suggested. Depending on the nature of the response, each scale may require a different statistical approach. Slope \bar{X} and Slope of Slope \bar{X} are likely to remain as the two most important variables throughout, while the scale at which Backscatter \bar{X} becomes more important than Depth σ is to be determined. A logical algorithmic succession of models developed at various spatial scales could potentially lead to very accurate future fish population predictions.

SITE-WIDE MODEL VALIDATION

The models describing the site-wide relationship between fish abundance and seafloor morphometrics can be used to make cautious predictions on the relative abundance of fish counts between sites that were not surveyed by the EK60. The four sites without fish data are Bull's Scarp, Charleston Deep Artificial Reef MPA, North of North Florida MPA and South of North Florida MPA (Figure 36). If water column data for these sites is collected at a future data, it would be interesting to explore how well the site-wide model predicts counts at each site.

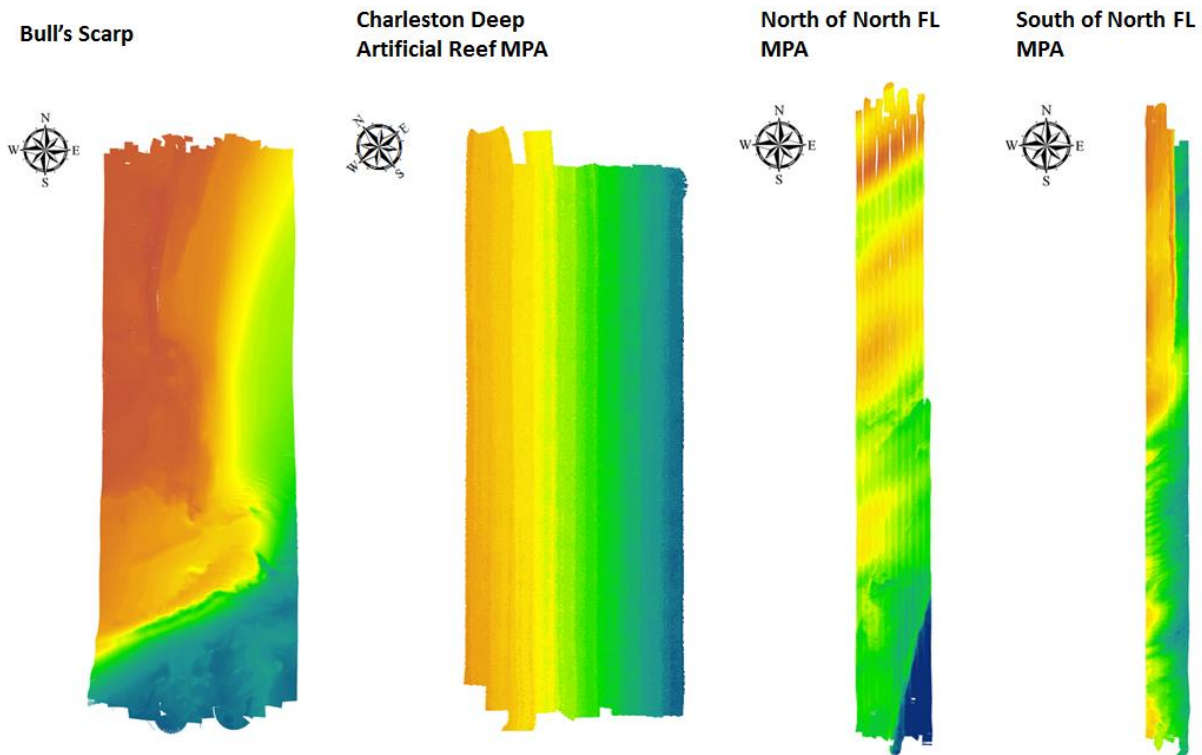


Figure 36. Survey sites without EK60 water column data. Sites not depicted to scale.

SEAFLOOR CLASSIFICATION

In the US Virgin Islands NOAA's Biogeography Branch has conducted a successful seafloor classification by examining the principal components that distinguish different seafloor habitats and are derived from seafloor morphometrics (Costa, et al. 2009). This type of effort, combining ROV surveys, acoustic seafloor and water column mapping is needed within the southeast Atlantic fishery to better map and characterize Essential Fish Habitat. In the past, stock assessments have focused on visually assessing single species distributions using ROVs and mapping the seafloor while ignoring acoustic water column data. Combining visual habitat assessments with classified seascapes and acoustically measured fish presences within the water column will provide a more complete picture of fish habitat throughout the southeast Atlantic and hopefully aid in effective marine spatial planning efforts by the SAFMC.

RECOMMENDATIONS

Acoustic surveys of fish abundance allow for rapid fishery ecosystem assessment, compared to conventional SCUBA, ROV and trawl methods (Costa, et al. 2014). On average, 20 km² of bathymetry were surveyed by the ME70 MBES in a single night. The area surveyed by the EK60 SBES was only a fraction of that. The ME70 system on the *Pisces* is scheduled to be equipped with the complete SIMRAD bathymetry package in early 2015 and will be able to acquire both bathymetric and water column data simultaneously. Once this upgrade has taken place, the average entire 20 km² of seafloor surveyed on given night will contain data for both bathymetry and fish abundance. This will provide baseline datasets for comprehensive training and evaluation of future models. With presence/absence modeling techniques conducted at multiple spatial scales and the augmentation of the water column datasets through acquisition by the ME70 MBES, future modeling approaches will better explain the spatial variance in fish

abundances and contribute to the effective planning and execution of fisheries surveys. Seafloor morphometrics identified here can be integrated in future modeling to help identify Essential Fish Habitat.

Acoustic surveying using the ME70 MBES for bathymetry and water column data collection is a promising method for rapid, sequential and comprehensive ecosystem assessment. Data collected in this study represents a mere snapshot in time of fish-seascape interactions. Because diurnal and nocturnal fish movement patterns change (Sedberry and Van Dolah 1984), acquiring a time-series dataset at Snowy Wreck Two would be valuable to better understand temporal variability. Snowy Wreck Two displays the greatest abundance of fish in all size classes per km² and provides a strong baseline for modeling fish site fidelity. A monthly, 24 hour survey, split into two 12 hour sections, each covering the same area is suggested. This survey is to be repeated monthly or quarterly, at the height of temperate seasons in the northern hemisphere. Training and evaluating models on such a dataset can potentially be applied to predictions of fish abundances across the southeast Atlantic. Once an acceptable model has been generated, predictive habitat maps can be created upon existing bathymetry and backscatter data, to aid in the planning and execution of successful future stock assessment surveys, and ultimately supply the SAFMC with stronger evidence for place-based management strategies.

REFERENCES

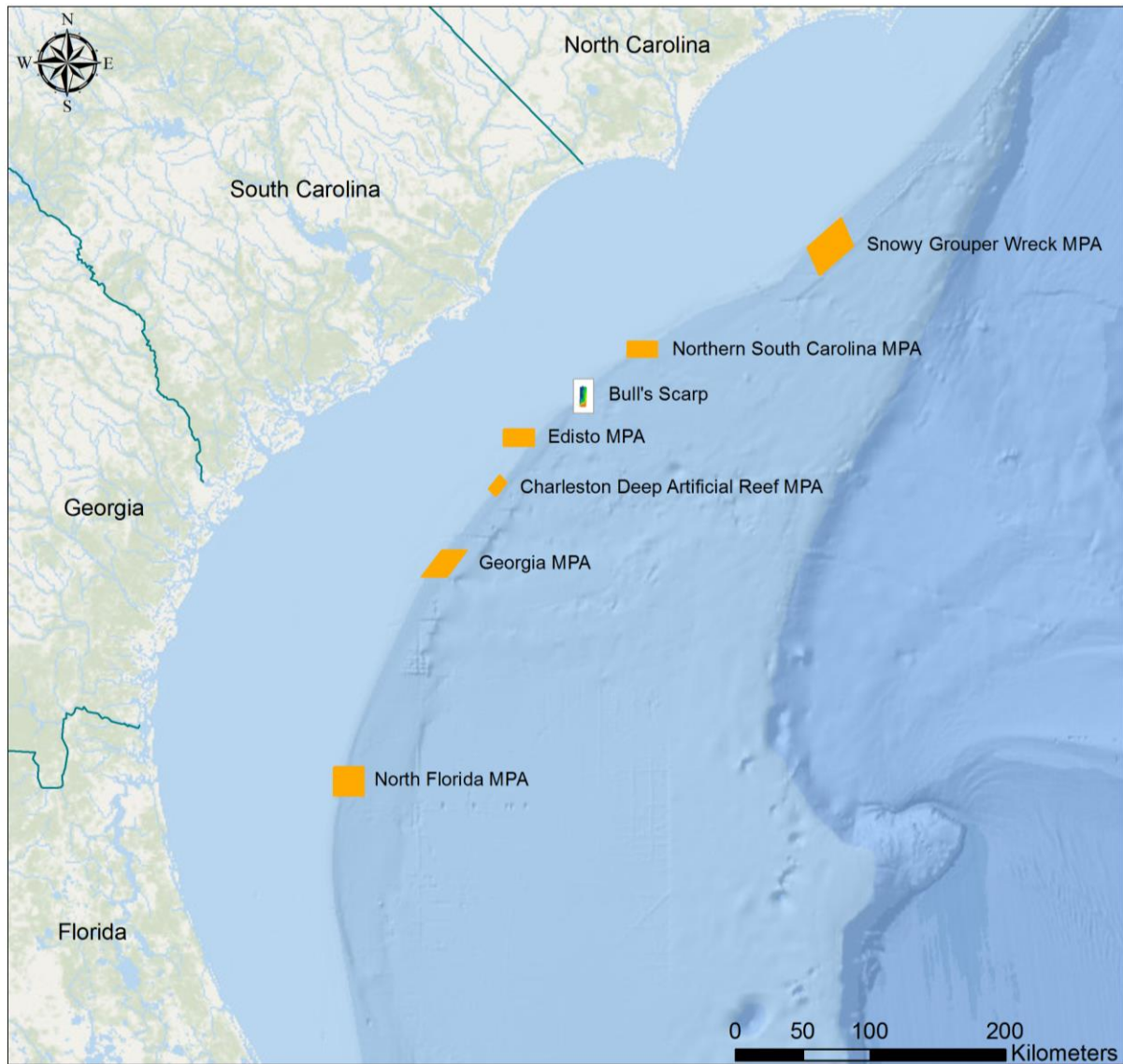
- Abesamis, Rene A., and Garry R. Russ. "Density-dependent spillover from marine reserve: long-term evidence." *Ecological applications* 15, no. 5 (2005): 1798-1812.
- Beverton, Raymond J.H., and Sydney J. Holt. *On the dynamics of exploited fish populations*. London: Chapman & Hall, 1957.
- Brown, Craig J., Stephen J. Smith, Peter Lawton, and John T. Anderson. "Benthic habitat mapping: A review of progress towards improved understanding." *Estuarine, Coastal and Shelf Science* 92, no. 4 (2011): 598 - 606.
- Christie, Mark R., et al. "Larval connectivity in an effective network of marine protected areas." *PloS one* 5, no. 12 (2010): e15715.
- Costa, Bryan M., Lauria J. Bauer, Timothy A. Battista, Peter W. Mueller, and Mark E. Monaco. "Moderate-Depth Benthic Habitats of St. John, U.S. Virgin Islands." *NOAA Technical Memorandum NOS NCCOS*, 2009: 57 pp.
- Costa, Bryan, J. Christopher Taylor, Laura Kracker, Tim Battista, and Simon Pittman. "Mapping Reef Fish and the Seascape: Using Acoustics and Spatial Modeling to Guide Coastal Management." *PloS one* 9, no. 1 (2014): e85555.
- Cutter, George R., Laurent Berger, and David A. Demer. "A comparison of bathymetry mapped with the Simrad ME70 multibeam echosounder operated in bathymetry and fisheries modes." *ICES Journal of Marine Science*, 2010: 1301-1309.
- Eggleston, David B., and Darren M. Parsons. "Disturbance-induced 'spill-in' of Caribbean spiny lobster to marine reserves." *Marine Ecology Progress Series*, no. 371 (2008): 213-220.
- ESRI. *Interpreting Exploratory Regression results*. 04 18, 2013.
<http://resources.arcgis.com/en/help/main/10.1/index.html#//005p00000052000000> (accessed 11 16, 2014).
- Favali, Paolo, Roland Person, Chris R. Barnes, Yoshiyuki Kaneda, John R. Delaney, and ShuKun Hsu. "Seafloor observatory science." *OceanObs'09*. Venice: ESA Publication, 2010. 21-25.
- Fishery Councils. *US Regional Fishery Management Councils*. 05 09, 2013.
www.fisherycouncils.org (accessed 11 24, 2014).

- Flom, Peter Leslie. *Multicollinearity diagnostics for multiple regression: A Monte Carlo Study*. Thesis Dissertation, New York: Fordham University, 1999, 1-149.
- Foote, Kenneth. "Linearity of fisheries acoustics, with addition theorems." *The Journal of the Acoustical Society of America*, 1983: 1932 - 1940.
- Gerber, Leah R., Selina S. Heppell, Ford Ballantyne, and Enric Sala. "The role of dispersal and demography in determining the efficacy of marine reserves." *Canadian Journal of Fisheries and Aquatic Sciences* 62, no. 4 (2005): 863-871.
- Grüss, Arnaud, David M. Kaplan, Sylvie Guénette, Callum M. Roberts, and Louis W. Botsford. "Consequences of adult juvenile movement for marine protected areas." *Biological Conservation* 144, no. 2 (2011): 692-702.
- Harter, Stacey L., Marta M. Ribera, Andrew N. Shepard, and Reed John K. "Assessment of fish populations and habitat on Oculina Bank, a deep-sea coral marine protected area off eastern Florida." *Fishery Bulletin* 107, no. 2 (2009): 195-206.
- Hashimoto, Takafumi. *Equipment for hydrographic survey*. 06 15, 2013. <http://ccom.unh.edu/gebco2013/survey.html> (accessed 10 30, 2014).
- Jeness, Jeff. *DEM Surface Tools*. Flagstaff, AZ, May 13, 2013.
- Kendall, M. S., et al. *Benthic Habitats of Gray's Reef*. Technical Report, Silver Spring, Maryland: NOAA/National Ocean Service/National Centers for Coastal Ocean Science/Center for Coastal Monitoring and Assessment, 2003.
- Kendall, Matthew S., Laurie J. Bauer, and Christopher F.G. Jeffrey. *Characterization of the benthos, marine debris and bottom fish at Gray's Reef National Marine Sanctuary*. Technical Memorandum, Silver Spring: NCCOS NOAA, 2007.
- Kongsberg Maritime, AS. *Technology for Sustainable Fisheries*. 09 01, 2014. <http://www.simrad.com/me70> (accessed 10 30, 2014).
- Kracker, L M, J C Taylor, E F Ebert, Battista T A, and Menza C. "Integration of fisheries acoustics surveys and bathymetric mapping to characterize midwater-seafloor habitats of US Virgin Islands and Puerto Rico." *NOAA Technical Memorandum*, 2010: 130-144.
- Kracker, Laura, Matt Kendall, and Greg McFall. "Benthic features as a determinant for fish biomass in Gray's Reef National Marine Sanctuary." *Marine Geodesy* 31, no. 4 (2008): 267-280.
- Magnuson-Stevens. *Magnuson-Stevens Fishery Conservation and Management Act*. Washington D.C., January 12, 2007.
- NOAA. *NOAA Ship Pisces*. 09 17, 2013. <http://www.moc.noaa.gov/pc/> (accessed 10 30, 2014).

- Pittman, Simon J, Bryan M. Costa, and Tim A. Battista. "Using lidar bathymetry and boosted regression trees to predict the diversity and abundance of fish and corals." *Journal of Coastal Research*, 2009: 27-38.
- Russ, Garry R., Angel C. Alcala, Aileen P. Maypa, Hilconida P. Calumpong, and Alan T. White. "Marine reserve ebenefits local fisheries." *Ecological applications* 14, (2004): 597-606.
- SAFMC. *Essential Fish Habitat*. 06 18, 2013. <http://www.safmc.net/ecosystem-management/essential-fish-habitat> (accessed 11 19, 2014).
- SAFMC, *MPA Information Page*. 06 18, 2013. <http://safmc.net/MPAInformationPage> (accessed 10 30, 2014).
- SAFMC/SEAMAP/MARMAP. *SAFMC Habitat and Ecosystem Viewer*. 09 01, 2014. http://ocean.floridamarine.org/safmc_atlas/ (accessed 10 30, 2014).
- SAMFC, *Snapper Grouper Page*. 06 18, 2013. safmc.net/resource-library/snapper-grouper (accessed 11 24, 2014).
- Sedberry, George R., and Robert F. Van Dolah. "Demersal fish assemblages associated with hard bottom habitat in the South Atlantic Bight of the USA." *Environmental Biology of Fishes* 11, no. 4 (1984): 241-258.
- Steele, Brian. *Chapter 16: Log-linear regression for Poisson counts*. 11 24, 2014. www.math.umt.edu/steele/STAT542/Chapter%2016-542.pdf (accessed 11 24, 2014).
- U.S. Geological Survey. *The North American Atlas*. 10 30, 2014. <http://nationalatlas.gov/atlasftp-na.html> (accessed 10 30, 2014).
- United Nations. *United Nations Conference on the Law of the Sea*. Memorandum, Geneva Switzerland: Unite Nations, 1958.
- University of Massachusets. *The Poisson Distribution*. August 24, 2007. <http://www.umass.edu/wsp/resources/poisson/> (accessed November 17, 2014).
- White, J. Wilson, Louis W. Botsford, Marissa L. Baskett, Lewis A.K. Barnett, R. Jeffrey Barr, and Alan Hastings. "Linking models with monitoring data for assessing performance of no-take marine reserves." *Frontiers in Ecology and the Environment* 9 (2011): 390-399.
- Williams, I. D., W. J. Walsh, J. T. Claisse, B. N. Tissot, and K. A. Stamoulis. "Impacts of a Hawaiian marine protected area network on the abundance and fishery sustainability of the yellow tang *Zebrasoma flavescens*." *Biological Conservation* 142, no. 5 (2009): 1066-1073.

APPENDIX A, MORPHOMETRICS

BULL'S SCARP



Legend

- State Boundaries
- Survey Site Bull's Scarp
- Marine Protected Areas (MPAs)

Friedrich Knuth (c)
College of Charleston
2014

Source: SAFMC online GIS database, NOAA,
SEAMAP, MARMAP, ESRI (base layer)

Coordinate System: WGS 1984 Web Mercator

Figure 37. Location of Bull's Scarp survey site relative to existing MPAs.

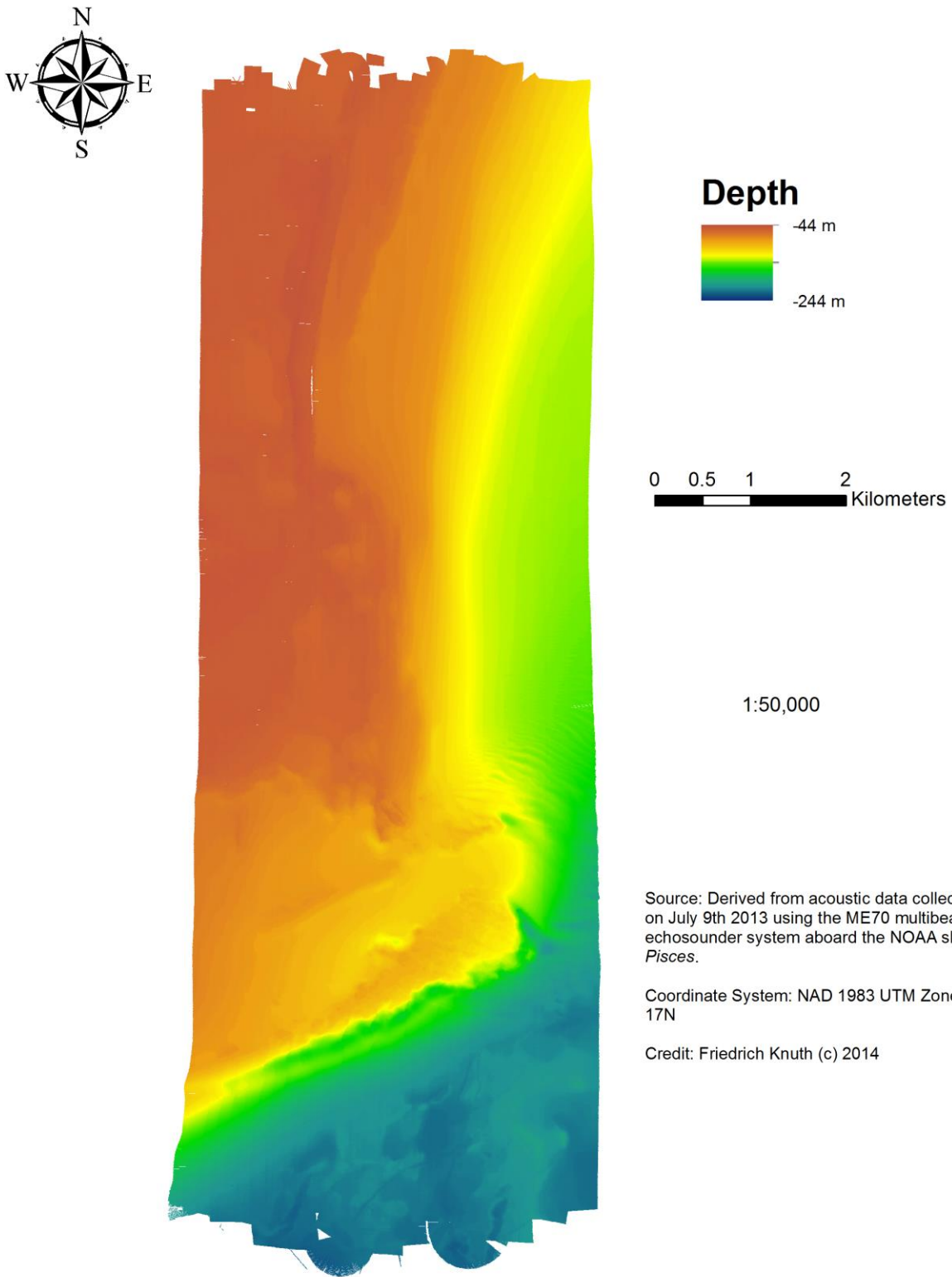
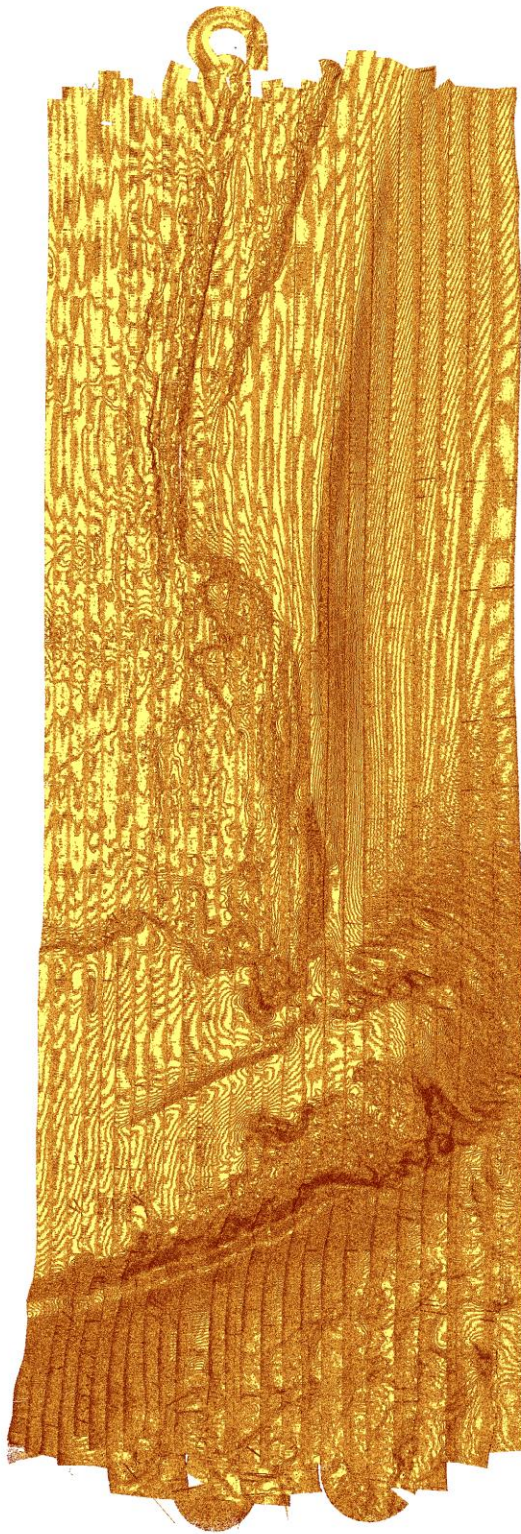


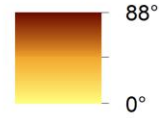
Figure 38. Depth of sea level to seafloor at Bull's Scarp.



Figure 39. Maximum rate of change in depth between 2 x 2 m raster cell and eight neighbors at Bull's Scarp.



Slope of Slope



1:50,000

Source: Derived from acoustic data collected on July 9th 2013 using the ME70 multibeam echosounder system aboard the NOAA ship *Pisces*.

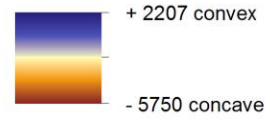
Coordinate System: NAD 1983 UTM Zone 17N

Credit: Friedrich Knuth (c) 2014

Figure 40. Maximum rate of change in slope between cell and eight neighbors at Bull's Scarp.



Plan Curvature



1:50,000

Source: Derived from acoustic data collected on July 9th 2013 using the ME70 multibeam echosounder system aboard the NOAA ship *Pisces*.

Coordinate System: NAD 1983 UTM Zone 17N

Credit: Friedrich Knuth (c) 2014

Figure 41. Rate of change in curvature across the surface at Bull's Scarp.

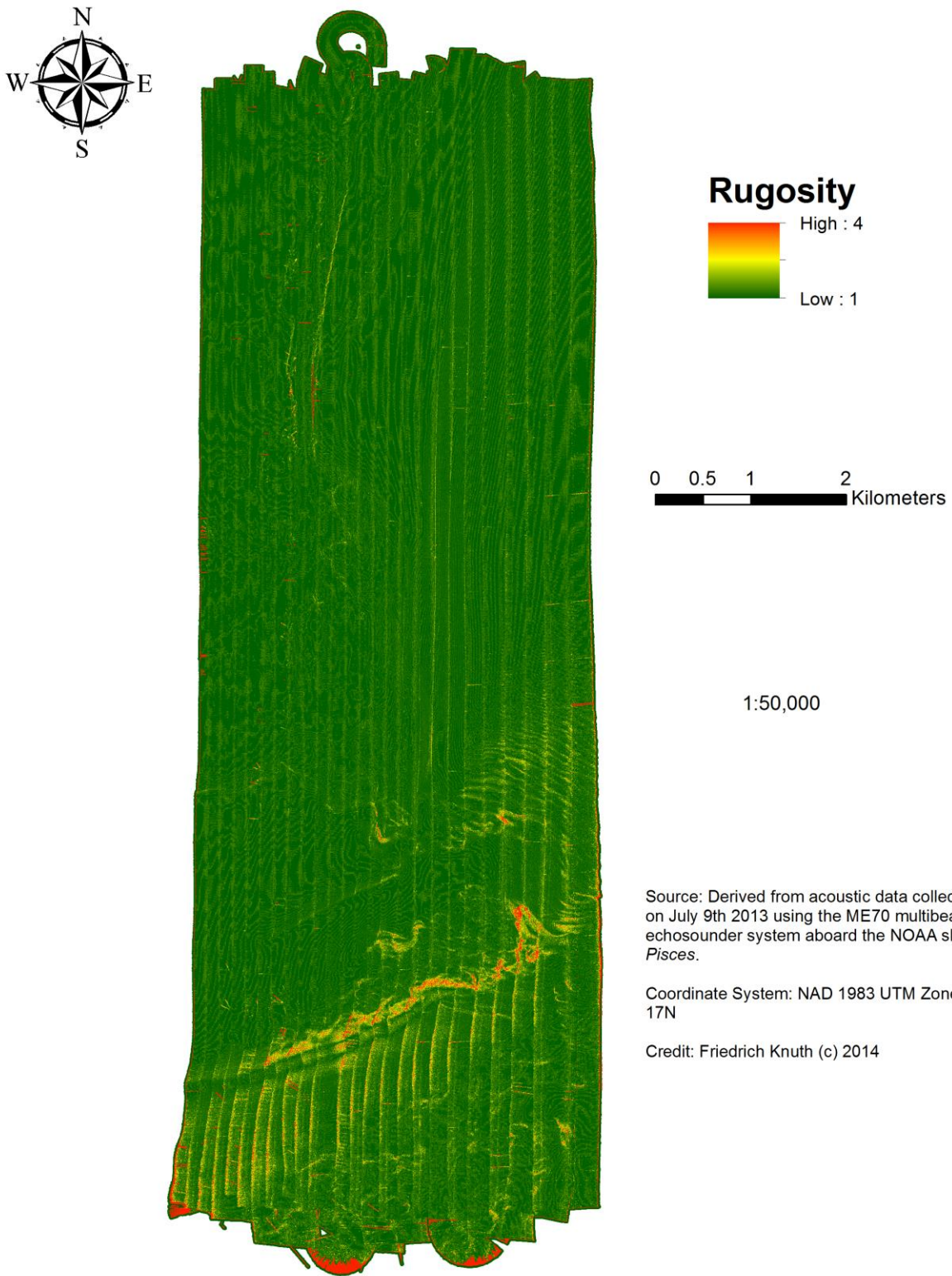


Figure 42. Ratio of surface area to planar surface area at Bull's Scarp.

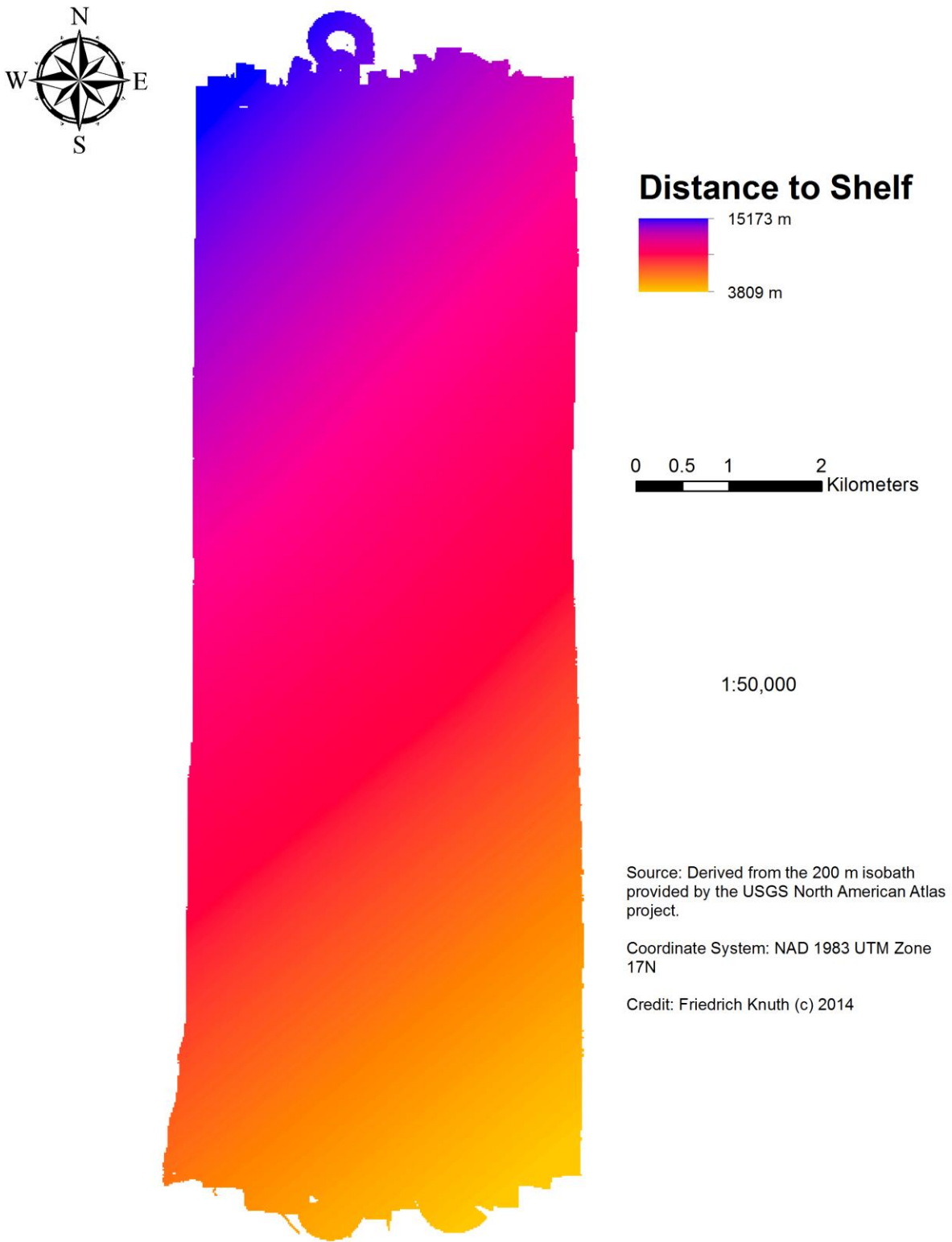


Figure 43. Distance of each 2x2 m raster cell to 200 m isobaths at Bull's Scarp.

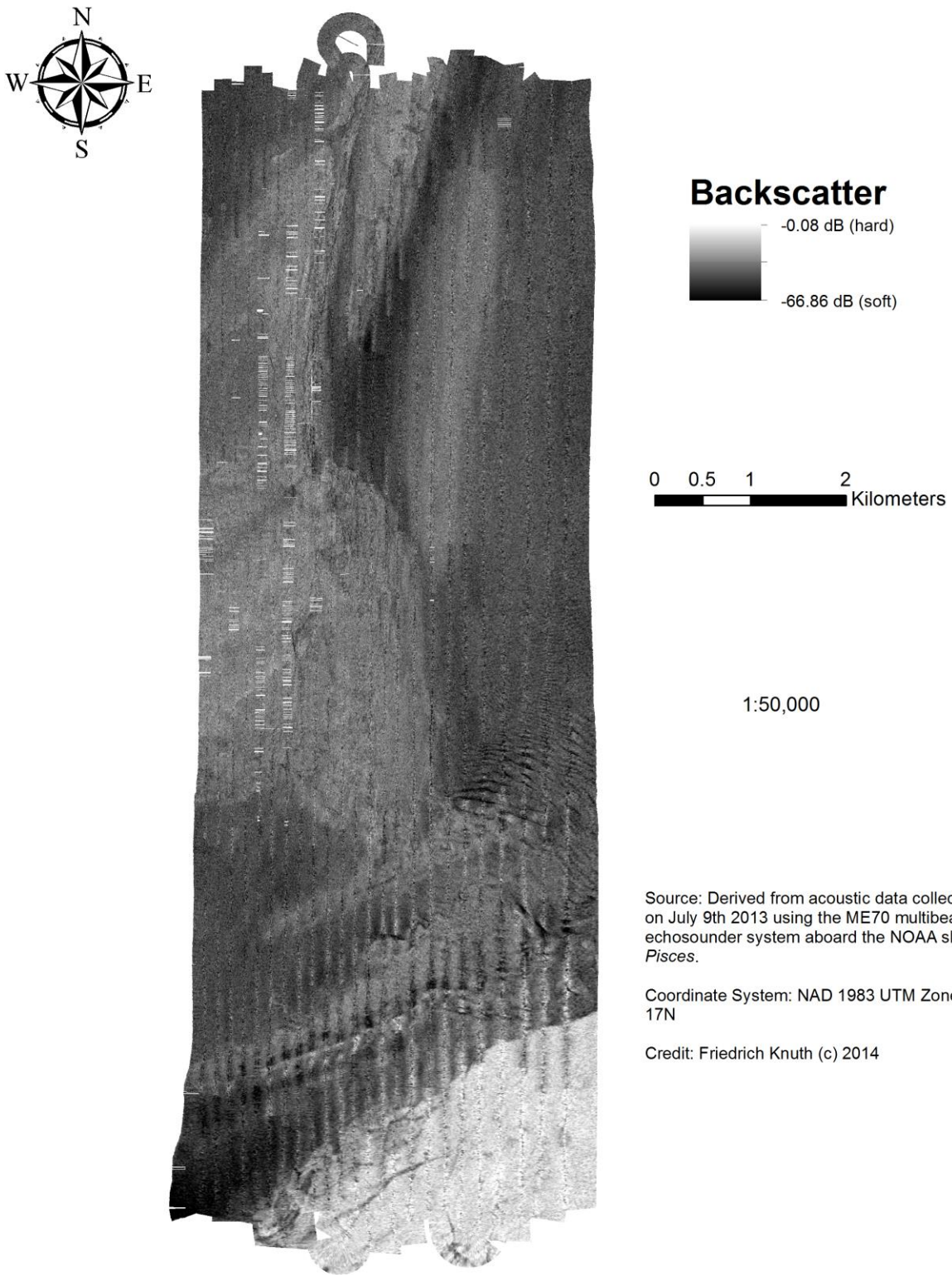
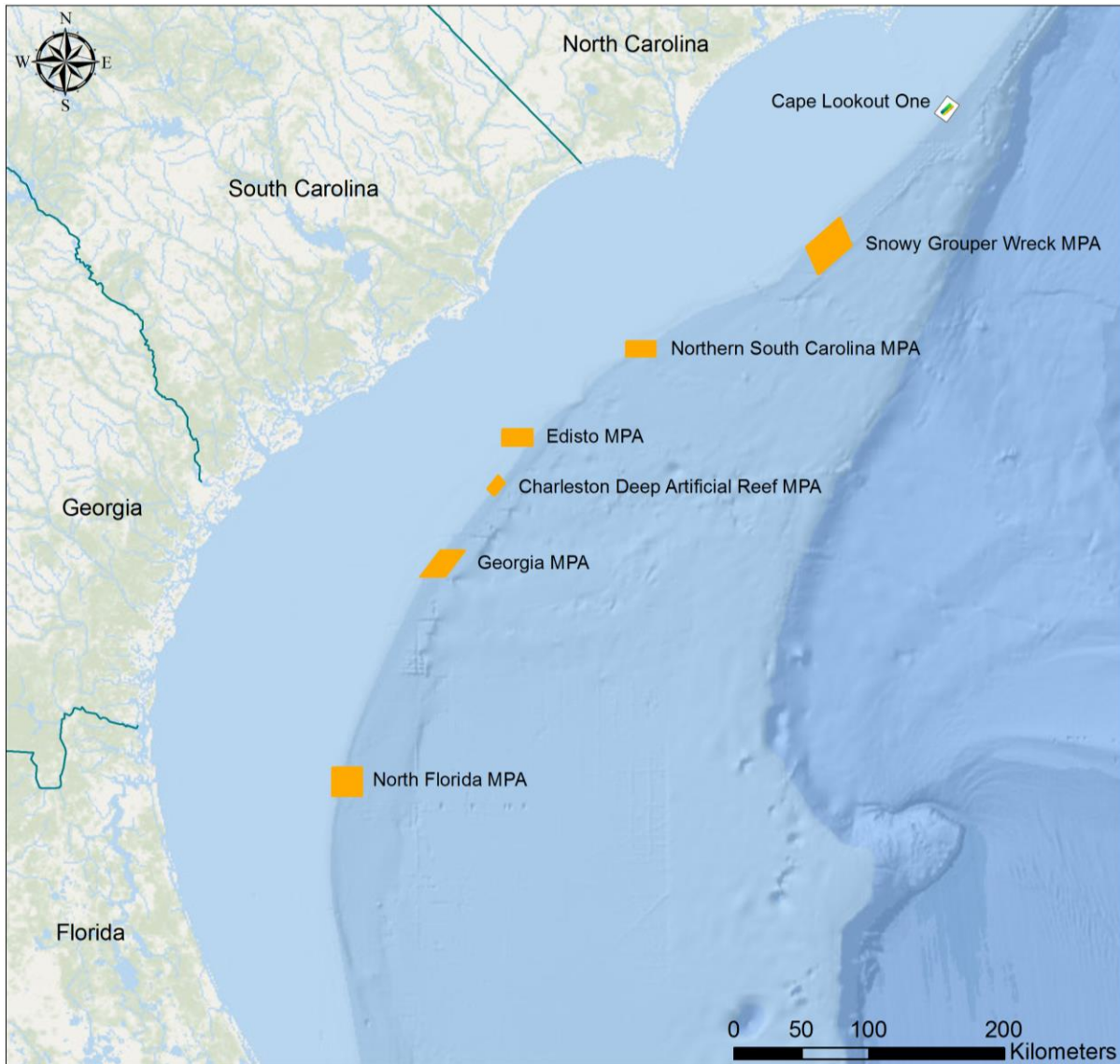


Figure 44. Intensity of the acoustic return at Bull's Scarp.

CAPE LOOKOUT ONE



Legend

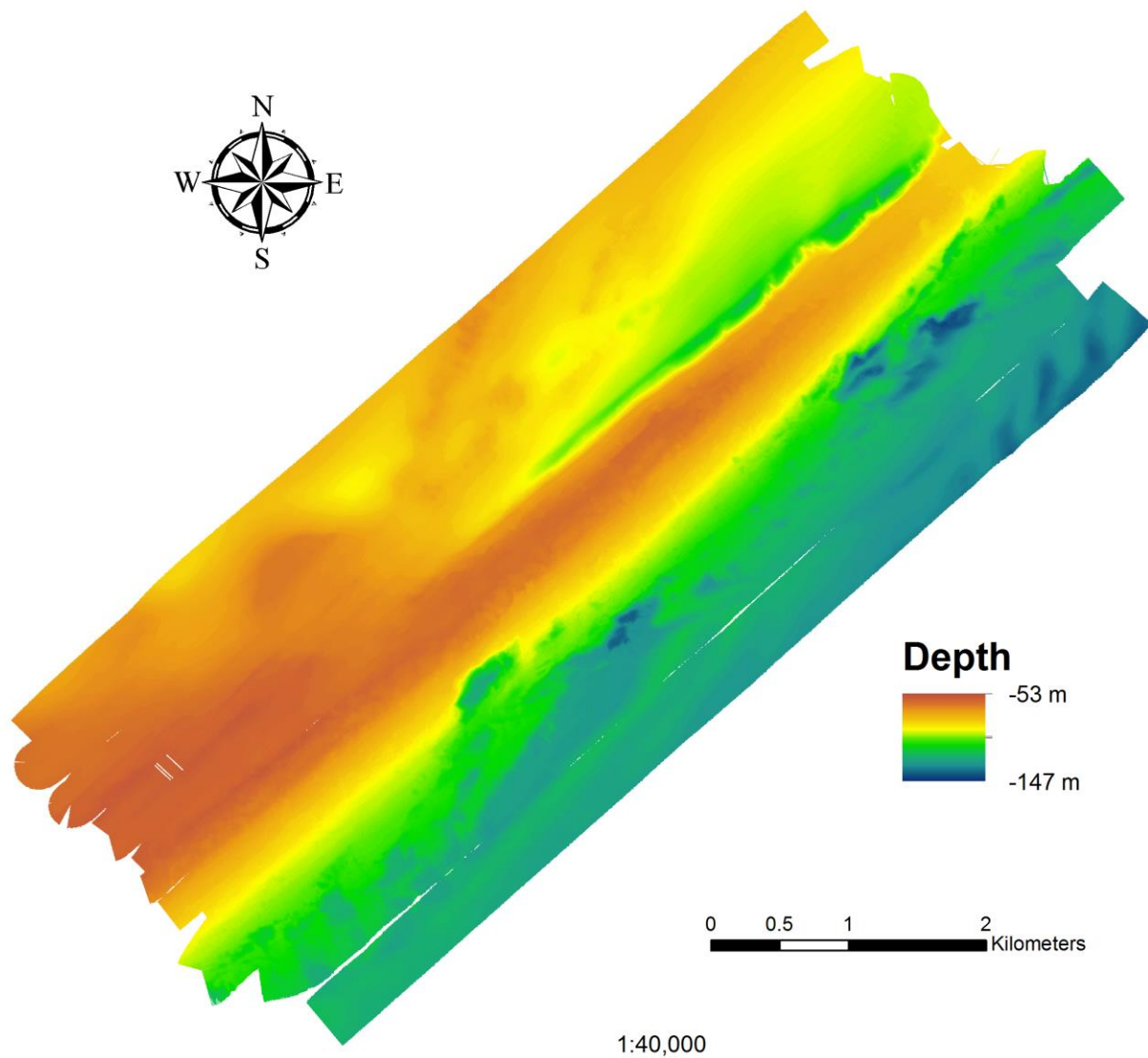
-  State Boundaries
-  Survey Site Cape Lookout One
-  Marine Protected Areas (MPAs)

Friedrich Knuth (c)
College of Charleston
2014

Source: SAFMC online GIS database, NOAA,
SEAMAP, MARMAP, ESRI (base layer)

Coordinate System: WGS 1984 Web Mercator

Figure 45. Location of Cape Lookout One survey site relative to existing MPAs.

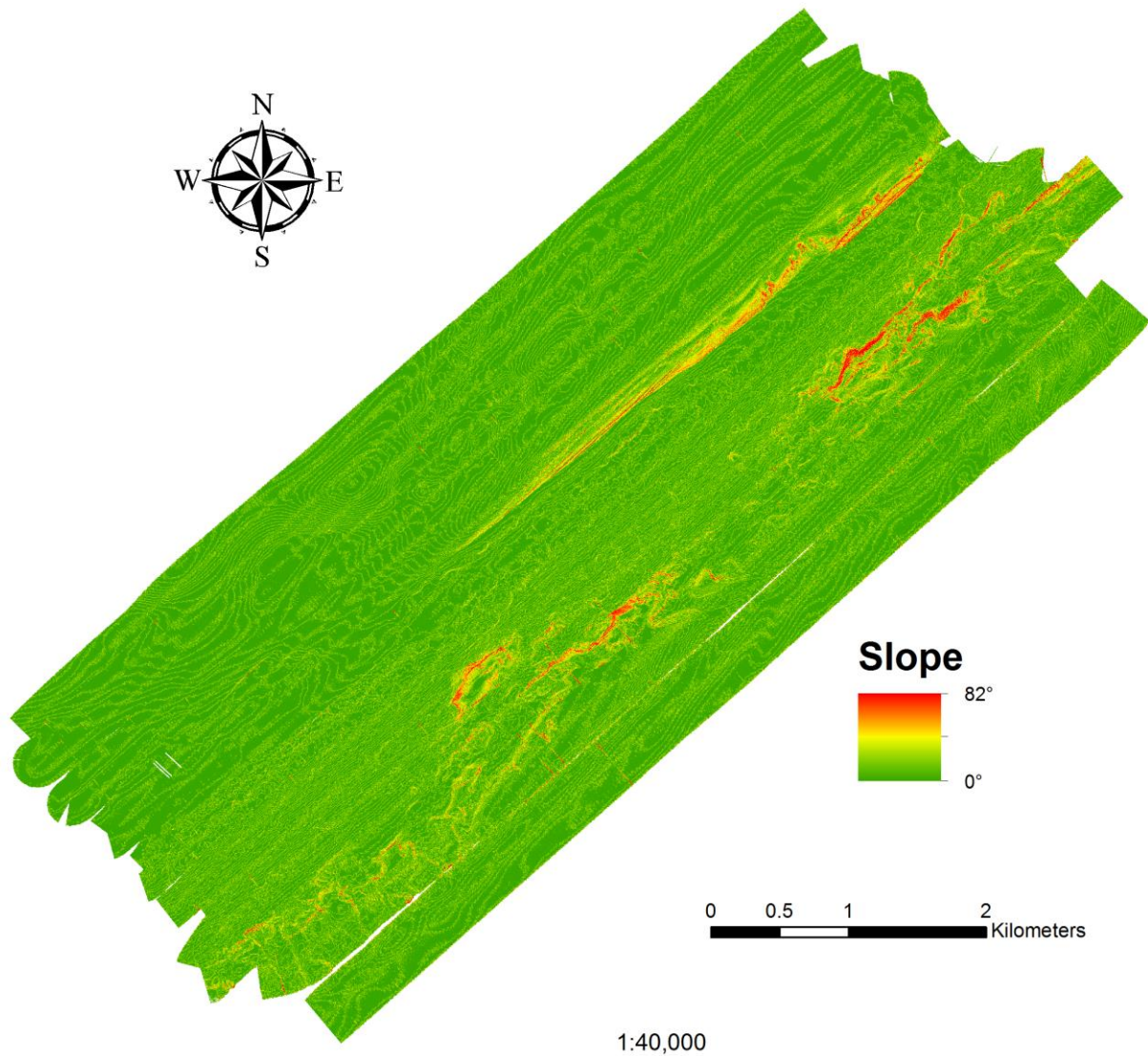


Source: Derived from bathymetric data collected on July 7th 2013 using the ME70 multibeam echosounder system aboard the NOAA ship *Pisces*.

Coordinate System: NAD 1983 UTM Zone 18N

Credit: Friedrich Knuth (c) 2014

Figure 46. Depth of sea level to seafloor at Cape Lookout One.

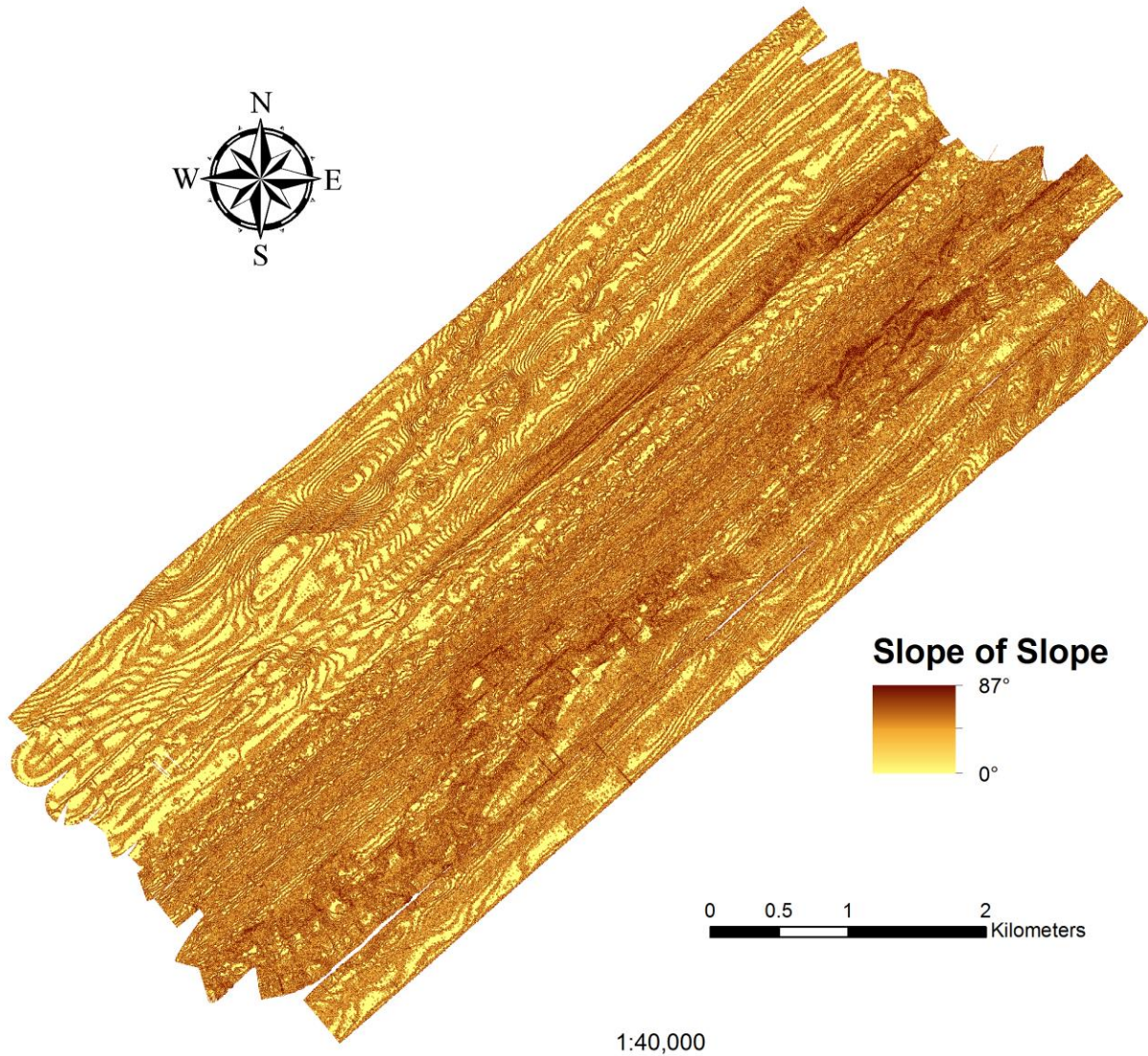


Source: Derived from bathymetric data collected on July 7th 2013 using the ME70 multibeam echosounder system aboard the NOAA ship *Pisces*.

Coordinate System: NAD 1983 UTM Zone 18N

Credit: Friedrich Knuth (c) 2014

Figure 47. Maximum rate of change in depth between 2 x 2 m raster cell and eight neighbors at Cape Lookout One.

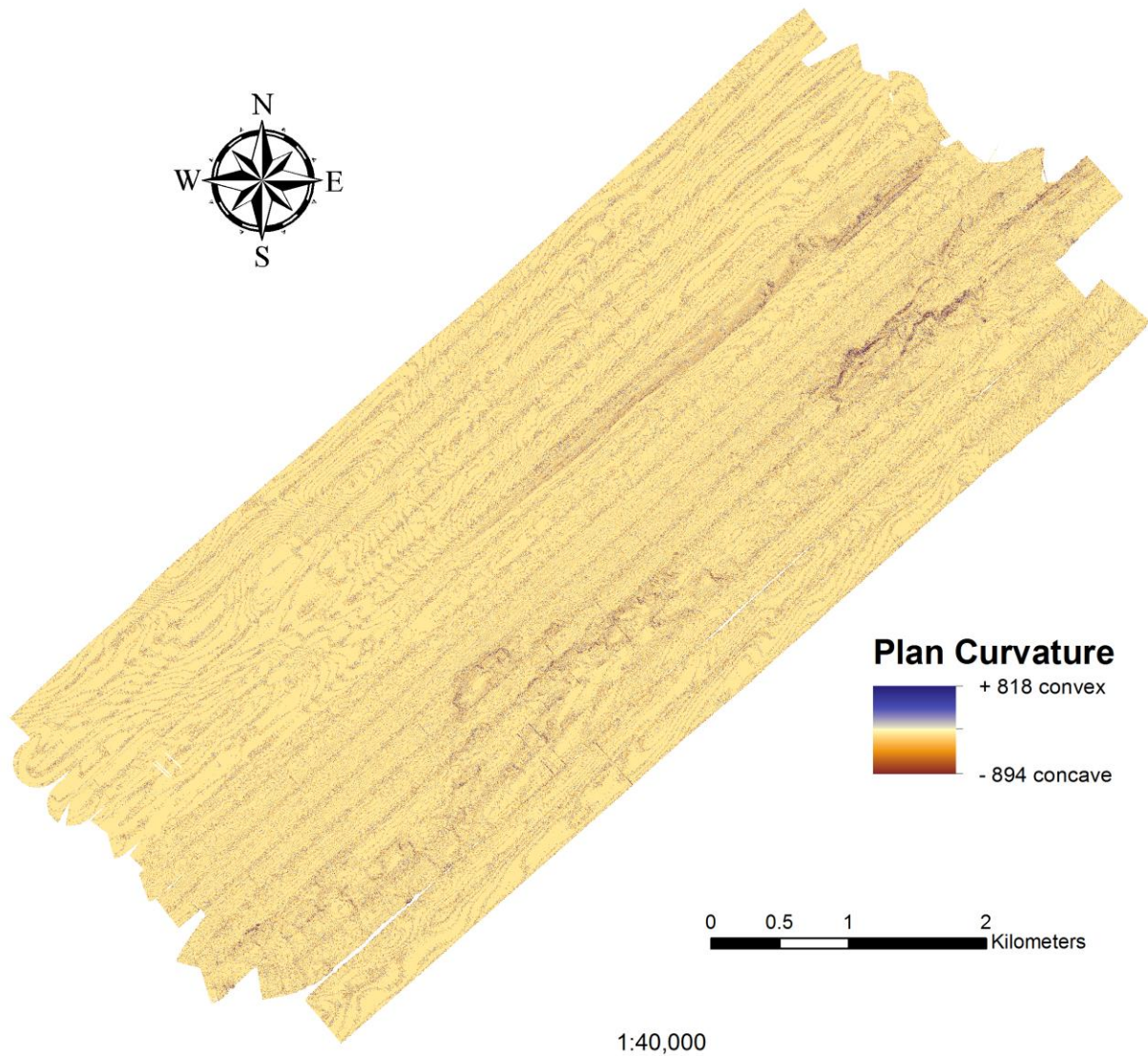


Source: Derived from bathymetric data collected on July 7th 2013 using the ME70 multibeam echosounder system aboard the NOAA ship *Pisces*.

Coordinate System: NAD 1983 UTM Zone 18N

Credit: Friedrich Knuth (c) 2014

Figure 48. Maximum rate of change in slope between cell and eight neighbors at Cape Lookout One.

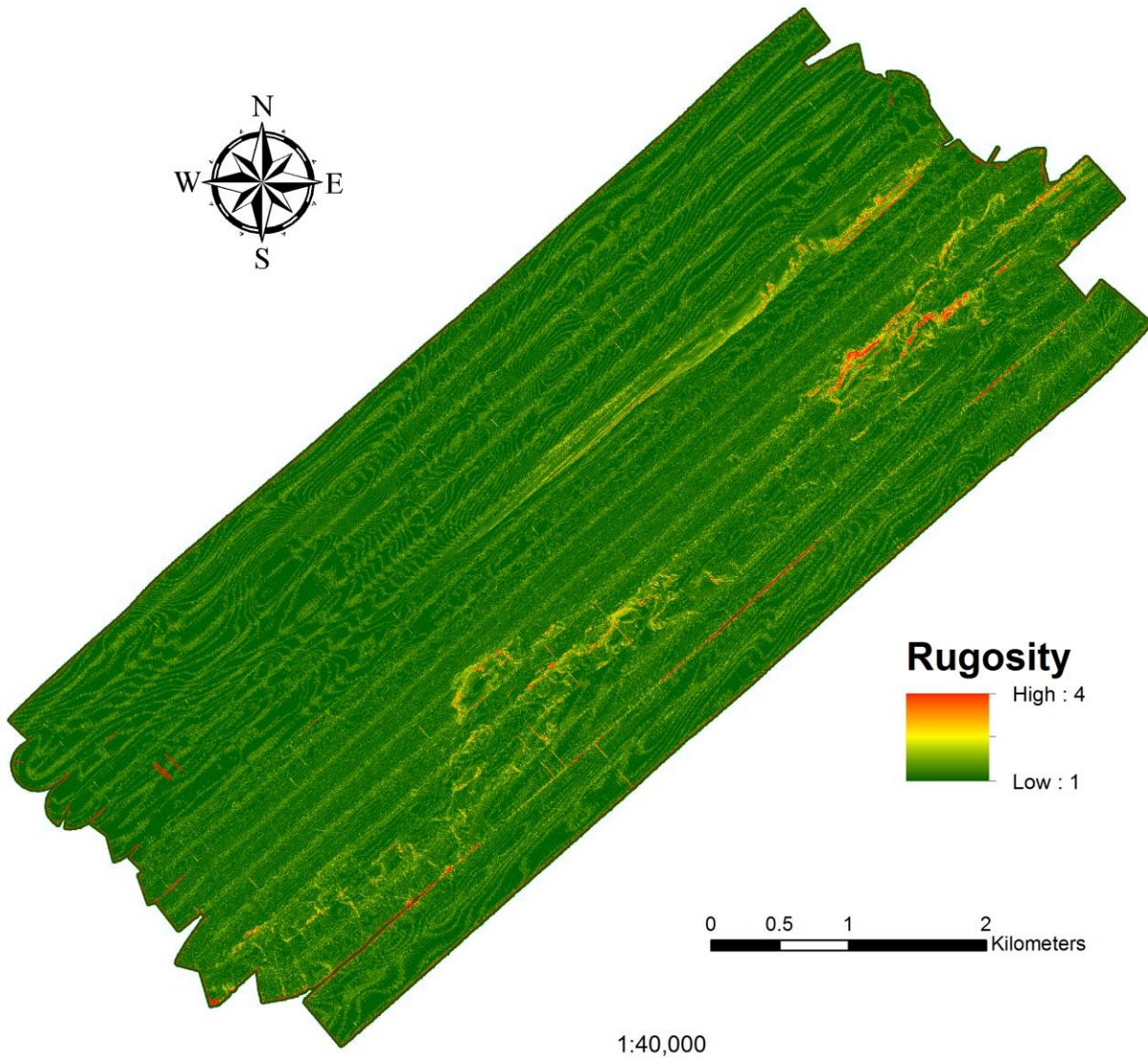


Source: Derived from bathymetric data collected on July 7th 2013 using the ME70 multibeam echosounder system aboard the NOAA ship *Pisces*.

Coordinate System: NAD 1983 UTM Zone 18N

Credit: Friedrich Knuth (c) 2014

Figure 49. Rate of change in curvature across the surface at Cape Lookout One.

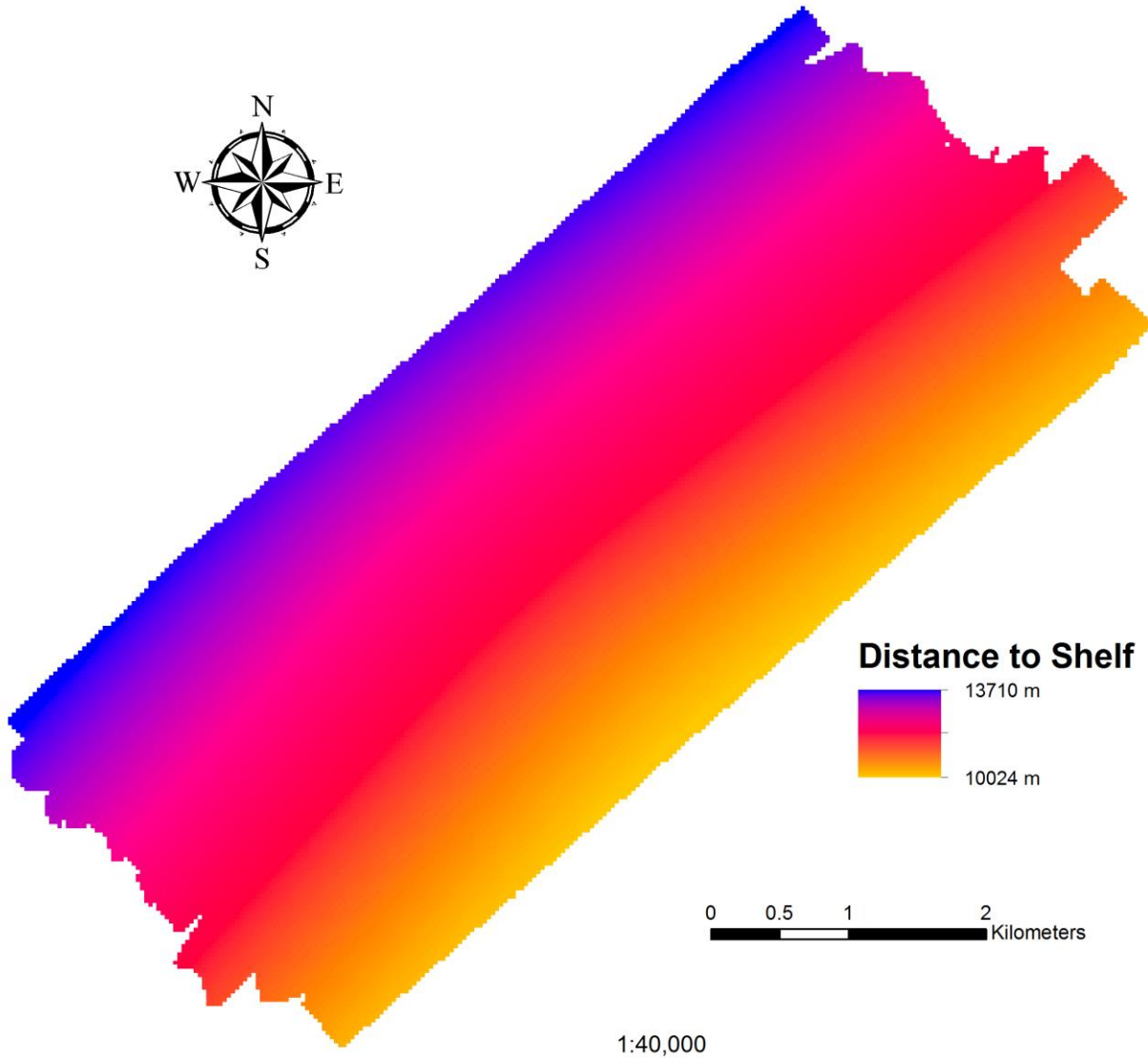


Source: Derived from bathymetric data collected on July 7th 2013 using the ME70 multibeam echosounder system aboard the NOAA ship *Pisces*.

Coordinate System: NAD 1983 UTM Zone 18N

Credit: Friedrich Knuth (c) 2014

Figure 50. Ratio of surface area to planar surface area at Cape Lookout One.

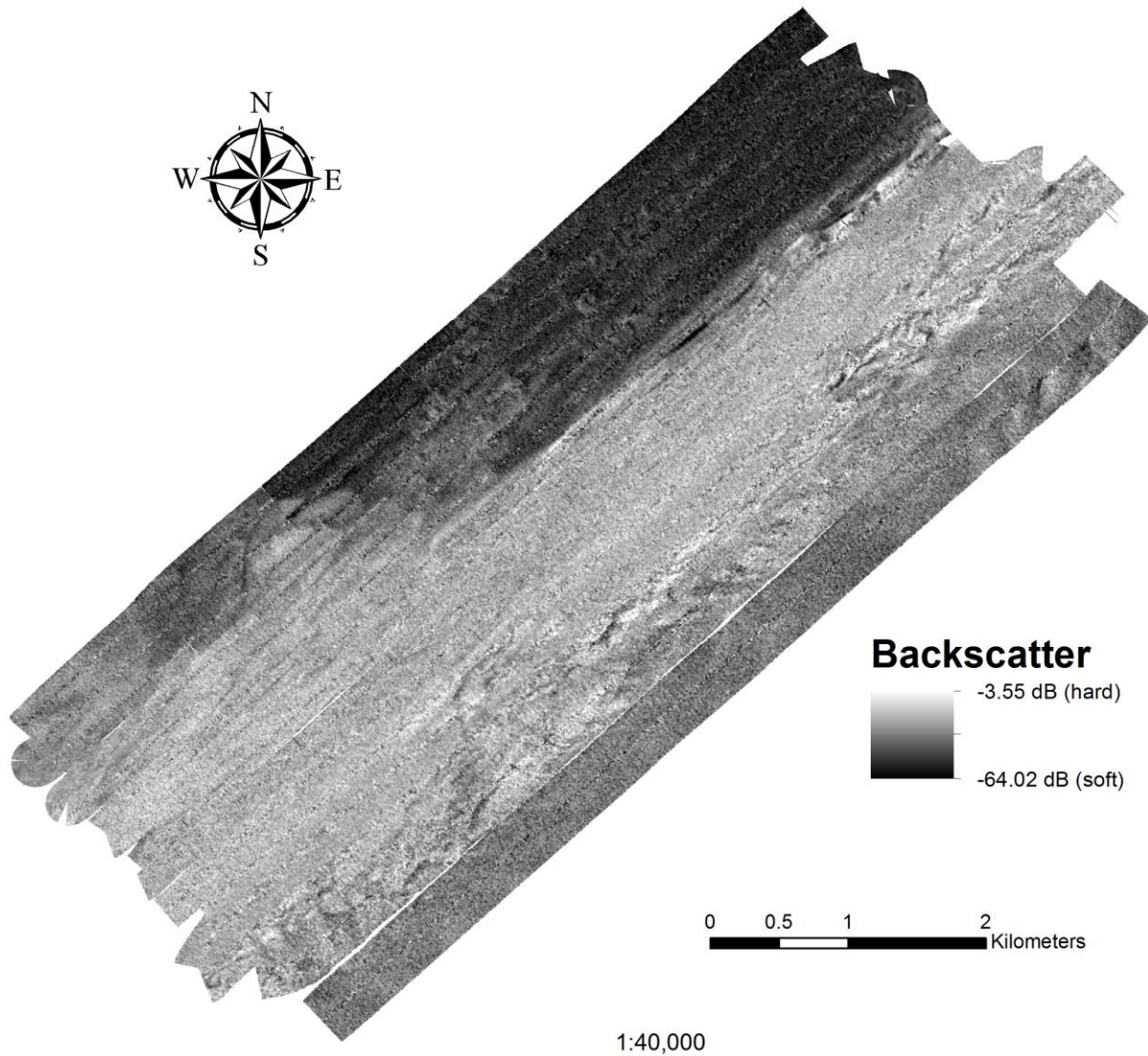


Source: Derived from bathymetric data collected on July 7th 2013 using the ME70 multibeam echosounder system aboard the NOAA ship *Pisces*.

Coordinate System: NAD 1983 UTM Zone 18N

Credit: Friedrich Knuth (c) 2014

Figure 51. Distance of each 2x2 m raster cell to 200 m isobaths at Cape Lookout One.



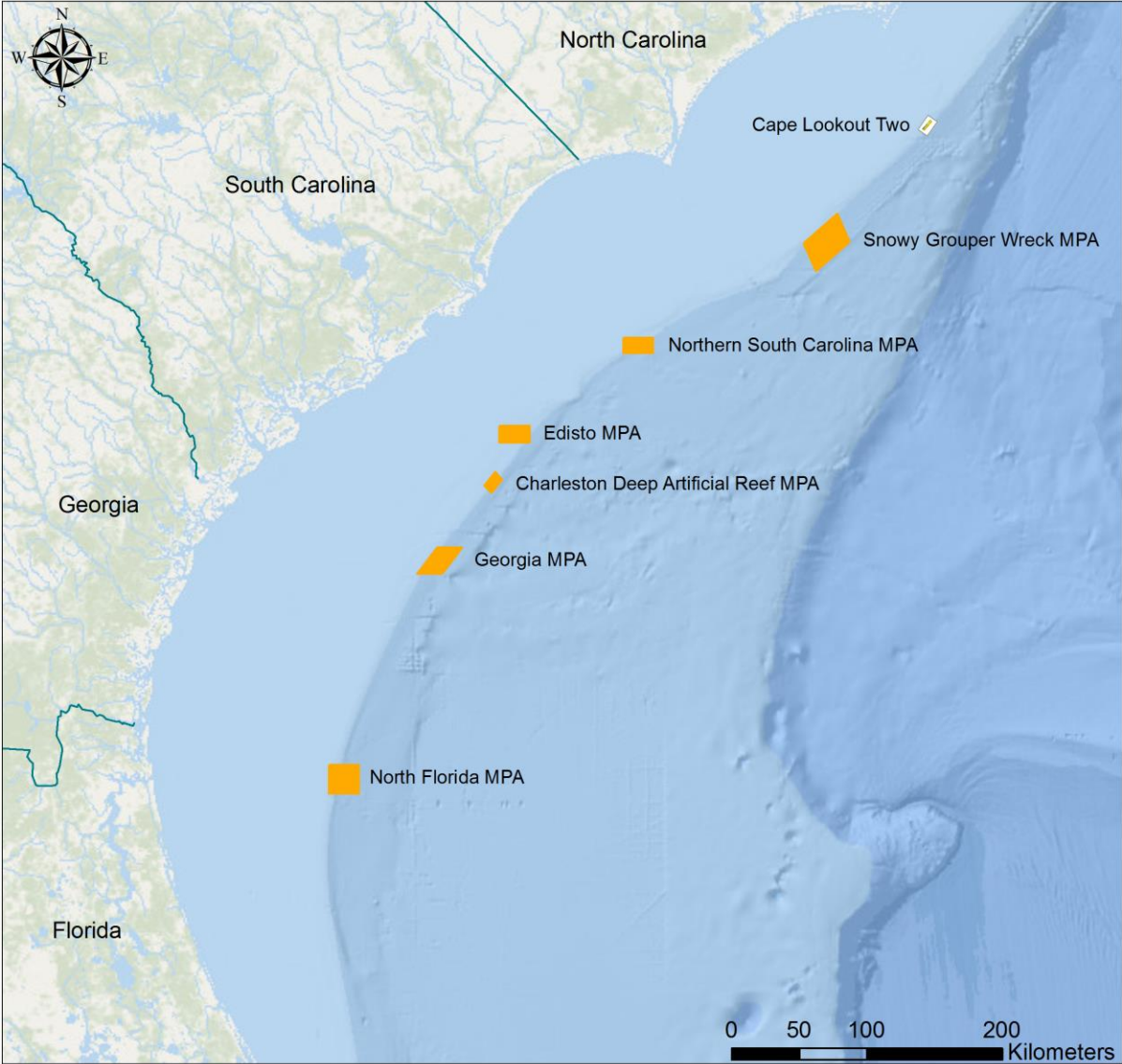
Source: Derived from acoustic data collected on July 7th 2013 using the ME70 multibeam echosounder system aboard the NOAA ship *Pisces*.

Coordinate System: NAD 1983 UTM Zone 18N

Credit: Friedrich Knuth (c) 2014

Figure 52. Intensity of the acoustic return at Cape Lookout One.

CAPE LOOKOUT TWO



Legend

- State Boundaries
- Survey Site Cape Lookout Two
- Marine Protected Areas (MPAs)

Friedrich Knuth (c)
College of Charleston
2014

Source: SAFMC online GIS database, NOAA, SEAMAP, MARMAP, ESRI (base layer)
Coordinate System: WGS 1984 Web Mercator

Figure 53. Location of Cape Lookout Two survey site relative to existing MPAs.

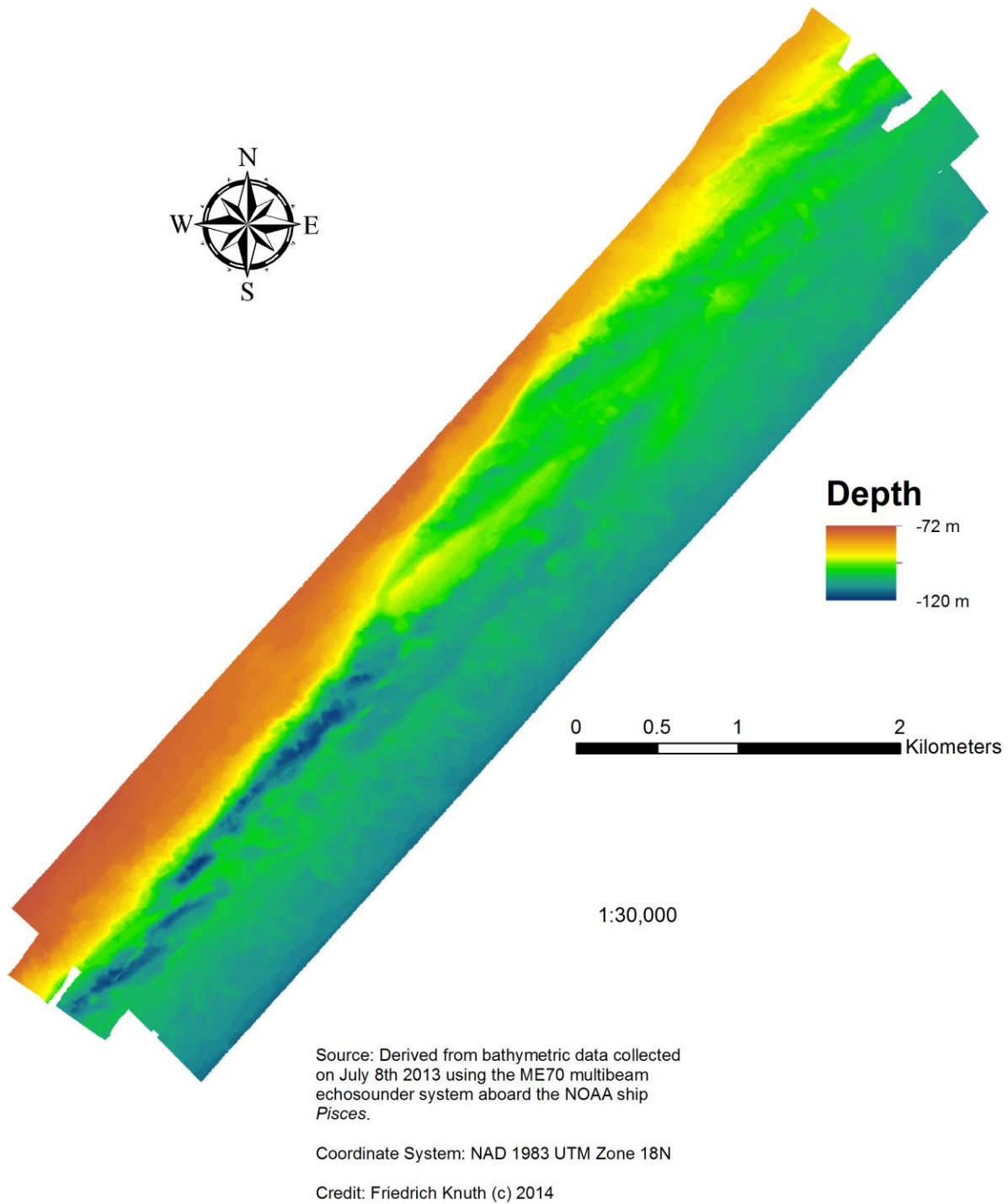
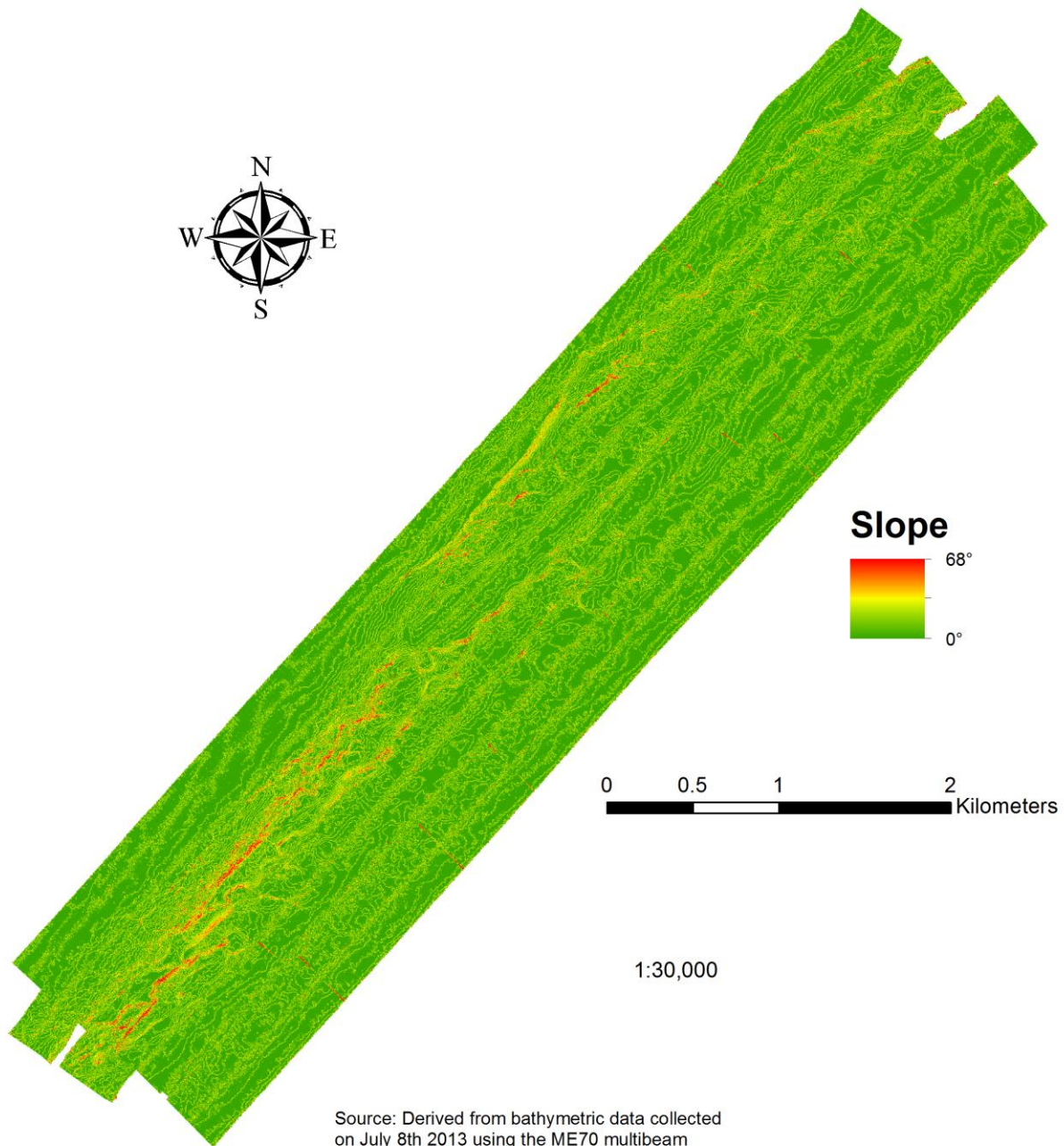


Figure 54. Depth of sea level to seafloor at Cape Lookout Two.



Source: Derived from bathymetric data collected on July 8th 2013 using the ME70 multibeam echosounder system aboard the NOAA ship *Pisces*.

Coordinate System: NAD 1983 UTM Zone 18N

Credit: Friedrich Knuth (c) 2014

Figure 55. Maximum rate of change in depth between 2 x 2 m raster cell and eight neighbors at Cape Lookout Two.

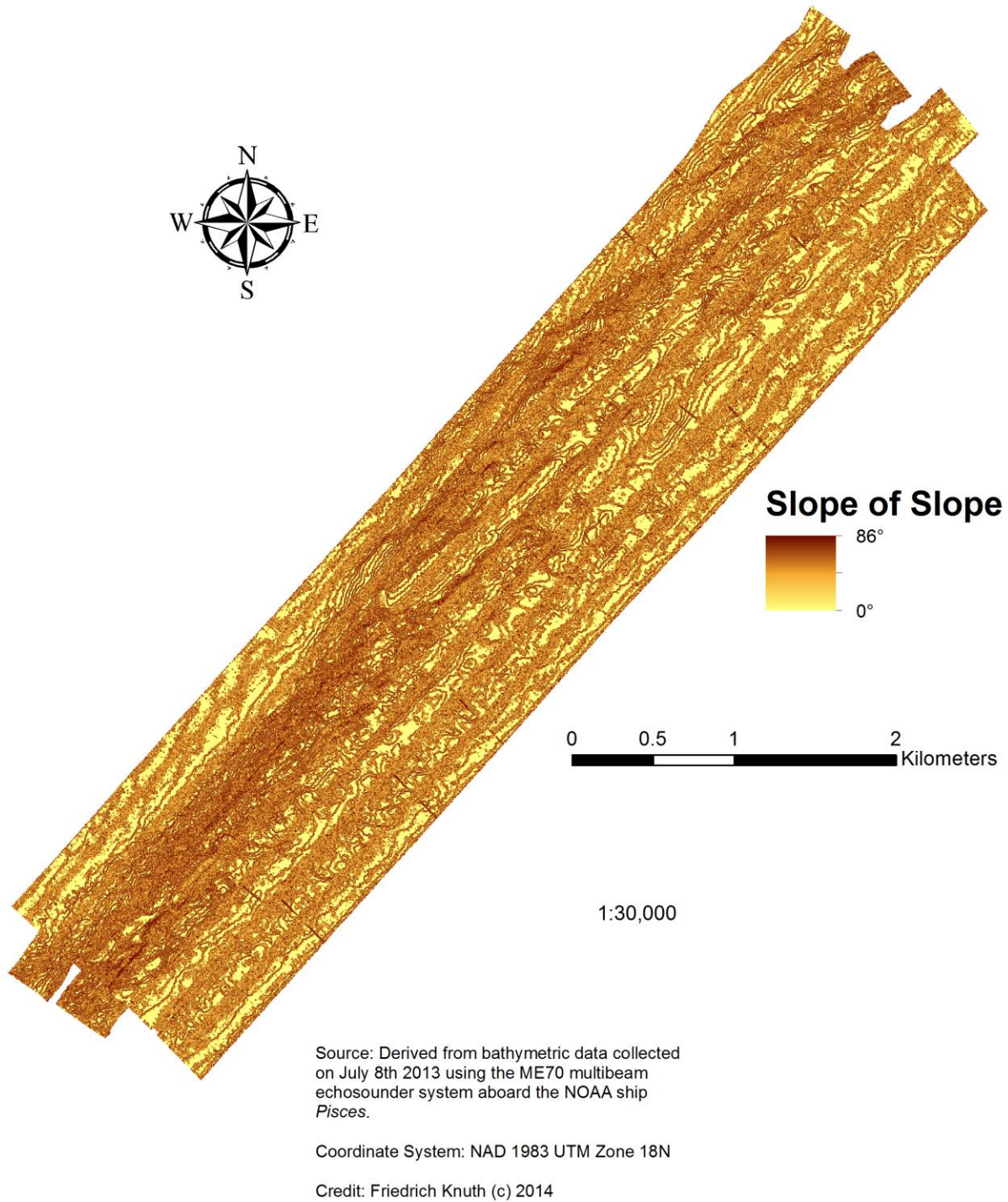


Figure 56. Maximum rate of change in slope between cell and eight neighbors at Cape Lookout Two.

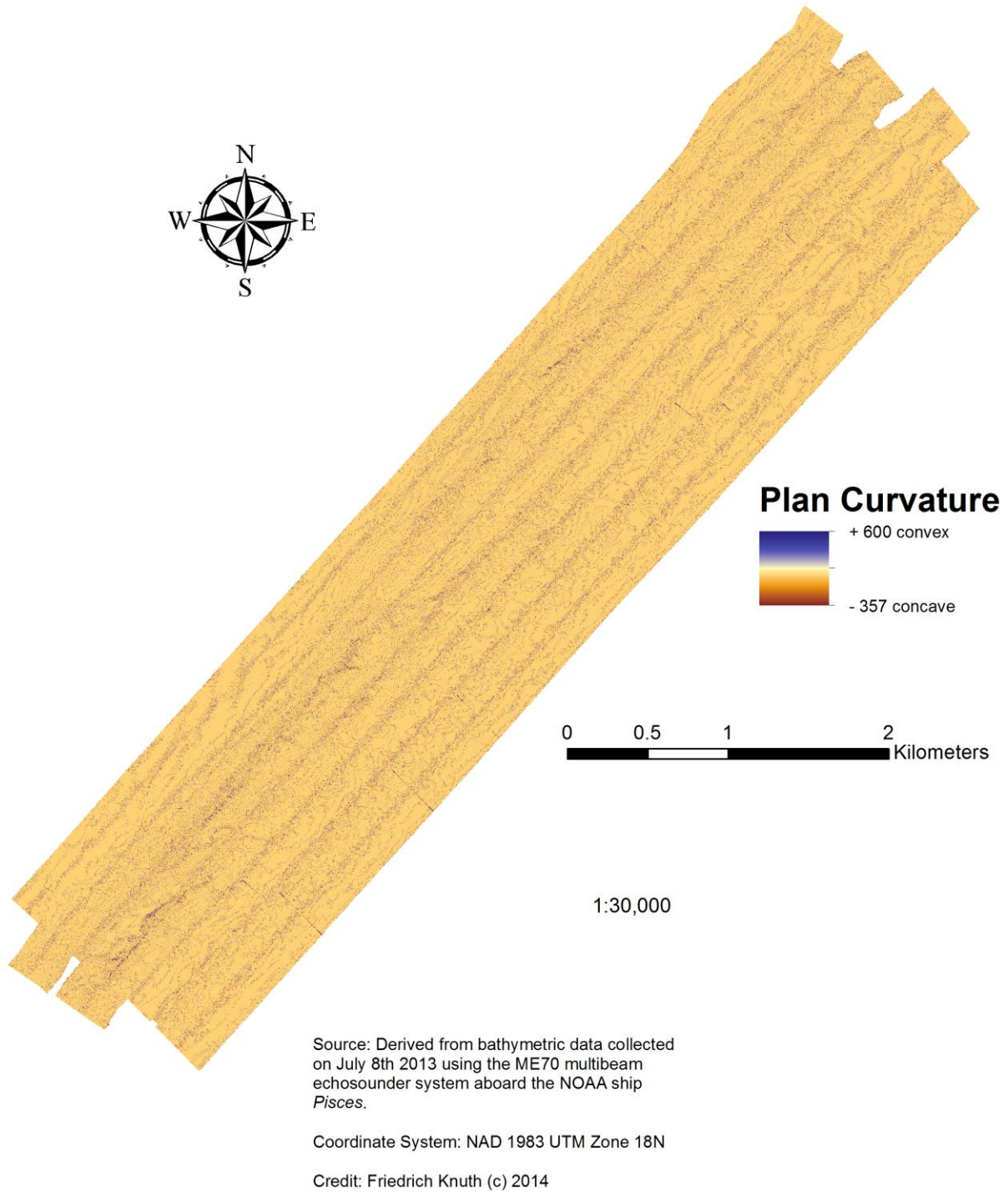


Figure 57. Rate of change in curvature across the surface at Cape Lookout Two.

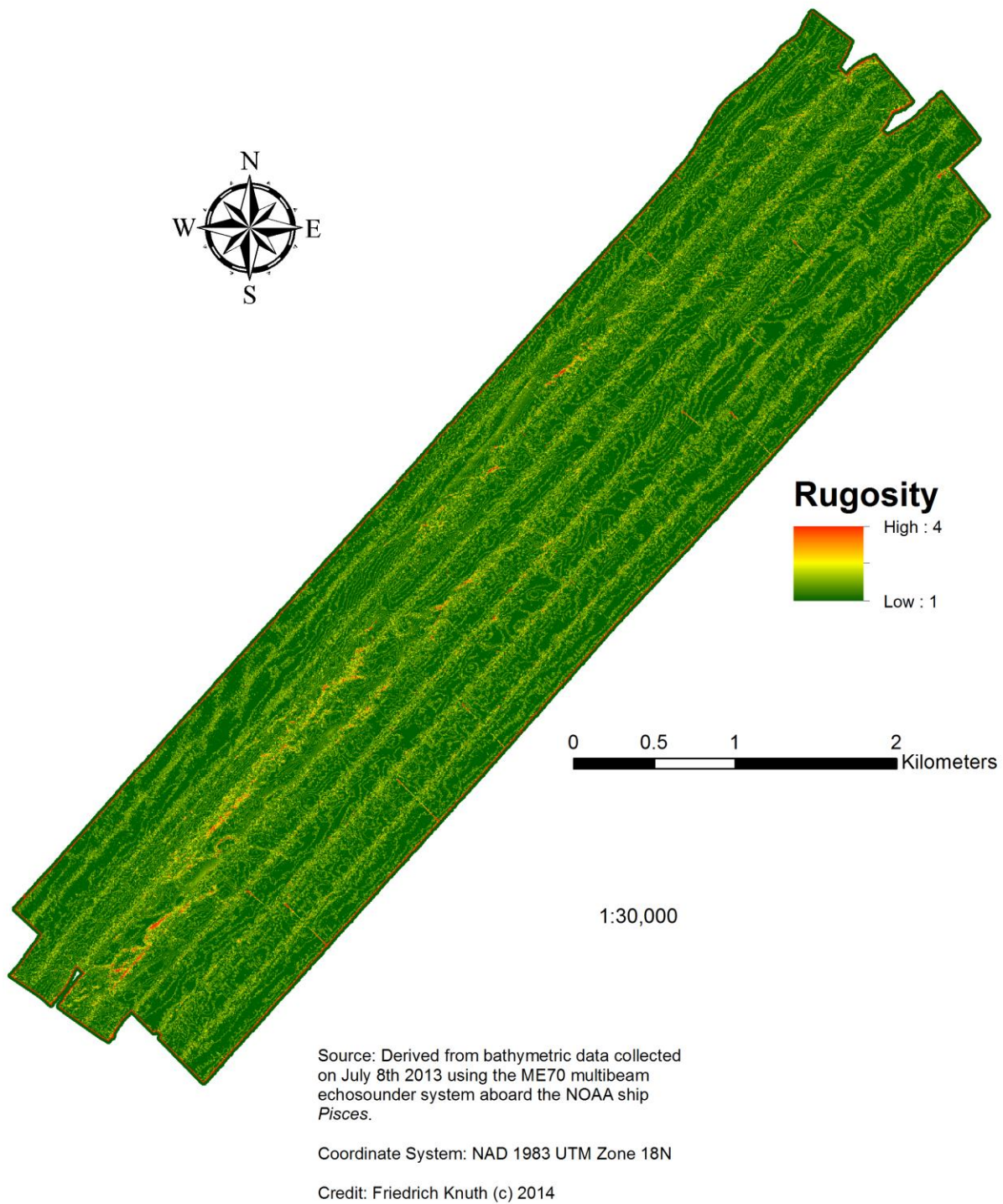


Figure 58. Ratio of surface area to planar surface area at Cape Lookout Two.

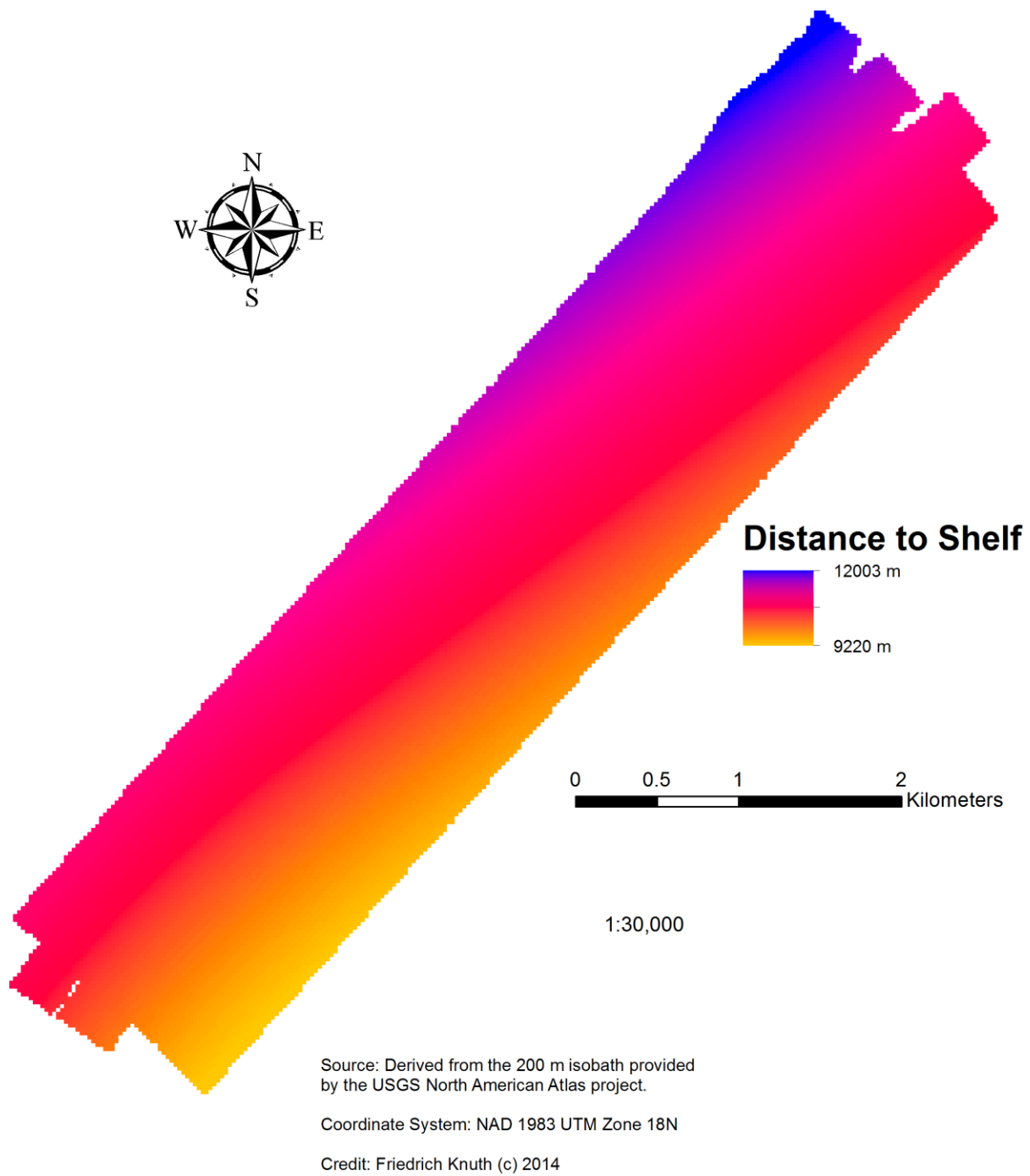
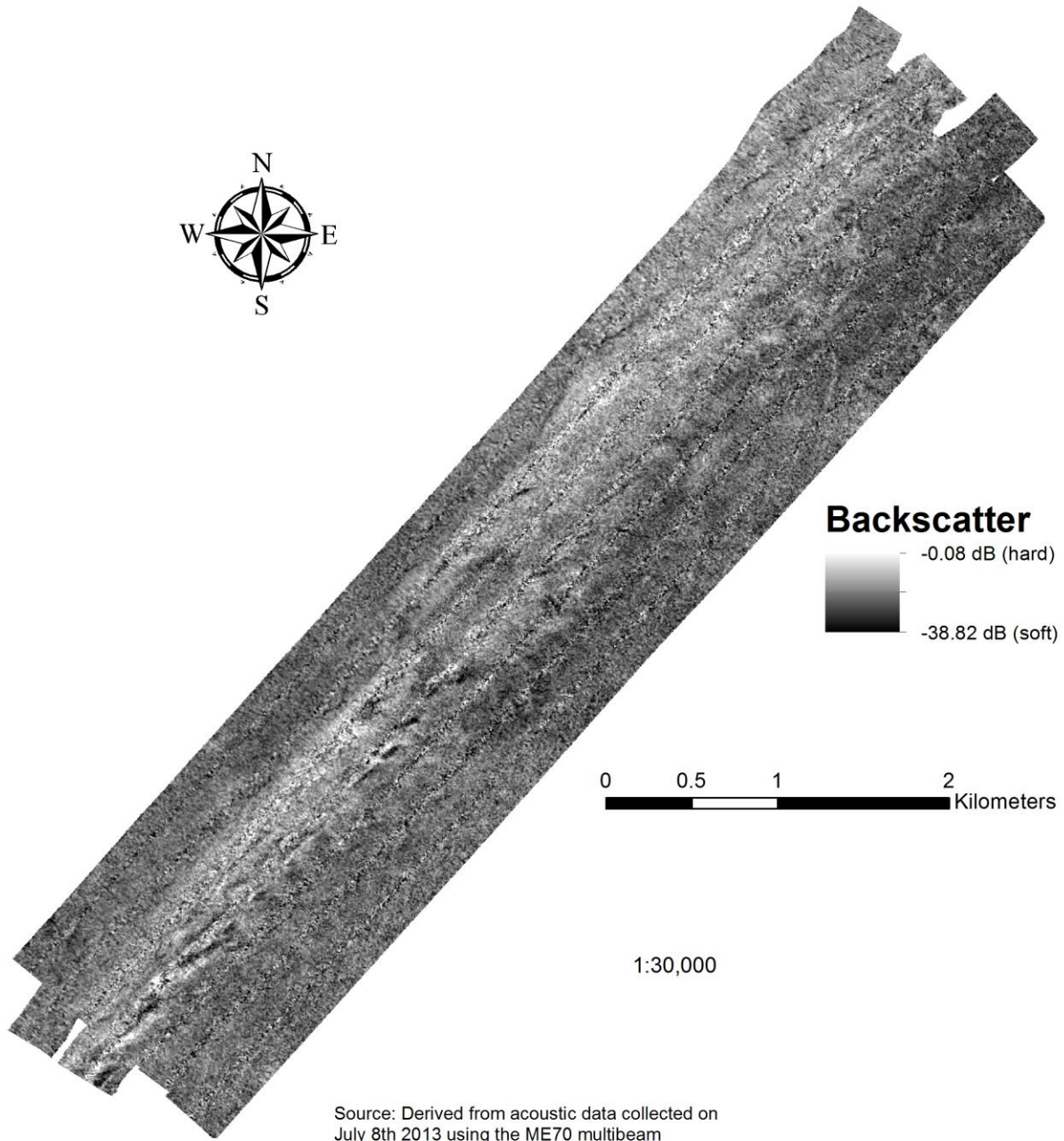


Figure 59. Distance of each 2x2 m raster cell to 200 m isobaths at Cape Lookout Two.



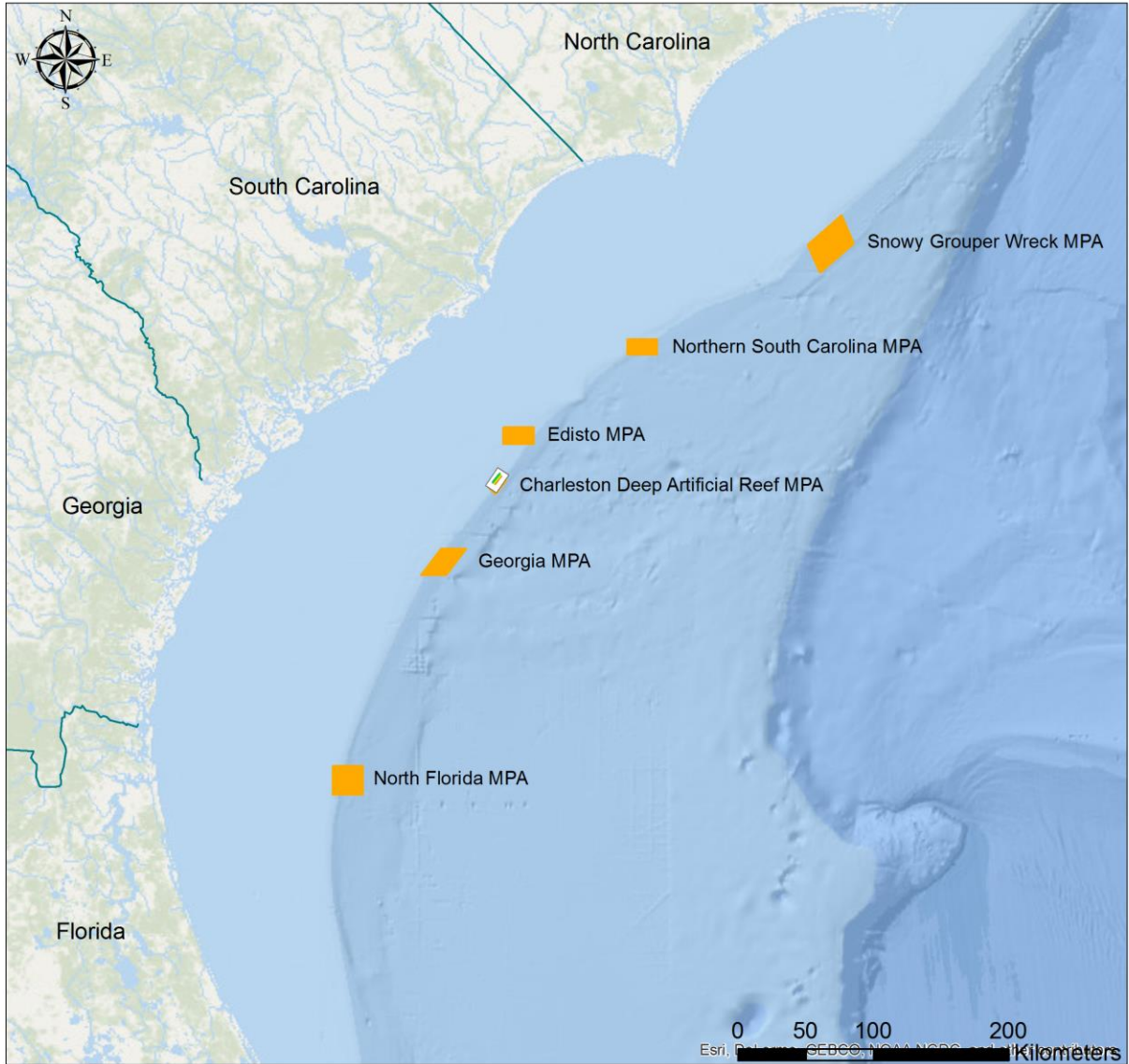
Source: Derived from acoustic data collected on July 8th 2013 using the ME70 multibeam echosounder system aboard the NOAA ship *Pisces*.

Coordinate System: NAD 1983 UTM Zone 18N

Credit: Friedrich Knuth (c) 2014

Figure 60. Intensity of the acoustic return at Cape Lookout Two.

CHARLESTON DEEP ARTIFICIAL REEF MPA



Legend

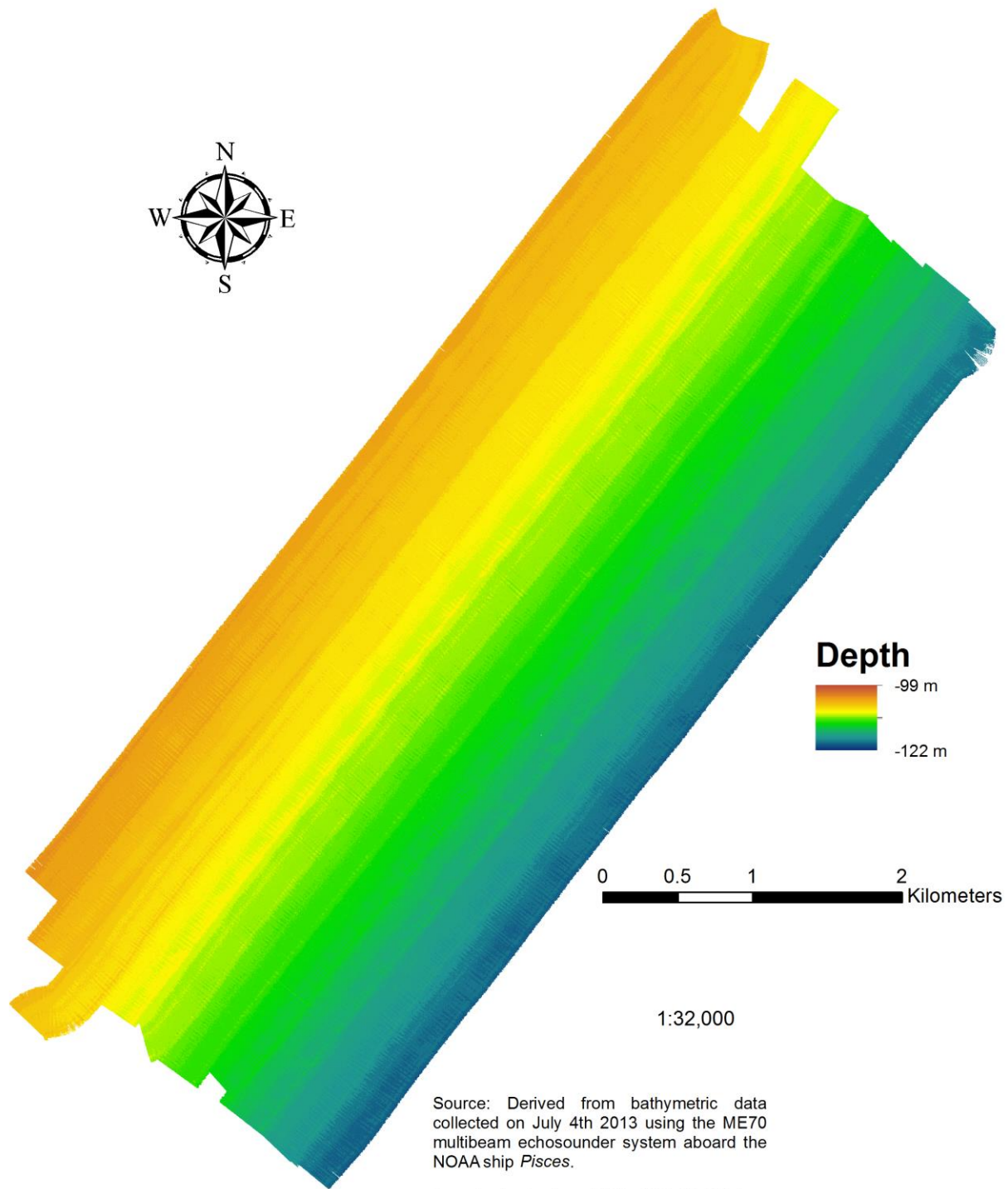
- State Boundaries
- Survey Site Edisto New MPA
- Marine Protected Areas (MPAs)

Friedrich Knuth (c)
College of Charleston
2014

Source: SAFMC online GIS database, NOAA, SEAMAP, MARMAP, ESRI (base layer)

Coordinate System: WGS 1984 Web Mercator

Figure 61. Location of Charleston DAR MPA survey site relative to other MPAs.

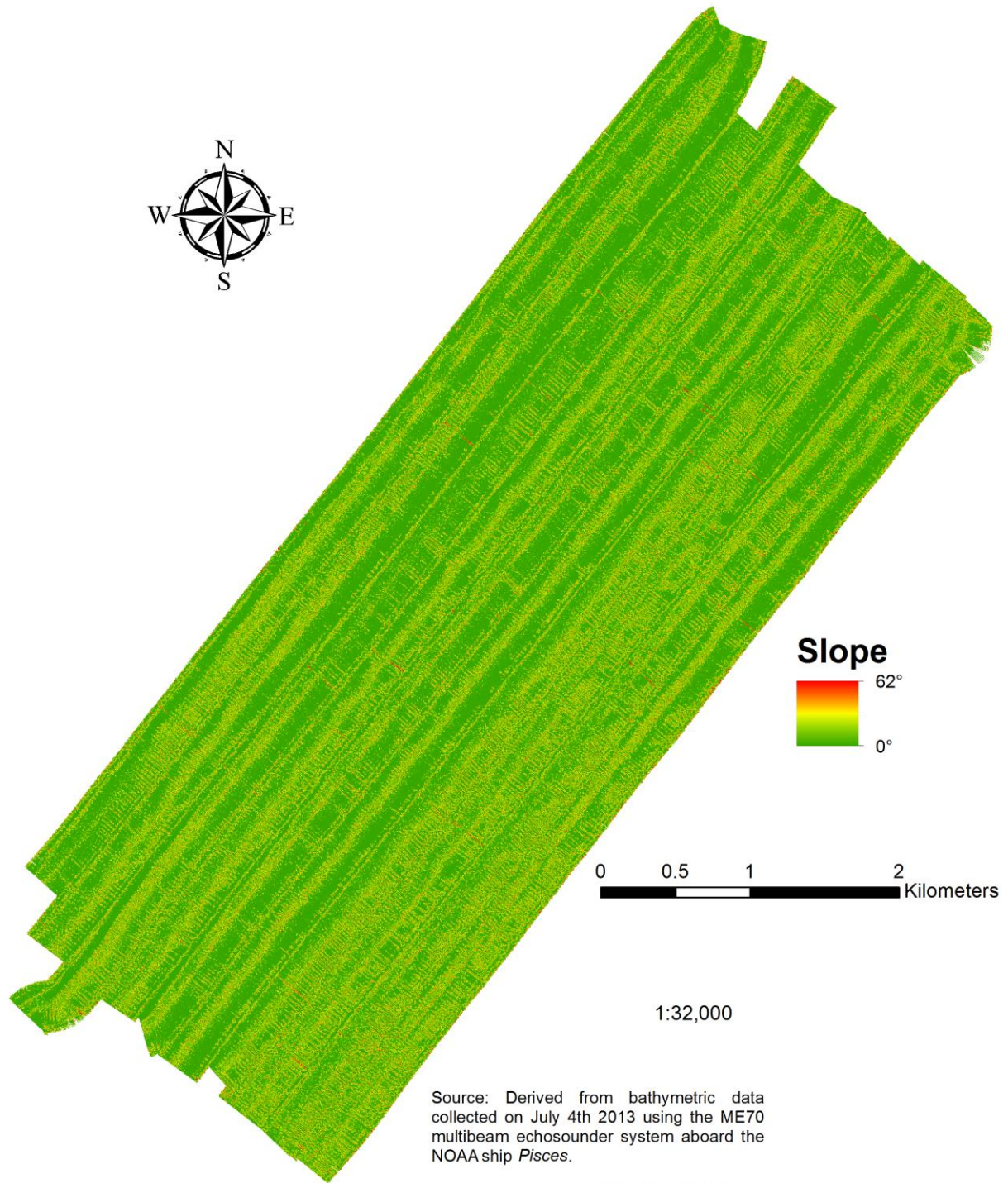


Source: Derived from bathymetric data collected on July 4th 2013 using the ME70 multibeam echosounder system aboard the NOAA ship *Pisces*.

Coordinate System: NAD 1983 UTM Zone 17N

Credit: Friedrich Knuth (c) 2014

Figure 62. Depth of sea level to seafloor at Charleston DAR MPA.



Coordinate System: NAD 1983 UTM Zone 17N

Credit: Friedrich Knuth (c) 2014

Figure 63. Maximum rate of change in depth between 2 x 2 m raster cell and eight neighbors at Charleston DAR MPA.

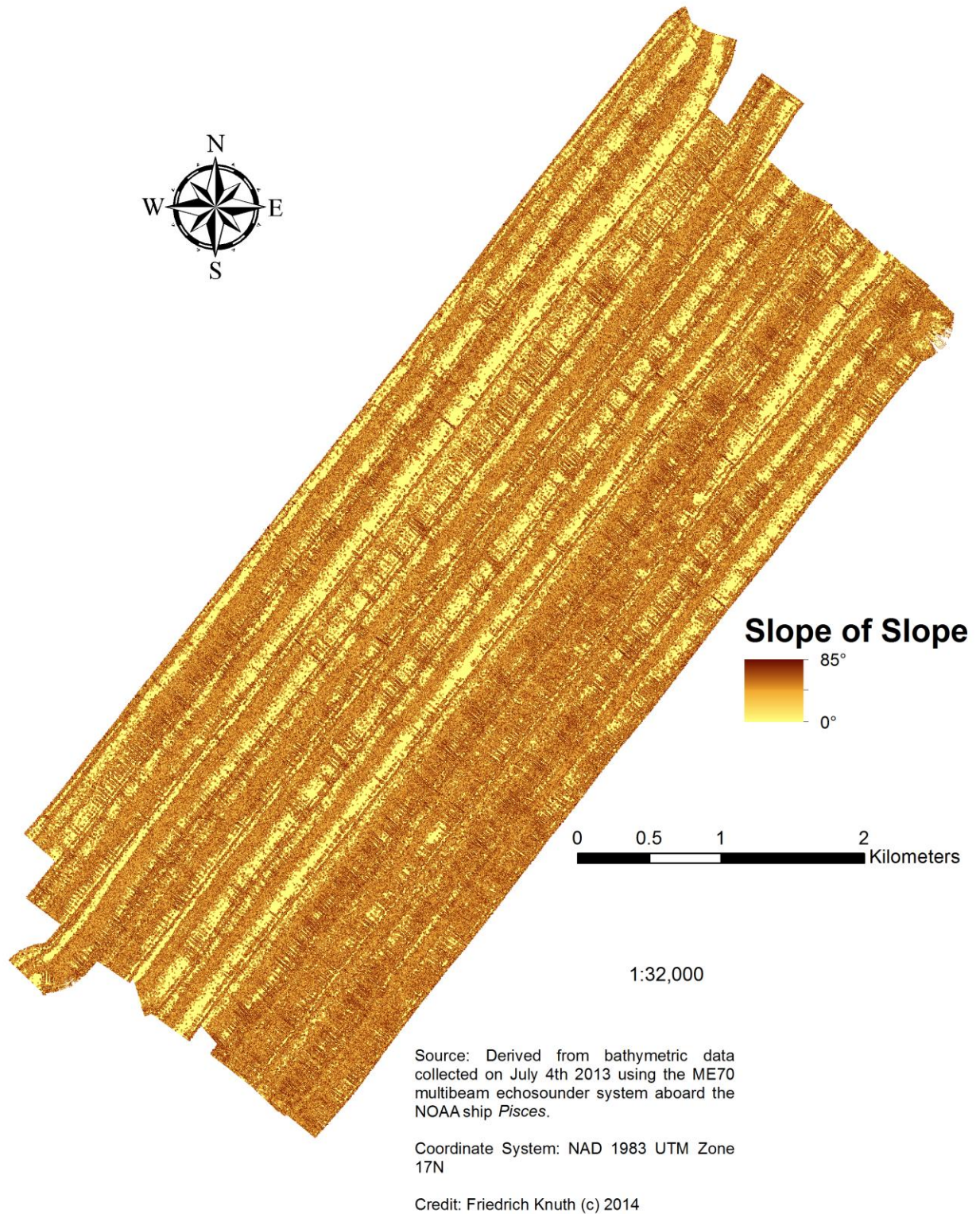


Figure 64. Maximum rate of change in slope between cell and eight neighbors at Charleston DAR MPA.

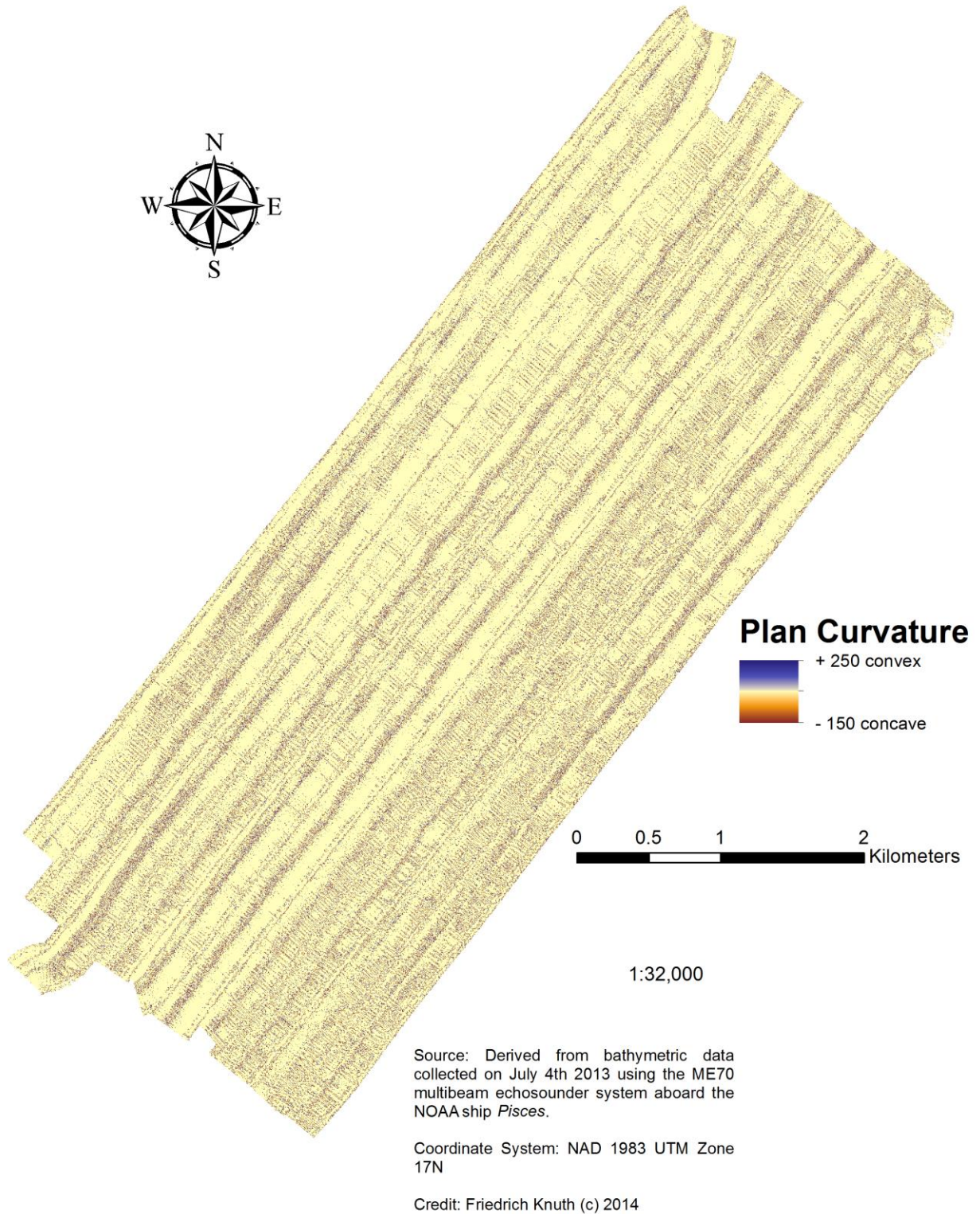


Figure 65. Rate of change in curvature across the surface at Charleston DAR MPA.

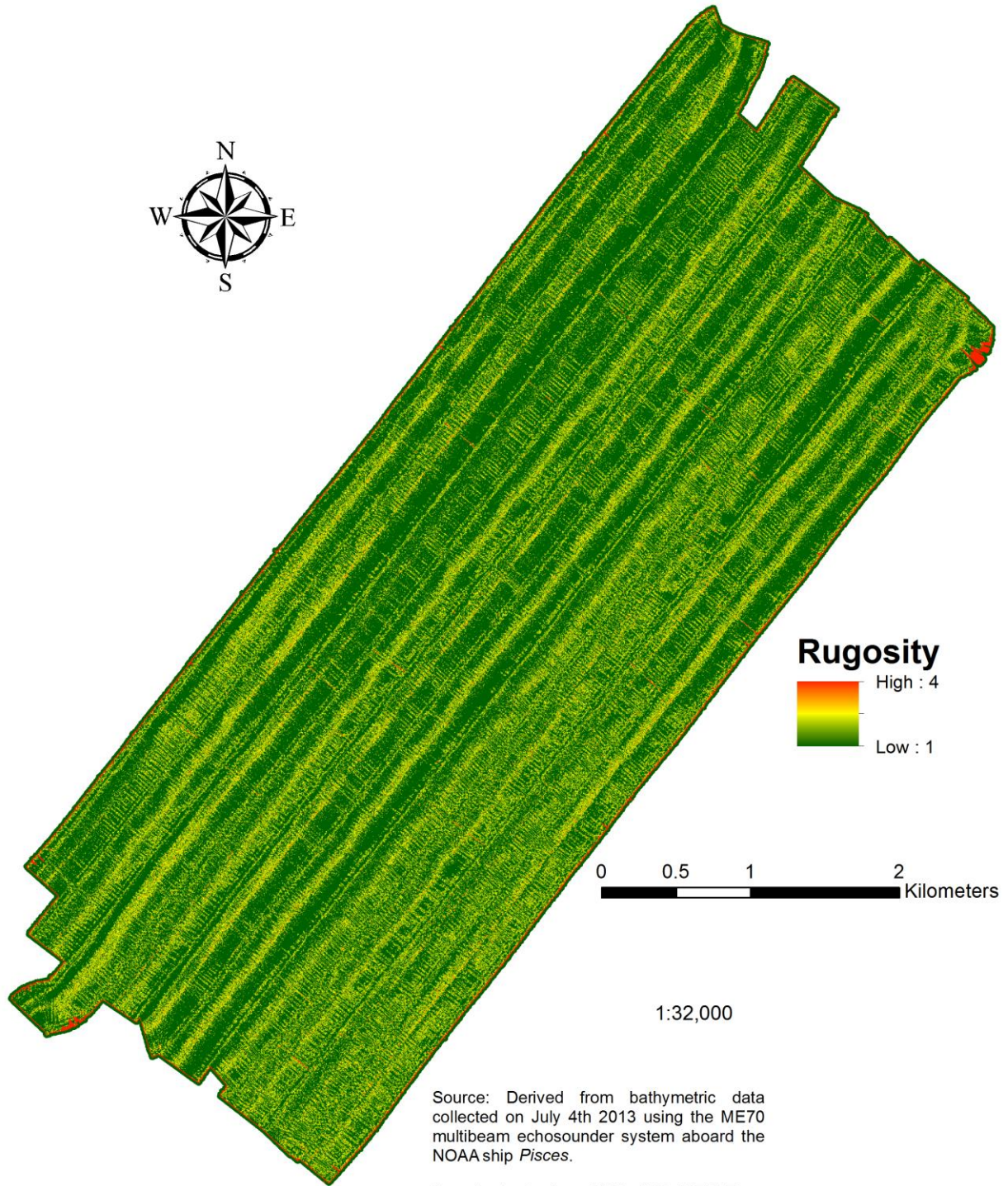


Figure 66. Ratio of surface area to planar surface area at Charleston DAR MPA.

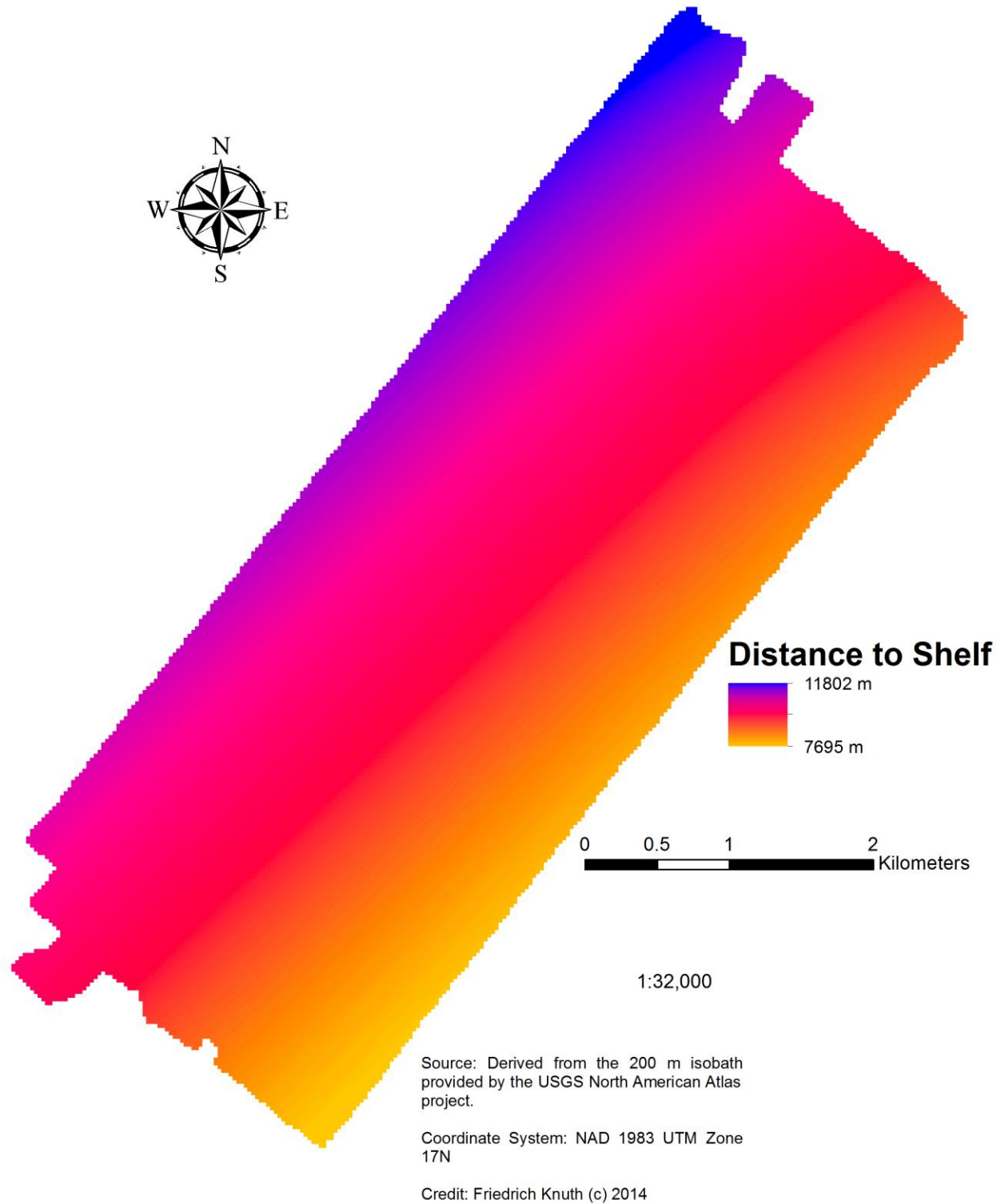


Figure 67. Distance of each 2x2 m raster cell to 200 m isobaths at Charleston DAR MPA.

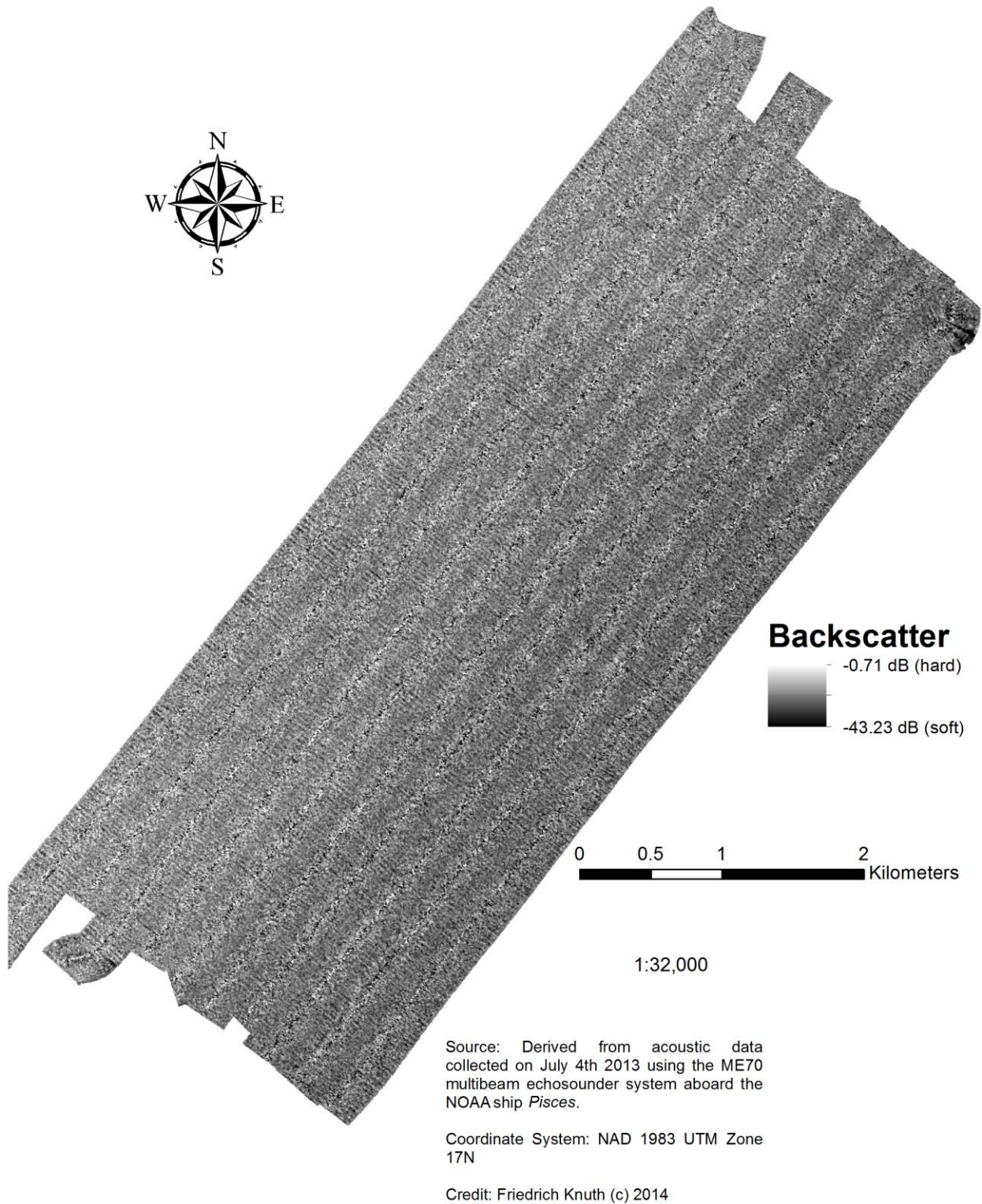
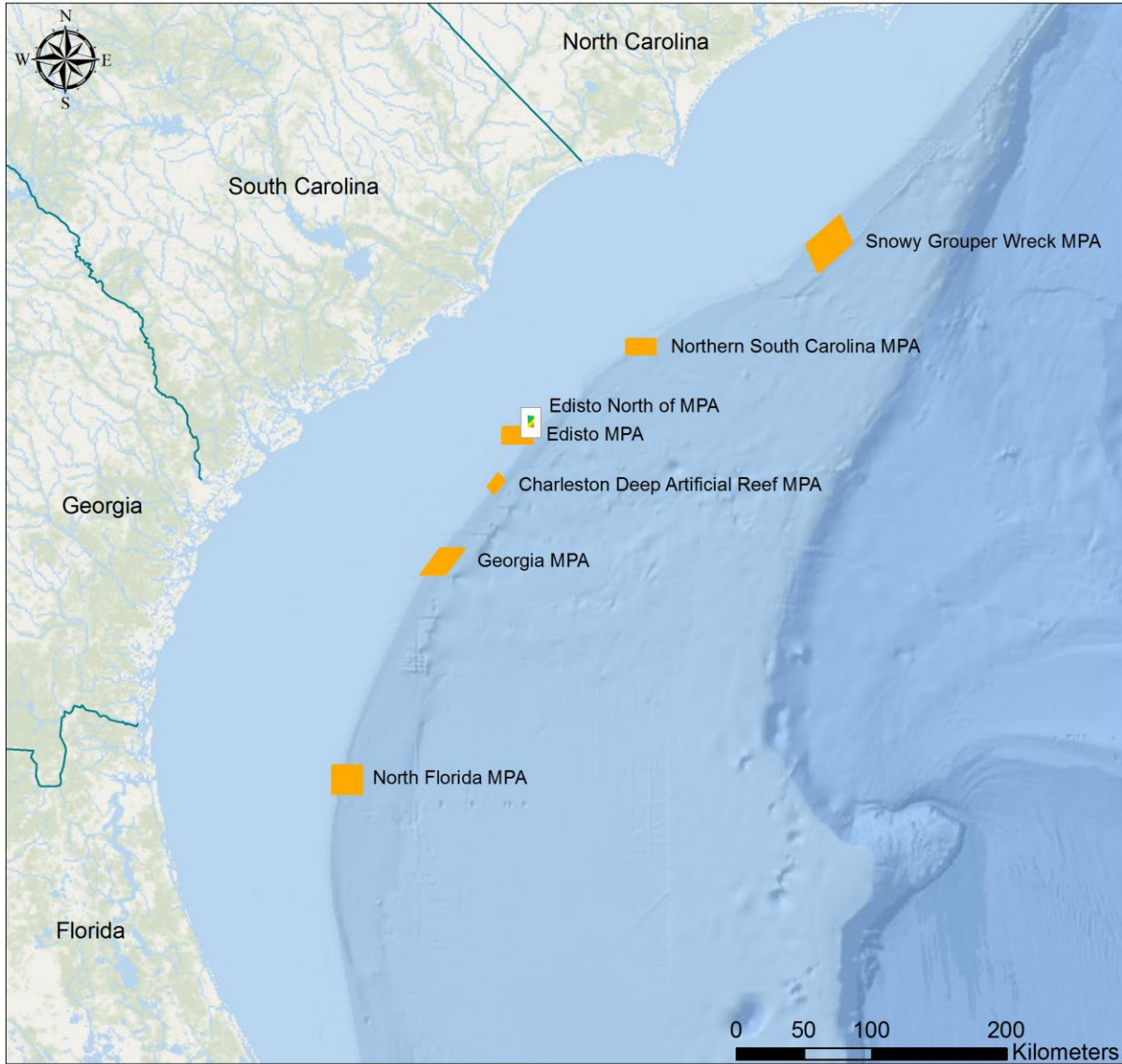


Figure 68. Intensity of the acoustic return at Charleston DAR MPA.

NORTH OF EDISTO MPA



Legend

- State Boundaries
- Survey Site Edisto North of MPA
- Marine Protected Areas (MPAs)

Friedrich Knuth (c)
College of Charleston
2014

Source: SAFMC online GIS database, NOAA, SEAMAP, MARMAP, ESRI (base layer)

Coordinate System: WGS 1984 Web Mercator

Figure 69. Location of N of Edisto MPA survey site relative to existing MPAs.

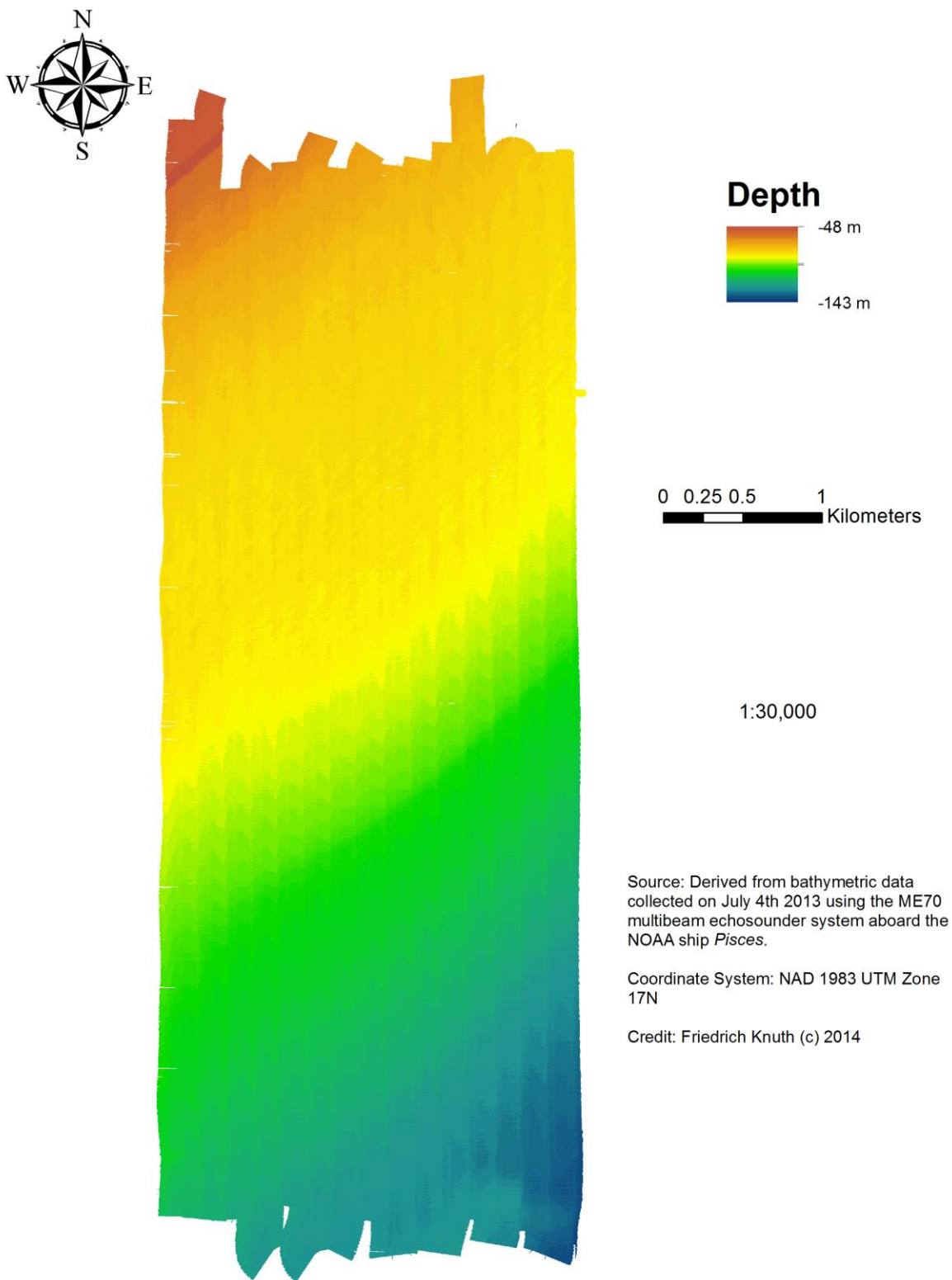


Figure 70. Depth of sea level to seafloor at N of Edisto MPA.

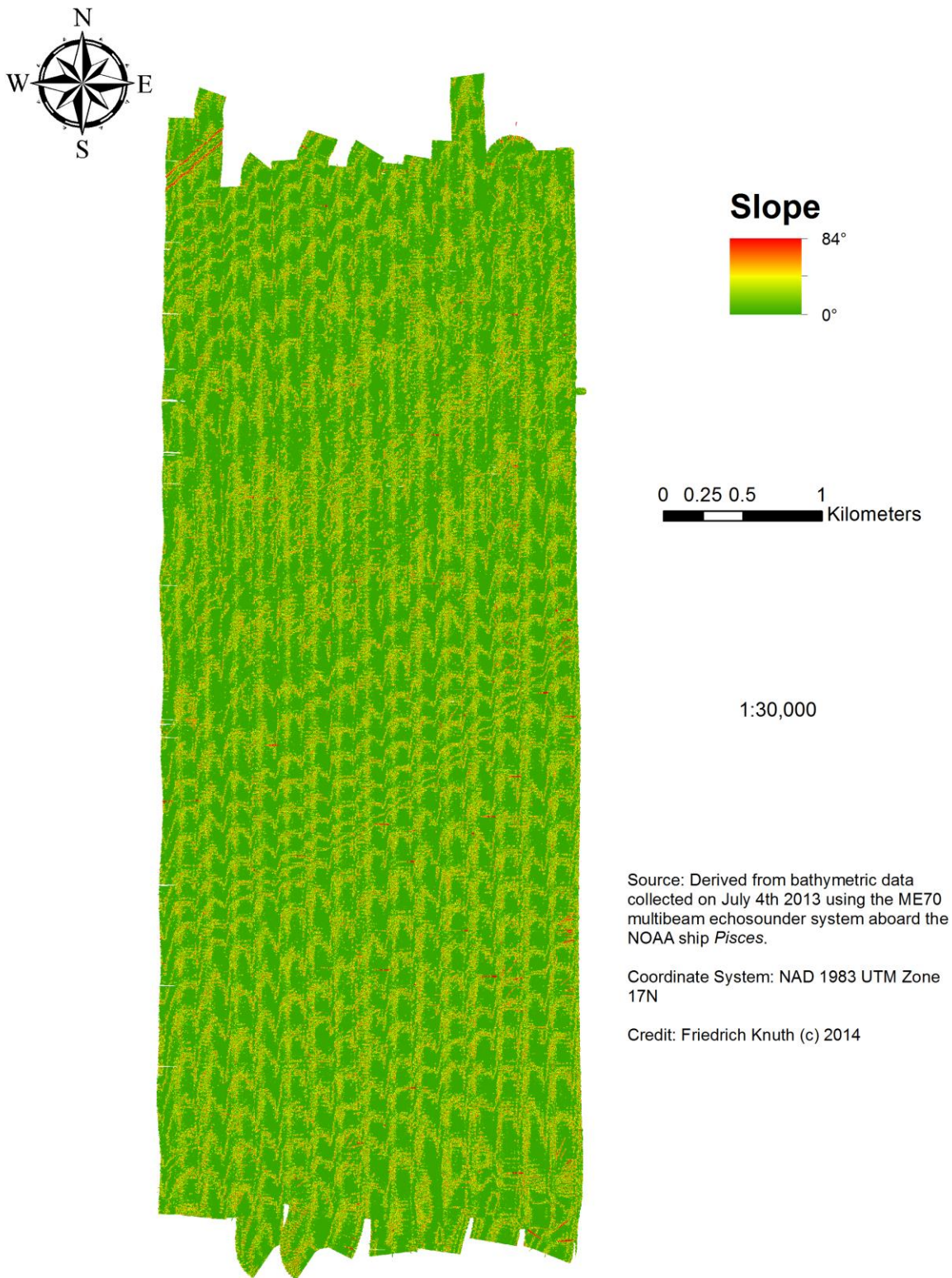
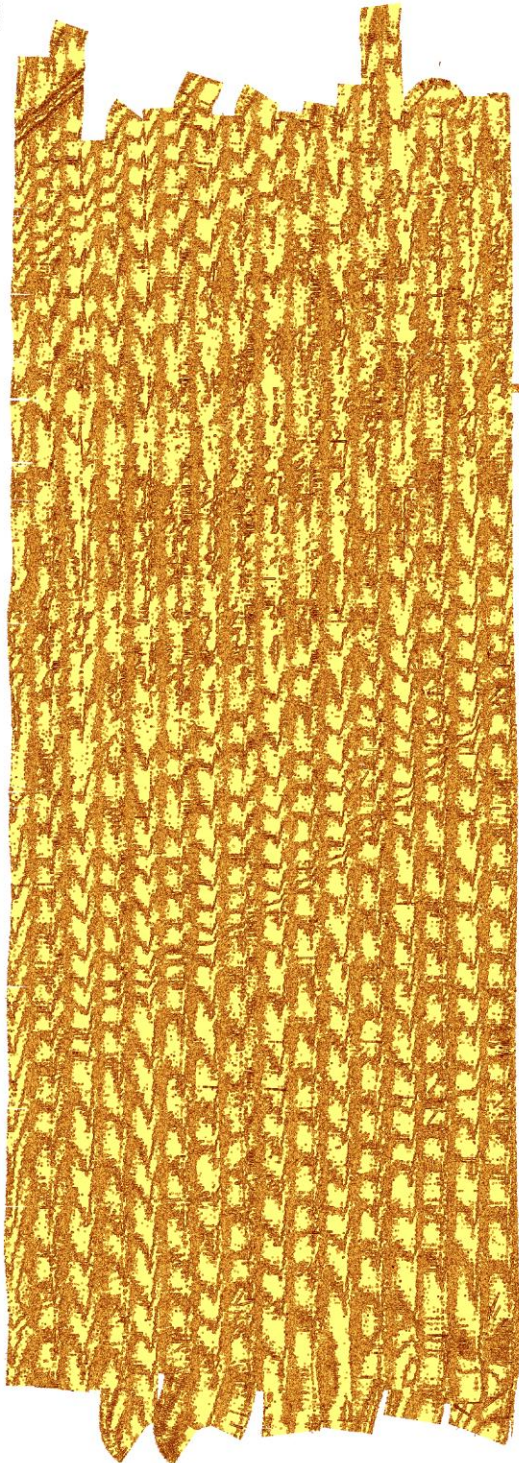
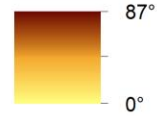


Figure 71. Maximum rate of change in depth between 2 x 2 m raster cell and eight neighbors at N of Edisto MPA.



Slope of Slope



0 0.25 0.5 1
Kilometers

1:30,000

Source: Derived from bathymetric data collected on July 4th 2013 using the ME70 multibeam echosounder system aboard the NOAA ship *Pisces*.

Coordinate System: NAD 1983 UTM Zone 17N

Credit: Friedrich Knuth (c) 2014

Figure 72. Maximum rate of change in slope between cell and eight neighbors at N of Edisto MPA.

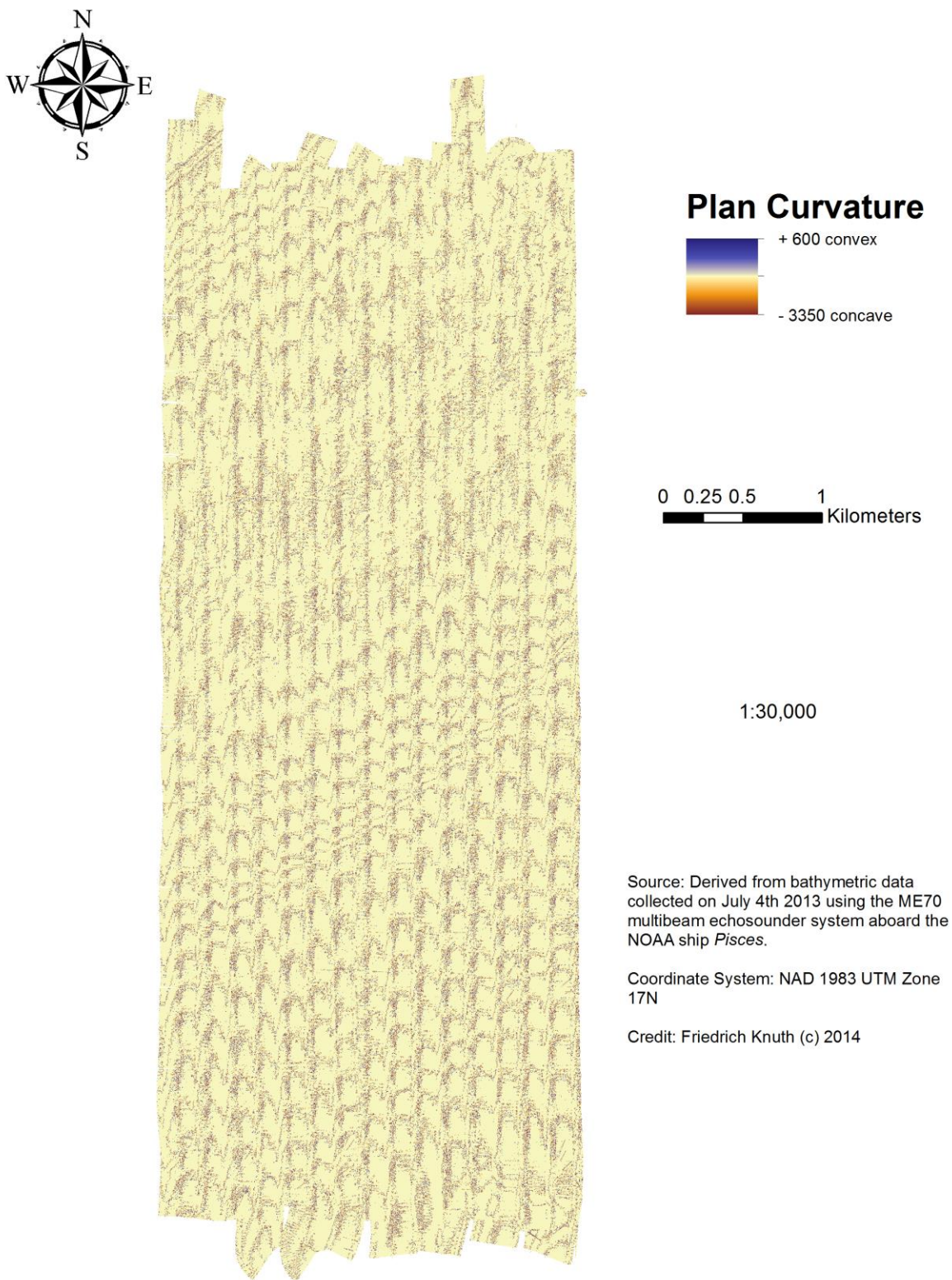


Figure 73. Rate of change in curvature across the surface at N of Edisto MPA.

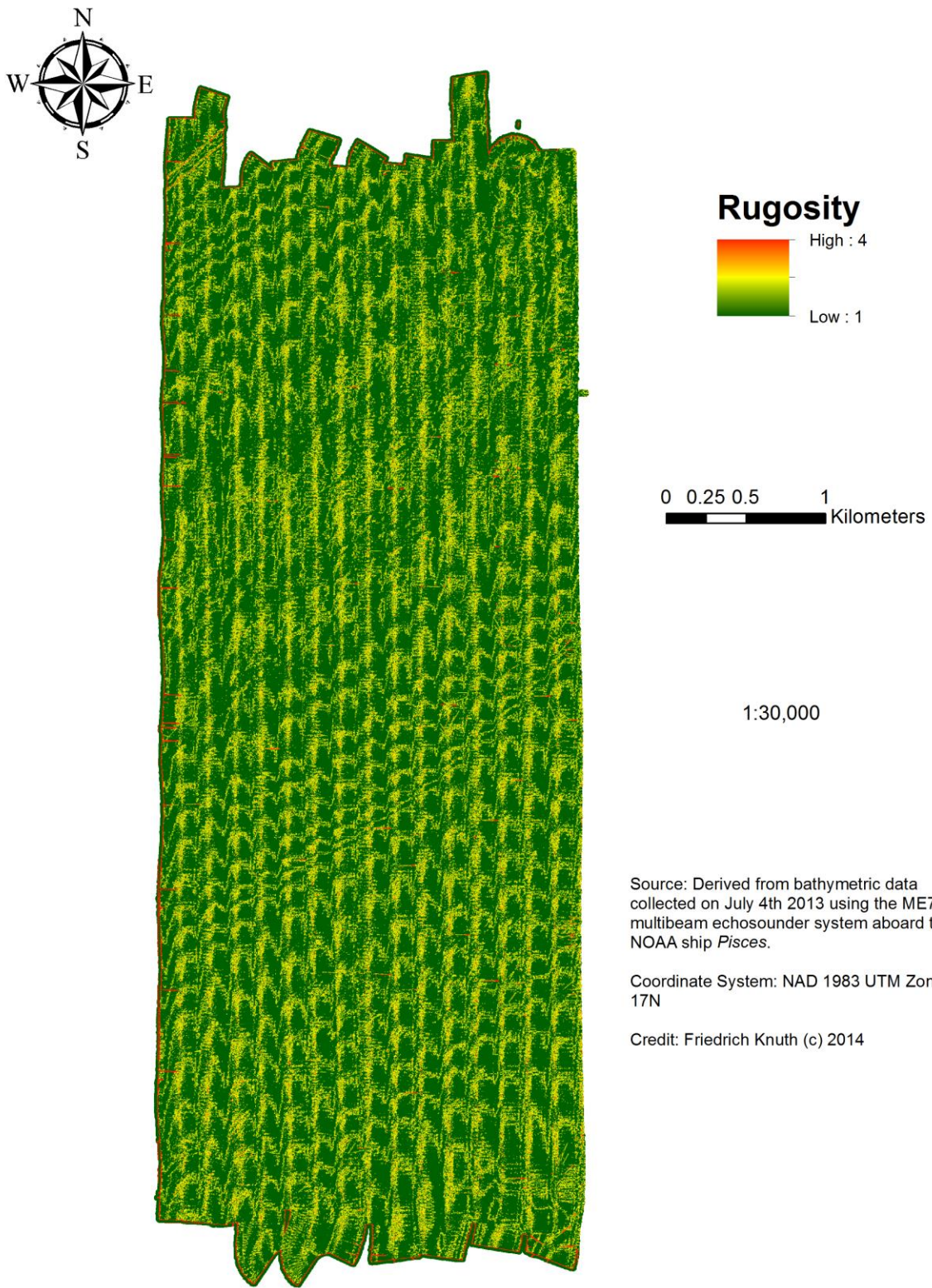


Figure 74. Ratio of surface area to planar surface area at N of Edisto MPA.

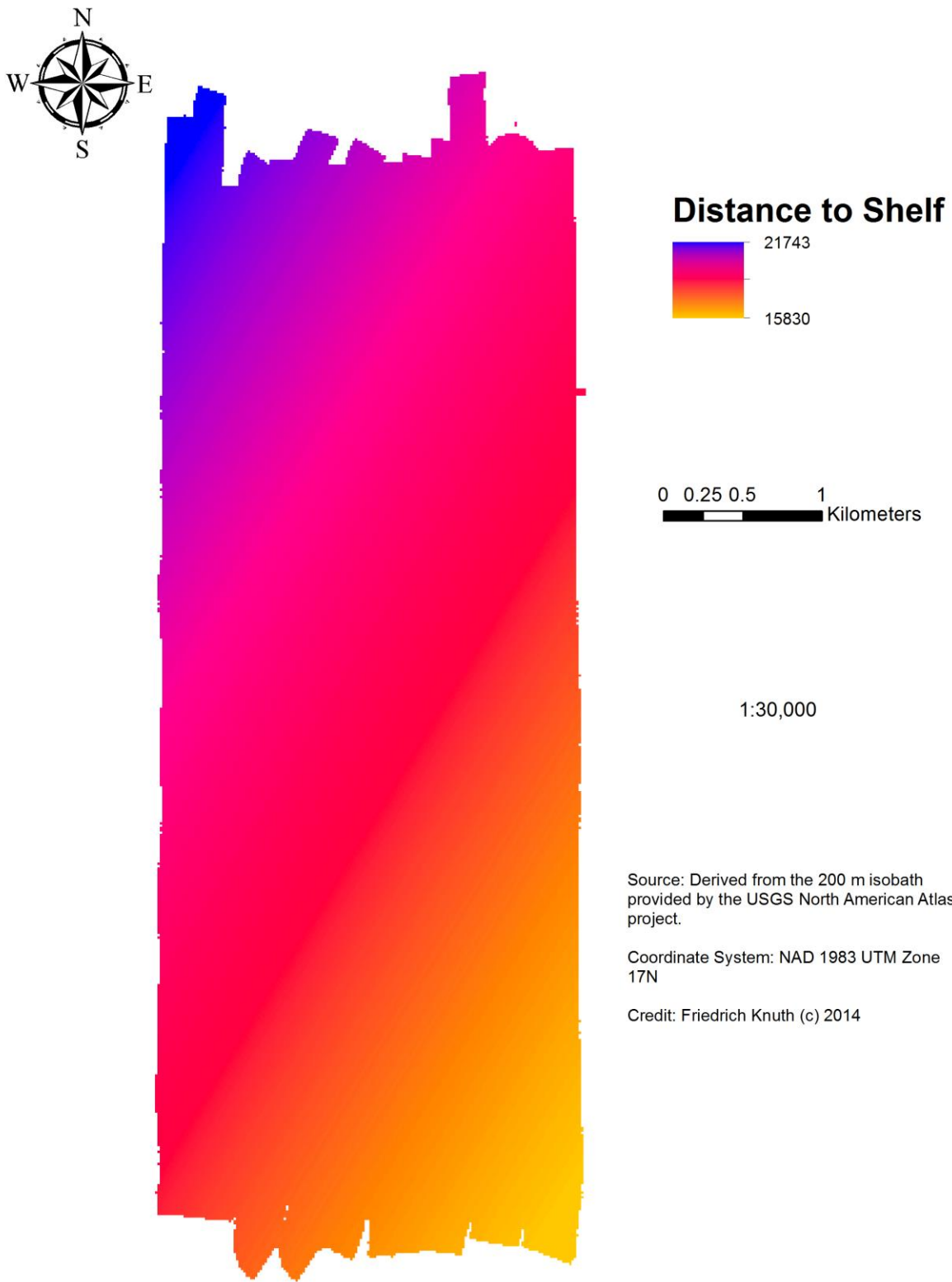


Figure 75. Distance of each 2x2 m raster cell to 200 m isobaths at N of Edisto MPA.

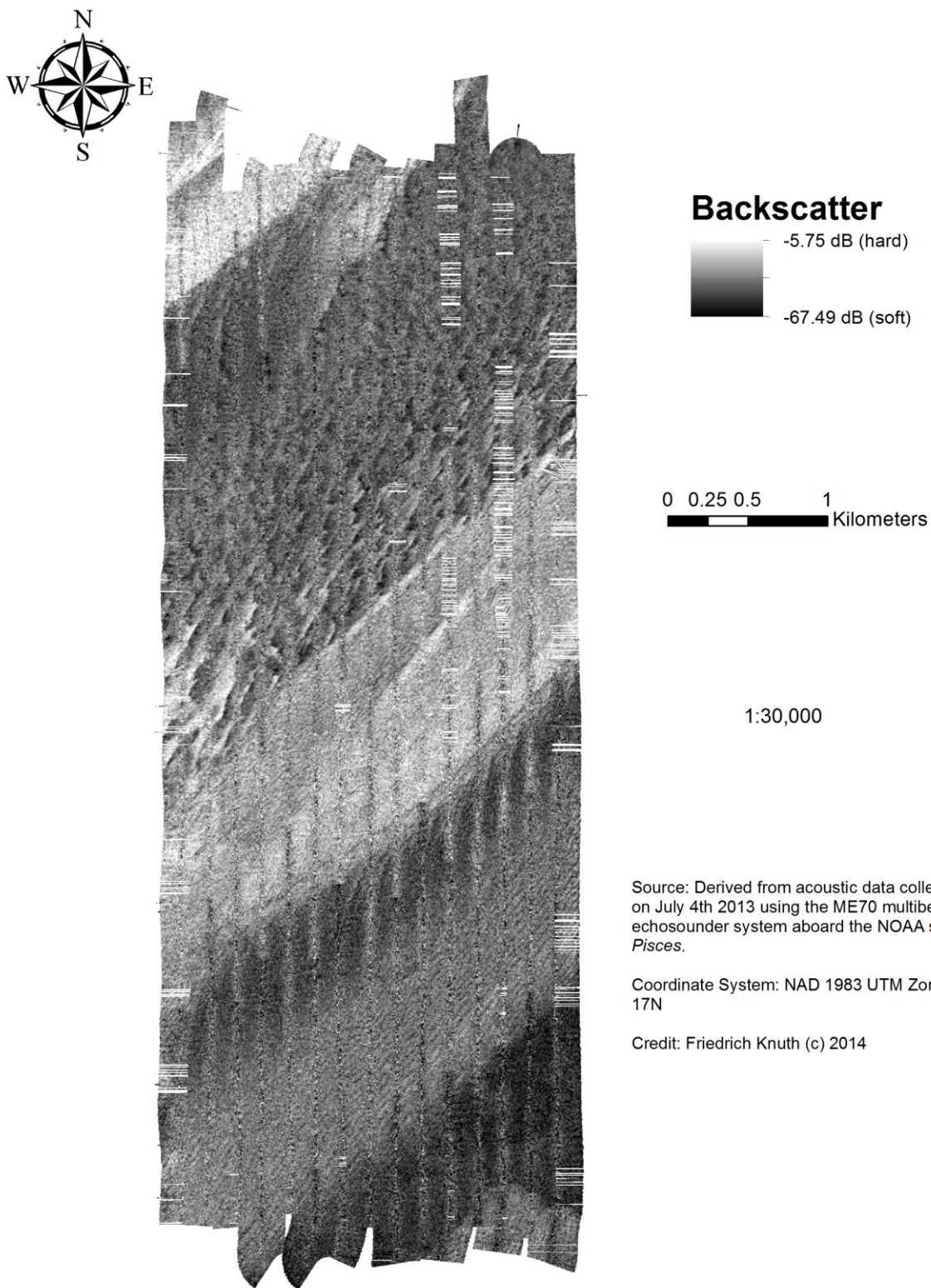
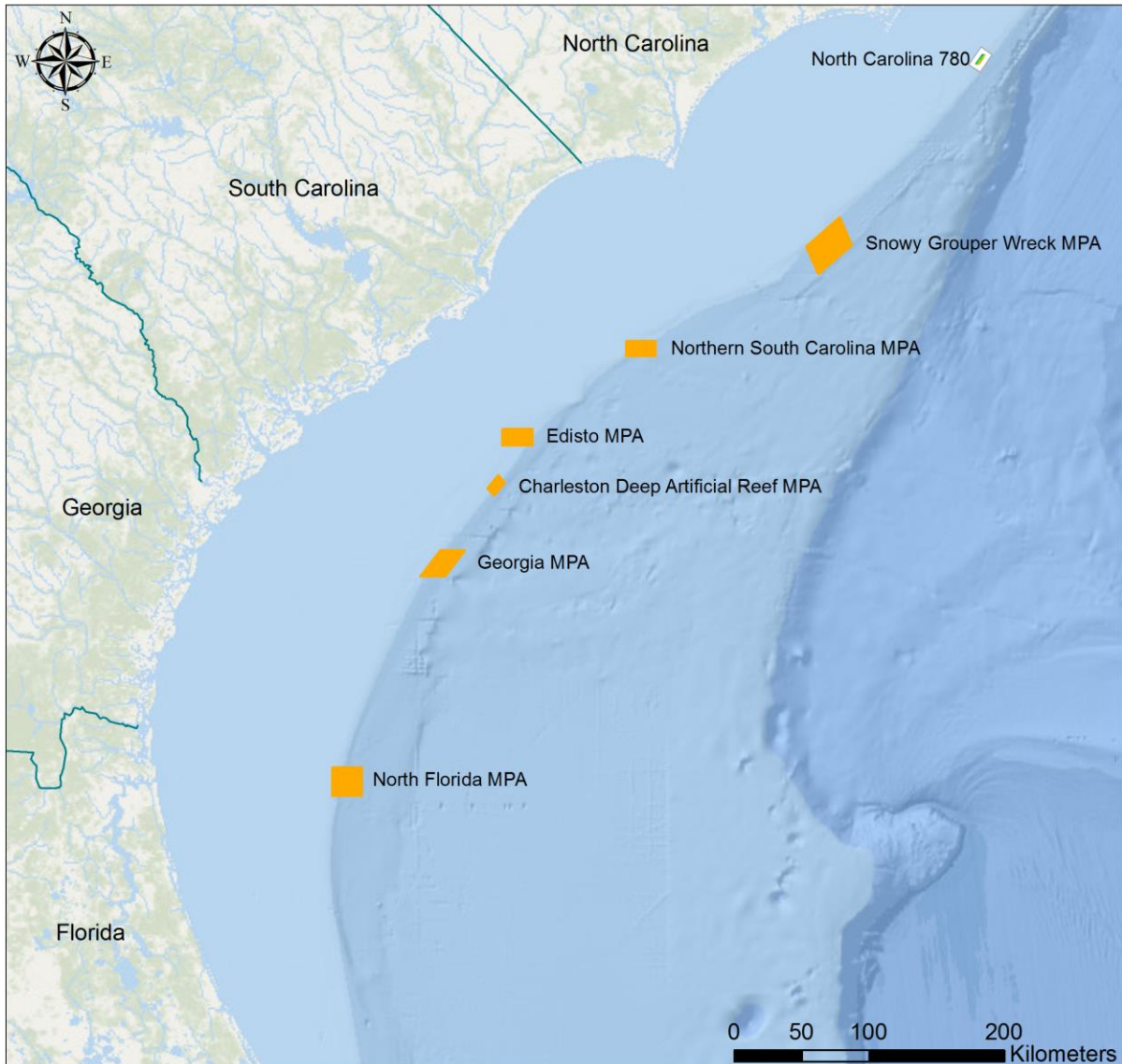


Figure 76. Intensity of the acoustic return at N of Edisto MPA.

NORTH CAROLINA 780



Legend

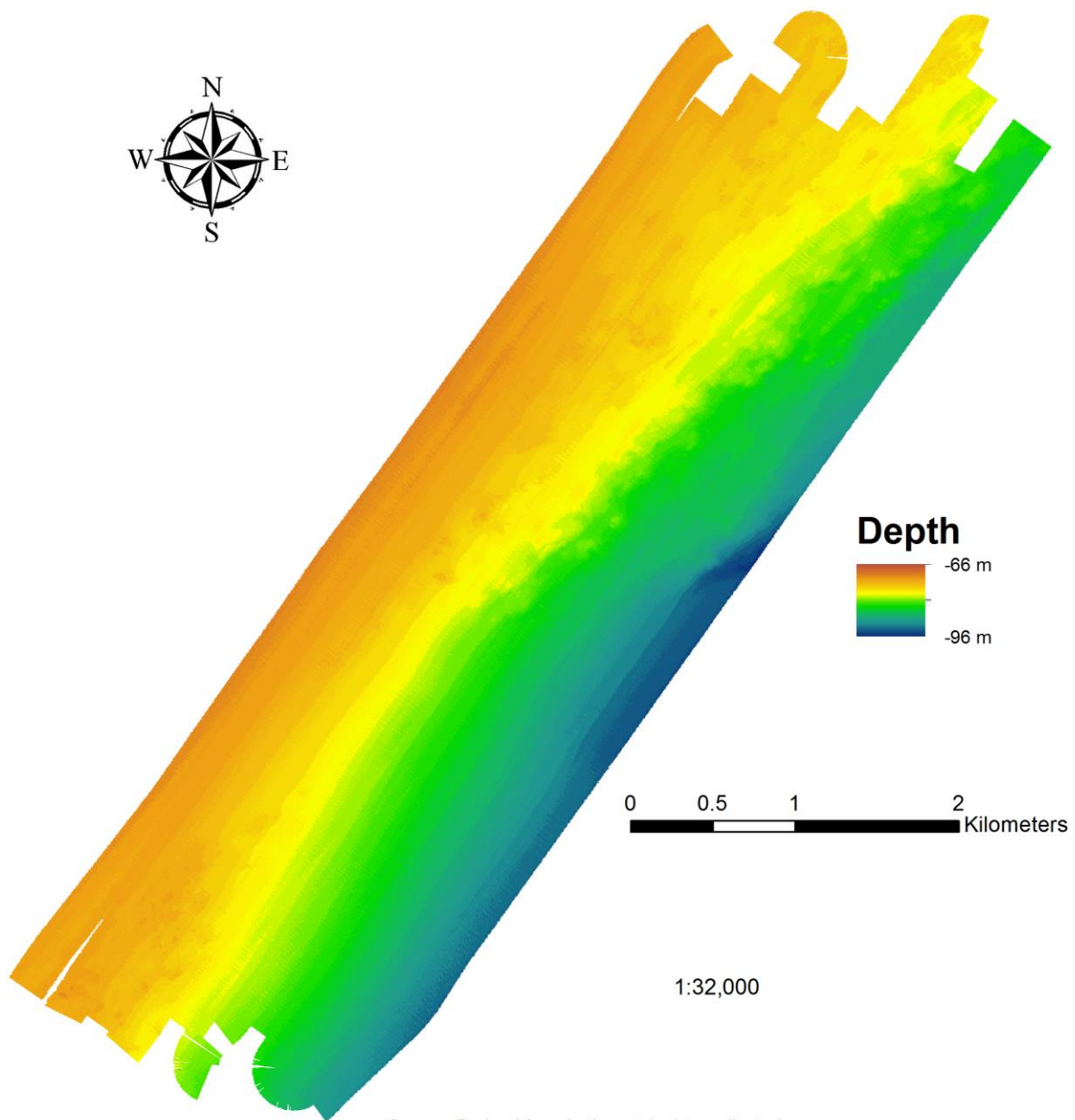
- State Boundaries
- Survey Site North Carolina 780
- Marine Protected Areas (MPAs)

Friedrich Knuth (c)
College of Charleston
2014

Source: SAFMC online GIS database, NOAA, SEAMAP, MARMAP, ESRI (base layer)

Coordinate System: WGS 1984 Web Mercator

Figure 77. Location of North Carolina 780 survey site relative to existing MPAs.

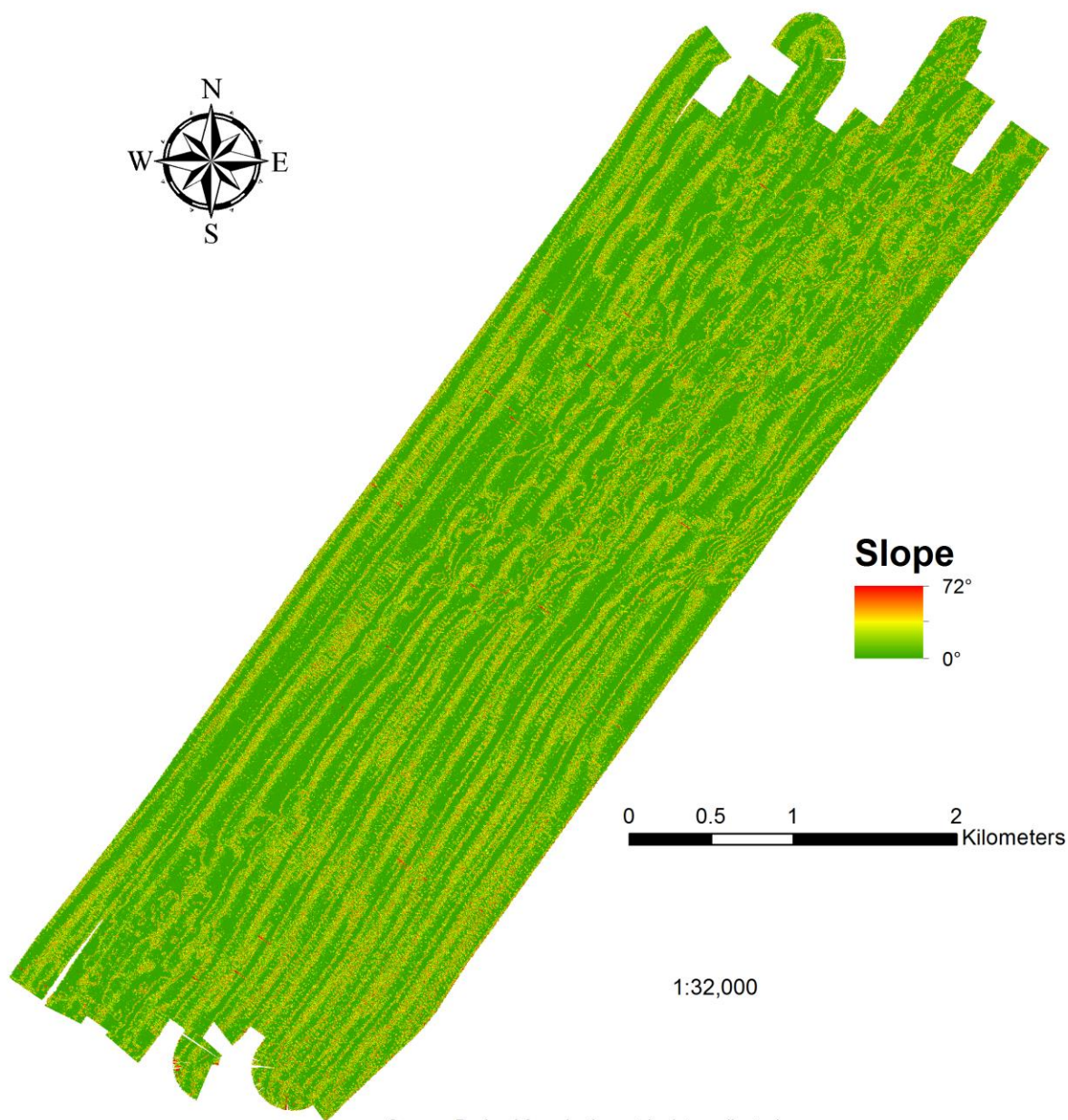


Source: Derived from bathymetric data collected on July 7th 2013 using the ME70 multibeam echosounder system aboard the NOAA ship *Pisces*.

Coordinate System: NAD 1983 UTM Zone 18N

Credit: Friedrich Knuth (c) 2014

Figure 78. Depth of sea level to seafloor at North Carolina 780.

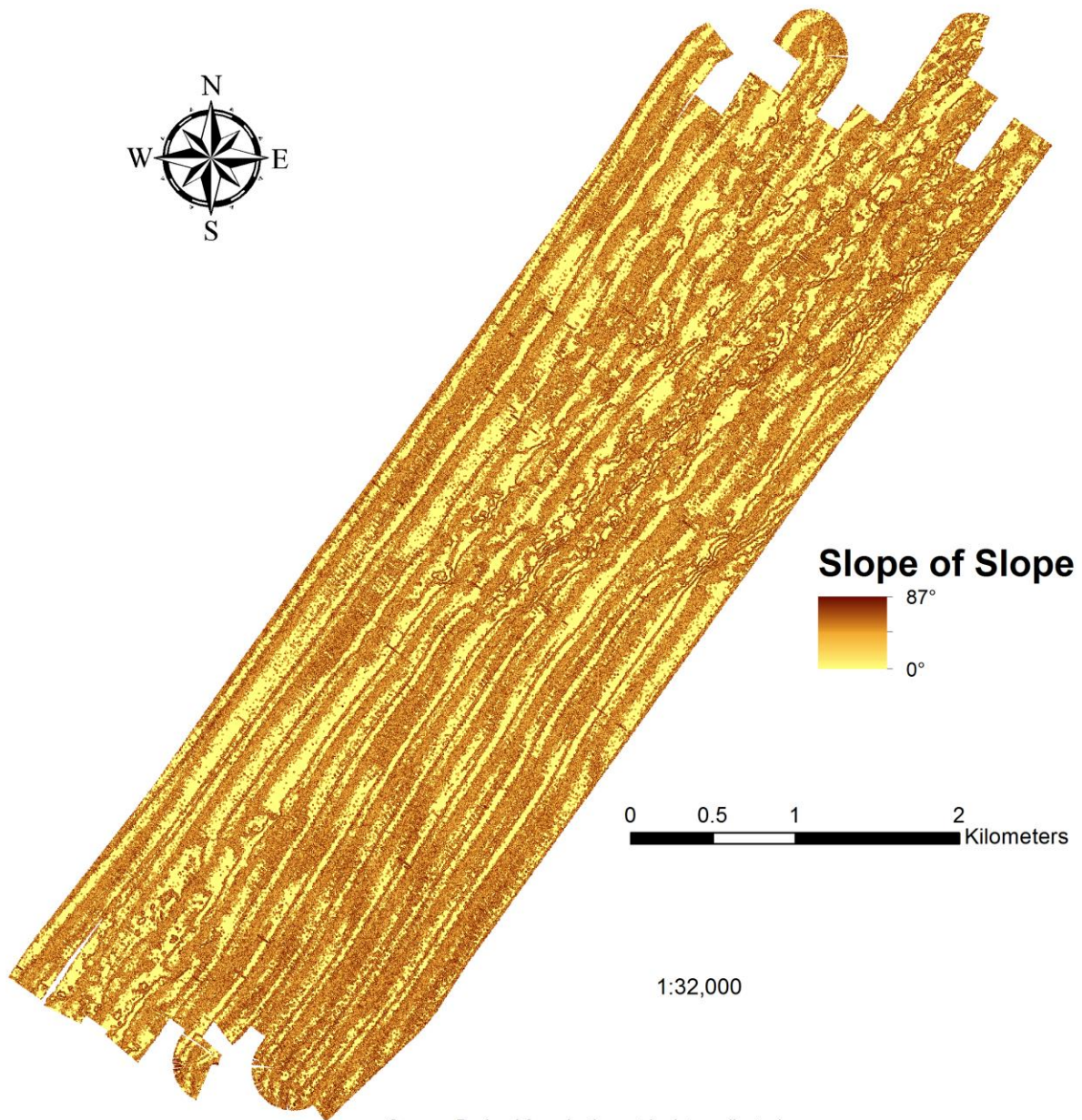


Source: Derived from bathymetric data collected on July 7th 2013 using the ME70 multibeam echosounder system aboard the NOAA ship *Pisces*.

Coordinate System: NAD 1983 UTM Zone 18N

Credit: Friedrich Knuth (c) 2014

Figure 79. Maximum rate of change in depth between 2 x 2 m raster cell and eight neighbors at North Carolina 780.



Source: Derived from bathymetric data collected on July 7th 2013 using the ME70 multibeam echosounder system aboard the NOAA ship *Pisces*.

Coordinate System: NAD 1983 UTM Zone 18N

Credit: Friedrich Knuth (c) 2014

Figure 80. Maximum rate of change in slope between cell and eight neighbors at North Carolina 780.

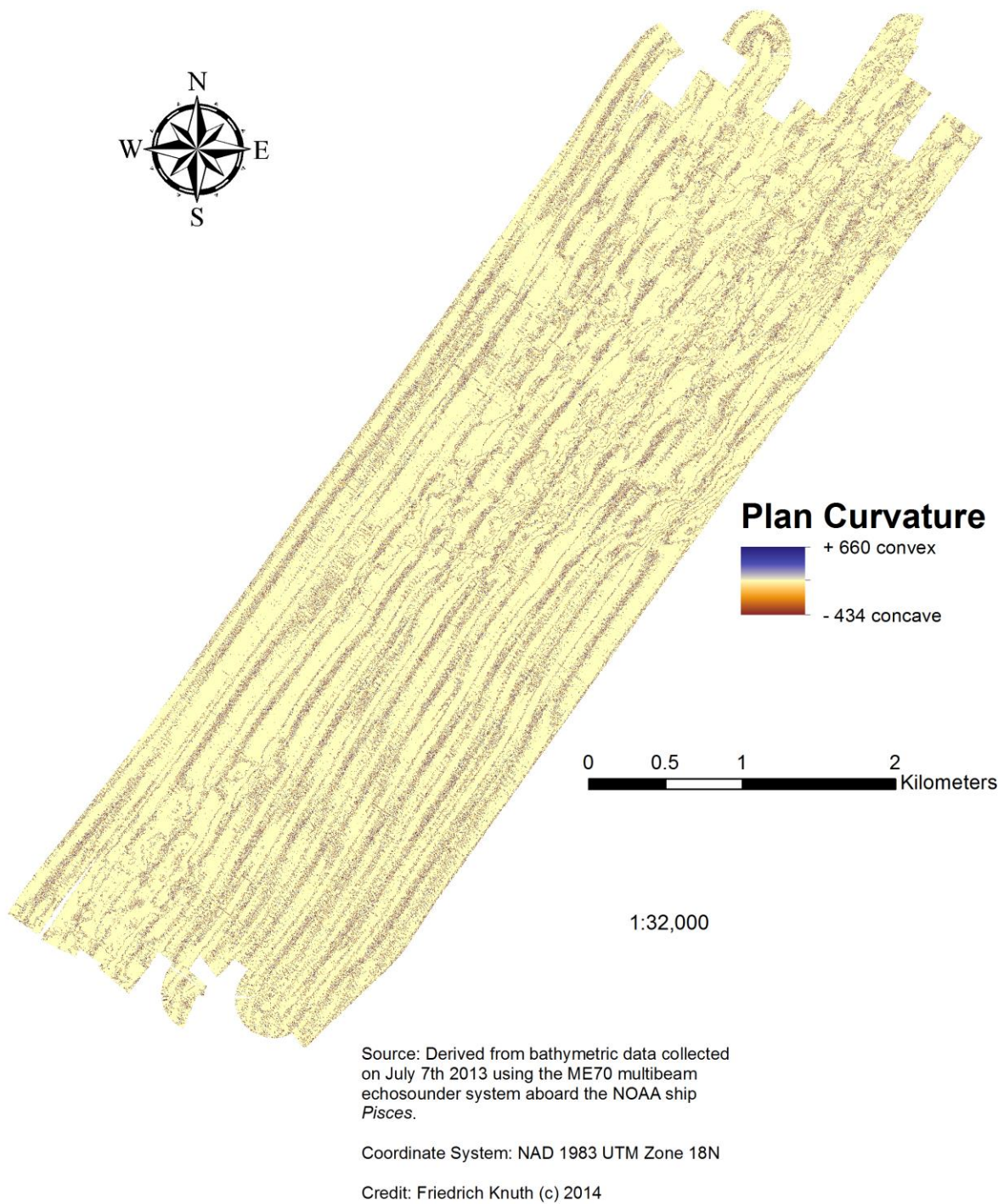


Figure 81. Rate of change in curvature across the surface at North Carolina 780.



Source: Derived from bathymetric data collected on July 7th 2013 using the ME70 multibeam echosounder system aboard the NOAA ship *Pisces*.

Coordinate System: NAD 1983 UTM Zone 18N

Credit: Friedrich Knuth (c) 2014

Figure 82. Ratio of surface area to planar surface area at North Carolina 780.

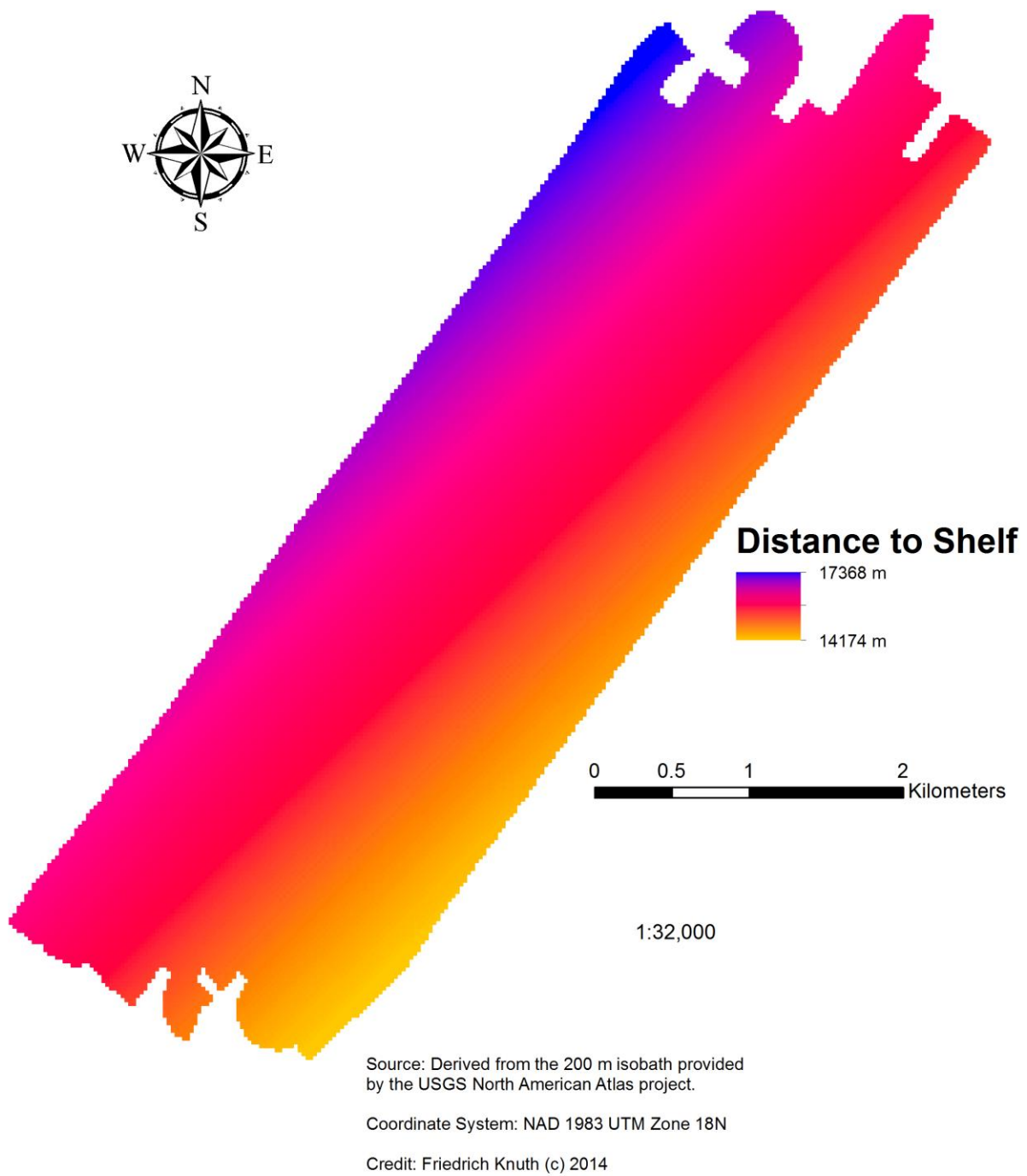
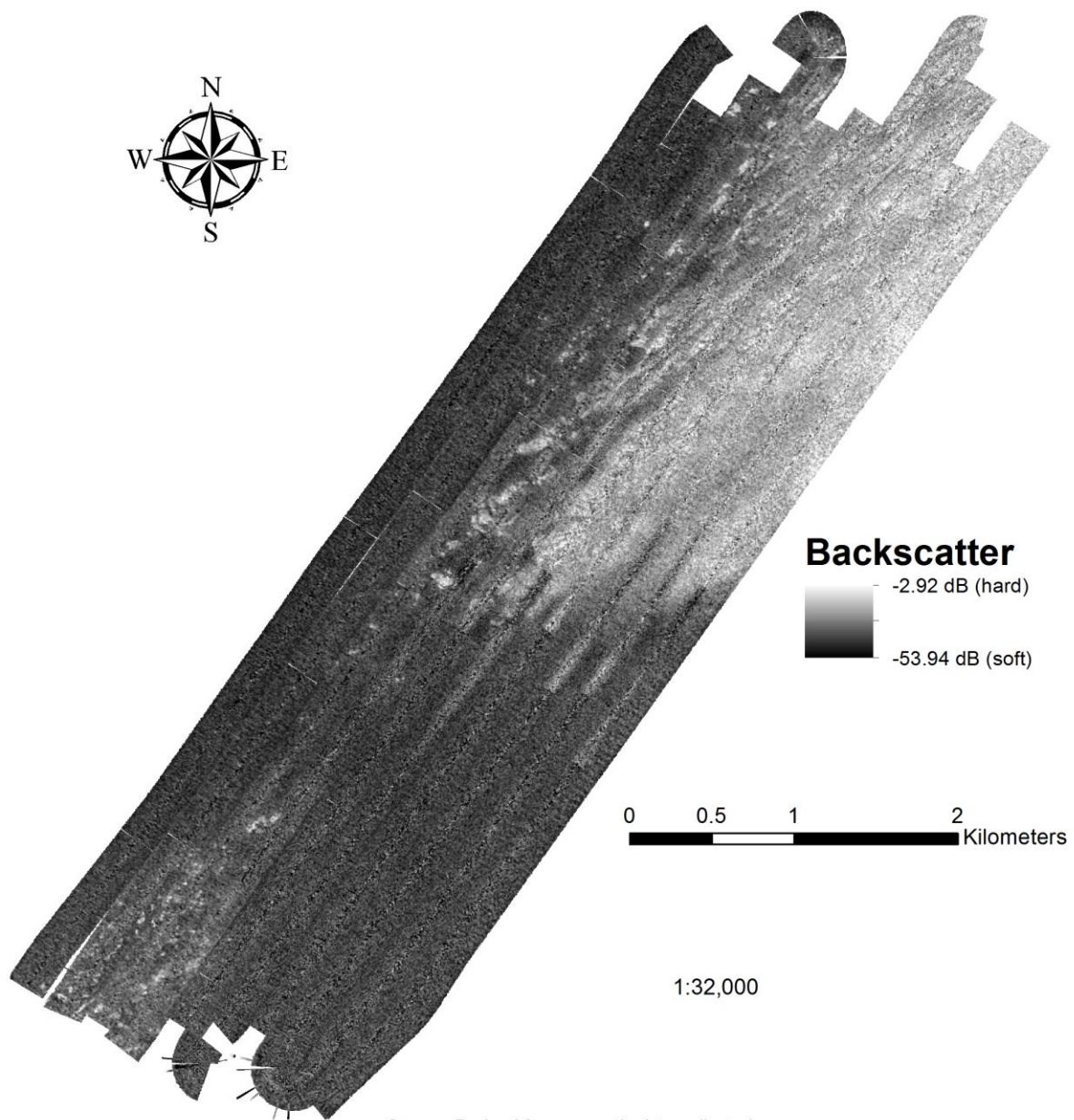


Figure 83. Distance of each 2x2 m raster cell to 200 m isobaths at North Carolina 780.



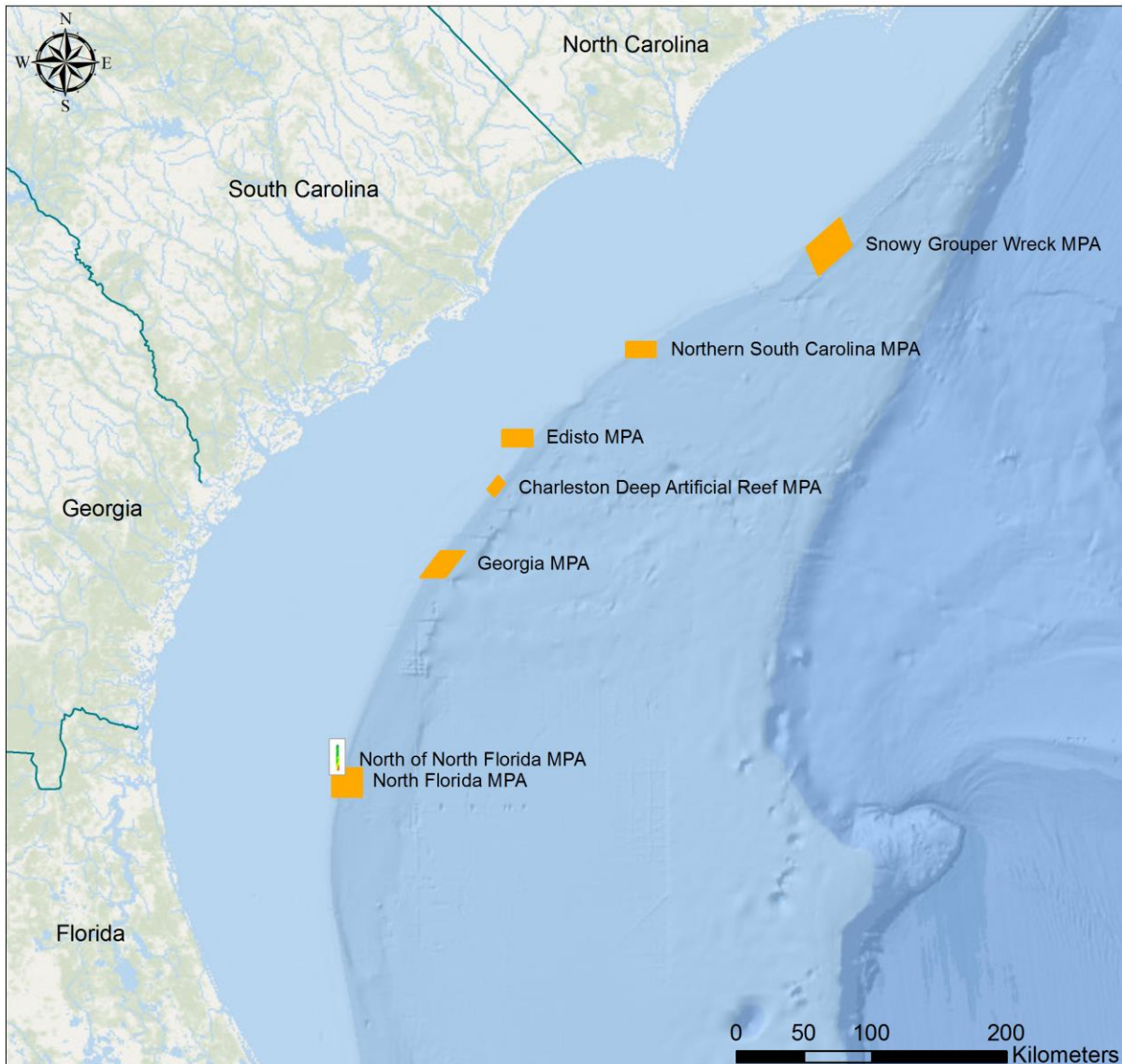
Source: Derived from acoustic data collected on July 7th 2013 using the ME70 multibeam echosounder system aboard the NOAA ship *Pisces*.

Coordinate System: NAD 1983 UTM Zone 18N

Credit: Friedrich Knuth (c) 2014

Figure 84. Intensity of the acoustic return at North Carolina 780.

NORTH OF NORTH FLORIDA MPA



Legend

- State Boundaries
- Survey Site North of North Florida MPA
- Marine Protected Areas (MPAs)

Friedrich Knuth (c)
College of Charleston
2014

Source: SAFMC online GIS database, NOAA, SEAMAP, MARMAP, ESRI (base layer)

Coordinate System: WGS 1984 Web Mercator

Figure 85. Location of North Carolina 780 survey site relative to existing MPAs.

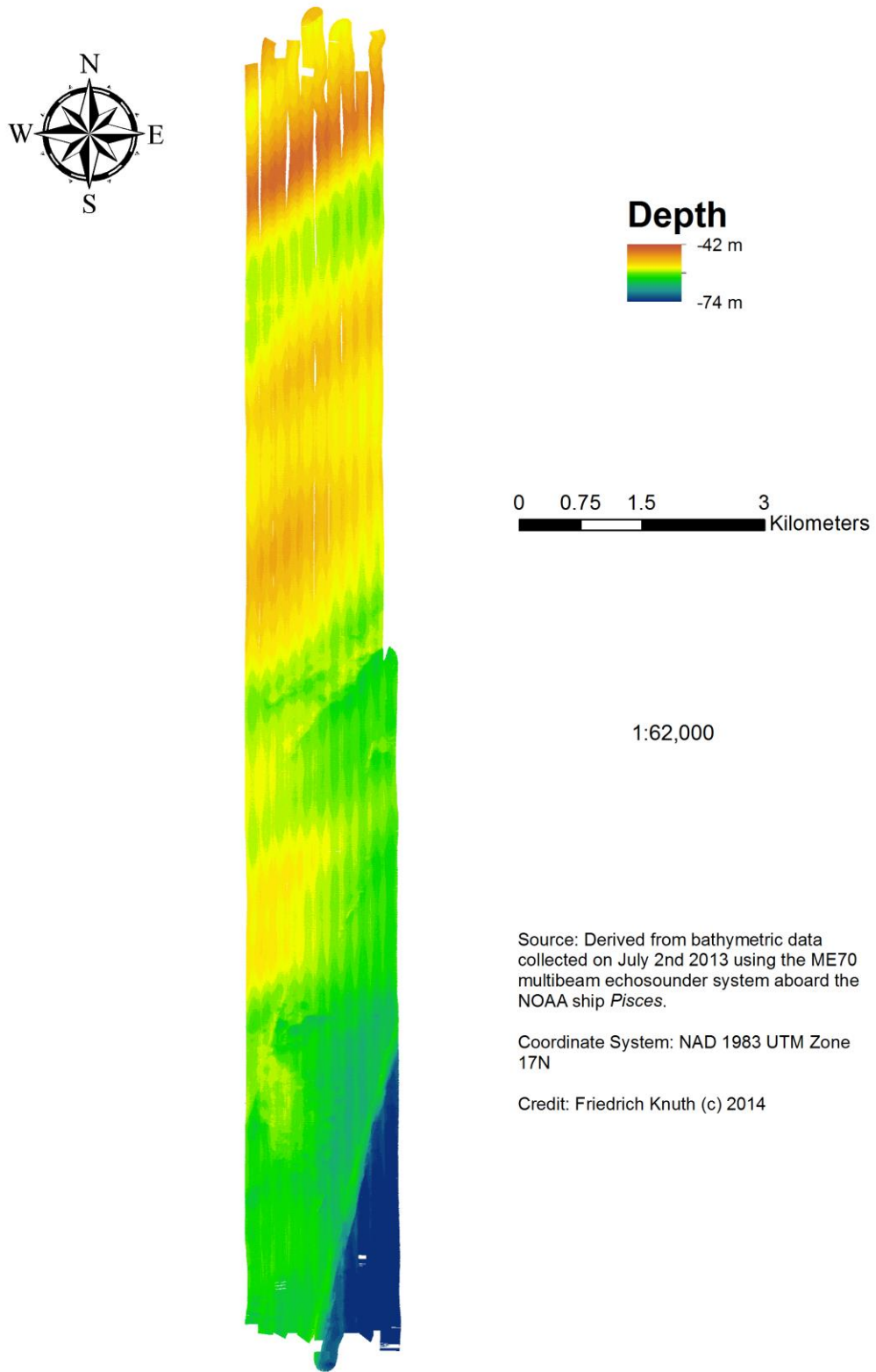


Figure 86. Depth of sea level to seafloor at North Carolina 780.

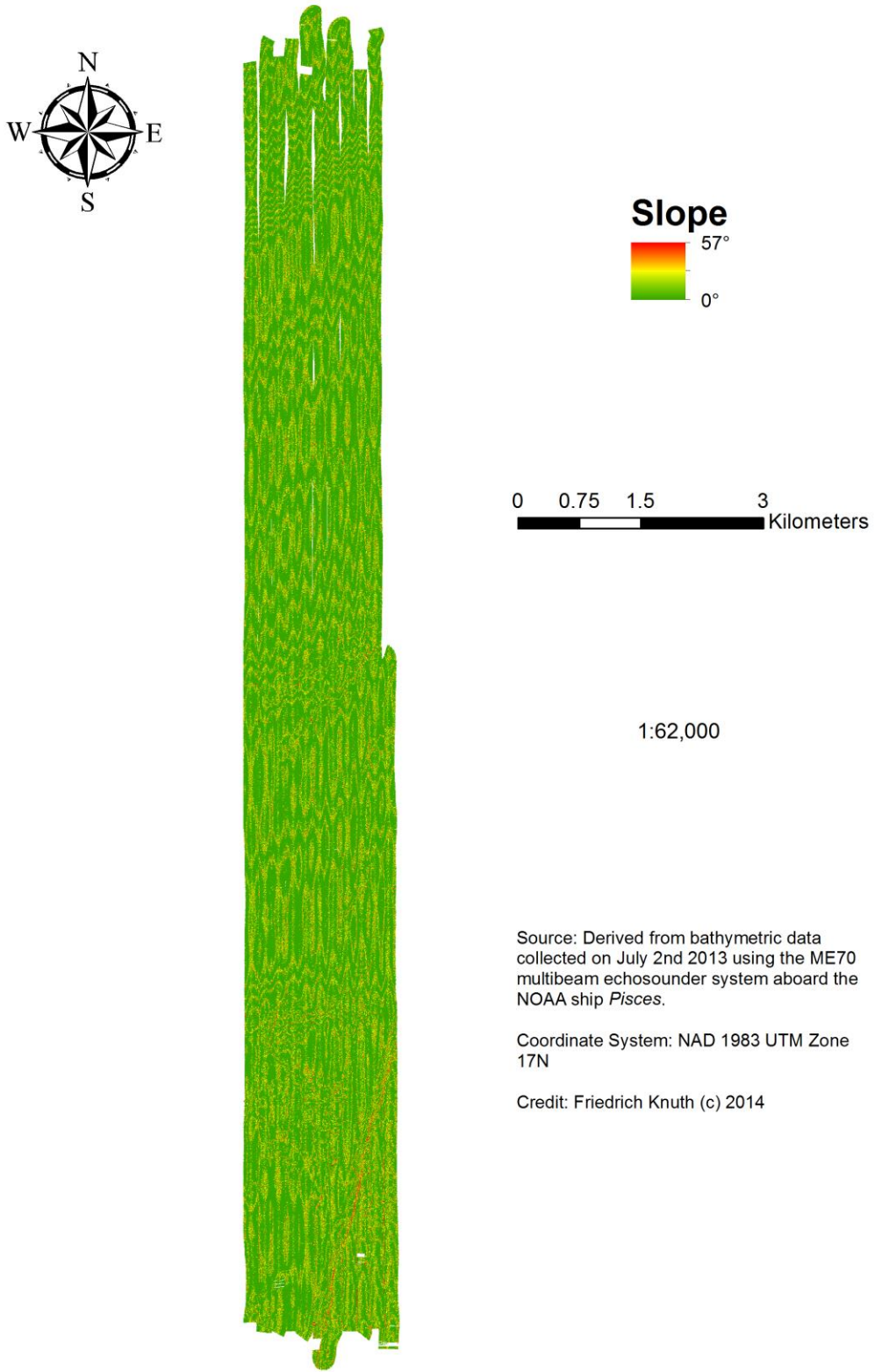


Figure 87. Maximum rate of change in depth between 2 x 2 m raster cell and eight neighbors at North Carolina 780.

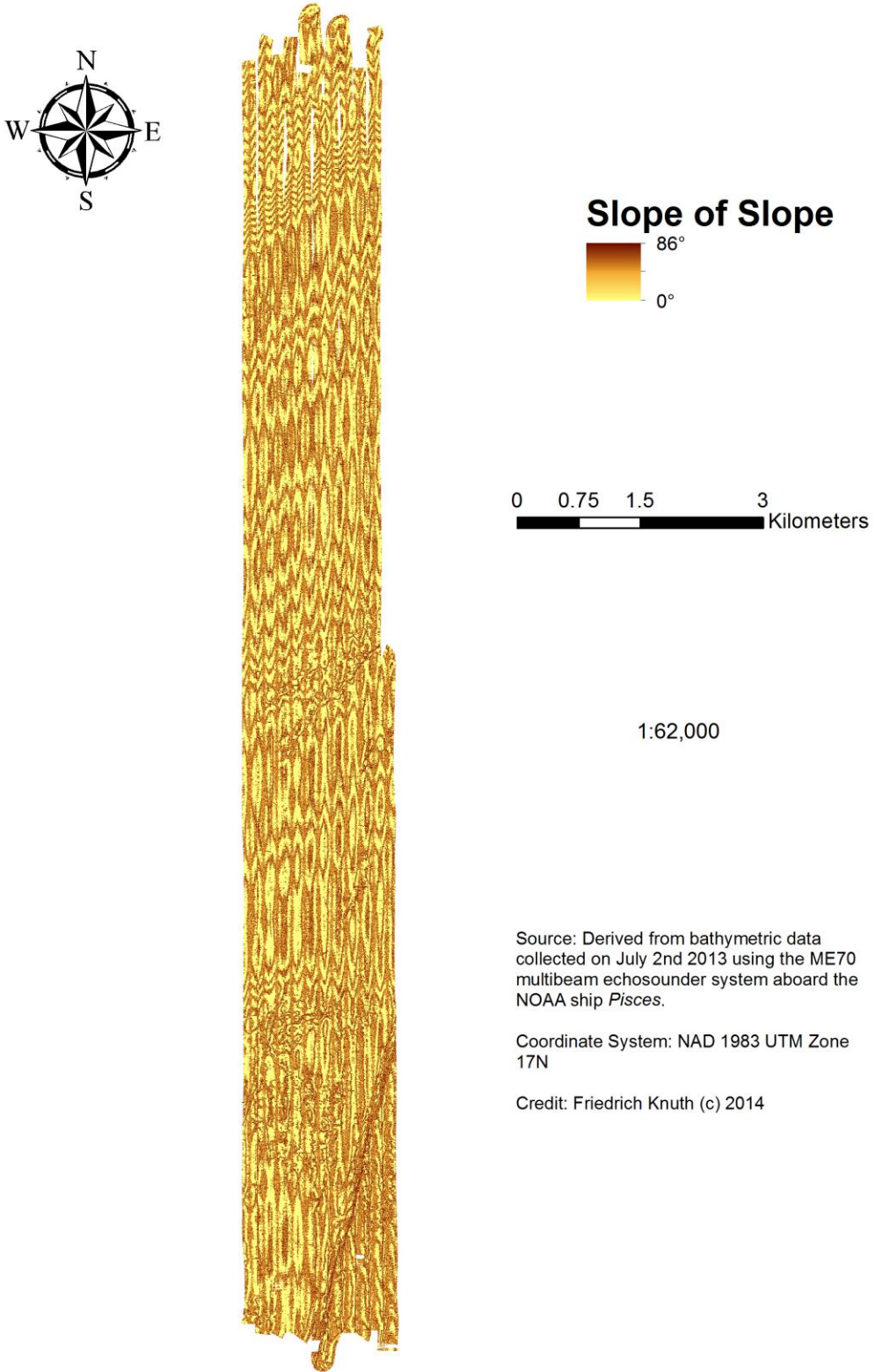


Figure 88. Maximum rate of change in slope between cell and eight neighbors at North Carolina 780.

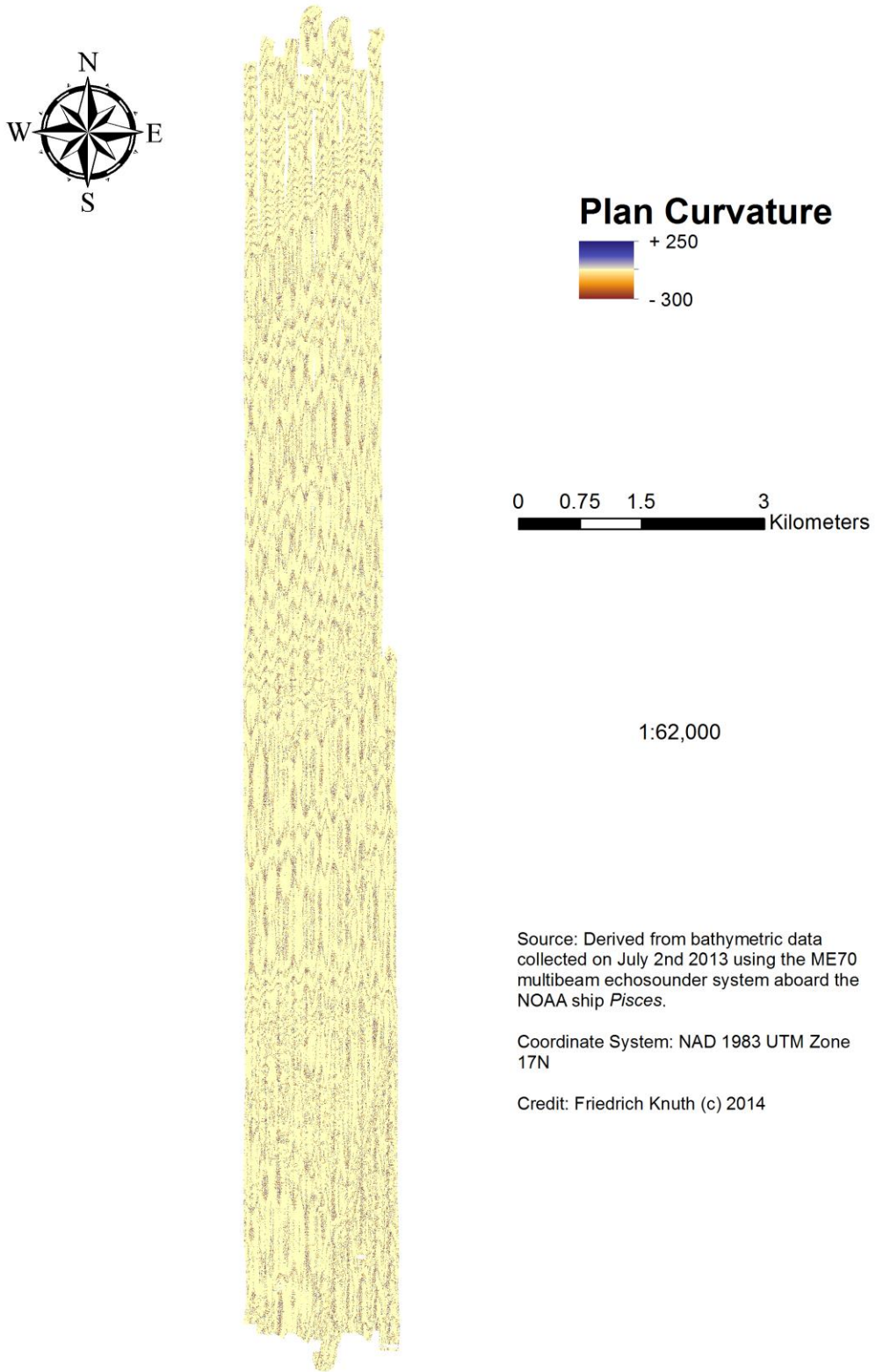


Figure 89. Rate of change in curvature across the surface at North Carolina 780.

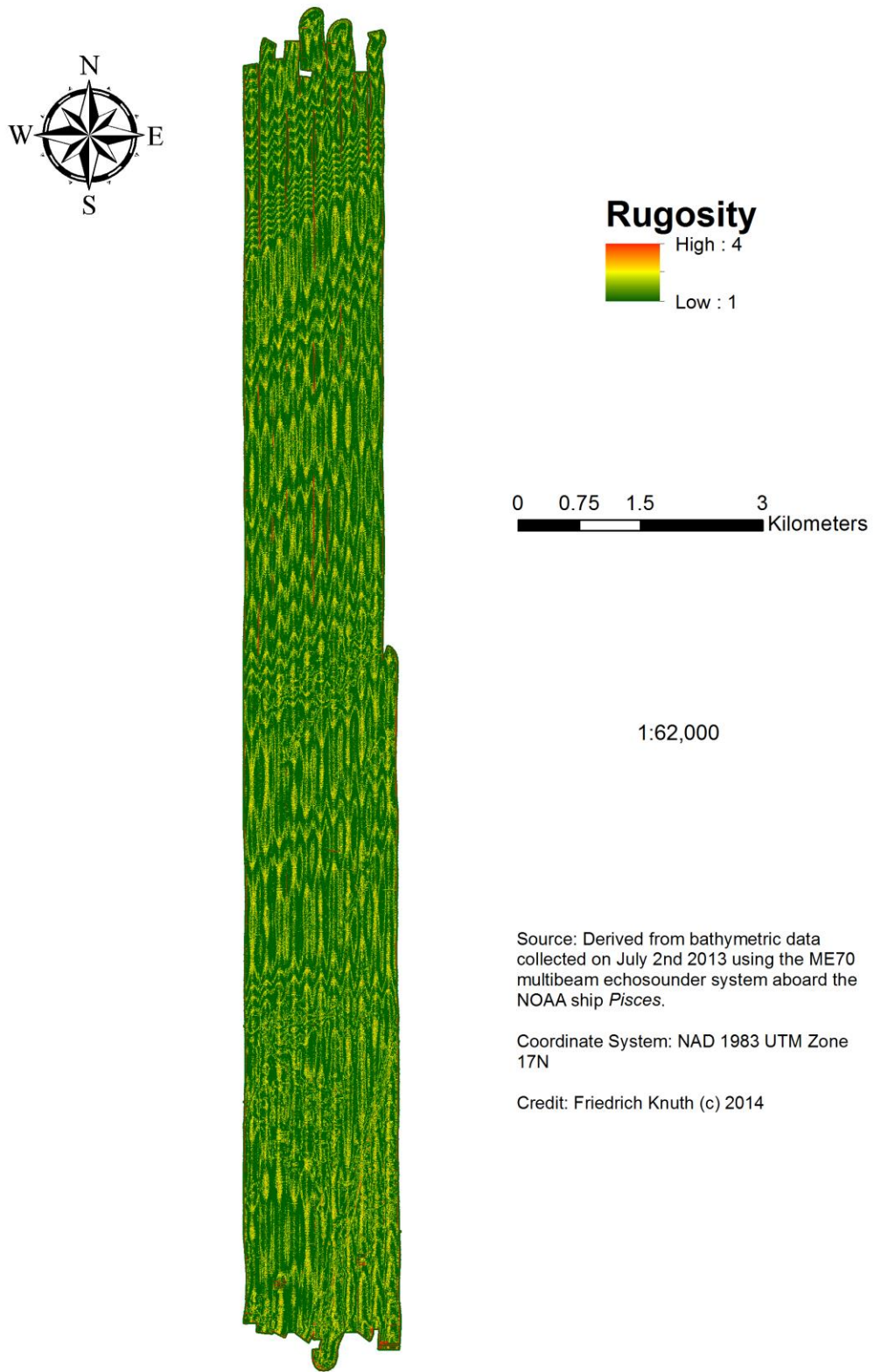


Figure 90. Ratio of surface area to planar surface area at North Carolina 780.

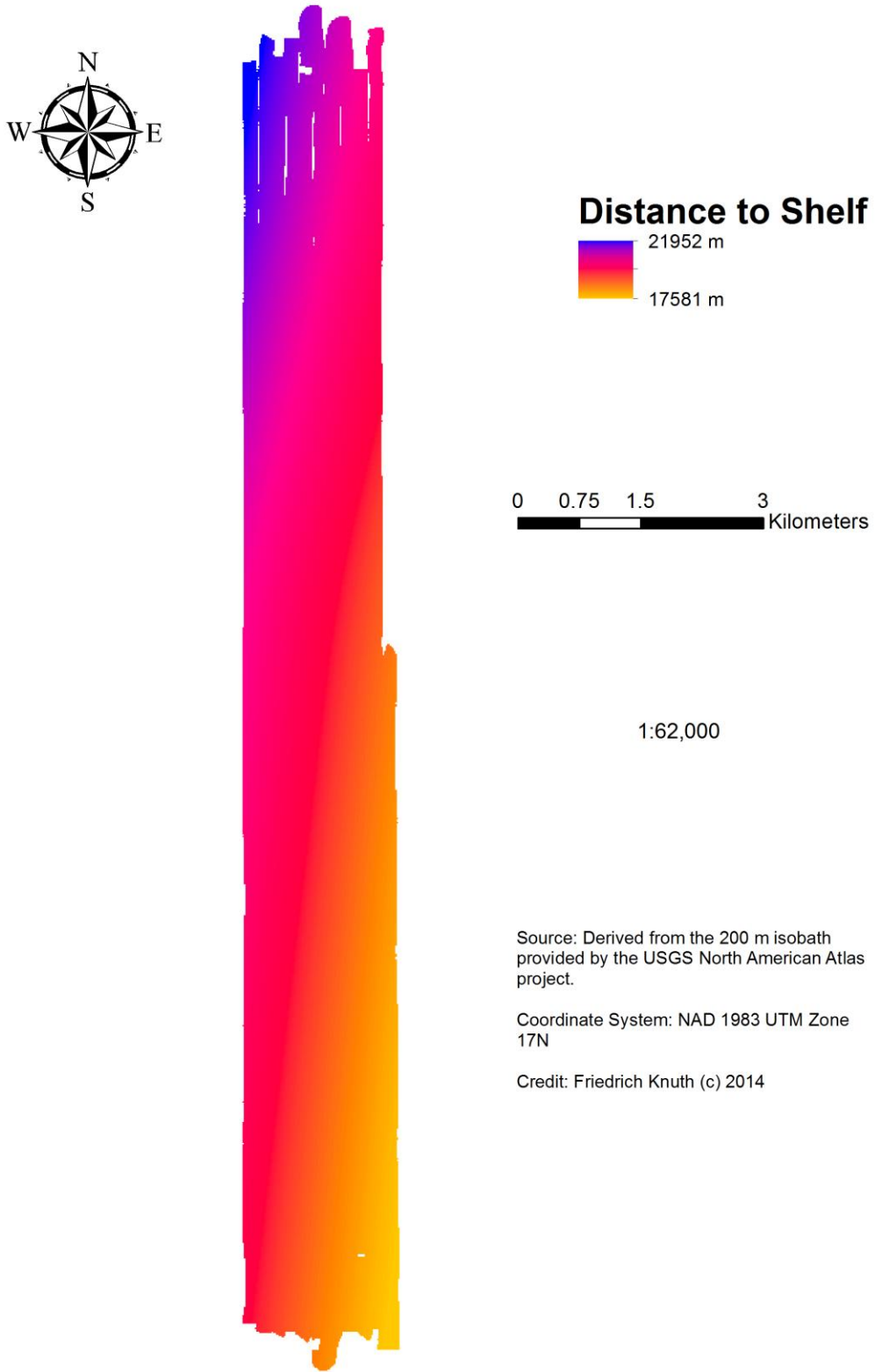


Figure 91. Distance of each 2x2 m raster cell to 200 m isobaths at North Carolina 780.

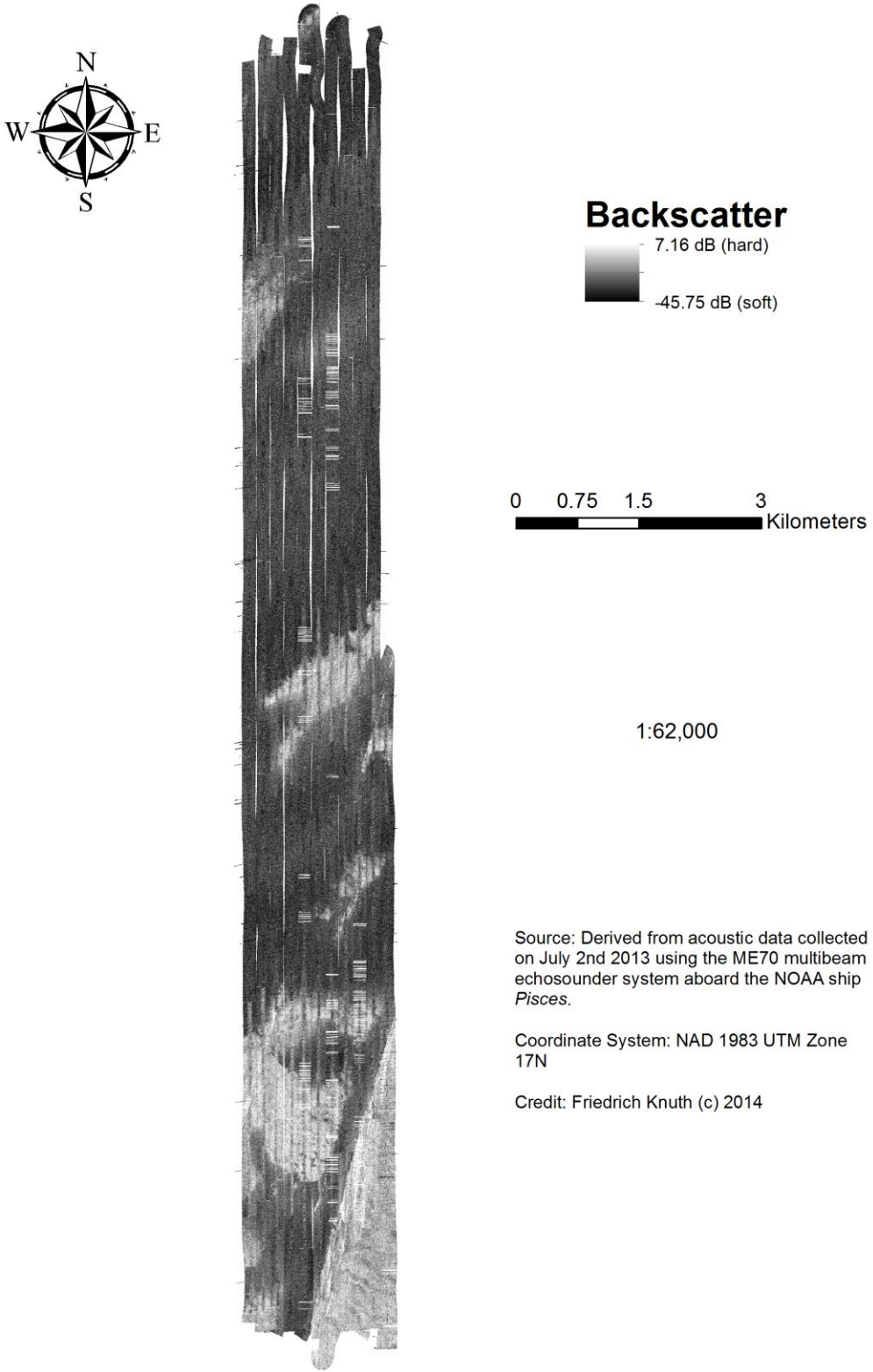
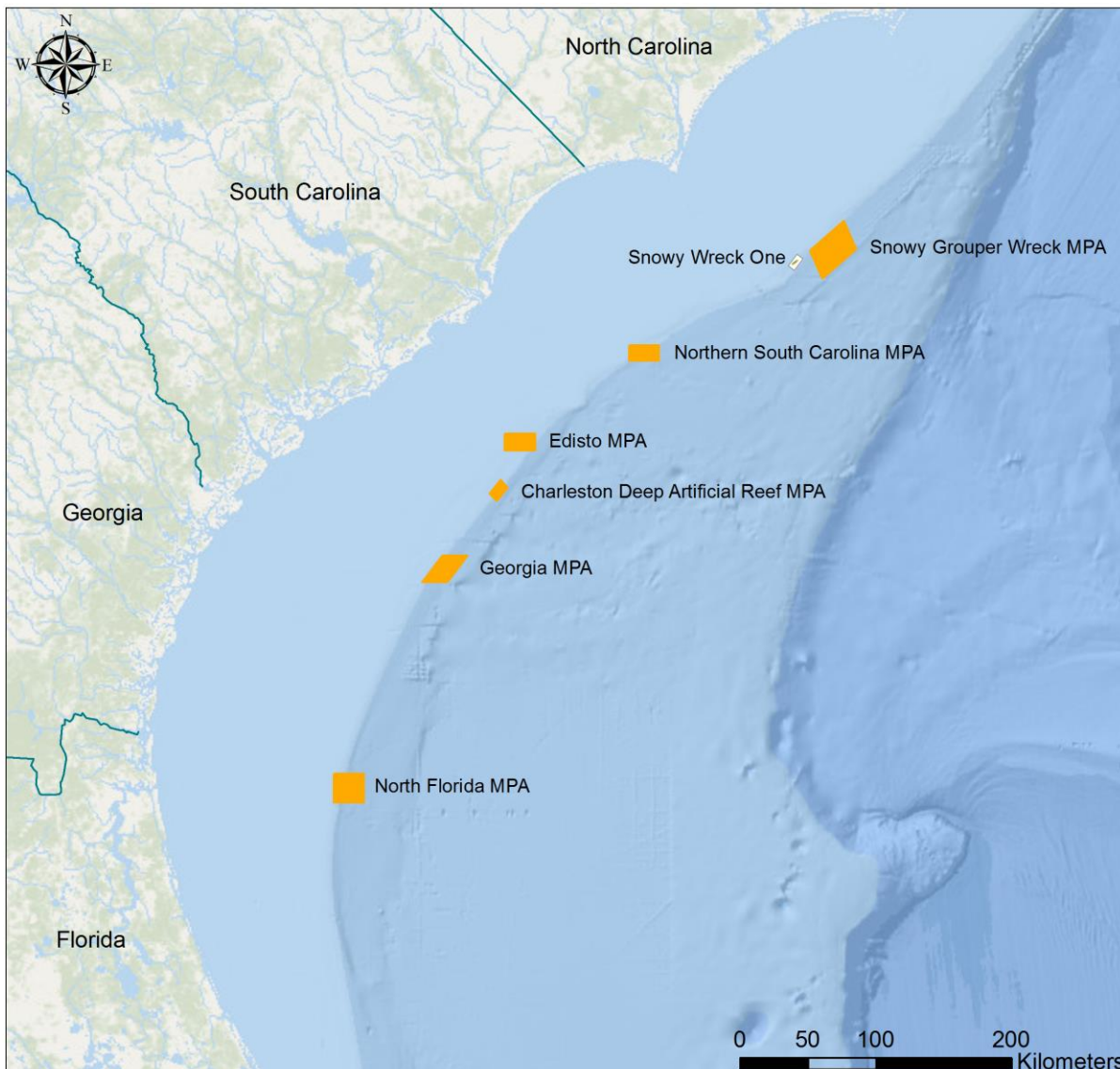


Figure 92. Intensity of the acoustic return at North Carolina 780.

SNOWY WRECK ONE



Legend

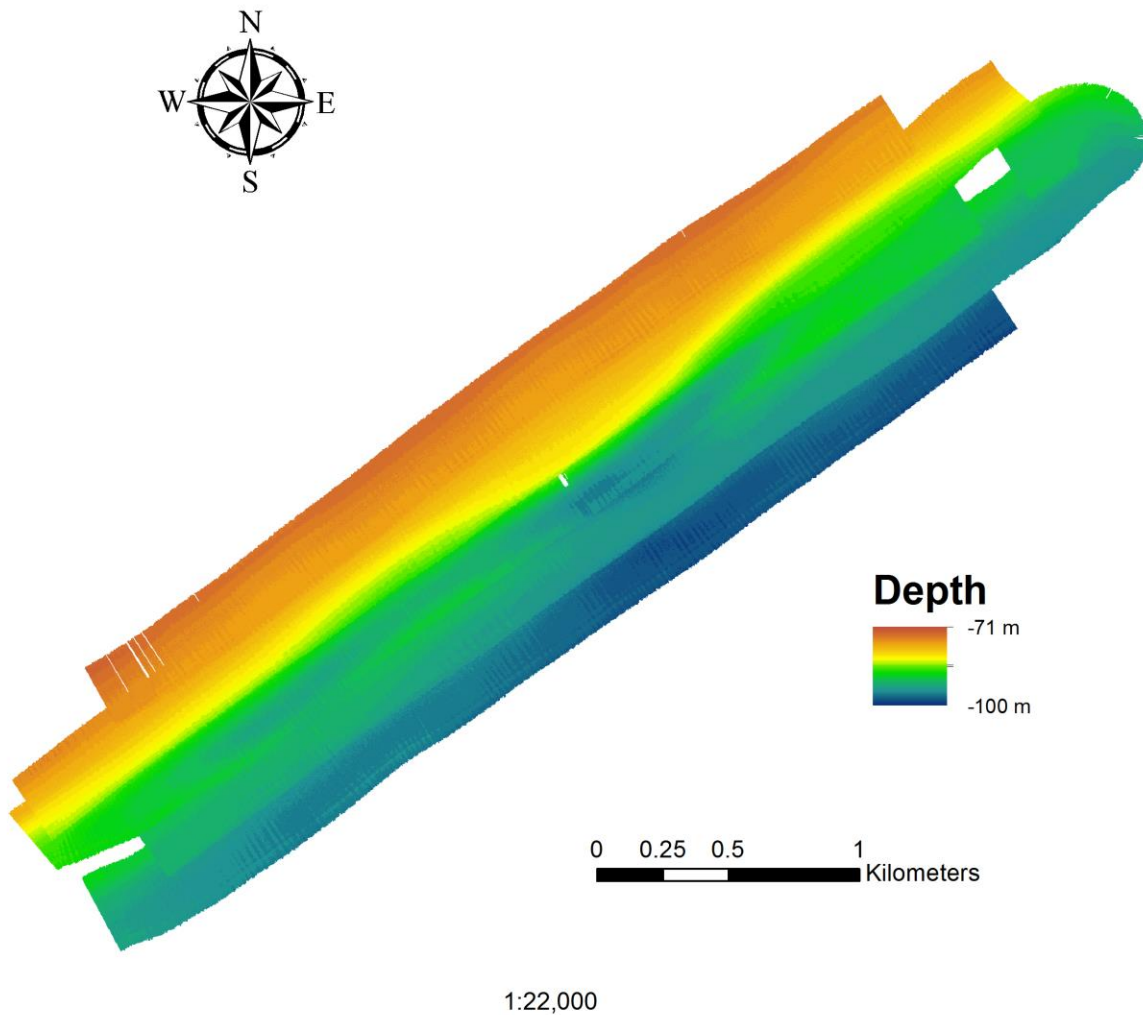
- State Boundaries
- Survey Site Snowy Wreck One
- Marine Protected Areas (MPAs)

Friedrich Knuth (c)
College of Charleston
2014

Source: SAFMC online GIS database, NOAA, SEAMAP, MARMAP, ESRI (base layer)

Coordinate System: WGS 1984 Web Mercator

Figure 93. Location of Snowy Wreck One survey site relative to existing MPAs.

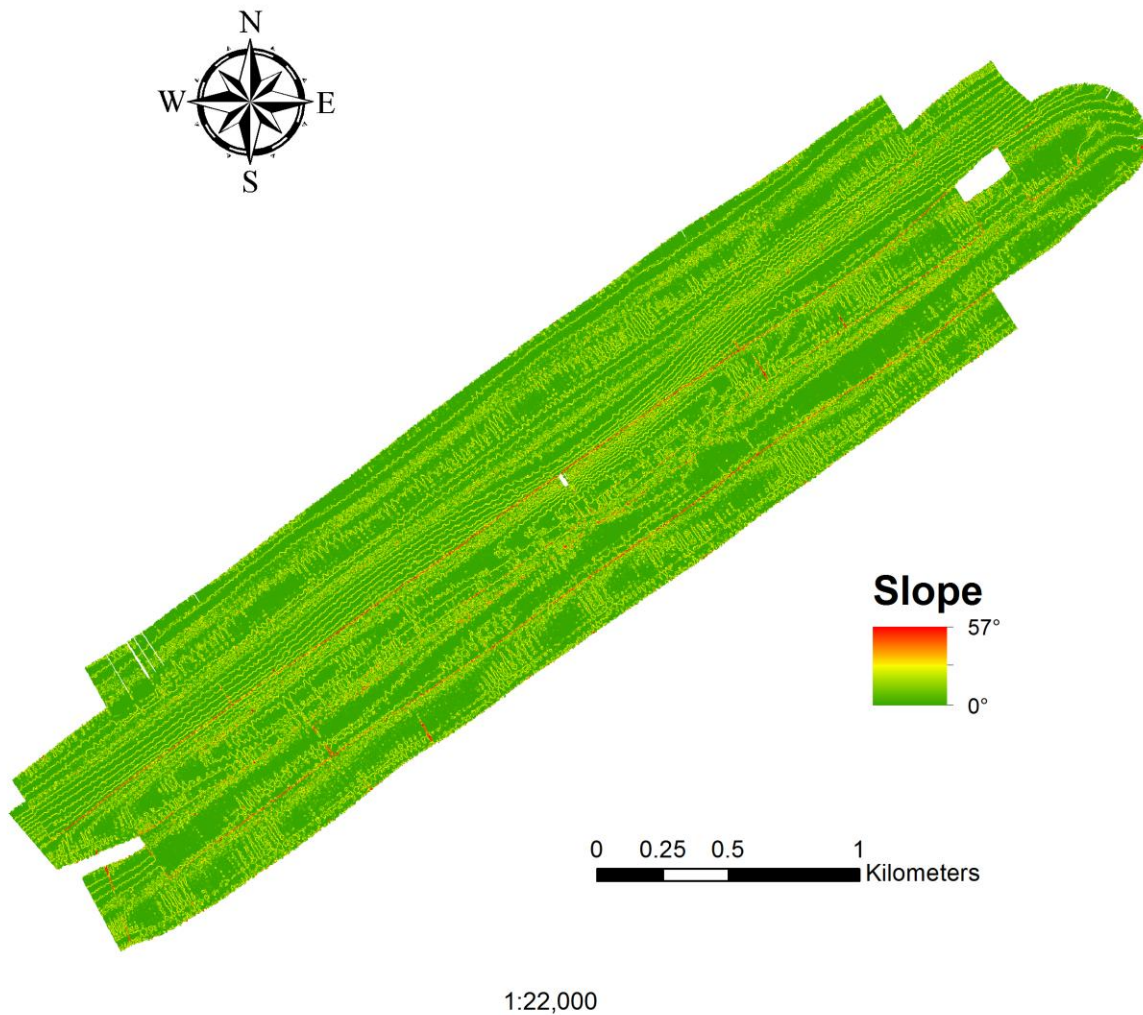


Source: Derived from bathymetric data collected on July 6th 2013 using the ME70 multibeam echosounder system aboard the NOAA ship *Pisces*.

Coordinate System: NAD 1983 UTM Zone 18N

Credit: Friedrich Knuth (c) 2014

Figure 94. Depth of sea level to seafloor at Snowy Wreck One.

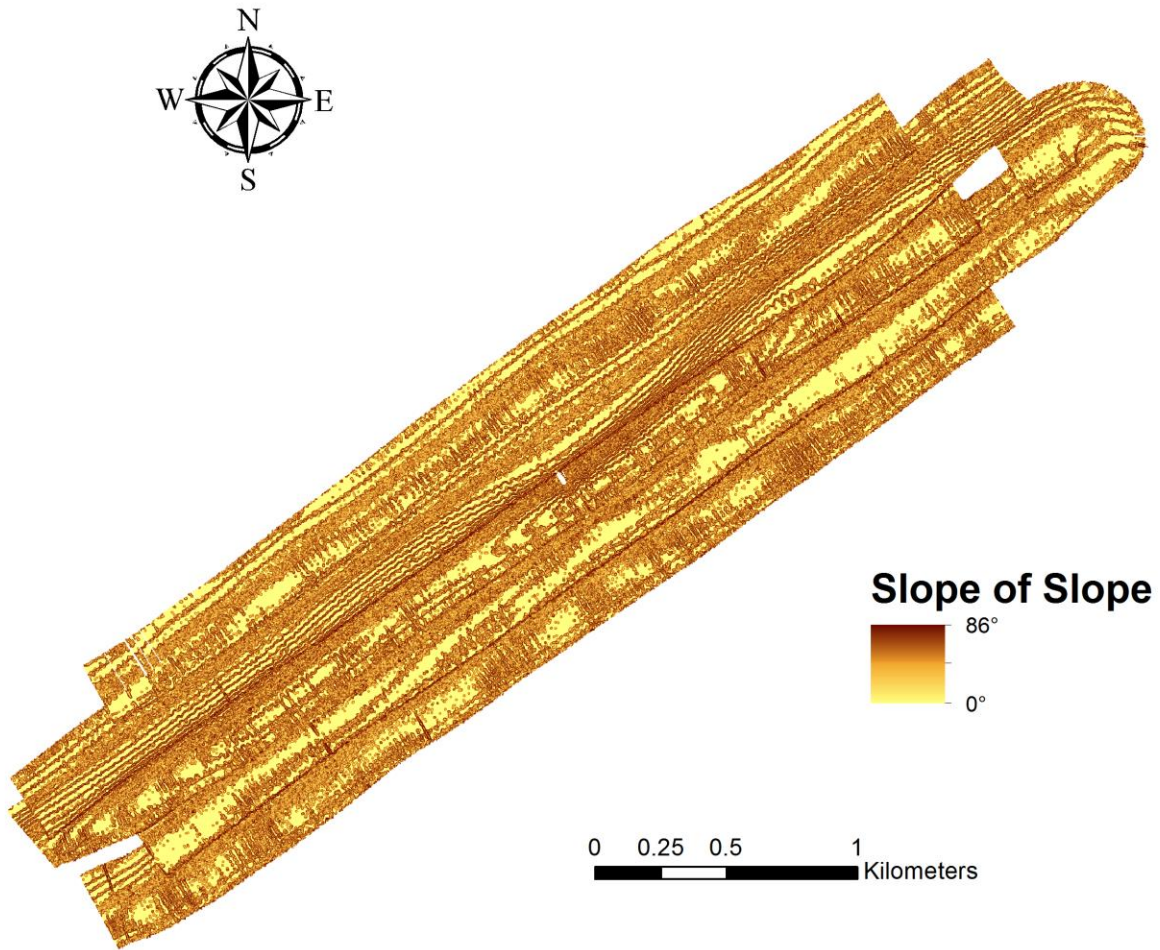


Source: Derived from bathymetric data collected on July 6th 2013 using the ME70 multibeam echosounder system aboard the NOAA ship *Pisces*.

Coordinate System: NAD 1983 UTM Zone 18N

Credit: Friedrich Knuth (c) 2014

Figure 95. Maximum rate of change in depth between 2 x 2 m raster cell and eight neighbors at Snowy Wreck One.



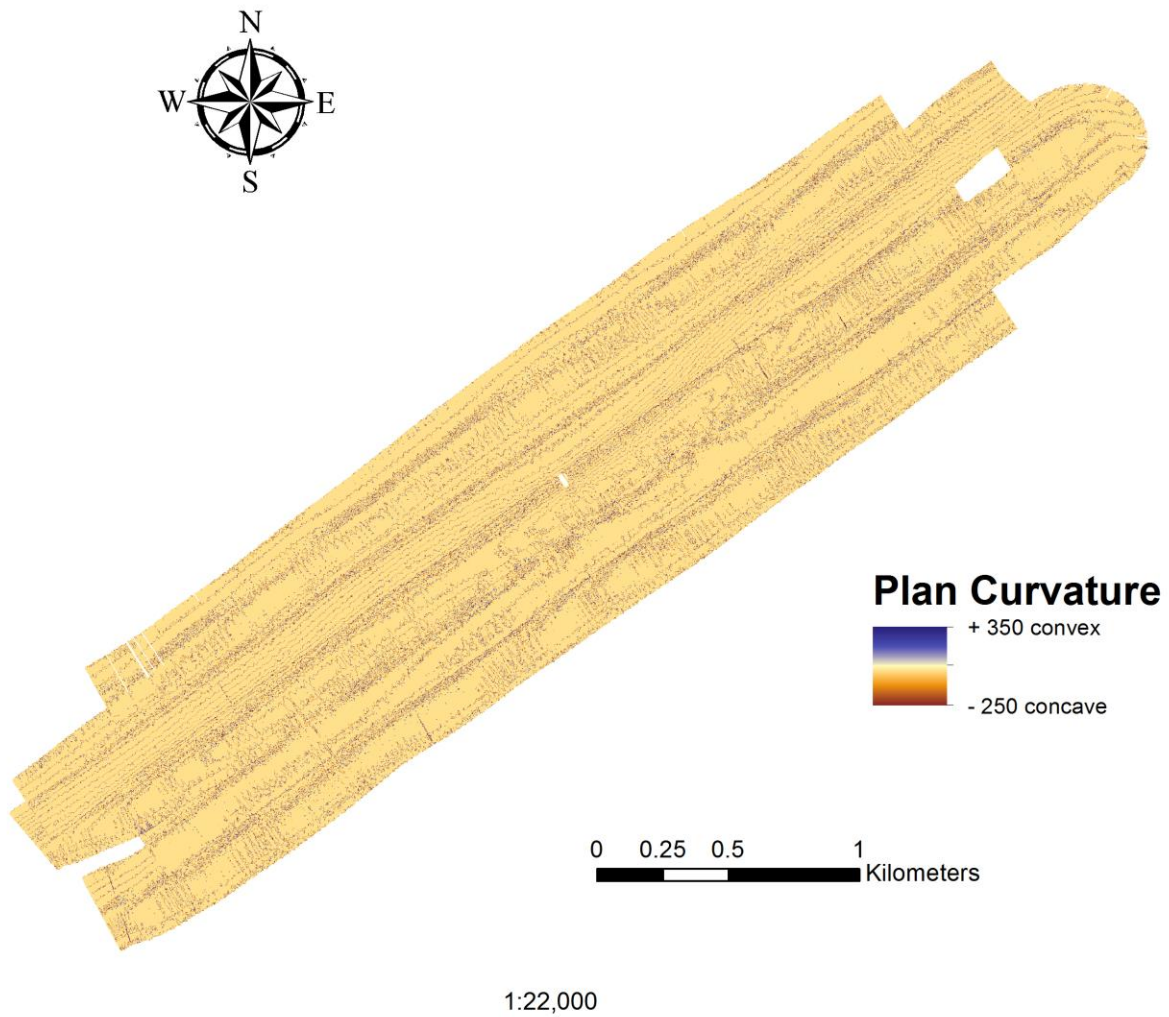
1:22,000

Source: Derived from bathymetric data collected on July 6th 2013 using the ME70 multibeam echosounder system aboard the NOAA ship *Pisces*.

Coordinate System: NAD 1983 UTM Zone 18N

Credit: Friedrich Knuth (c) 2014

Figure 96. Maximum rate of change in slope between cell and eight neighbors at Snowy Wreck One.

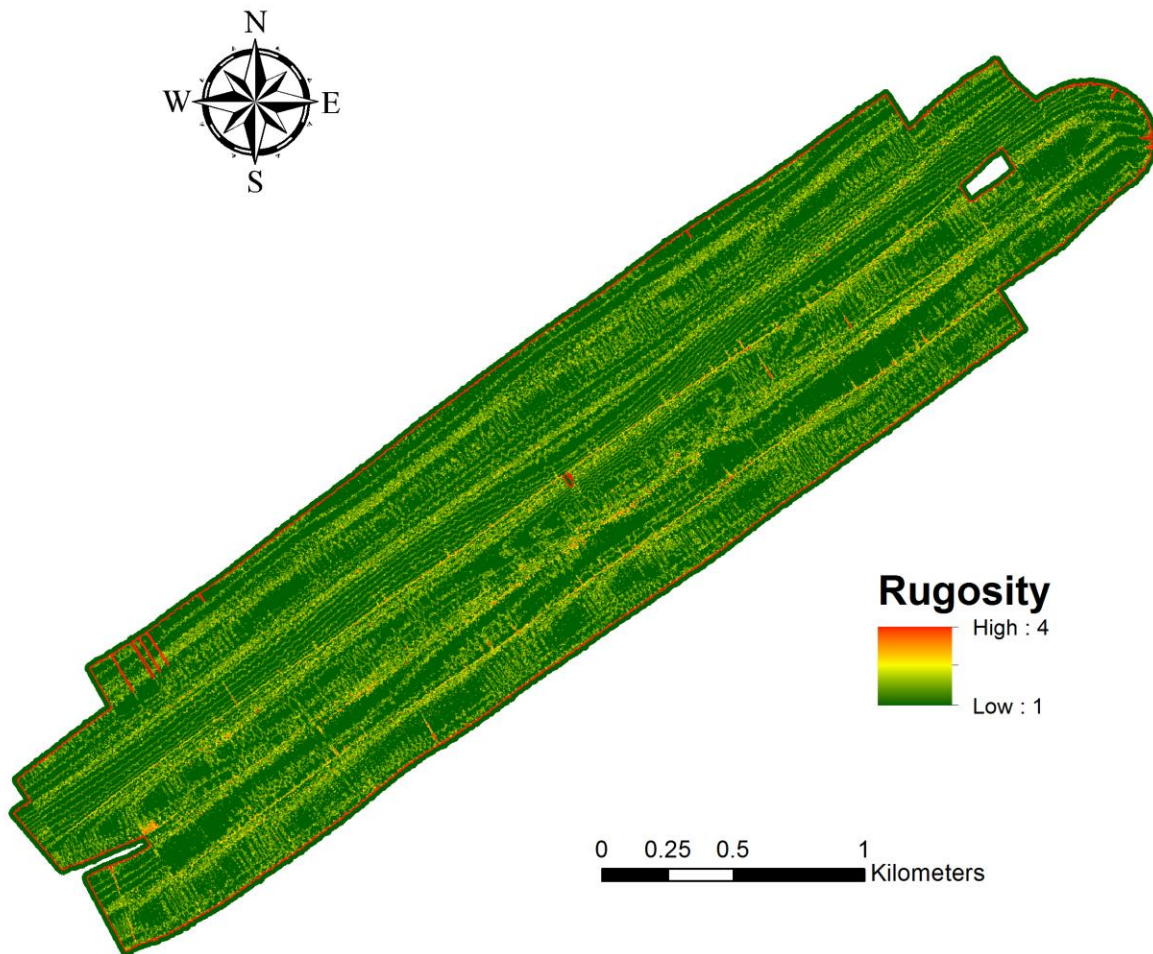


Source: Derived from bathymetric data collected on July 6th 2013 using the ME70 multibeam echosounder system aboard the NOAA ship *Pisces*.

Coordinate System: NAD 1983 UTM Zone 18N

Credit: Friedrich Knuth (c) 2014

Figure 97. Rate of change in curvature across the surface at Snowy Wreck One.



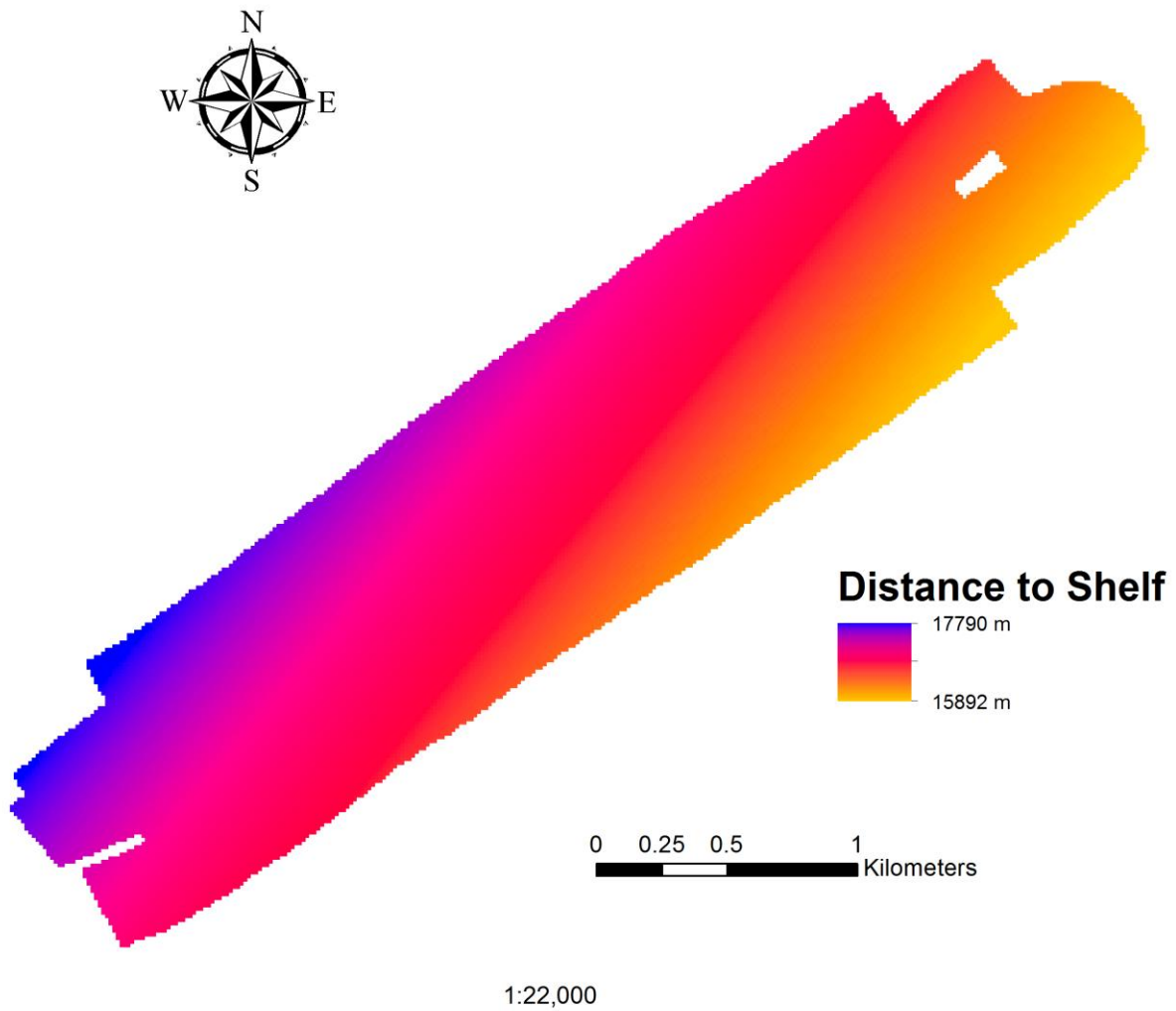
1:22,000

Source: Derived from bathymetric data collected on July 6th 2013 using the ME70 multibeam echosounder system aboard the NOAA ship *Pisces*.

Coordinate System: NAD 1983 UTM Zone 18N

Credit: Friedrich Knuth (c) 2014

Figure 98. Ratio of surface area to planar surface area at Snowy Wreck One.

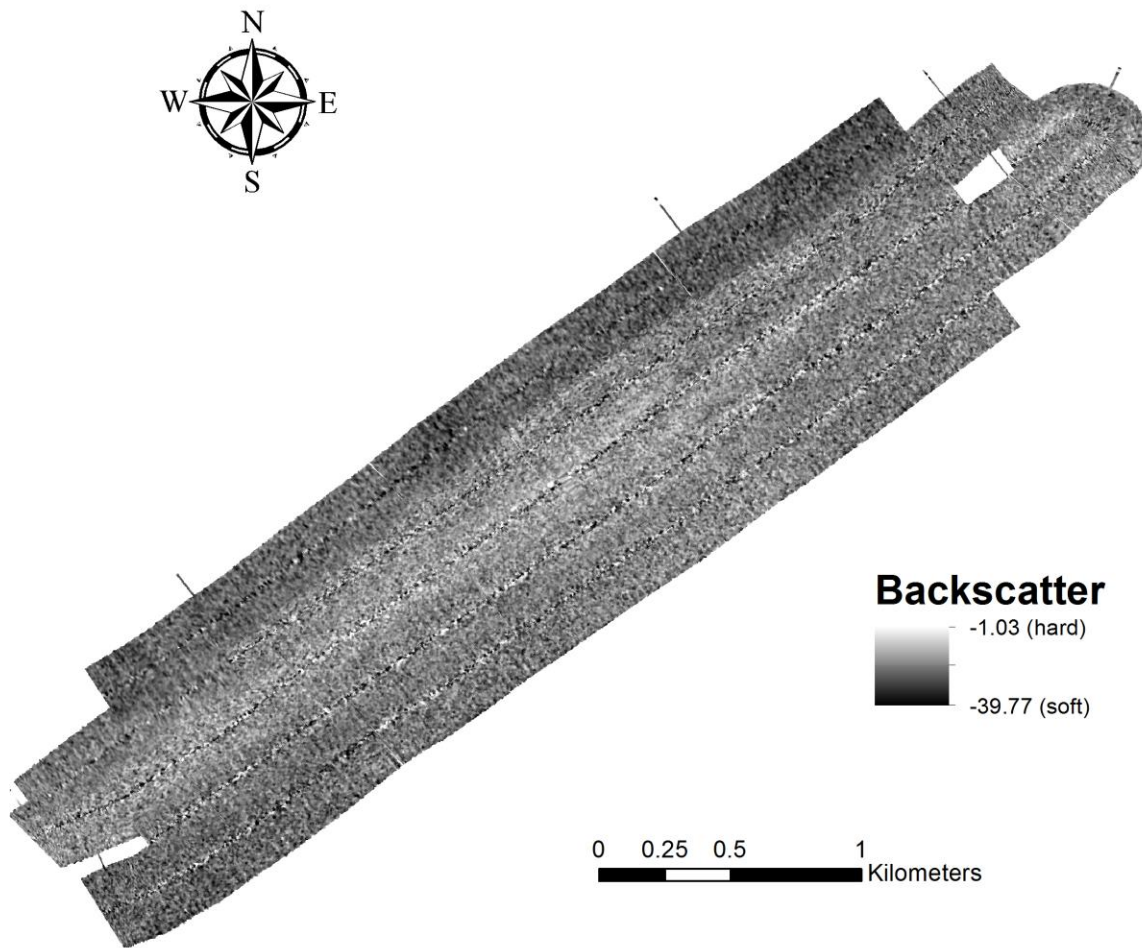


Source: Derived from the 200 m isobath provided by the USGS North American Atlas project.

Coordinate System: NAD 1983 UTM Zone 18N

Credit: Friedrich Knuth (c) 2014

Figure 99. Distance of each 2x2 m raster cell to 200 m isobaths at Snowy Wreck One.



1:22,000

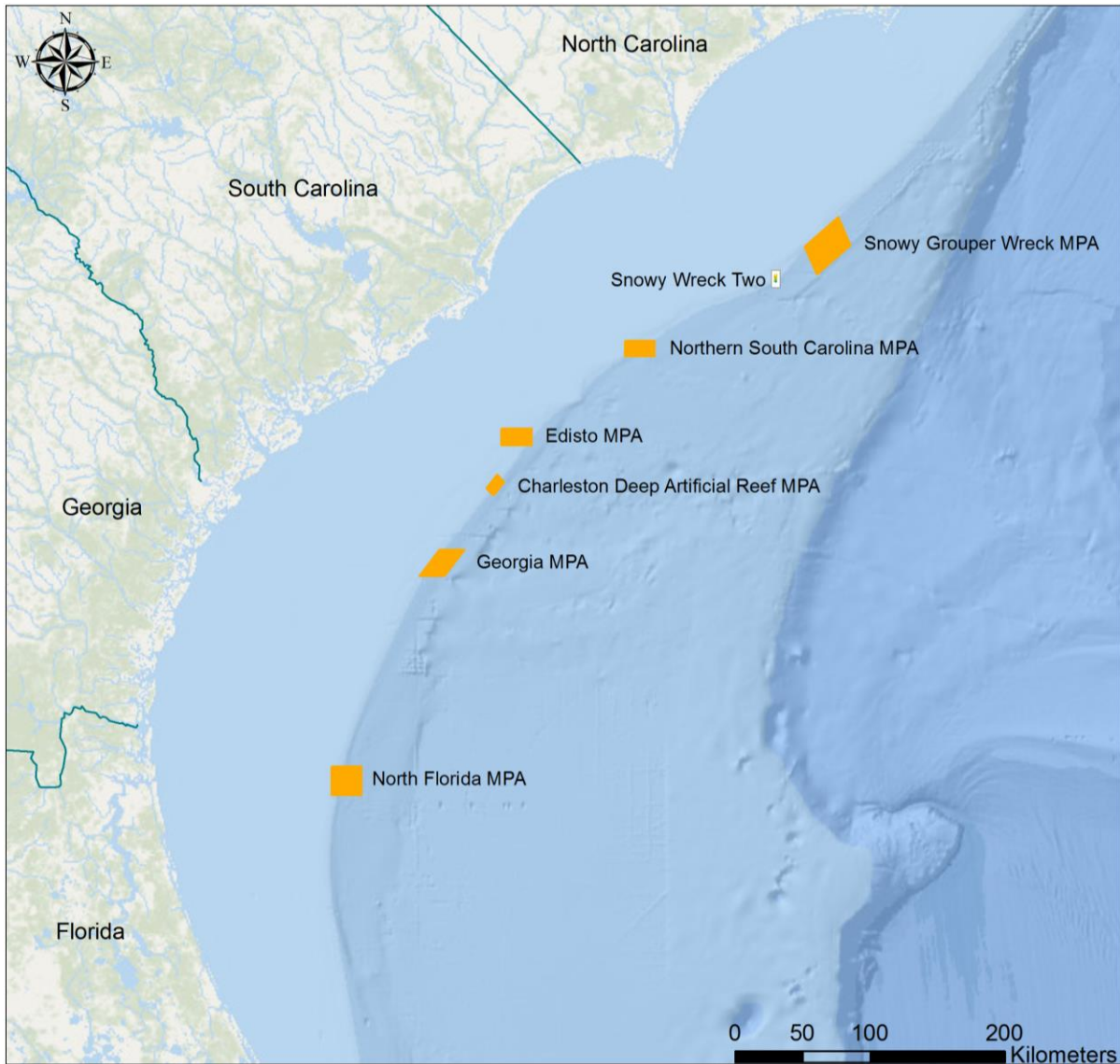
Source: Derived from acoustic data collected on July 6th 2013 using the ME70 multibeam echosounder system aboard the NOAA ship *Pisces*.

Coordinate System: NAD 1983 UTM Zone 18N

Credit: Friedrich Knuth (c) 2014

Figure 100. Intensity of the acoustic return at Snowy Wreck One.

SNOWY WRECK TWO



Legend

- State Boundaries
- Survey Site Snowy Wreck Two
- Marine Protected Areas (MPAs)

Friedrich Knuth (c)
College of Charleston
2014

Source: SAFMC online GIS database, NOAA, SEAMAP, MARMAP, ESRI (base layer)

Coordinate System: WGS 1984 Web Mercator

Figure 101. Location of Snowy Wreck Two survey site relative to existing MPAs.

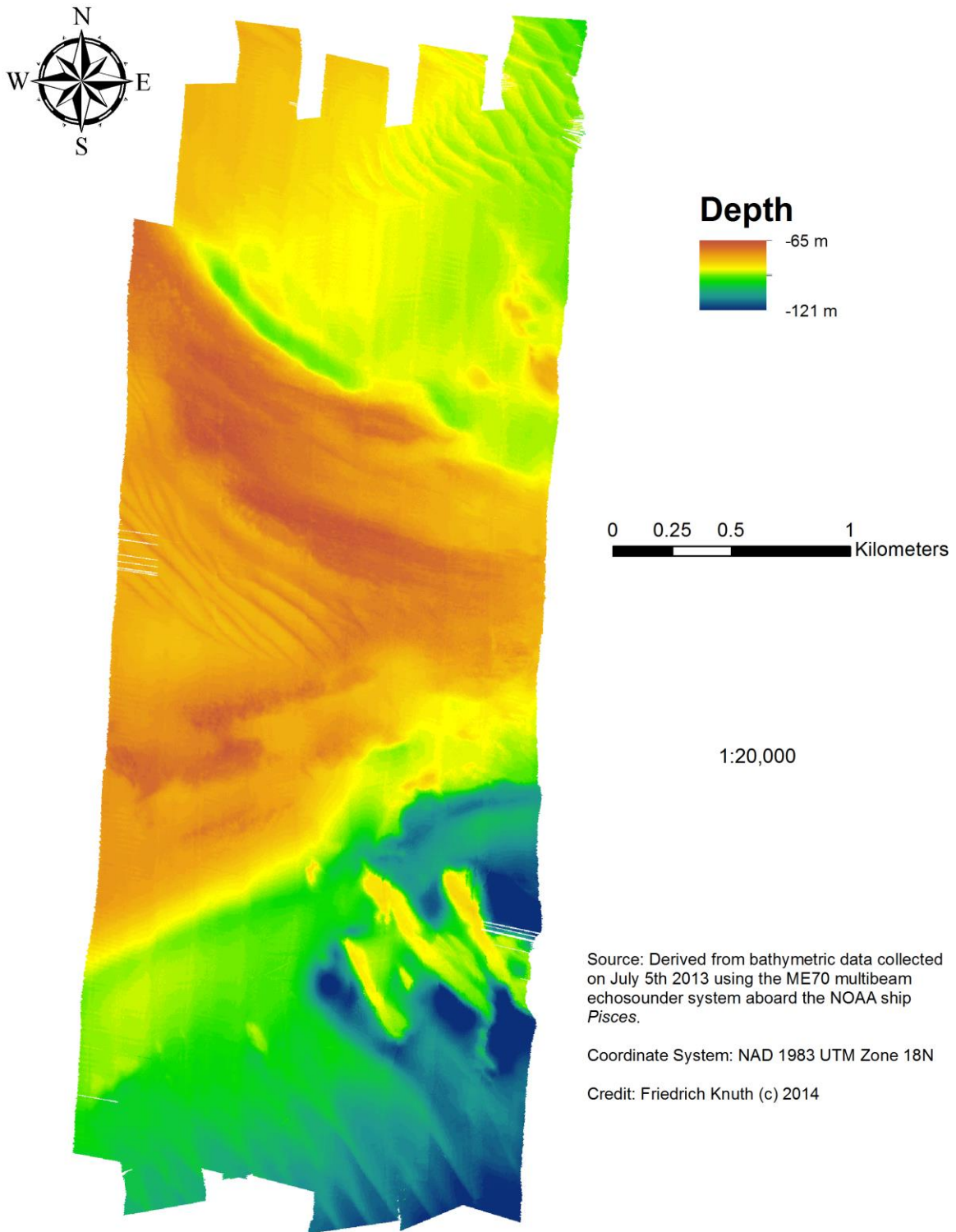


Figure 102. Depth of sea level to seafloor at Snowy Wreck Two.



Figure 103. Maximum rate of change in depth between 2 x 2 m raster cell and eight neighbors at Snowy Wreck Two.

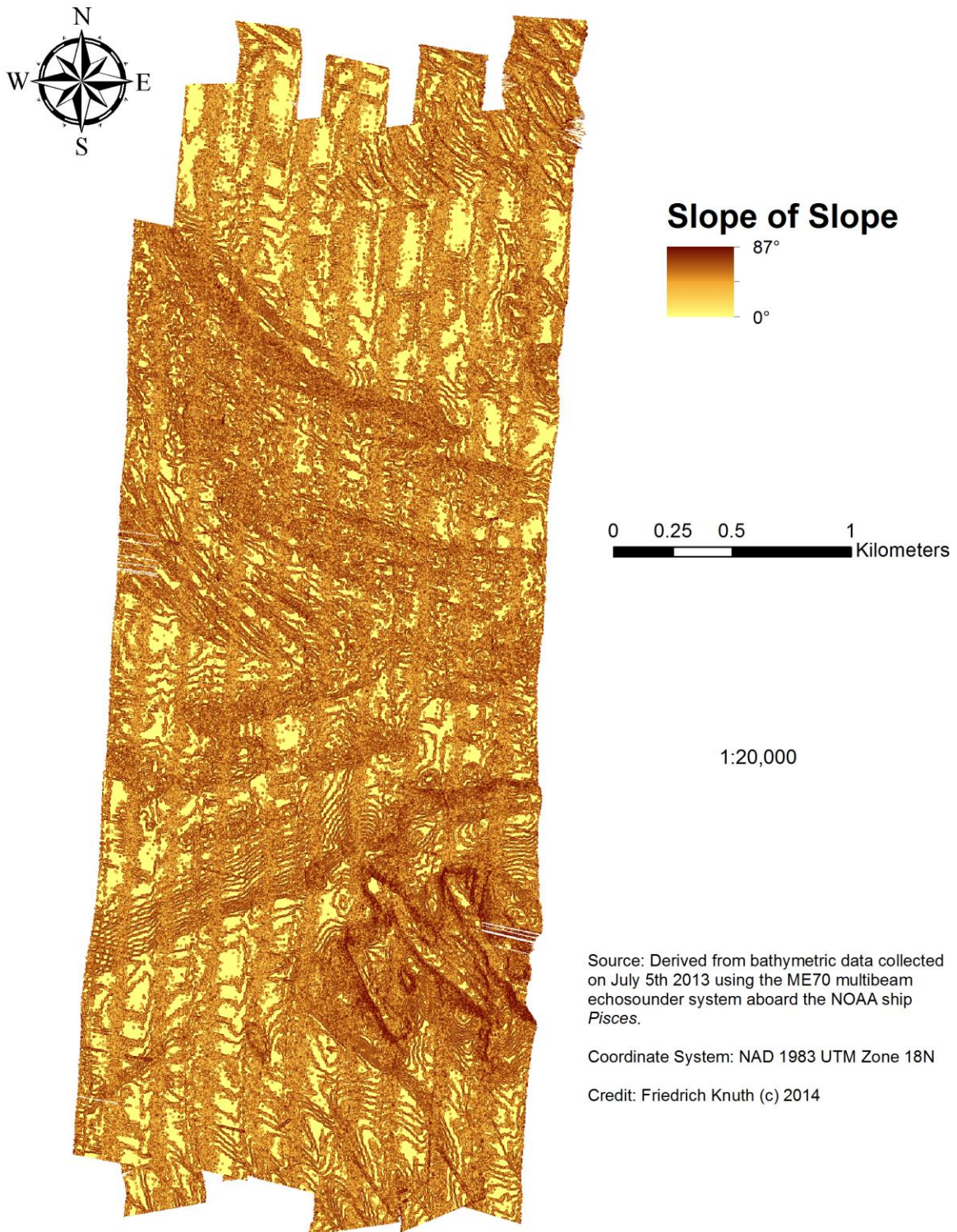


Figure 104. Maximum rate of change in slope between cell and eight neighbors at Snowy Wreck Two.

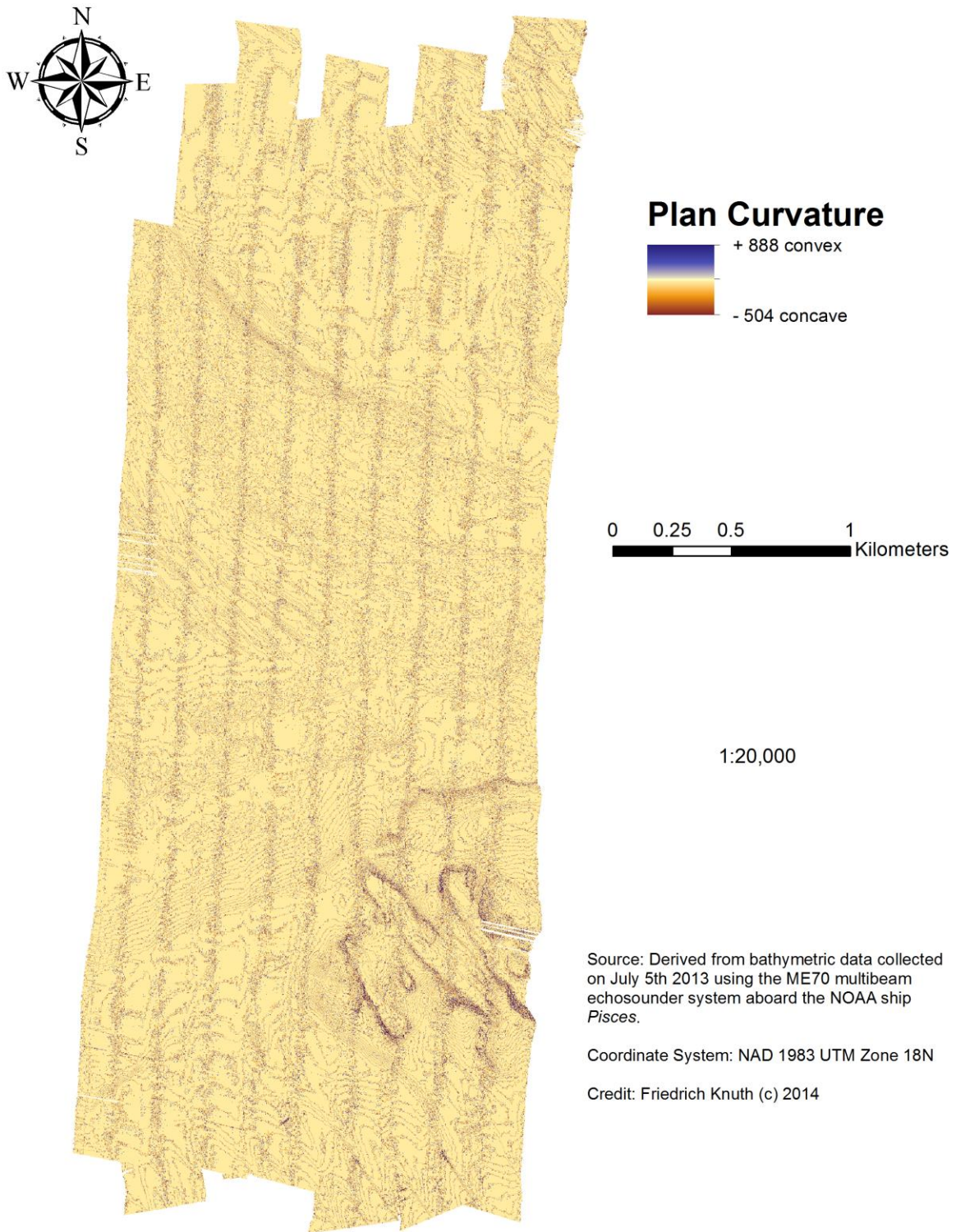


Figure 105. Rate of change in curvature across the surface at Snowy Wreck Two.

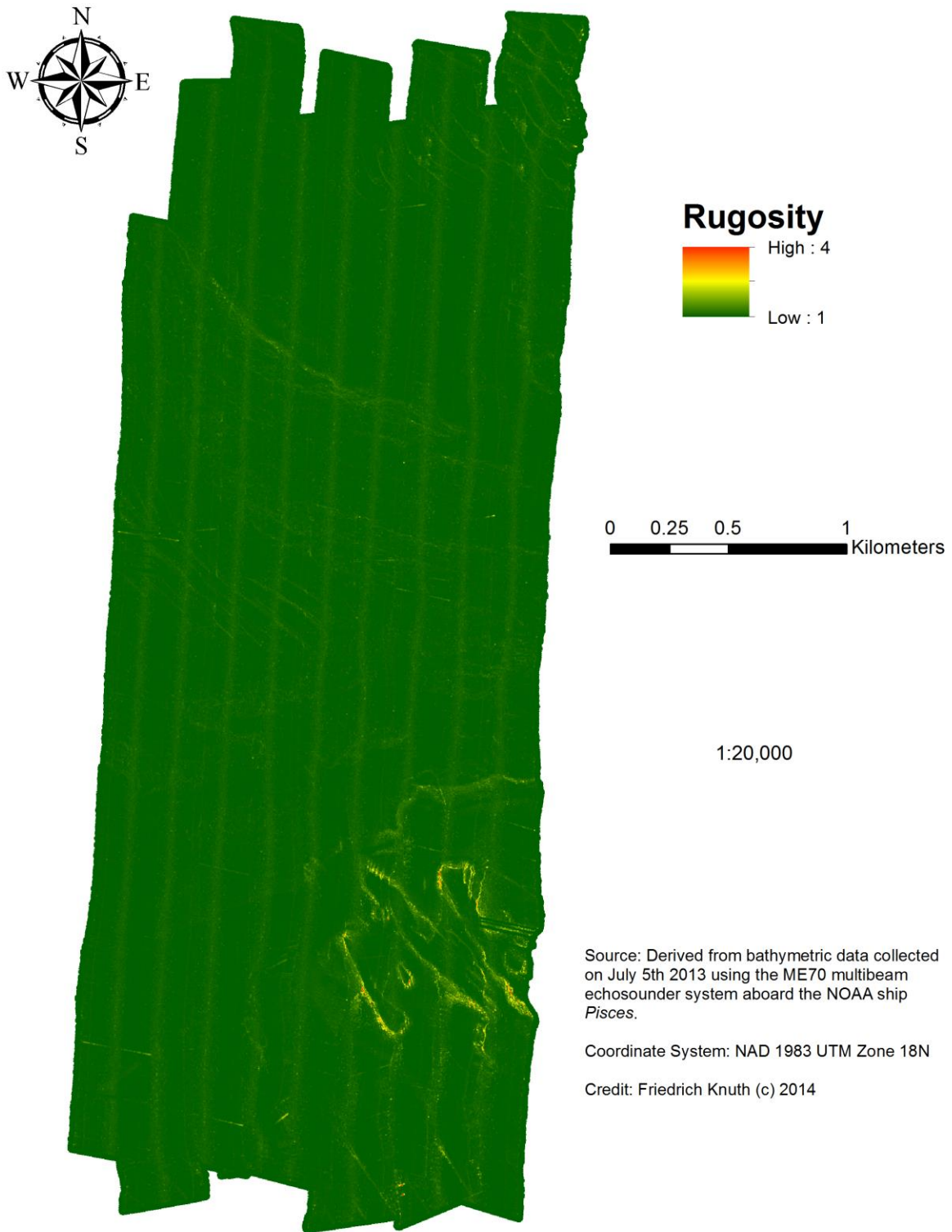


Figure 106. Ratio of surface area to planar surface area at Snowy Wreck Two.

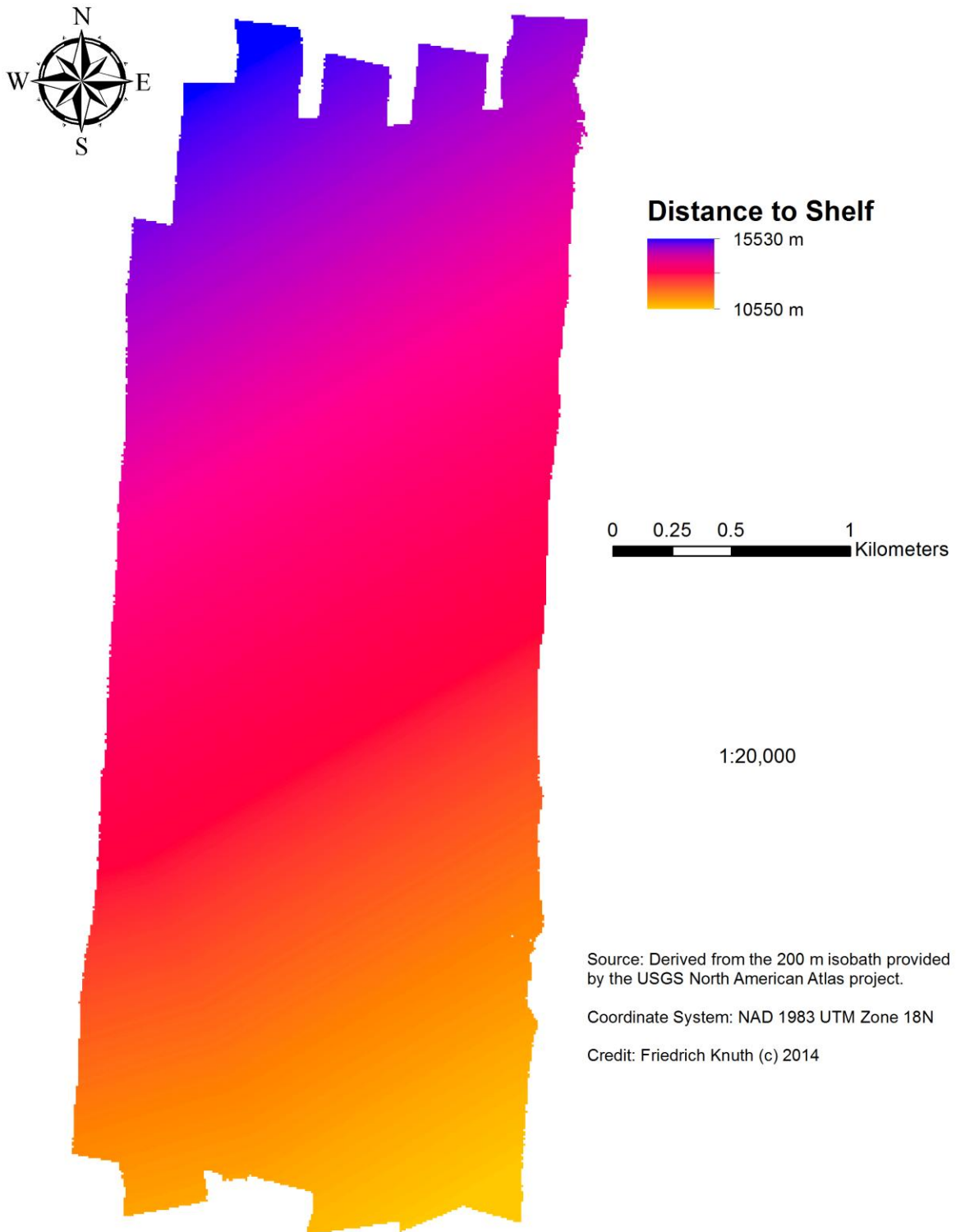


Figure 107. Distance of each 2x2 m raster cell to 200 m isobaths at Snowy Wreck Two.

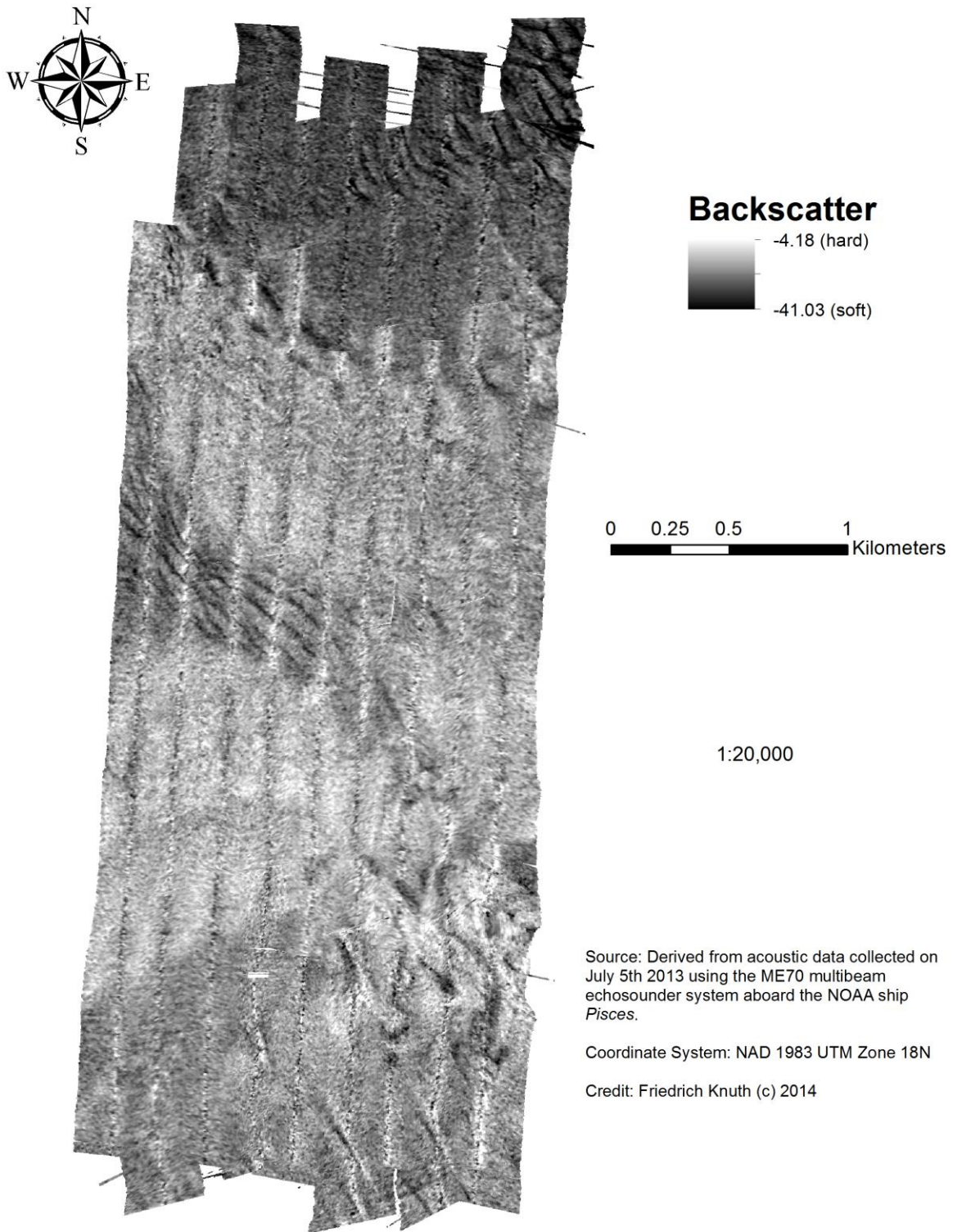
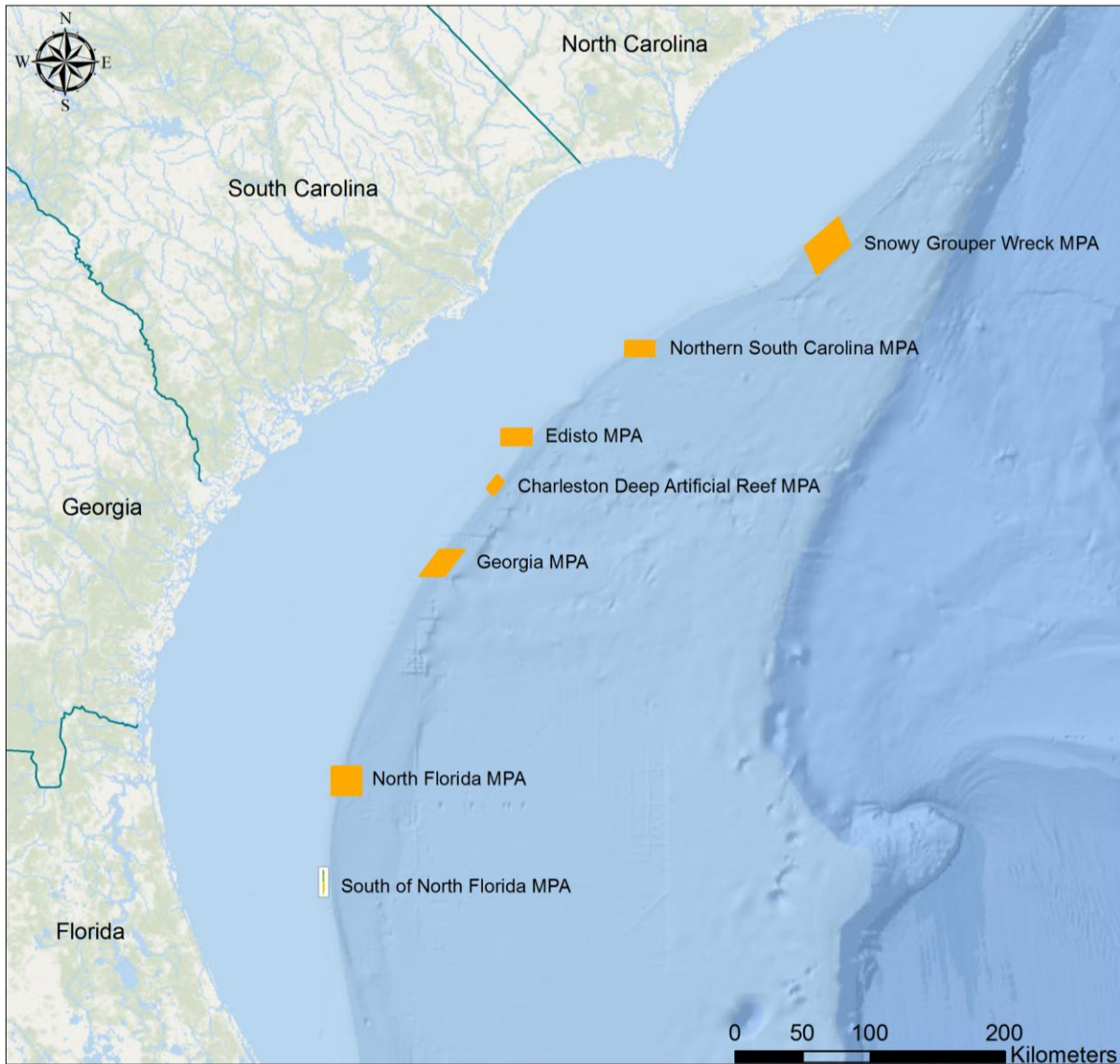


Figure 108. Intensity of the acoustic return at Snowy Wreck Two.

SOUTH OF NORTH FLORIDA MPA



Legend

- State Boundaries
- Survey Site South of North Florida MPA
- Marine Protected Areas (MPAs)

Friedrich Knuth (c)
College of Charleston
2014

Source: SAFMC online GIS database, NOAA, SEAMAP, MARMAP, ESRI (base layer)

Coordinate System: WGS 1984 Web Mercator

Figure 109. Location of South of North Florida MPA survey site relative to existing MPAs.

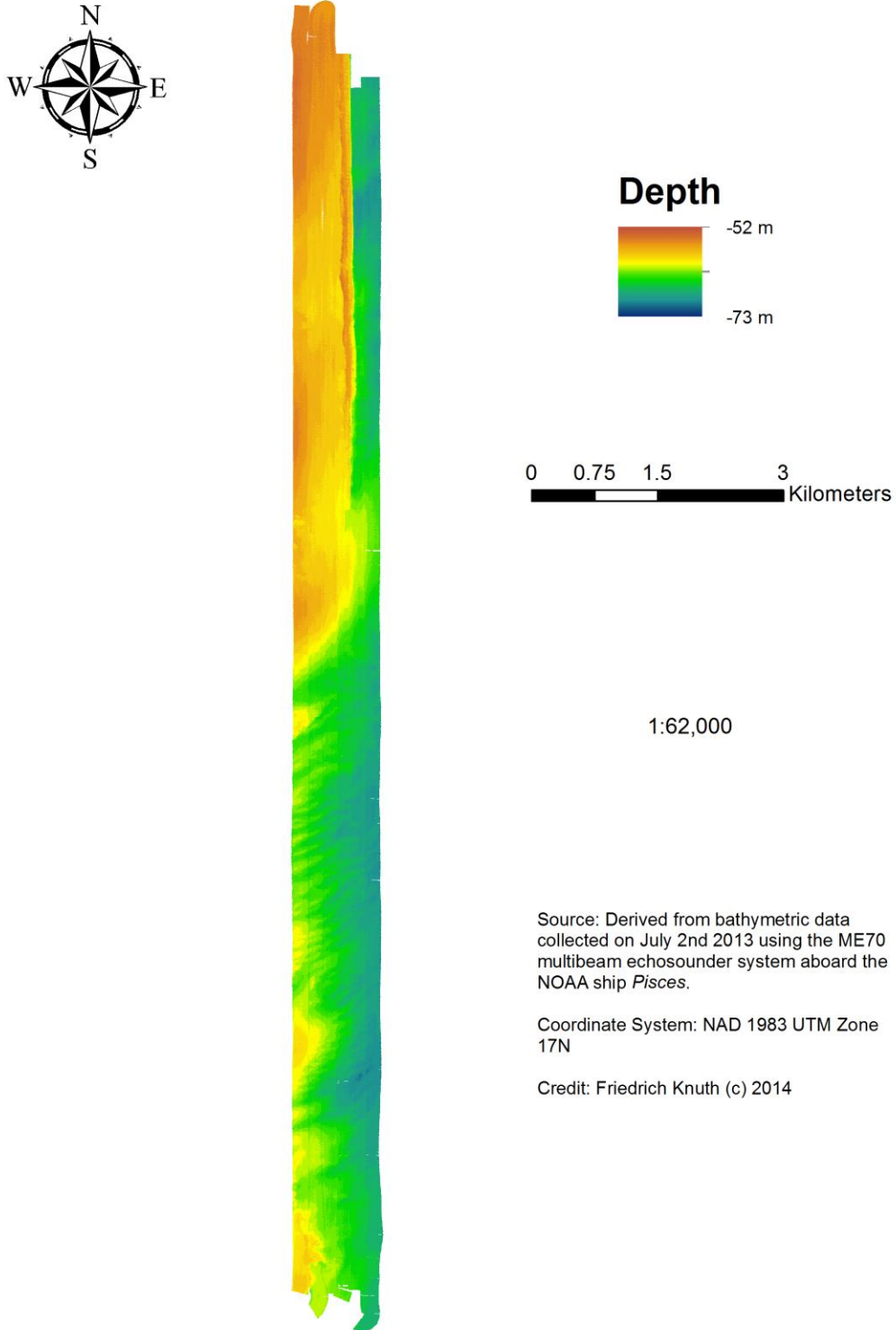


Figure 110. Depth of sea level to seafloor at South of North Florida MPA.

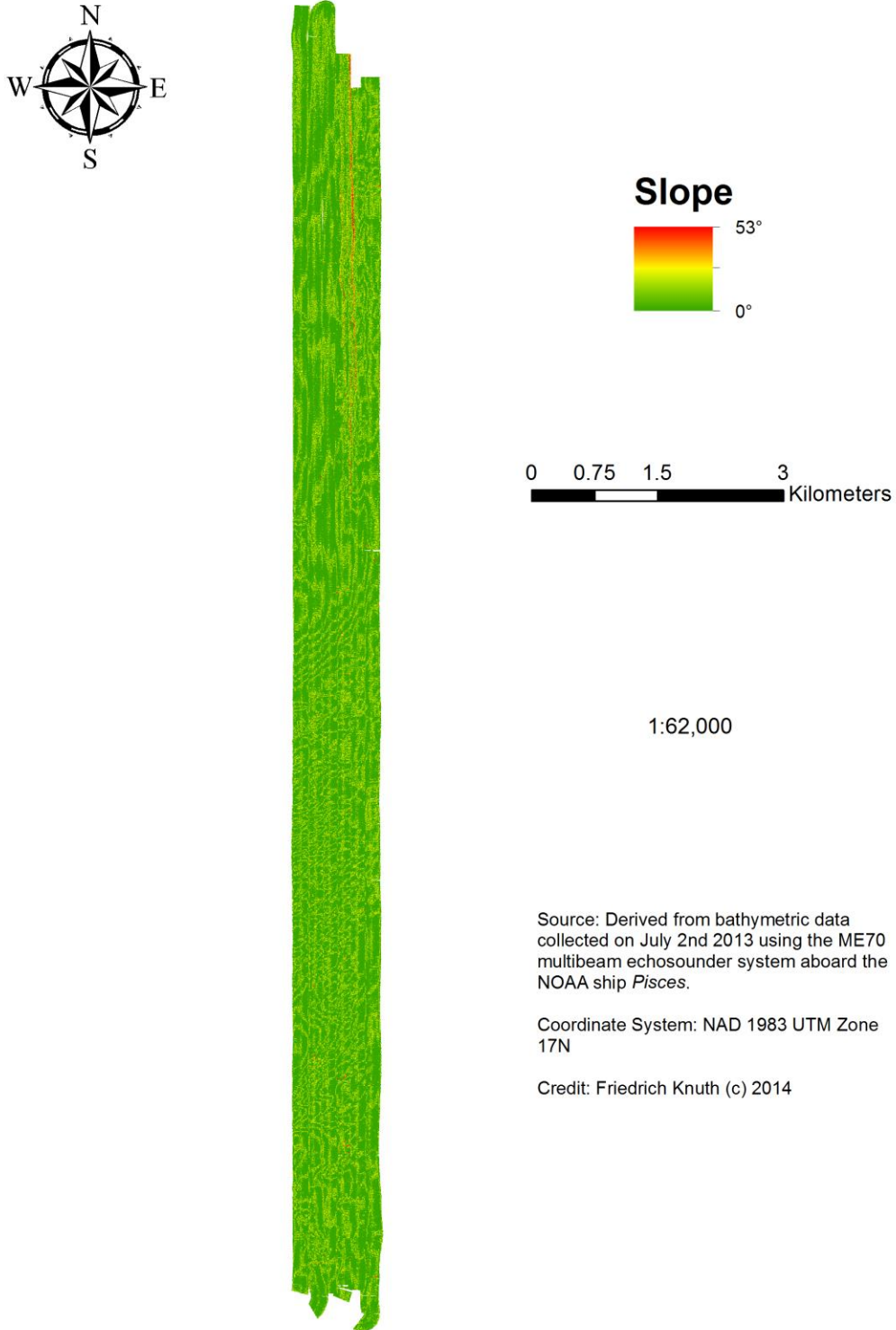
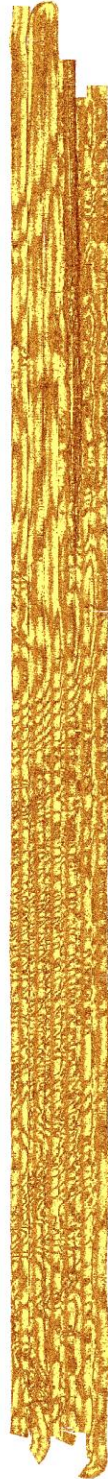
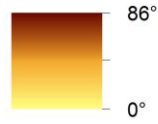


Figure 111. Maximum rate of change in depth between 2 x 2 m raster cell and eight neighbors at South of North Florida MPA.



Slope of Slope



1:62,000

Source: Derived from bathymetric data collected on July 2nd 2013 using the ME70 multibeam echosounder system aboard the NOAA ship *Pisces*.

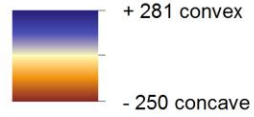
Coordinate System: NAD 1983 UTM Zone 17N

Credit: Friedrich Knuth (c) 2014

Figure 112. Maximum rate of change in slope between cell and eight neighbors at South of North Florida MPA.



Plan Curvature



1:62,000

Source: Derived from bathymetric data collected on July 2nd 2013 using the ME70 multibeam echosounder system aboard the NOAA ship *Pisces*.

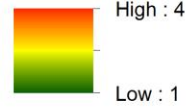
Coordinate System: NAD 1983 UTM Zone 17N

Credit: Friedrich Knuth (c) 2014

Figure 113. Rate of change in curvature across the surface at South of North Florida MPA.



Rugosity



1:62,000

Source: Derived from bathymetric data collected on July 2nd 2013 using the ME70 multibeam echosounder system aboard the NOAA ship *Pisces*.

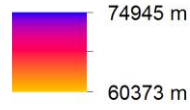
Coordinate System: NAD 1983 UTM Zone 17N

Credit: Friedrich Knuth (c) 2014

Figure 114. Ratio of surface area to planar surface area at South of North Florida MPA.



Distance to Shelf



1:62,000

Source: Derived from the 200 m isobath provided by the USGS North American Atlas project.

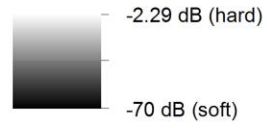
Coordinate System: NAD 1983 UTM Zone 17N

Credit: Friedrich Knuth (c) 2014

Figure 115. Distance of each 2x2 m raster cell to 200 m isobaths at South of North Florida MPA.



Backscatter



1:62,000

Source: Derived from acoustic data collected on July 2nd 2013 using the ME70 multibeam echosounder system aboard the NOAA ship *Pisces*.

Coordinate System: NAD 1983 UTM Zone 17N

Credit: Friedrich Knuth (c) 2014

Figure 116. Intensity of the acoustic return at South of North Florida MPA.

APPENDIX B, FISH COUNTS

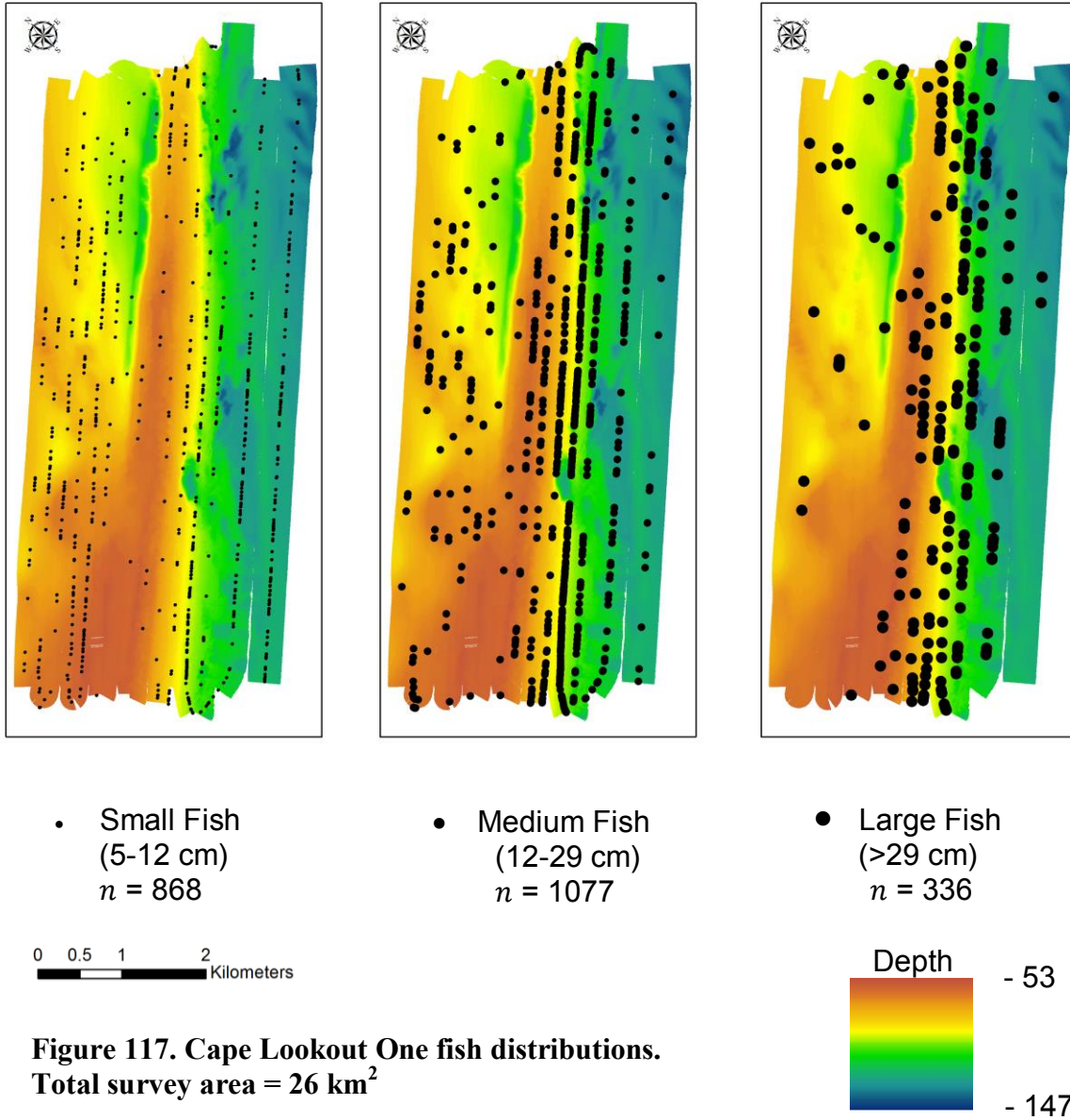
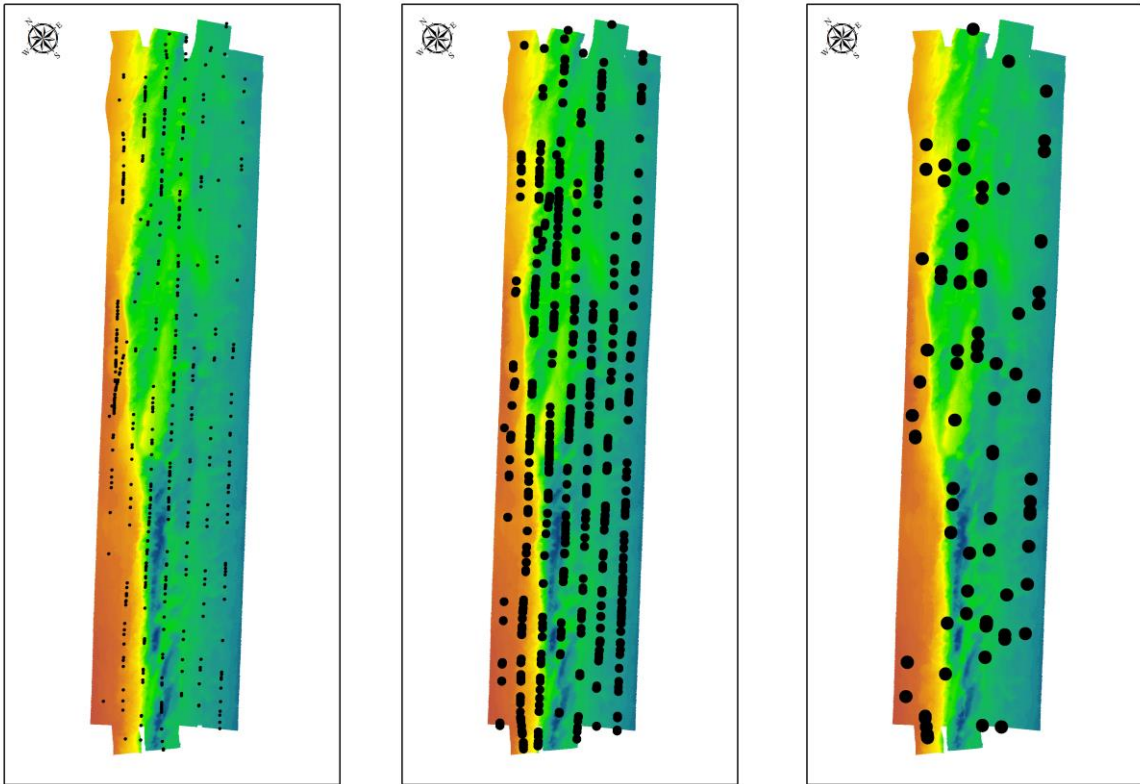


Figure 117. Cape Lookout One fish distributions.
Total survey area = 26 km²



- Small Fish
(5-12 cm)
 $n = 504$

- Medium Fish
(12-29 cm)
 $n = 569$

- Large Fish
(>29 cm)
 $n = 91$

0 0.5 1 2 Kilometers

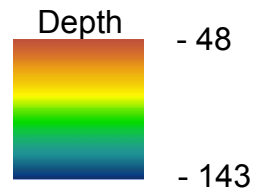
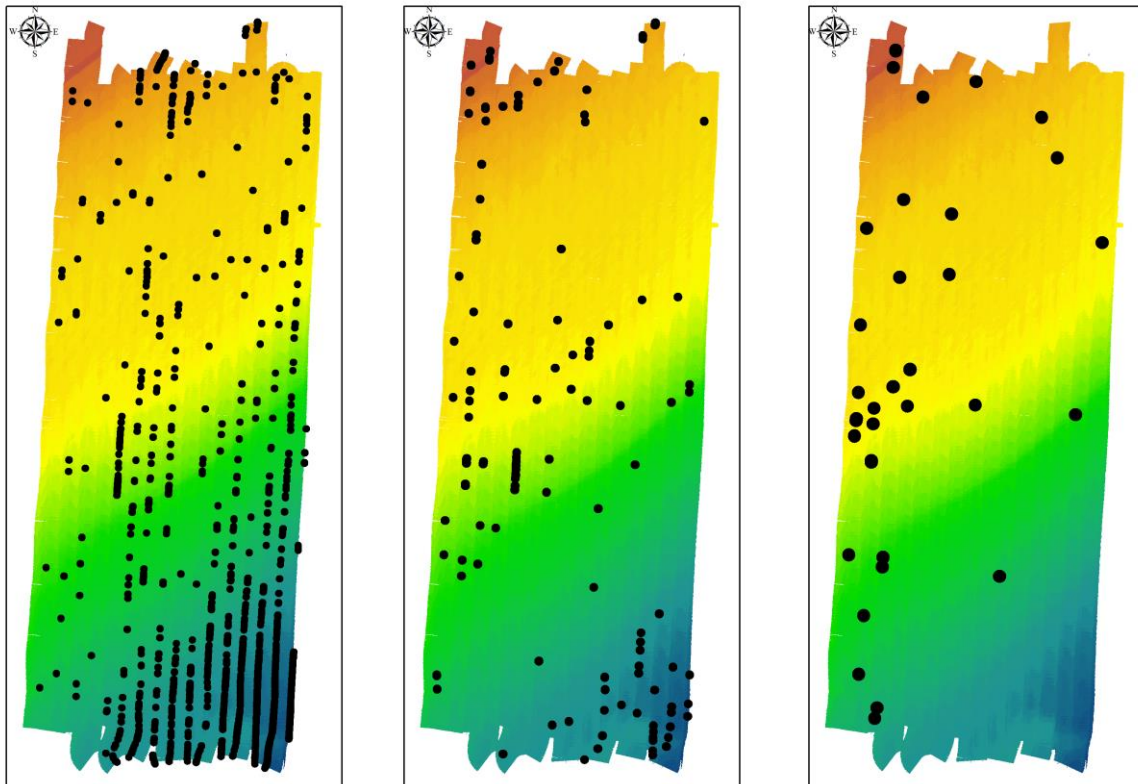


Figure 118. Cape Lookout Two fish distributions.
Total survey area = 10 km²



- Small Fish
(5-12 cm)
 $n = 181$

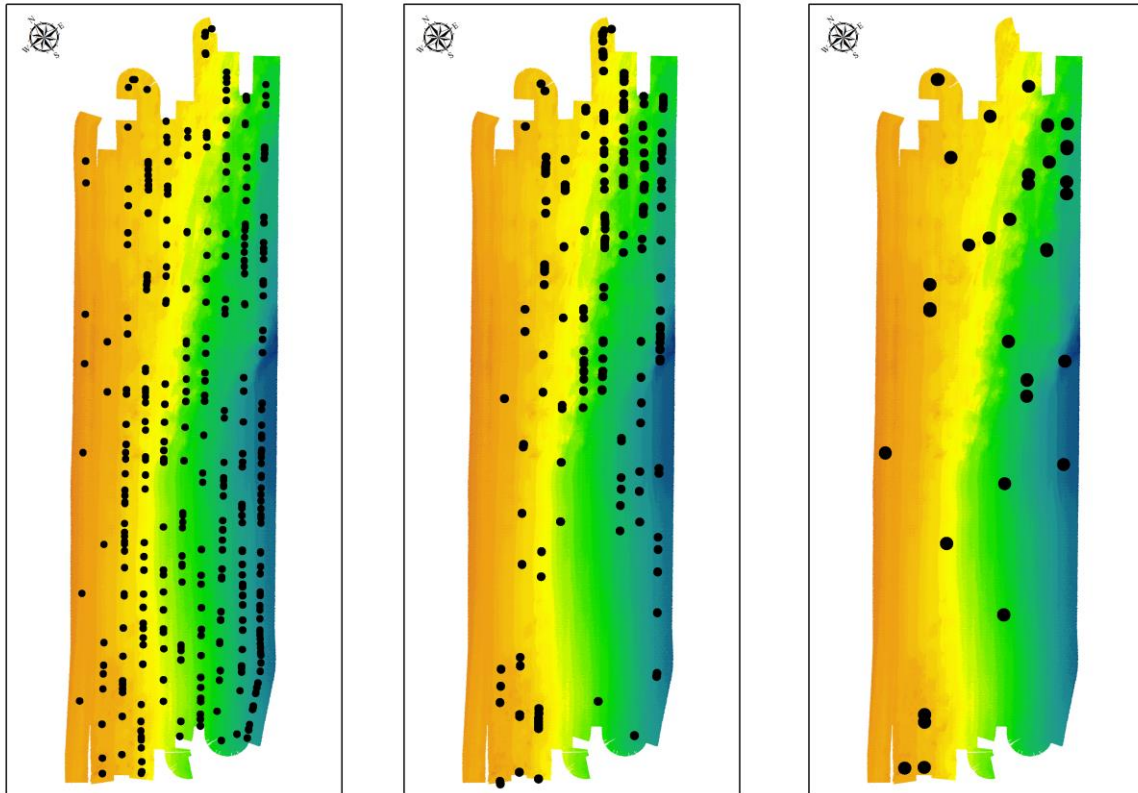
- Medium Fish
(12-29 cm)
 $n = 26$

- Large Fish
(>29 cm)
 $n = 7$

0 0.5 1 2 Kilometers

Depth - 53
- 147

Figure 119. North of Edisto MPA fish distributions.
Total survey area = 25 km²



- Small Fish
(5-12 cm)
 $n = 379$

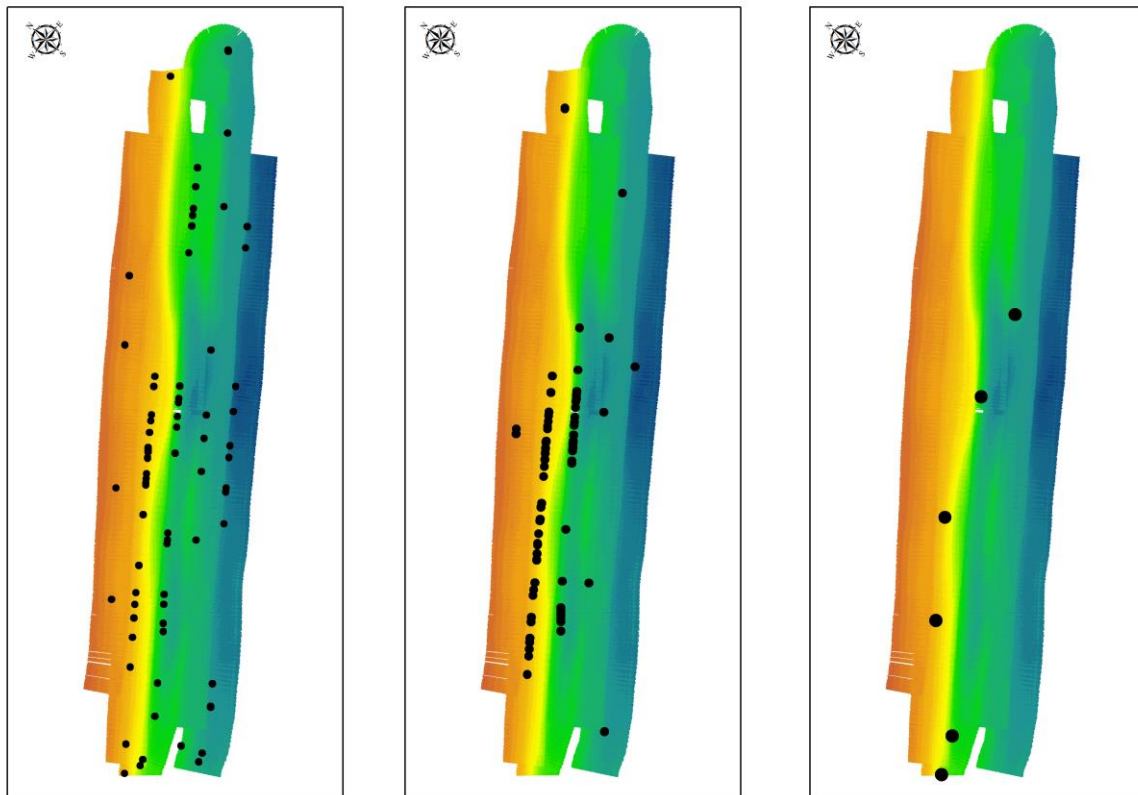
- Medium Fish
(12-29 cm)
 $n = 230$

- Large Fish
(>29 cm)
 $n = 48$

0 0.5 1 2 Kilometers

Depth - 66
- 96

Figure 120. North Carolina 780 fish distributions.
Total survey area = 14 km²



- Small Fish
(5-12 cm)
 $n = 77$

- Medium Fish
(12-29 cm)
 $n = 74$

- Large Fish
(>29 cm)
 $n = 6$

0 0.5 1 2 Kilometers

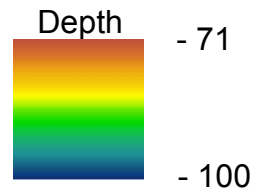
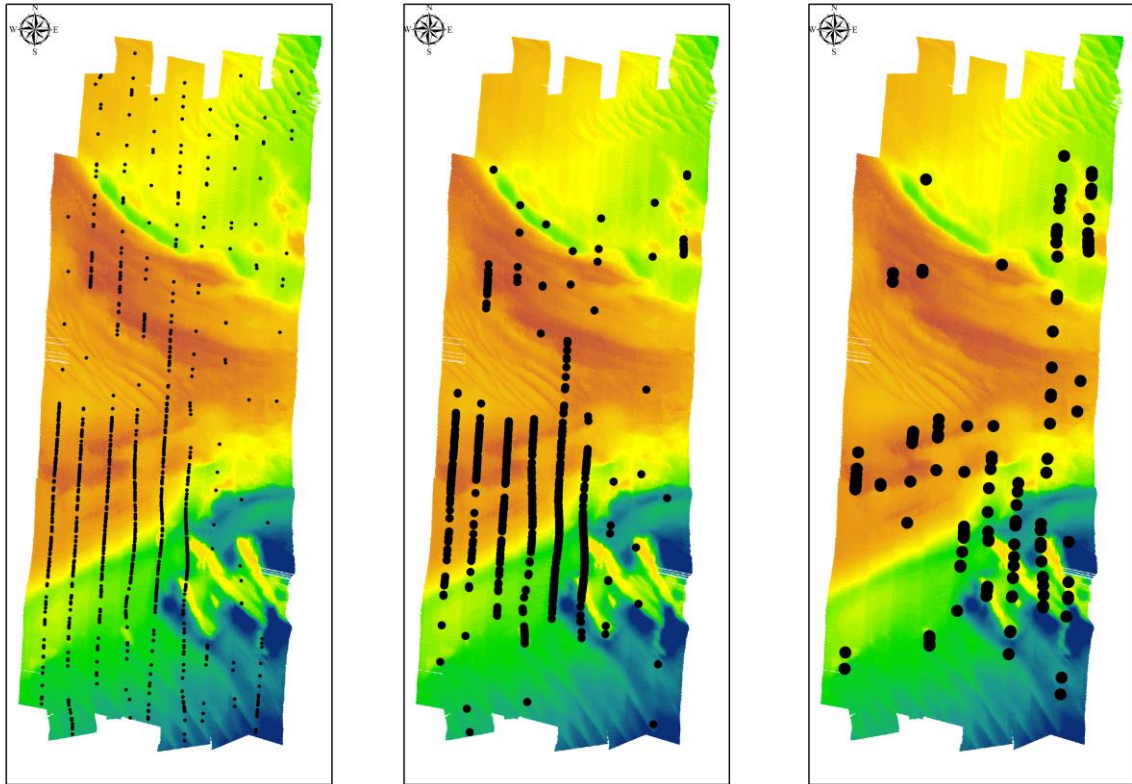


Figure 121. Snowy Wreck One fish distributions.
Total survey area = 4 km²



- Small Fish
(5-12 cm)
 $n = 1126$

- Medium Fish
(12-29 cm)
 $n = 766$

- Large Fish
(>29 cm)
 $n = 160$

0 0.5 1 2 Kilometers

Depth - 65
- 121

Figure 122. Snowy Wreck Two fish distributions.
Total survey area = 9 km²

APPENDIX C, MULTIVARIATE OUTPUTS

Poisson Regression Analysis: large_fish versus depth_mean_5, depth_std_50, depth_rangev, ...

Method

Link function Natural log
 Rows used 10796

Stepwise Selection of Terms

α to enter = 0.05, α to remove = 0.05

Deviance Table

Source	DF	Adj Dev	Adj Mean	Chi-Square	P-Value
Regression	5	672.24	134.447	672.24	0.000
depth_std_50m	1	53.61	53.614	53.61	0.000
depth_rangevariety_50m	1	65.21	65.208	65.21	0.000
slopeofslope_mean_50m	1	101.72	101.720	101.72	0.000
rugosity_std_50m	1	9.38	9.384	9.38	0.002
backscatter_mean_50	1	103.21	103.207	103.21	0.000
Error	10790	3877.06	0.359		
Total	10795	4549.30			

Model Summary

Deviance R-Sq	Deviance R-Sq(adj)	AIC
14.78%	14.67%	4941.33

Coefficients

Term	Coef	SE Coef	VIF
Constant	-2.525	0.564	
depth_std_50m	0.746	0.103	12.46
depth_rangevariety_50m	-0.00844	0.00129	10.35
slopeofslope_mean_50m	0.06372	0.00700	1.85
rugosity_std_50m	0.857	0.251	1.43
backscatter_mean_50	0.1604	0.0167	1.21

Regression Equation

large_fish = exp(Y')

Y' = -2.525 + 0.746 depth_std_50m - 0.00844 depth_rangevariety_50m
 + 0.06372 slopeofslope_mean_50m + 0.857 rugosity_std_50m
 + 0.1604 backscatter_mean_50

Poisson Regression Analysis: large_fish versus depth_rangevariety_50m, slopeofslope_mean_50m, rugosity_std_50m, ...

Method

Link function Natural log
 Rows used 10796

Stepwise Selection of Terms

α to enter = 0.05, α to remove = 0.05

Deviance Table

Source	DF	Adj Dev	Adj Mean	Chi-Square	P-Value
Regression	4	618.62	154.656	618.62	0.000
depth_rangevariety_50m	1	11.60	11.598	11.60	0.001
slopeofslope_mean_50m	1	210.96	210.956	210.96	0.000
rugosity_std_50m	1	17.09	17.090	17.09	0.000
backscatter_mean_50	1	124.58	124.576	124.58	0.000
Error	10791	3930.68	0.364		
Total	10795	4549.30			

Model Summary

Deviance	Deviance	AIC
R-Sq	R-Sq(adj)	
13.60%	13.51%	4992.94

Coefficients

Term	Coef	SE Coef	VIF
Constant	-2.806	0.571	
depth_rangevariety_50m	-0.001276	0.000419	1.52
slopeofslope_mean_50m	0.08453	0.00679	1.63
rugosity_std_50m	1.125	0.232	1.09
backscatter_mean_50	0.1732	0.0165	1.18

Regression Equation

large_fish = exp(Y')

Y' = -2.806 - 0.001276 depth_rangevariety_50m + 0.08453 slopeofslope_mean_50m
 + 1.125 rugosity_std_50m + 0.1732 backscatter_mean_50

Poisson Regression Analysis: large_fish versus slopeofslope_mean_50m, backscatter_mean_50

Method

Link function Natural log
 Rows used 10796

Stepwise Selection of Terms

α to enter = 0.05, α to remove = 0.05

Deviance Table

Source	DF	Adj Dev	Adj Mean	Chi-Square	P-Value
Regression	2	597.1	298.563	597.13	0.000
slopeofslope_mean_50m	1	228.4	228.352	228.35	0.000
backscatter_mean_50	1	127.6	127.615	127.61	0.000
Error	10793	3952.2	0.366		
Total	10795	4549.3			

Model Summary

Deviance	Deviance	AIC
R-Sq	R-Sq(adj)	
13.13%	13.08%	5010.44

Coefficients

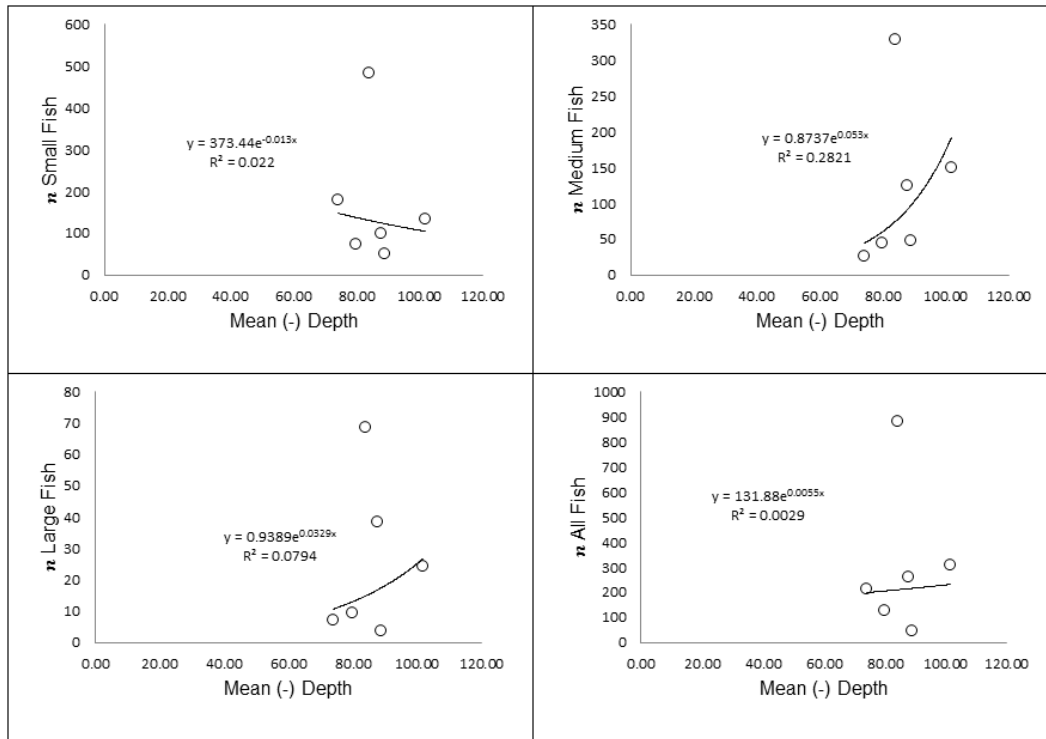
Term	Coef	SE Coef	VIF
Constant	-2.355	0.532	
slopeofslope_mean_50m	0.07697	0.00556	1.17
backscatter_mean_50	0.1753	0.0165	1.17

Regression Equation

large_fish = exp(Y')

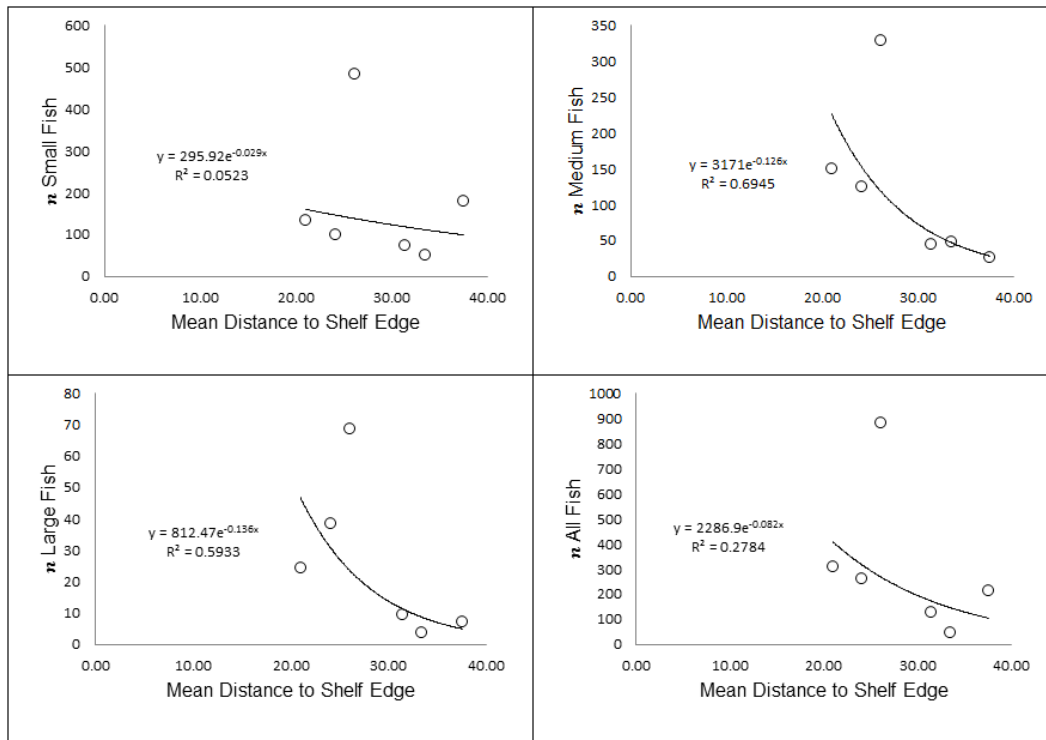
Y' = -2.355 + 0.07697 slopeofslope_mean_50m + 0.1753 backscatter_mean_50

APPENDIX D, BIVARIATE OUTPUTS



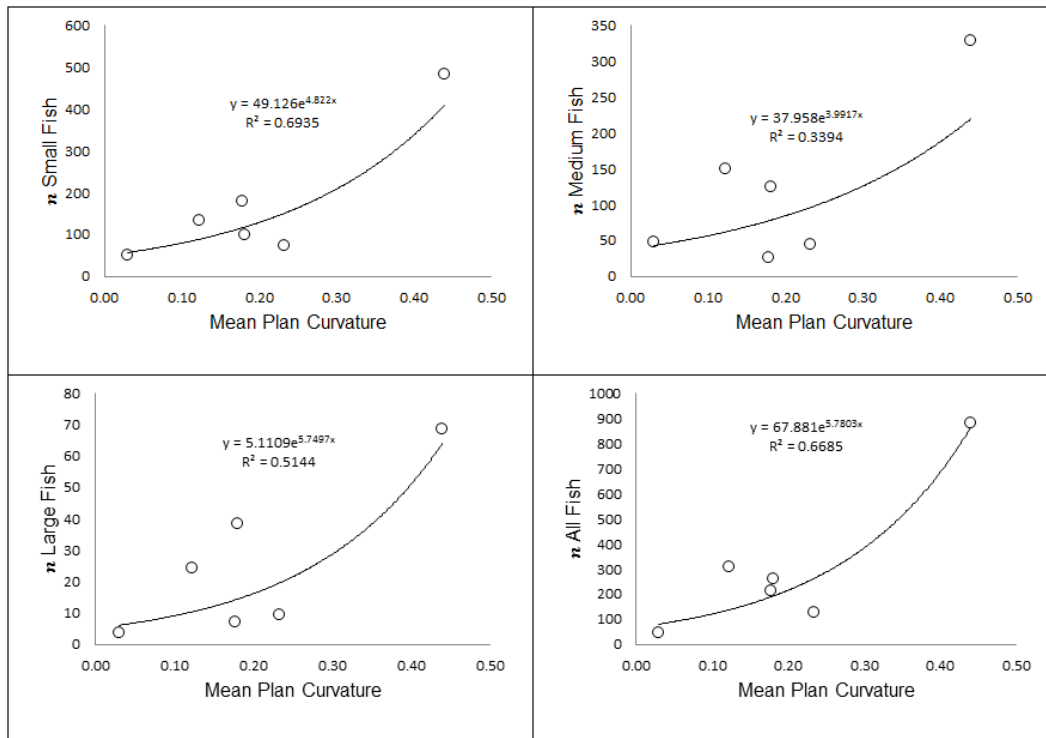
Site	\bar{X} Depth	All Fish	Large Fish	Medium Fish	Small Fish
Snowy Wreck Two	-84.05	881	69	329	483
Cape Lookout One	-87.79	263	39	124	100
Cape Lookout Two	-101.64	309	24	150	135
North Carolina 780	-79.80	127	9	44	73
N of Edisto MPA	-73.87	214	7	26	181
Snowy Wreck One	-88.72	47	4	47	49

Figure 123. Relationship between \bar{X} Depth and Fish Count by site. Highest $R^2 = 28\%$



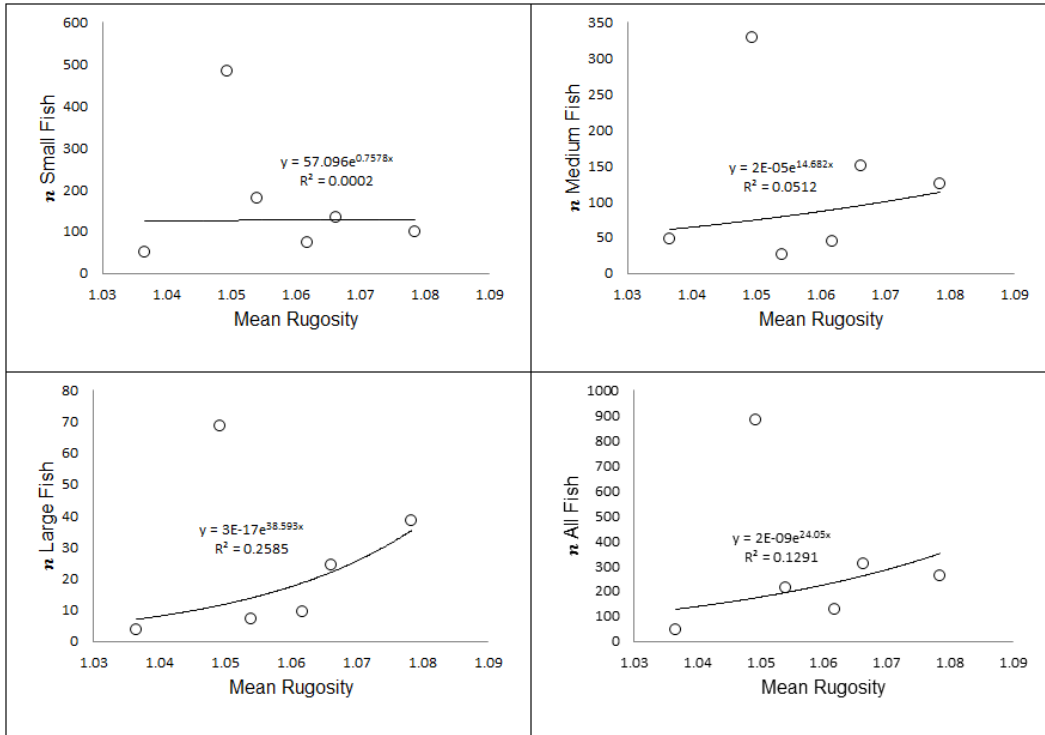
Site	\bar{X} Distance to Shelf Edge	All Fish	Large Fish	Medium Fish	Small Fish
Snowy Wreck Two	26.13	881	69	329	483
Cape Lookout One	24.14	263	39	124	100
Cape Lookout Two	21.02	309	24	150	135
North Carolina 780	31.43	127	9	44	73
N of Edisto MPA	37.58	214	7	26	181
Snowy Wreck One	33.49	47	4	47	49

Figure 124. Relationships between \bar{X} Distance to Shelf Edge and Fish Count by site. Highest $R^2 = 69\%$



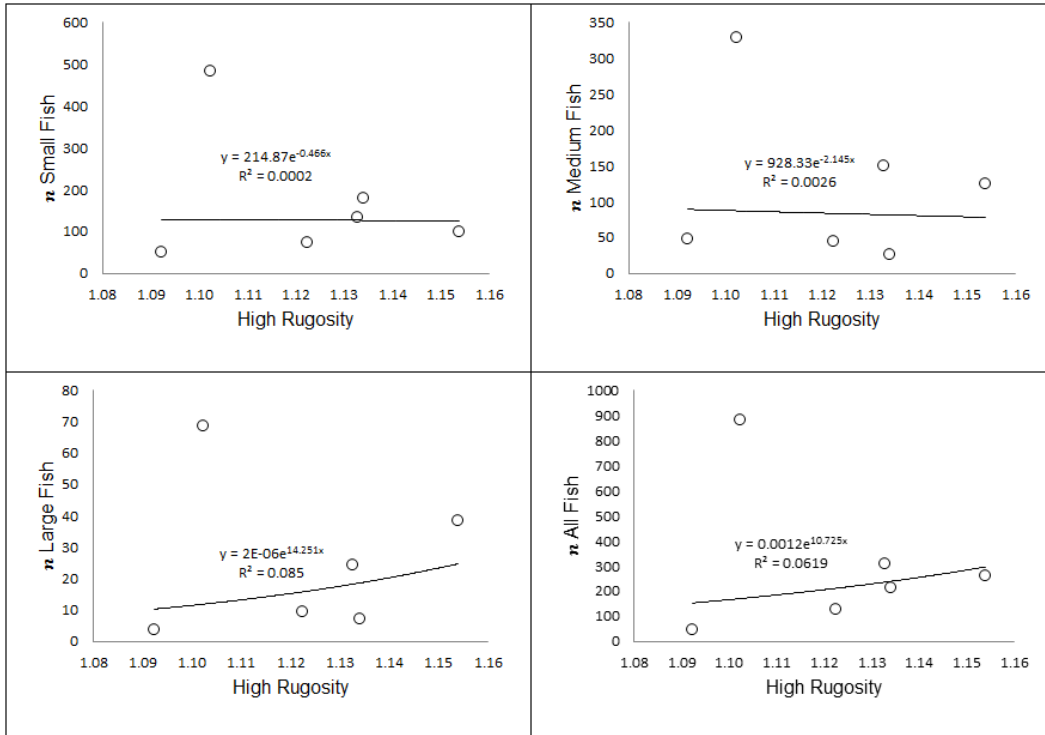
Site	\bar{X} Plan Curvature	All Fish	Large Fish	Medium Fish	Small Fish
Snowy Wreck Two	0.44	881	69	329	483
Cape Lookout One	0.18	263	39	124	100
Cape Lookout Two	0.12	309	24	150	135
North Carolina 780	0.23	127	9	44	73
N of Edisto MPA	0.18	214	7	26	181
Snowy Wreck One	0.03	47	4	47	49

Figure 125. Relationships between \bar{X} Plan Curvature and Fish Count by site. Highest $R^2 = 69\%$



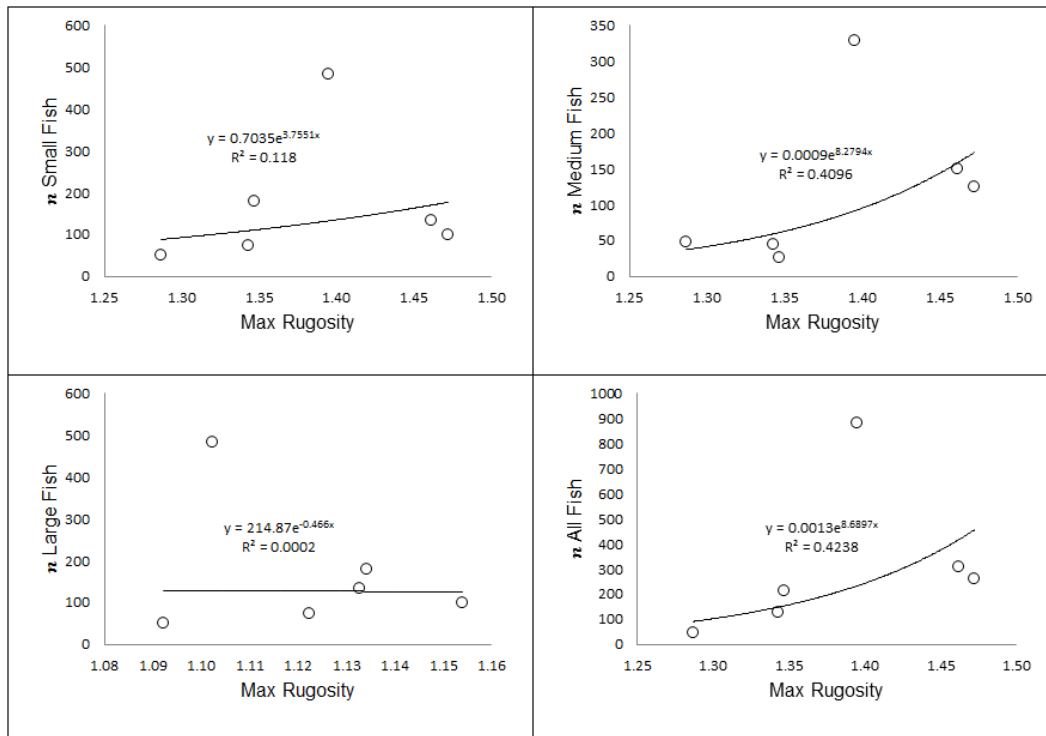
Site	\bar{X} Rugosity	All Fish	Large Fish	Medium Fish	Small Fish
Snowy Wreck Two	1.05	881	69	329	483
Cape Lookout One	1.08	263	39	124	100
Cape Lookout Two	1.07	309	24	150	135
North Carolina 780	1.06	127	9	44	73
N of Edisto MPA	1.05	214	7	26	181
Snowy Wreck One	1.04	47	4	47	49

Figure 126. Relationships between \bar{X} Rugosity and Fish Count by site. Highest $R^2 = 26\%$



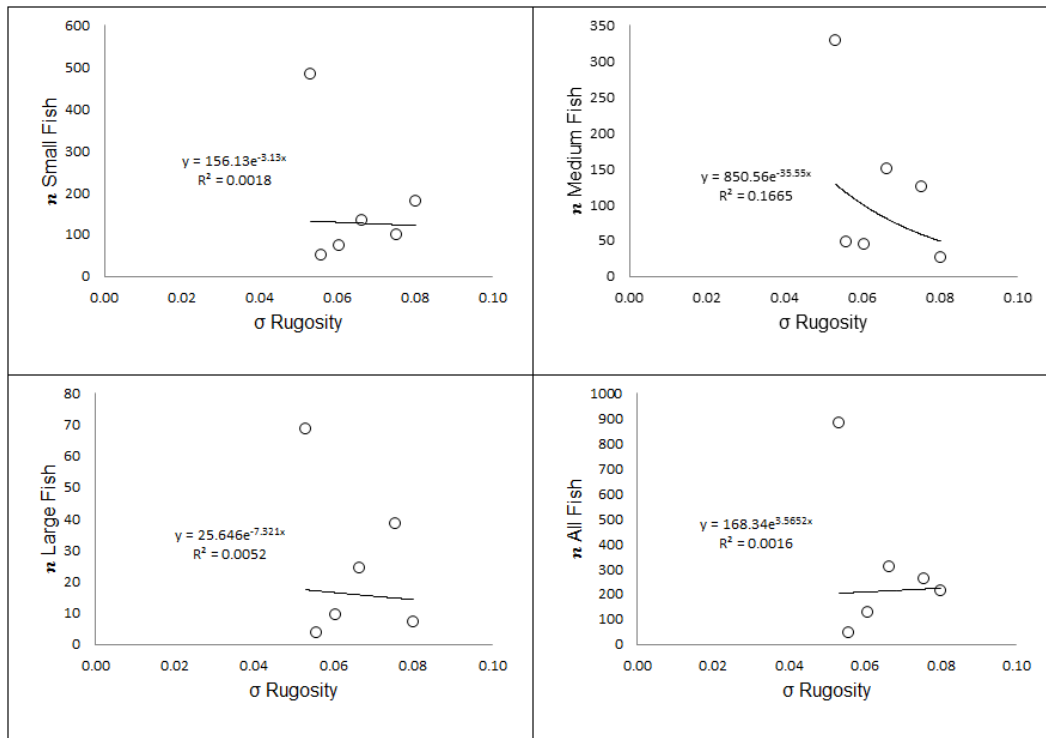
Site	\bar{X} High Rugosity	All Fish	Large Fish	Medium Fish	Small Fish
Snowy Wreck Two	1.10	881	69	329	483
Cape Lookout One	1.15	263	39	124	100
Cape Lookout Two	1.13	309	24	150	135
North Carolina 780	1.12	127	9	44	73
N of Edisto MPA	1.13	214	7	26	181
Snowy Wreck One	1.09	47	4	47	49

Figure 127. Relationships between \bar{X} High Rugosity and Fish Count by site. Highest $R^2 = 8\%$



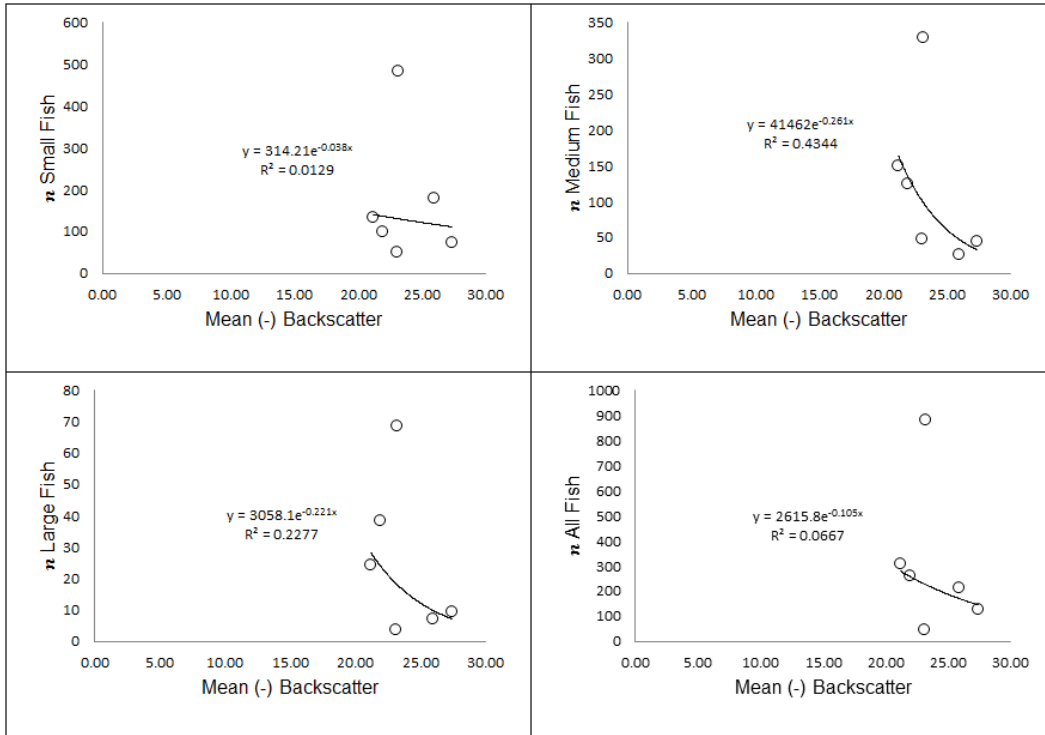
Site	\bar{X} Max Rugosity	All Fish	Large Fish	Medium Fish	Small Fish
Snowy Wreck Two	1.39	881	69	329	483
Cape Lookout One	1.47	263	39	124	100
Cape Lookout Two	1.46	309	24	150	135
North Carolina 780	1.34	127	9	44	73
N of Edisto MPA	1.35	214	7	26	181
Snowy Wreck One	1.29	47	4	47	49

Figure 128. Relationships between \bar{X} Max Rugosity and Fish Count by site. Highest $R^2 = 42\%$



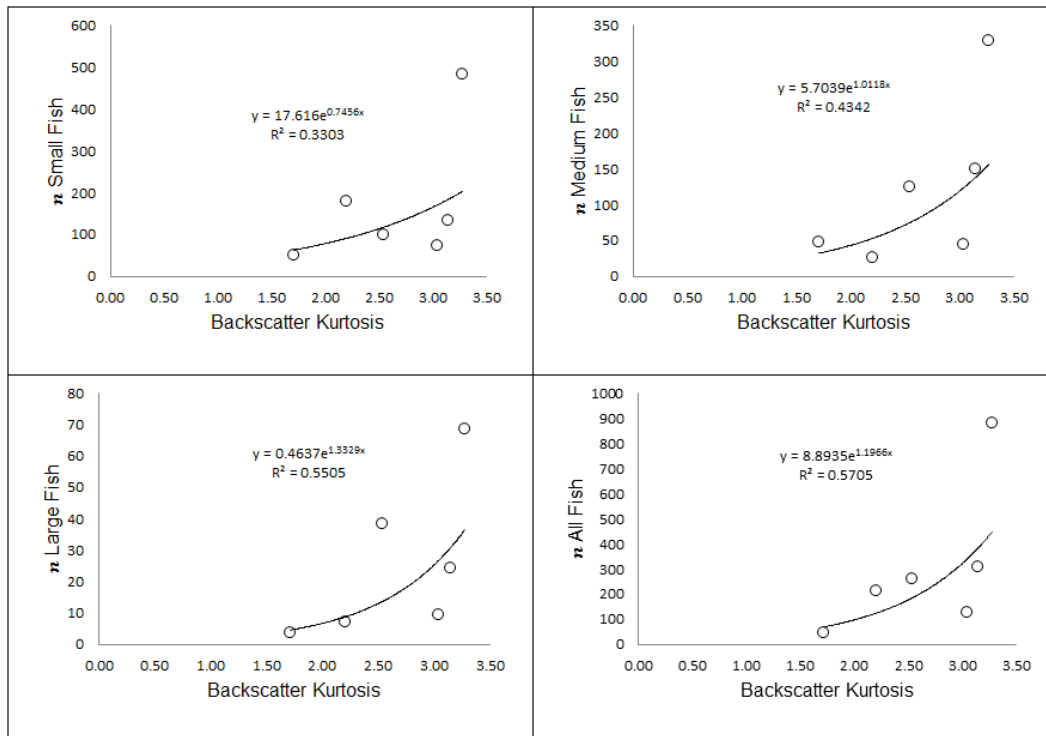
Site	σ Rugosity	All Fish	Large Fish	Medium Fish	Small Fish
Snowy Wreck Two	1.39	881	69	329	483
Cape Lookout One	1.47	263	39	124	100
Cape Lookout Two	1.46	309	24	150	135
North Carolina 780	1.34	127	9	44	73
N of Edisto MPA	1.35	214	7	26	181
Snowy Wreck One	1.29	47	4	47	49

Figure 129. Relationships between σ Rugosity and Fish Count by site. Highest $R^2 = 17\%$



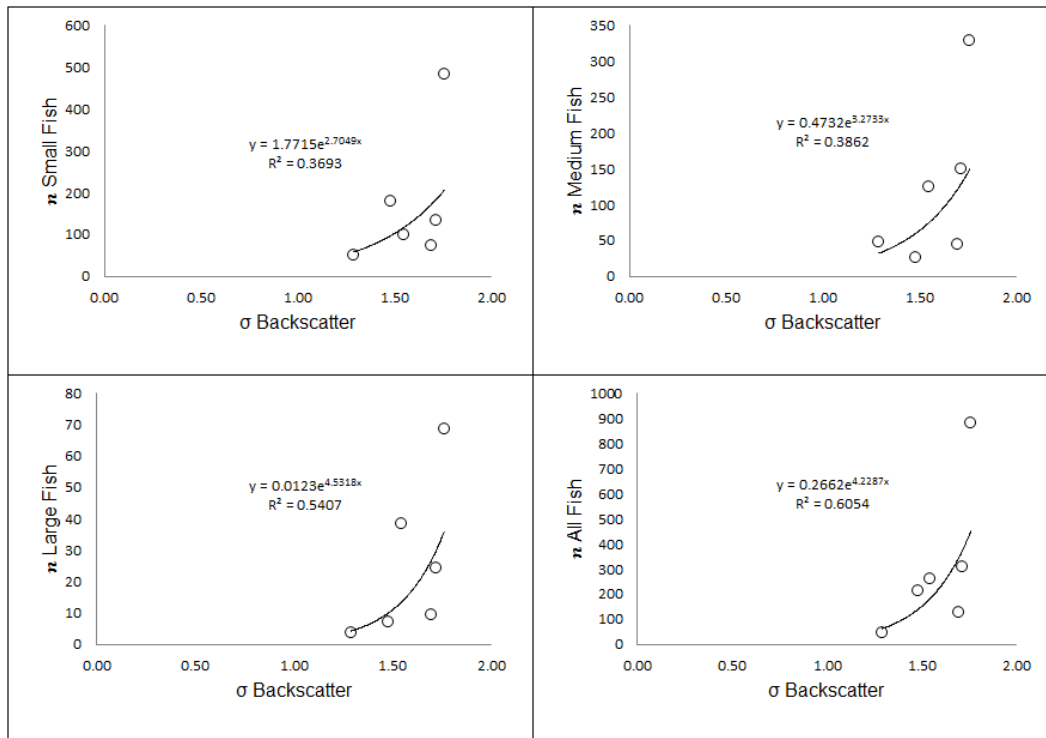
Site	\bar{X} Backscatter	All Fish	Large Fish	Medium Fish	Small Fish
Snowy Wreck Two	-23.21	881	69	329	483
Cape Lookout One	-21.97	263	39	124	100
Cape Lookout Two	-21.23	309	24	150	135
North Carolina 780	-27.41	127	9	44	73
N of Edisto MPA	-25.93	214	7	26	181
Snowy Wreck One	-23.10	47	4	47	49

Figure 130. Relationships between \bar{X} Backscatter and Fish Count by site. Highest $R^2 = 43\%$



Site	Backscatter Kurtosis	All Fish	Large Fish	Medium Fish	Small Fish
Snowy Wreck Two	3.27	881	69	329	483
Cape Lookout One	2.54	263	39	124	100
Cape Lookout Two	3.15	309	24	150	135
North Carolina 780	3.04	127	9	44	73
N of Edisto MPA	2.20	214	7	26	181
Snowy Wreck One	1.71	47	4	47	49

Figure 131. Relationships between Backscatter Kurtosis and Fish Count by site. Highest $R^2 = 57\%$



Site	σ Backscatter	All Fish	Large Fish	Medium Fish	Small Fish
Snowy Wreck Two	1.76	881	69	329	483
Cape Lookout One	1.55	263	39	124	100
Cape Lookout Two	1.72	309	24	150	135
North Carolina 780	1.69	127	9	44	73
N of Edisto MPA	1.48	214	7	26	181
Snowy Wreck One	1.29	47	4	47	49

Figure 132. Relationships between σ Backscatter and Fish Count by site. Highest $R^2 = 61\%$